DLR-FB-2017-59

Lidar-based Wake Identification and Impact Alleviation

Forschungsbericht

Autor: Jana Schwithal

Deutsches Zentrum
DLR für Luft- und Raumfahrt

Forschungsbericht 2017-59

Lidar-based Wake Identification and Impact Alleviation

Jana Schwithal

Deutsches Zentrum für Luft- und Raumfahrt
Institut für Flugsystemtechnik
Braunschweig

188 Seiten
105 Bilder
15 Tabellen
138 Literaturstellen

Deutsches Zentrum
DLR für Luft- und Raumfahrt

TU Braunschweig – Niedersächsisches Forschungszentrum für Luftfahrt

Berichte aus der Luft- und Raumfahrttechnik

Forschungsbericht 2017-22

Lidar-based Wake Identification and Impact Alleviation

Jana Schwithal

Deutsches Zentrum für Luft- und Raumfahrt
Institut für Flugsystemtechnik
Braunschweig

Diese Veröffentlichung wird gleichzeitig in der Berichtsreihe „NFL - Forschungsberichte“ geführt.

Diese Arbeit erscheint gleichzeitig als von der Fakultät für Maschinenbau der Technischen Universität Carolo-Wilhelmina zu Braunschweig zur Erlangung des akademischen Grades einer Doktor-Ingenieurin genehmigte Dissertation.

Lidar-based Wake Identification and Impact Alleviation

Bei der Fakultät für Maschinenbau
der Technischen Universität Carolo-Wilhelmina zu Braunschweig
zur Erlangung der Würde
einer Doktor-Ingenieurin (Dr.-Ing.)
genehmigte Dissertation

von:	Dipl.-Ing. Jana Schwithal, geb. Ehlers
aus:	Achim

eingereicht am:	08.12.2016
mündliche Prüfung am:	01.09.2017

Gutachter:	Prof. Dr.-Ing. S. Levedag
	Prof. Dr.-Ing. P. Hecker

2017

Abstract

Wake vortices can pose a serious safety hazard for air traffic. If an aircraft encounters the wake of another aircraft, this can cause sudden, unexpected aircraft reactions such as a strong rolling motion. In order to avoid these critical wake-induced aircraft reactions the International Civil Aviation Organization (ICAO) introduced specific separation minima for aircraft during approach and departure. The drawback of these separation requirements is, however, their resulting capacity limiting effect. A possible way to mitigate the wake-induced aircraft response during wake encounters is to improve the wake resistance of an aircraft by equipping it with a special wake impact alleviation control system. Such a control system could, on the one hand, lead to a significant safety improvement during wake vortex encounters and, on the other hand, represent a potential solution to relax the current wake-vortex-based separation minima for following aircraft equipped with such a control system while maintaining the current safety level. The resulting capacity gain would allow reducing arrival delays, which would, besides bringing economic benefits, also be attractive from the environmental point of view (because it implies lower fuel and noise emission) as well as from a comfort point of view for the passengers. Furthermore, the capacity gain could be used to increase the traffic flow and hence represent a possible solution to the future air traffic growth.

This thesis presents a possible approach for a wake impact alleviation control system, which is based on remote lidar wind sensing and online wake identification. The wake impact alleviation system, called OWIDIA (Online Wake IDentification and Wake Impact Alleviation), uses the information of a forward-looking Doppler lidar sensor to identify a model of the wake vortex disturbance and generates control commands to compensate the wake impact on the aircraft. This special wake vortex control system is integrated into the overall control architecture of a modern Fly-by-Wire aircraft and analyzed with respect to its potential to mitigate the aircraft reaction during wake vortex encounters. This analysis also includes an investigation of the requirements the OWIDIA system implies on the used lidar sensor.

The analysis of the attainable wake impact alleviation of the OWIDIA system is based on realistic boundary conditions and is performed on a system level covering the complex interdependencies of the different modules. It includes the investigation of the theoretical limits of the developed control system in the case of a perfectly identified disturbance during different encounter scenarios with varying encounter geometries and vortex strengths. The performance of the system is thereby evaluated by considering the achievable mitigation of the wake-induced bank angle, which represents the most relevant disturbance during encounters during the approach. In a second step, the sensitivity of the bank angle reduction performance with respect to the estimated parameters of the wake vortex model is performed to get insight of the required accuracy of the wake identification. Finally, the alleviation performance of the complete system including a realistic application of the wake identification is extensively investigated for different encounter scenarios including diverse encounter geometries and vortex ages as well as for different lidar sensor configurations. The analysis demonstrates that the system performance of the OWIDIA is strongly dependent on the characteristics of the lidar sensor. In combination with suitable sensor configurations with a good spatial resolution and low measurement noise,

the OWIDIA system shows very promising results. For straight wake vortices the system works very well and reduces the maximum bank angle by about $70\,\%$ on average during typical encounters of the approach flight phase and by up to $90\,\%$ during particular encounter scenarios. This alleviation performance suggests that the OWIDIA system would most likely be able to allow aircraft spacing at minimum radar separation. If the vortex age increases and the wake vortex starts to deform, the current version of the OWIDIA system can still be applied up to vortex ages involving moderately deformed vortices (such as 64-s-old wake vortices in atmospheric conditions with moderate turbulence and neutral stratification).

Altogether the analysis in this thesis shows that the lidar-based wake identification and impact alleviation system represents a very promising approach to mitigate the impact of wake vortices and seems to be realizable on the basis of future lidar sensor technology.

Kurzzusammenfassung

Wirbelschleppen können ein ernsthaftes Risiko für den Luftverkehr darstellen. Wenn ein Flugzeug in die Wirbelschleppe eines anderen Flugzeuges einfliegt, kann dies zu plötzlichen und unerwarteten Flugzeugreaktionen wie einer starken Rollbewegung führen. Um dies zu verhindern hat die Internationale Zivilluftfahrtorganisation ICAO (International Civil Aviation Organization) spezielle minimale Staffelungsabstände für Start und Landung festgelegt. Der Nachteil dieser Staffelungsabstände ist, dass sie die Kapazität des Luftraums begrenzen. Eine Möglichkeit, die Flugzeugreaktion bei Wirbelschleppendurchflügen zu verringern, besteht darin, das Flugzeug mit einem speziellen Steuerungssystem zur Abmilderung der wirbelinduzierten Flugzeugreaktion auszustatten. Für Flugzeuge mit einem solchen Steuerungssystem könnte auf der einen Seite ein signifikanter Sicherheitsgewinn während der Wirbelschleppendurchflüge erzielt und auf der anderen Seite eine mögliche Lockerung der minimalen wirbelschleppenbasierten Staffelungsabstände zum vorausfliegenden Flugzeug bei mindestens gleichbleibender Sicherheit erreicht werden. Der resultierende Kapazitätsgewinn würde es ermöglichen, die Verzögerung ankommender Flugzeug zu reduzieren. Dies wäre neben wirtschaftlichen Vorteilen und Komfortaspekten für die Passagiere auch aus Umweltgesichtspunkten attraktiv, da dadurch der Treibstoffausstoß und die Lärmbelästigung reduziert werden könnten. Außerdem könnte der Kapazitätsgewinn für eine Steigerung des Verkehrsflusses genutzt werden und somit eine mögliche Lösung für das prognostizierte weiter ansteigende Luftverkehrsaufkommen darstellen.

Diese Arbeit präsentiert einen möglichen Ansatz für ein Steuerungssystem zur Reduktion der Flugzeugreaktion bei Wirbelschleppendurchflügen. Das OWIDIA (Online Wake IDentification and Wake Impact Alleviation) genannte Steuerungssystem nutzt die Informationen eines vorausschauenden Doppler Lidars Sensors, um ein Modell der Wirbelschleppe zu identifizieren und auf dessen Basis Steuerflächenausschläge zu generieren, die die wirbelinduzierte Störung kompensieren. Dieses Steuerungssystem wird in die gesamte Flugsteuerungsarchitektur eines modernen Fly-by-Wire Flugzeuges integriert und hinsichtlich seines Potentials zur Reduktion der wirbelinduzierten Flugzeugreaktion analysiert. Daraus werden Anforderungen an zukünftige Lidar Sensoren für die Nutzung mit dem OWIDIA System abgeleitet.

Die Analyse der erreichbaren Reduktion der wirbelinduzierten Flugzeugreaktion durch das OWIDIA System stellt eine Systembetrachtung dar, in der statt der einzelnen Komponenten das vollständige Gesamtsystem unter realistischen Rahmenbedingungen untersucht wird. Es werden zunächst die theoretischen Grenzen des entwickelten Steuerungssystems unter der Annahme eines perfekt identifizierten Wirbels untersucht und der maximal auftretende Hängewinkel während Wirbelschleppendurchflügen mit verschiedenen Einflugszenarien und Wirbelstärken betrachtet. Anschließend wird die Sensitivität der erzielbaren Reduktion des Hängewinkels in Abhängigkeit der Genauigkeit der identifizierten Wirbelparameter analysiert. Abschließend wird das Potential des gesamten OWIDIA Systems einschließlich der Wirbelidentifizierung während verschiedener Wirbelschleppendurchflüge mit unterschiedlichen Einfluggeometrien und variierenden Wirbelaltern detailliert untersucht. Die Analyse zeigt, dass die Leistung des OWIDIA Systems stark von den Eigenschaften des Lidar Sensors abhängt. Wenn das System in Kombination mit geeigneten Sensoren mit guter räumlicher Auflösung der Messun-

gen und geringem Messrauschen angewendet wird, können sehr vielversprechende Ergebnisse erzielt werden. Bei geraden Wirbeln funktioniert das Steuerungssystem sehr gut und kann den maximalen Hängewinkel bei typischen Wirbelschleppendurchflügen im Landeanflug um durchschnittlich ca. $70\,\%$ und in einigen Fällen sogar um bis zu $90\,\%$ reduzieren. Diese Ergebnisse legen nahe, dass mit dem OWIDIA System eine Reduktion der Staffelungsabstände bis auf Radarstaffelung möglich sein könnte. Bei zunehmendem Wirbelalter ist das aktuelle OWIDIA System bis zu Wirbelaltern mit moderater Deformierung (wie bei $64\,\mathrm{s}$ alten Wirbeln bei atmosphärischen Bedingungen mit moderater Turbulenz und neutraler Schichtung) anwendbar.

Insgesamt zeigen die Analysen in dieser Arbeit, dass das untersuchte, auf vorausschauenden Lidar Messungen und Wirbelidentifizierung basierende Steuerungssystem OWIDIA ein vielversprechendes Potential zur Reduktion der wirbelinduzierten Flugzeugreaktion aufweist und mit zukünftig voraussichtlich verfügbarer Sensortechnologie realisierbar zu sein scheint.

Acknowledgments

This thesis has been accomplished during my employment as a research scientist at the Institute of Flight Systems of DLR (German Aerospace Center).

Firstly, I would like to thank my advisor Prof. Dr.-Ing. Stefan Levedag for his support of my thesis and for the constructive advice with respect to my work. I would like to thank Prof. Dr.-Ing. Peter Hecker for his effort of reviewing my thesis as co-examiner and for his helpful comments on my research. Also, I would like to express my gratitude to Prof. Dr.-Ing. Rolf Radespiel for being the chairman of the examination board.

Furthermore, my special thanks go to all of my colleagues from the department of Flight Dynamics and Simulation and from the Institute of Atmospheric Physics who supported my work with helpful assistance. I greatly appreciate the contributions from all of them and would like to acknowledge in particular the productive discussions with Carsten Schwarz, Dennis Vechtel, Dietrich Fischenberg, Dominik Niedermeier, Dr. Patrick Vrancken, and Jonas Herbst. I thank the head of my department Prof. Dr.-Ing. Klaus-Uwe Hahn for his continuous support and for giving me the opportunity to accomplish my thesis in the course of my work at DLR. Finally, my profound thanks go to Dr.-Ing. Nicolas Fezans for his sustained and remarkable support, his constructive criticism, and his fruitful inputs.

Last but not least I would like to acknowledge the valuable exchange and productive discussions with the members of the WakeNet community.

Braunschweig, 2017 Jana Schwithal

Contents

List of Figures

List of Tables

Nomenclature

Symbols

α	angle of attack (rad)
β	sideslip angle (rad)
β_{est}	estimated sideslip angle (rad)
β_{K}	flight path sideslip angle (rad)
Γ	circulation (m^2/s)
γ	flight path angle (rad)
Δ	difference (-)
δ_i	deflection of control surface i (rad)
Δt_{delay}	time delay between control deflection command generation and command realization (s)
Δt_{s}	sample time (s)
ϵ	eddy dissipation rate (m^2/s^3)
ϵ^*	normalized eddy dissipation rate (-)
Θ	pitch angle (rad), potential temperature (K)
λ	wave length (m), traffic flow (1/h)
μ	capacity (1/h)
Φ	bank angle (rad)
ρ	air density (kg/m^3)
σ	standard deviation (-)
χ	flight path azimuth (rad)
Ψ	heading (rad)
b	wing span (m)
b'	lateral separation of vortex cores (m)
$C_{i,j}$	nondimensional aerodynamic derivative of control surface j with respect to moment i (-)
c	velocity of light (m/s)
g	gravity force (m/s^2)
f	frequency (Hz)
H	height (m)
K_{FF}	feedforward gain (-)
K_I	integral gain (-)
K_P	proportional gain (-)
$K_{\delta_{\text{ail}}\delta_{\text{SP}}}$	factor between aileron deflection and deflection difference of left and right spoiler pair (-)
L	lift (N)
L_{WV}	wake-induced rolling moment (Nm)
l_μ	mean aerodynamic chord (m)
$\underline{M}_{i,j}$	transformation matrix from j to i coordinates (-)
M_{WV}	wake-induced pitching moment (Nm)
m	mass (kg)

N_{WV}	wake-induced yawing moment (Nm)
N^*	normalized Brunt-Väisälaä frequency (-)
N_{a}	number of measurement points along axis (-)
N_{h}	number of horizontal measurement axes (-)
N_{MP}	number of measurement points (-)
N_{v}	number of vertical measurement axes (-)
p	roll rate (rad/s)
$\overline{q}$	dynamic pressure ($\mathrm{N/m^2}$)
r	distance from vortex core (m), yaw rate (rad/s)
r_c	core radius (m)
$r_{x,\mathrm{MP}}$	body-fixed x-component of measurement range (m)
S	wing area ($\mathrm{m^2}$)
s	half span of wing (m)
t	time (s)
t_0	reference time in which sinking distance of wake vortex corresponds to initial vortex spacing b_0 (s)
u	longitudinal velocity (m/s)
V	velocity (m/s)
V_Θ	tangential velocity (m/s)
v	lateral velocity (m/s)
w	vertical velocity (m/s)
X	longitudinal force (N)
x	horizontal position (m)
$x_{\mathrm{mean,lidar}}$	average body-fixed x-component of the measurement range of all stored measurement points (m)
x_p	integrated error of bank angle deviation from command value (rad)
x_r	integrated error of sideslip angle deviation from command value (rad)
Y	lateral force (N)
y	lateral position (m)
Z	vertical force (N)
Z_{WV}	wake-induced vertical force (N)
z	vertical position (m)

Indices

0	inital value (for wake vortex: value right after formation)
A	aerodynamic coordinate system
AC	aircraft
ADS-B	value provided via ADS-B
age	vortex age
ail	aileron
atmos	resulting from atmosphere

b	body-fixed coordinate system
cmd	command value
Crow	Crow instability
ctrl	output value of controller
elev	elevator
ID	identification coordinate system in OWI
LoS	Line-of-Sight components
L-R	deflection difference of left and right side
l	rolling moment
m	pitching moment
max	maximum value
motion	resulting from aircraft motion
model	simulated parameter resulting from model
NED	north-east-down coordinate system
n	yawing moment
OWI	value identified by OWI
pedal	commanded value via pedal input of pilot
req	required
rud	rudder
scan	related to scan angles
SP	spoiler
TAS	true airspeed
true	true value
wind	wind components
WV	wake vortex

Abbreviations

ADS-B	Automatic Dependent Surveillance - Broadcast
AIM	Aerodynamic Interaction Model
ANN	Artificial Neural Networks
ASRS	Aviation Safety Reporting System
ATRA	Advanced Technology Research Aircraft
ATTAS	Advanced Technologies Testing Aircraft System
AWIATOR	Aircraft Wing with Advanced Technology OpeRation
CREDOS	Crosswind-REDuced Separations for Departure OperationS
CW	Continuous-Wave
DLR	Deutsches Zentrum für Luft- und Raumfahrt (German Aerospace Center)
DoF	Degrees of Freedom
DELICAT	DEmonstration of LIdar based Clear Air Turbulence detection
EU	Europeran Union
FAA	Federal Aviation Administration
FRA	FRankfurt Airport

HMI	Human Machine Interface
ICAO	International Civil Aviation Organization
IMC	Instrument Meteorological Conditions
IAE	International Aero Engines
IR	InfraRed
JAXA	Japan Aerospace Exploration Agency
KIAS	Knots Indicated AirSpeed
LASER	Light Amplification through Stimulated Emission of Radiation
LGW	London Gatewick Airport
LH	Left-Hand side
LIDAR	LIght Detection And Ranging
LoS	Line-of-Sight
MFLAME	Multifunction Future Laser Atmospheric Measuring Equipment
MOPA	Master Oscillator Power Amplifier
MP	Measurement Point
MRAC	Model Reference Adaptation Control
MTOW	Maximum Take-Off Weight
NASA	National Aeronautics and Space Administration
N	Noise
OWI	Online Wake Identification
OWIDIA	Online Wake IDentification and Impact Alleviation
P	Point
PID	Proportional-Integral-Derivative
QP	Quadratic Programming
RCR	Roll Control Ratio
RH	Right-Hand side
SHAPe	Simplified Hazard Area Predrediction
S	Signal
SNR	Signal-to-Noise Ratio
STD	STandard Deviation
TAP	Terminal Area Productivity
UK	United Kingdom
US	United States
UV	UltraViolet
WEAA	Wake Encounter Avoidance and Advisory
WIAC	Wake Impact Alleviation Control

1 Introduction

1.1 Overview and Motivation

Wake vortices represent a serious safety risk for air traffic. They are the undesired by-product of the lift generated by an aircraft. They result from the pressure difference on the upper and lower side of the aircraft wing[1] when the wing generates lift. The pressure difference leads to a circulating airflow, which rolls up shortly behind the aircraft to form a counter-rotating wake vortex pair.

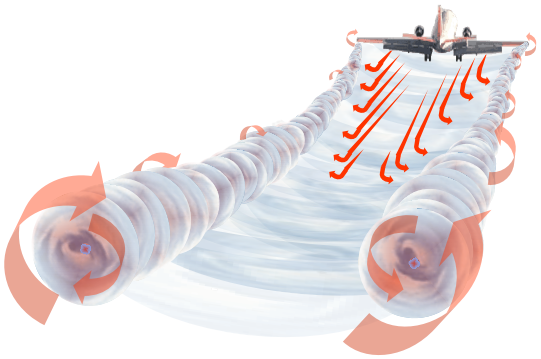

Figure 1.1: Wake vortex formation behind an aircraft[2]

This so-called wake vortex can pose a serious safety hazard for subsequent aircraft. If an aircraft encounters the wake vortex of another aircraft, this may cause dangerous aircraft reactions such as a sudden rapid rolling motion, undesired accelerations and critical deviations from the flight path. The wake induced aircraft response produces a considerable workload for the pilot. It may lead to injuries of the passengers and crew and can cause structural damages.

In order to reduce the risk of hazardous wake vortex encounters the ICAO (International Civil Aviation Organization) introduced separation minima for aircraft during approach and departure.[3] These separation requirements are generally considered to be safe. Their drawback, however, is that they limit the air traffic capacity at airports and in the airspace. An example of the consequences of the separation minima is outlined in a Boeing study which investigates the impact of different wake vortex separation schemes on the airport capacity.[4] The simulation of the 10 major US airports showed that the current FAA (Federal Aviation Administration) wake vortex separation standards during IMC (Instrument Meteorological Conditions), which are very similar to the ICAO wake vortex separation standards[5], reduce the airport capacity

[1] The same effect occurs on all lift-generating surfaces at the aircraft, such as vertical and horizontal stabilizers and high-lift flaps, as well. However, the main influence results from the wing.
[2] Hahn and Schwarz (2009), p. 29, Article about measurement flights into wake vortices.
[3] ICAO (2007), ICAO document providing rules for air traffic management.
[4] Robinson (1996), Paper presenting the results of a capacity study for different wake turbulence separations.
[5] The FAA wake separation minima are applied in the United States. The categories and minimum distances

by approximately $12\,\%$ compared to standard radar separations. *Hahn and Schwarz (2006)*[6] indicate that the theoretically achievable airport capacity gain of a relaxation of the current ICAO separation minima to minimum radar separation would be $66.7\,\%$ for aircraft parings of the ICAO HEAVY and MEDIUM class and $33.3\,\%$ for a pairing of two aircraft of the ICAO HEAVY class.

Even though the number of wake-vortex-induced incidents and accidents has greatly decreased since the introduction of the wake vortex separation minima, they still occur occasionally. An analysis of the US database ASRS (Aviation Safety Reporting System)[7] showed 488 events related to wake vortices including 58 cases with damages or injuries.[8] Examples of incidents resulting from wake vortex encounters with temporary loss of control and injuries of occupants are described in several incident reports.[9-12] In extreme cases a wake vortex encounter can even be the trigger for an accident such as in the case of Belle Harbour, New York, in 2001 where the pilot's reaction to a wake vortex encounter with excessive pedal commands led to the separation of the vertical stabilizer and the crash of the airplane.[13] Another example for a catastrophic result of a wake vortex encounter is the crash of an Israel Aircraft Industries 1124A that encountered the wake of a Boeing 757 in Santa Ana, California, in 1993.[14]

A possibility to reduce the impact of a wake vortex encounter is to develop a wake impact alleviation system. If the wake-induced aircraft response was avoided or at least significantly reduced by such a system, the risk of injuries of passengers and the crew as well as aircraft damages would be lowered and the pilot workload could be decreased. Furthermore, the application of a wake impact alleviation system could represent a potential chance to relax the current wake vortex separation minima. A relaxation of the separation standards while at least preserving the current safety level would be highly desirable from an operational and economical point of view. It could be a solution to deal with the growing air traffic. Figure 1.2 illustrates that the worldwide aircraft traffic has constantly been growing during the last years and forecasts,

differ slightly from the ICAO wake vortex separation minima, as shown in appendix A. The discrepancies between the two separation standards are, however, comparably small and the limiting effects on the capacity can be considered as similar.

6 Hahn and Schwarz (2006), Paper about the effects of wake vortex avoidance on landing capacity.

7 http://asrs.arc.nasa.gov/, Database of NASA with reports of pilots, air traffic controls, ground staff and other people involved in air traffic about events, disturbances and incidents in the US airspace.

8 Münster and Schwarz (2010), Report about the analysis of the ASRA database concerning wake vortex incidents in the US.

9 CIAIAC (2011), Report about the wake vortex incident of an Airbus A320 in high-level air space in north eastern Spain in 2006.

10 TSB (2010), Report about the wake vortex incident of an Airbus A319 in Washington State, USA on 10 January 2008.

11 NTSB (2001), Report about the wake vortex incident of a Boeing 737 at flight level 240 near Santa Barbara, California, USA.

12 ATSB (2009), Report about the wake vortex incident of a Saab 340b-229 at Sydney Airport in 2008.

13 NTSB (2004), Aircraft accident report about the accident with vertical stabilizer separation of American Airlines flight 587 in Belle Harbor New in 2001.

14 NTSB (1994), Report of the wake vortex accident of an Israel Aircraft Industries 1124A resulting in a crash close to John Wayne Airport, Santa Ana, California, USA in 1993.

e.g. by Eurocontrol[15], suggest it will continue to grow during the next decades. However, the construction of new runways will, at least in Europe, become more and more problematic since the corresponding consumption of limited land resources as well as the noise exposure are no longer accepted by the resident population. Therefore, alternative solutions that help towards the reduction of the separation minima such as a wake impact alleviation control system are becoming very attractive.

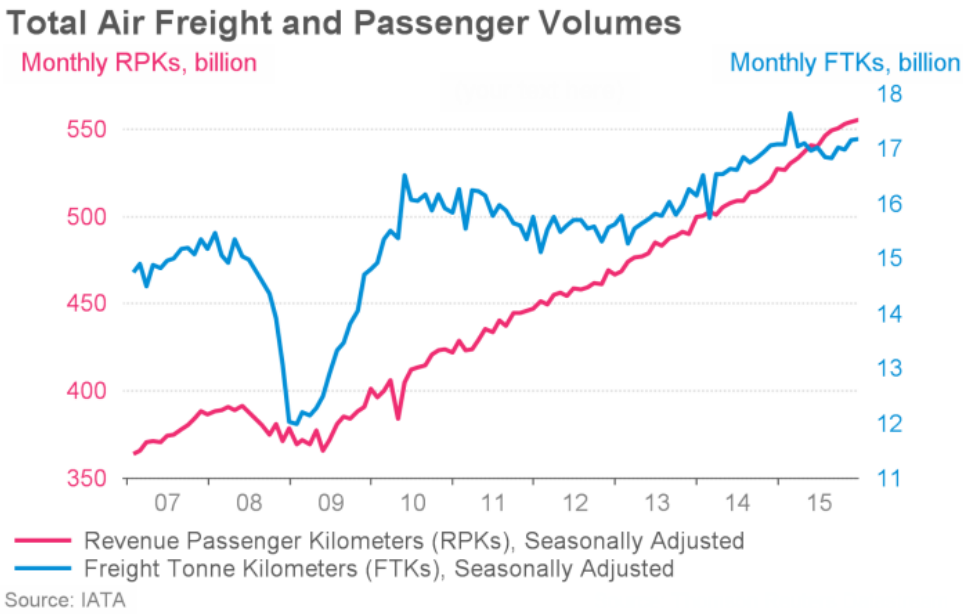

Figure 1.2: Development of global air traffic from 2007 to 2015[16]

A possible approach could be, for instance, that aircraft that are equipped with a wake impact alleviation system are allowed to fly with closer separation minima behind other aircraft than aircraft without such a system. The reduction of the wake-induced aircraft response due to a wake impact alleviation system could represent an equivalent safety finding that could guarantee the same safety level for closer separation minima as the safety level achieved by aircraft without a wake impact alleviation system in case of regular separation minima. This concept is also considered in the SESAR (Single European Sky ATM Research) project, in which it is suggested that "more wake resistant" aircraft are allowed to have closer separation distances than "less wake resistant" aircraft.[17] *Focking (2016)*[18] analyzed the potential capacity gain and resulting economical benefit if aircraft with a wake impact alleviation system were allowed to fly more closely behind other aircraft. The analysis was based on strong simplifications. However, the general trends and orders of magnitudes of potential benefits can be expected to be

[15] Eurocontrol (2013), Eurocontrol study about growth in air traffic and capacity for 2035.

[16] IATA (2015), p. 1, Analysis of air traffic passengers in December 2015 by International Air Transport Association. ©International Air Transport Association, 2015. Air Passenger Market Analysis - December 2015. All Rights Reserved.

[17] Eriksen (2010), p. 12, Presentation about workpackage 6.8.1 "Wake Vortex Research" of the SESAR Joint Undertaking.

[18] Focking (2016), By the author of this work supervised student project thesis about the economical benefit of a wake impact alleviation system.

correct. The capacity gain can be used in order to optimize two different aspects: It can either lead to a reduced delay or to an increase in the traffic flow as shown in Fig. 1.3. The upper curve μ_0 represents a given airport capacity. If the capacity is increased to curve μ_1, the average delay can be reduced by Δt_{Delay}, while maintaining the same traffic flow, or the traffic flow can be increased by $\Delta\lambda$ compared to the original delay. Besides these two extreme cases, a combined improvement of both benefits can also be achieved according to combinations of both parameters along the curve μ_1 between the values (λ_0, W_1) and (λ_1, W_0). That means that the traffic flow could, for instance, be slightly increased and the delay would still be lower than in case of the original capacity μ_0.

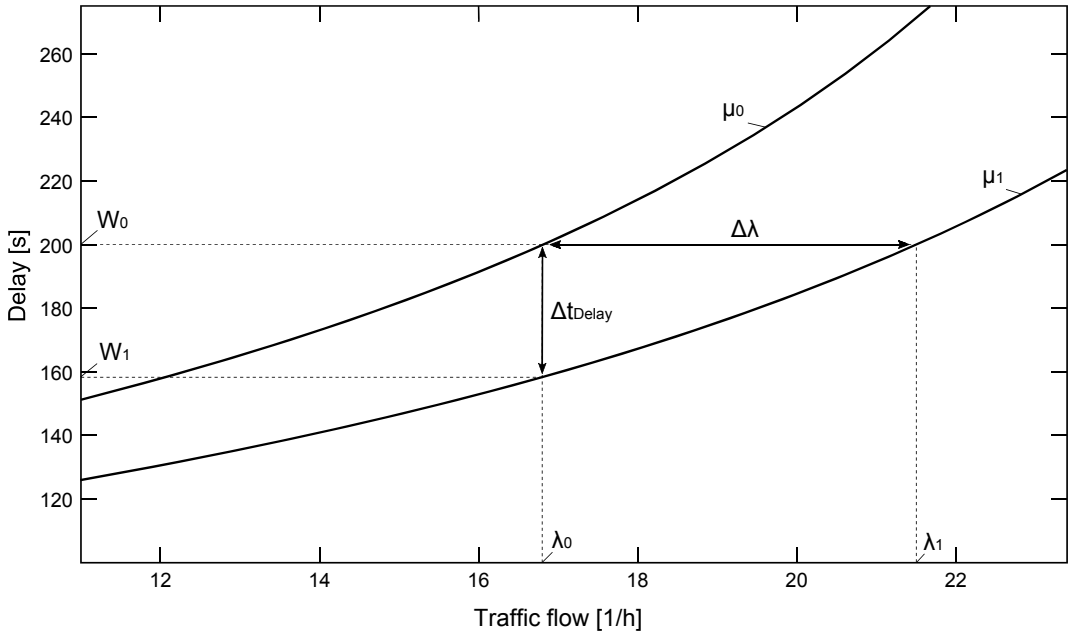

Figure 1.3: Correlation of traffic flow and delay for different capacities (based on *Focking (2016)*[19])

Focking estimates the approximately achievable increase in traffic flow and reduction of delay in holding under simplified assumptions[20]. The results are presented in Fig. 1.4 and 1.5. Different scenarios are considered concerning the percentage of aircraft equipped with a wake impact alleviation system and the distance the current separation minima could be reduced for aircraft with a wake impact alleviation system. The more aircraft possess such an alleviation system, the greater is obviously the capacity gain and the resulting maximum traffic flow increase or maximum delay reduction. Especially large airports, which are used as a hub by airlines that decided to equippe their complete fleet with the alleviation system, could therefore particularly

[19] Focking (2016), p. 18, Student project thesis about the economical benefit of a wake impact alleviation system, supervised by the author of this thesis.

[20] The analyses are performed for a generic airport exhibiting a traffic mix of aircraft types similar to Frankfurt Airport (FRA). Only one runway is considered, which is assumed to be operated in segregated mode and used for landing only. The runway is assumed to be used to capacity with an average delay derived from the average delay at London Gatewick Airport (LGW), selected as an example for a busy single runway airport operating to capacity.

benefit from the capacity gain. Up to what degree the current separation minima could be reduced thanks to a wake impact alleviation system depends on the system performances and will still have to be analyzed within the scope of the equivalent safety findings. Figures 1.4 and 1.5 show the effects for different distance reductions between -0.25 NM and -1 NM compared to the current ICAO separation minima.[21] The exact values in these figures are influenced by the assumptions[22] of the simplified study of Focking and might vary for other airports and conditions. The trends are, however, generally true.

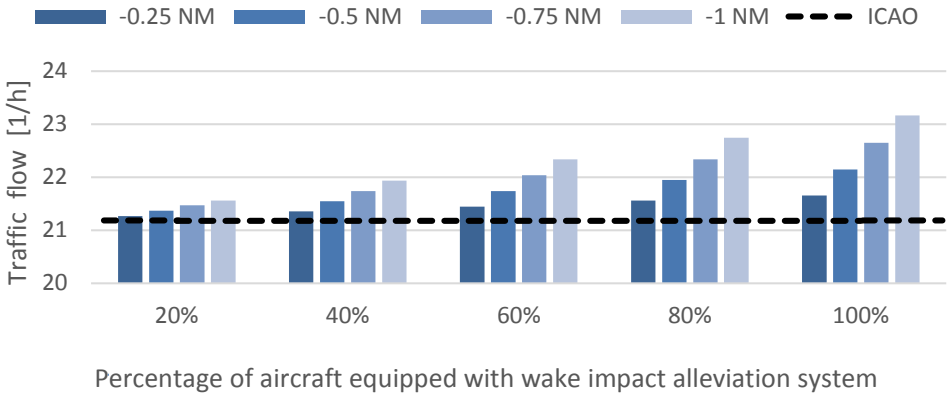

Figure 1.4: Increase in traffic flow for different percentages of aircraft with a wake impact alleviation system and reductions of the current separation minima by -0.25 NM to -1 NM (based on *Focking (2016)*[23])

An increase of the average traffic flow of one to two aircraft per hour could already be a huge benefit for an airport. By improving the traffic flow airports can operate more efficiently, which might in some cases even avoid the construction of additional runways. Furthermore, the airport would have a direct economical profit from the increased traffic flow. This could be partly transferred to the airlines, e.g. by means of reduced landing costs, and thus reduce the costs for the passengers as well.

A reduction of the average arrival delays of the aircraft would have economical as well as ecological benefits. Thanks to the shorter time spent in holding, the aircraft consume less fuel. This implies a lower environmental pollution and reduced costs for the airline due to fuel burn. Further economical benefits for the airline result, for instance, from reduced crew and maintenance costs due to shorter flight hours and lower compensation costs for delayed passengers. A report produced during NASA's Terminal Area Productivity (TAP) program[24] estimated that savings

[21] The separation is, in this context, never reduced below the minimum radar separation, which is assumed to be 2.5 NM here.

[22] The calculations are based on the assumption of an M/M/1 queue. The aircraft pairings are generated randomly, whereupon the traffic mix corresponds to a typical traffic mix at Frankfurt airport. The runway is assumed to be used in segregated mode for landing only. The reference value for the delay with ICAO separation minima is derived from a representative day at a highly frequented airport like Gatwick and set to 200 s.

[23] Focking (2016), p. 24, Student project thesis about the economical benefit of a wake impact alleviation system, supervised by the author of this thesis.

[24] Hemm et al. (1999), p. 1-8, Report about the estimated benefits of the Terminal Area Productivity (TAP) Program Technologies at 10 international US airport.

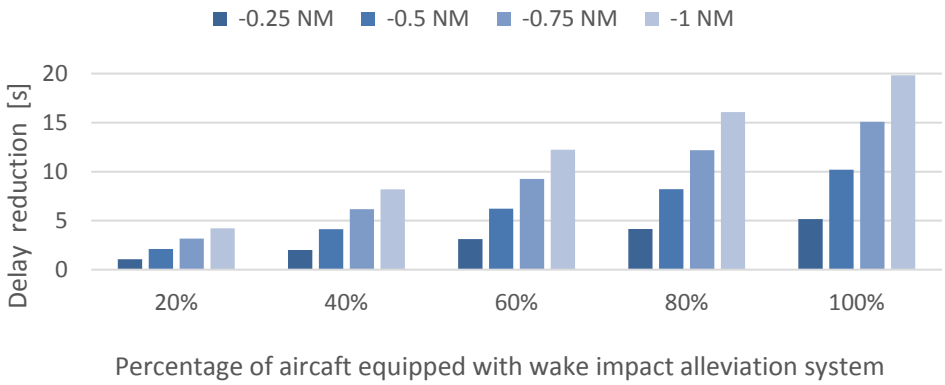

Figure 1.5: Reduction of delay in holding for different percentages of aircraft with a wake impact alleviation system and reductions of the current separation minima by -0.25 NM to -1 NM (based on *Focking (2016)*[23])

of about \$15 million per year and per airport could be achieved on average at 10 internal US airports thanks to reduced arrival delays if the separation minima could be reduced.[25] Additional benefits of the reduction of the holding time of the aircraft are a lower noise exposure of people living close to airports and reduced local environmental pollution while also providing a comfort gain for passengers thanks to fewer travel delays.

Therefore, it can be seen that the development of a control system to alleviate the wake-induced aircraft response would be beneficial from a safety, operational, economical, and ecological point of view.

1.2 State of the Art

At most airports in the world, the ICAO wake-vortex-based separation minima are applied today. An overview of these separation minima for the different weight-based aircraft pairings is given in table A.1 in appendix A. They have been developed with the goal to have a distance to leave enough time such that the wake vortex is not dangerous for the following aircraft anymore. After sufficient time the wake vortex can either have decayed to a negligible turbulence level or have been carried away by winds (cf. section 2.1). As the impact of the wake vortex on the following aircraft is strongly influenced by the size of this aircraft and the strength of the wake vortex, which is, in turn, proportional to the weight of the generator aircraft (cf. section 2.1), the separation minima are defined dependent on the maximum takeoff weight of the leading and following aircraft. The separation minima of the ICAO only represent a suggestion of safe distances between landing aircraft, which is applied in most countries in the world. If a country or airport wants to apply other separation standards this is possible if it can be shown that the alternative separations are safe as well. In the United States separation standards

[25] The analysis considers the effects of NASA's Aircraft Vortex Spacing System AVOSS. This system adjusts separation minima on the basis of the estimated weather-dependent vortex evaluation instead of allowing reduced spacing due to wake impact alleviation systems. Nevertheless, the results show the great potential benefit of relaxed separation minima even if the basis for the reduction is different in this case.

defined by the FAA are applied, which are shown in table A.2 in appendix A. Further alternative separations are, for instance, used at some airports in the United Kingdom and in Swiss (cf. Fig. A.1 in appendix A). All these separation minima are, however, very similar. As they are known to be rather conservative, serious effort has been posed on a revision of the current separation standards during the last years with the purpose to create a capacity gain. Within the RECAT (wake turbulence re-categorization) framework new separation minima have been developed that are based on additional aspects besides the weight of the follower aircraft. The first step is the installation of a new categorization of aircraft into six categories with adapted minimum separations. These separation minima are already in operation at specific airports in the US (e.g. at Memphis Internal Airport since 2012) and in Europe (at Paris Charles de Gaulle Airport since 2016). Appendix A shows the corresponding categories and distances for Europe (RECAT-EU) and the USA (RECAT-US), which are again slightly different. For future applications, further revisions of the wake-vortex-based separation standards are planned and currently in development, which include weather-dependent separation minima and specific separations for individual aircraft pairings. In this context, it could also be possible to allow shorter separations for aircraft that are particularly wake-resistant, e.g. because they possess a special wake impact alleviations system.

In the past different approaches have been taken to reduce the risk of wake vortex encounters with the purpose to improve the safety during flight on the one hand and to increase the airspace and airport capacity by closer wake vortex separation on the other hand. These approaches either focus on the generator aircraft and try to reduce the wake vortex during its generation or on the following aircraft and aim at the reduction of the danger of a given wake vortex for the encountering aircraft.

The intention of the research activities concerning the wake vortex alleviation at the generator aircraft is to influence the vortex strength and vortex decay by specific wing design or active devices at the wing. Different passive technologies such as spoilers, triangular flaps, splines or tail wings have been applied in order to weaken the generated wake vortices and to shorten their life span by accelerated decay.[26-28] Beyond that, active methods have been investigated in diverse approaches such as differential and oscillating flap settings[29,30], rapidly actuated seg-

[26] Croom (1977), Paper about the evaluation of the application of spoilers for wake impact alleviation in flight test.

[27] Ortega, Bristol, and Savas (2003), Paper about the experimental analysis of the instability of counter-rotating vortex pairs of unequal strength.

[28] Durston et al. (2005), Paper about the analysis of the alleviation of the far-field vortex wake of a generic wing-tail aircraft model.

[29] Voß et al. (2007), Paper about the numerical and experimental investigation of wake vortex alleviation using differential and oscillating flap setting.

[30] Crouch, Miller, and P.R. (2001), Paper about the application of periodic motion of the wing control surfaces for the breakup of aircraft trailing vortices.

mented Gurney flaps (miniature trailing-edge effectors)[31-33] or synthetic jets separating control along the span of the wing[34].

In addition to the research related to the alleviation of wake vortex generation, further research activity focused on the influence of the wake vortex on encountering aircraft during the last years. With the goal to reduce the risk of wake vortex encounters for a given wake vortex, different strategies have been investigated concerning the detection, avoidance and pilot awareness of wake vortices as well as control systems for the alleviation of the wake impact of the encountering aircraft.

The detection of wake vortices can be based on a prediction of the wake vortex location with prediction models such as the P2P[35-37], APA[38] or PVM[39]. These wake vortex prediction tools use information about the aircraft configuration of the generator aircraft and atmospheric conditions to estimate the evolution of the wake vortex circulation and position. If additional sensors such as a Doppler LIDAR (LIght Detection And Ranging) sensor are available on the aircraft, the wake vortex position can also be derived from the provided measurement data. *Feuerle, Steen, and Hecker (2015)*[40] suggest to apply a backward looking lidar sensor to detect the own wake vortex and to broadcast information about the wake vortex to following aircraft. Other applications assume a forward looking lidar sensor to measure the wake of aircraft flying ahead. The patent *Fischenberg (2013b)*[41] suggests using a wake vortex identification algorithm that determines a wake vortex model from lidar measurements with limited numbers of measurement spots. To evaluate whether the identified wake vortex represents a risk for the potentially encountering aircraft a wake hazard assessment method such as the DLR development SHAPe

[31] Matalanis and Eaton (2007b), Paper about the analysis of the potential of static segmented Gurney flaps for the active wake vortex alleviation.

[32] Matalanis and Eaton (2007a), Paper about the analysis of the potential of rapidly actuated segmented Gurney flaps for the active wake vortex alleviation.

[33] Matalanis, Nelson, and Eaton (2007), Paper about a novel aerodynamic decide specifically designed for active wake alleviation.

[34] Greenblatt et al. (2005), Paper about active control of a wing tip vortex by varying the degree of boundary layer separation with zero mass-flux perturbations.

[35] Holzäpfel (2003), Paper describing the probabilistic two-phase wake vortex decay and transport model developed at DLR.

[36] Holzäpfel (2004), Paper presenting the application and assessment of the probabilistic two-phase wake vortex decay and transport model developed at DLR.

[37] Holzäpfel (2006), Paper about further developments, applications and assessments of the probabilistic two-phase wake vortex decay and transport model developed at DLR.

[38] Sarpkaya, Robins, and Delisi (2001), Paper describing a wake vortex eddy-dissipation model and its comparison with lidar measurements.

[39] De Visscher et al. (2010), Paper presenting the 3D model for the prediction of wake vortex transport and decay developed at the Université catholique de Louvain (UCL).

[40] Feuerle, Steen, and Hecker (2015), Paper presenting a new concept for wake vortex hazard mitigation on the basis of onboard measurement equipment.

[41] Fischenberg (2013b), Patent of an online wake identification algorithm.

(Simplified Hazard Area Prediction)[42-44] can be applied, which determines areas of dangerous wake-induced roll moments around the detected wake vortex location. Based on this knowledge, avoidance strategies can be deployed, which either deliver a suggested flight path, the pilot should follow manually to evade the hazardous wake vortex area, or automatically steer the aircraft around the wake vortex if the autopilot is engaged. A possible algorithm to compute the flight path around the wake vortex can, for instance, be realized with path primitives.[45] Besides the detection and evasion of the wake vortices, another important aspect during the avoidance maneuver is the pilot awareness. *Kocks et al. (2010)*[46] present a concept for the graphical presentation of wake vortex hazard areas in existing cockpit displays. *Raab (2010b)*[47] describes an approach for a human-machine-interface (HMI) that informs the pilot about a detected wake vortex and displays the suggested avoidance maneuver, which the pilot either has to track himself or which the autopilot follows. In the latter case the information about the autopilot's goal helps to increase the pilot's situational awareness. The Wake Encounter Avoidance and Advisory (WEAA) system[48], developed by DLR, is a concept that combines all these elements of wake prediction (optionally including wake detection based on lidar measurements), avoidance, and awareness. It is intended to be a safety net function that performs small-scale evasion of wake vortex encounters and has successfully been tested in flight test with the DLR research aircraft ATRA (Advanced Technology Research Aircraft).[49,50] The MITRE Corporation's Center for Advanced Aviation System Development developed a similar system.[51] This system also displays the wake vortex tail of the leading aircraft (estimated on the basis of the generator aircraft class and current wind conditions) in the cockpit of subsequent aircraft and provides guidance for speed adjustments for achieving the spacing assigned by the air traffic controller. A wake hazard assessment and automatic avoidance maneuvers are not included in this approach. Further visualization systems for wake vortices for manual avoidance by the pilot are presented in *Nykl et al. (2011)*[52] and in the patent *Baranov et al. (2009)*[53].

The evasion of wake vortices is a very effective procedure to increase the safety of air traffic

[42] Hahn, Schwarz, and Friehmelt (2004), Paper about the development of a simplified hazard area prediction model.

[43] Schwarz and Hahn (2006), Paper presenting the results of a full-flight simulator study for the investigation of wake vortex hazard areas.

[44] Hahn and Schwarz (2007), Paper about the derivation of safe limits for wake penetration from pilot ratings during flight simulator studies and in-flight simulations.

[45] Vechtel (2012), DLR institute report about the design of an algorithm for the resolution of wake vortex conflicts in air traffic.

[46] Kocks et al. (2010), Paper introducing a wake vortex visualization concept for existing cockpit displays.

[47] Raab (2010b), DLR institute report about the conceptual design for the operation of a wake impact attenuation and avoidance system and its human machine interface.

[48] Bauer, Vechtel, and Raab (2012), Paper describing the development of an avoidance and advisory system for wake vortex encounters.

[49] Bauer et al. (2014), Paper about flight tests of the WEAA system developed at DLR.

[50] Sölch et al. (2016), Paper about the analysis of the accuracy of the wake prediction of the WEAA system on the basis of data from a flight test campaign in April 2014.

[51] Estes et al. (2011), Paper about the evaluation of wake turbulence avoidance automation.

[52] Nykl et al. (2011), Paper presenting a prototype of a flight tested instrument that tracks wake vortices and presents this information to the pilots.

[53] Baranov et al. (2009), Patent for a method and a system assisting an aircraft to prevent wake vortex encounters.

with respect to potential wake vortex encounters. However, it requires a long distance between the wake vortex and the position of the affected aircraft at the time of wake vortex detection in order to provide enough time to initiate appropriate maneuvers. In reality such long warning lead-times are not always given. Furthermore, the avoidance strategy requires a reliable detection of the wake vortex. If the wake vortex position is not correctly detected, the avoidance maneuver could, in the worst case, be ineffective and the aircraft might still encounter the wake vortex disturbance. Although this case cannot be excluded, the reduction of the probability to hit the vortex when applying the avoidance strategy (compared to the case without an avoidance assistance systems) is, however, certainly interesting and will lead to an increase in safety.

For scenarios in which an encounter with the wake vortex cannot be avoided (because the presence of a wake vortex is only known very shortly before the encounter or because evasion maneuvers are not possible), the application of specific flight control systems to attenuate the impact of the wake vortex represents a promising approach to increase the safety and comfort during the wake vortex encounter. Different approaches for wake impact flight control systems have been developed during the last years.
Looye, Lombaerts, and Kier (2012)[54] and *Rafi and Steck (2013)*[55] pursue the approach to design a general feedback control system and consider a wake vortex as one of the disturbances the controller should be able to cope with. They do not detect the wake vortex before the encounter but let the regular feedback law of their control system deal with the wake vortex as a general disturbance. During the DLR project "Wetter & Fliegen" (weather and flying)[56] Looye, Lombaerts and Kier tested a Rate-Command-Attitude-Hold control system based on a nonlinear dynamic inversion method on the DLR research aircraft ATTAS (Advanced Technologies Testing Aircraft System) for a wake vortex encounter and showed that it reduced the bank angle compared to a wake encounter without attitude hold control. Rafi and Steck equipped a general aviation aircraft with a Model Reference Adaption Control (MRAC) system and assessed the flight control system during wake vortex encounters. The flight control system consists of a PID controller combined with a dynamic inverse controller, which transforms the commanded accelerations of the PID controller into control surface deflection commands and thrust settings. Artificial Neural Networks (ANNs) generate additional commands, which are added to the commands of the PID controller if deviations from the desired aircraft dynamics occur. For the application of the control system during wake vortex encounters an envelope protection was added which deactivates the side force control if bank angle deviations of more than 40° from the command angle occur. Simulated wake vortex encounters with and without the control system showed that the controller reduced the occurring bank angle and speed loss during all considered encounters and the altitude loss in most cases.

The challenge of control systems which are based the on design of feedback control laws to cope with the wake vortex disturbance is the risk of generating undesired, high structural loads

[54] Looye, Lombaerts, and Kier (2012), Paper describing the design of feedback control laws for wake vortex encounters and the assessment of the control system in flight tests.
[55] Rafi and Steck (2013), Paper about the development and testing of a flight control system for wake vortex encounters including an envelope protection scheme.
[56] Gerz and Schwarz (2012), Research report of DLR project "Wetter & Fliegen" (Weather and Flying).

during the rest of the flight without the wake vortex. In order to alleviate the wake-induced aircraft reaction a dynamic control system with comparably high gains is required. However, during most of the flight time, when there is no wake vortex, these strong control dynamics are not required. They are even unfavorable as the controller reacts very sensitively to any kind of disturbance and constantly commands control actions, which can lead to harmful structural loads. In order to avoid these permanent structural loads, it would be favorable to apply the very dynamic control activities for the wake impact alleviation only during the actual wake vortex encounter. To realize this, the wake vortex encounter obviously needs to be known, which is usually not the case.

A promising concept for this purpose is the wake disturbance rejection on the basis of forward-looking flow field scanning sensors. This concept was originally developed at DLR[57-61], by Hahn et al. but was also analyzed at TU Berlin by *Kloidt (2007)*[62] and *Held (2003)*[63]. It assumes that a forward-looking sensor such as a lidar is equipped aboard the aircraft and provides information about the disturbance wind velocities in a short distance of about 100 - $200\,\mathrm{m}$ in front of the aircraft. The application of an Aerodynamic Interaction Model (AIM)[64] allows to derive the wake-induced forces and moments affecting the aircraft from the measured wind velocities. The developed flight control system finally computes the control surface deflections which compensate for the wake-vortex-induced disturbances. To avoid negative effects of sensor or actuator delays, the compensatory control surface deflections can be applied in advance with a fixed temporal offset corresponding to the known system delay.

This wake impact alleviation approach allows countervailing disturbance moments up to the control authority of the aircraft. If the wake induced rolling moment exceeds the roll control authority of the aircraft (i.e. the so-called Roll Control Ratio RCR[65,66] is larger than 1), a rolling motion can obviously not be entirely prevented. For wake vortex encounters with RCR values

[57] Schwarz and Hahn (2011), Paper about a control system for wake vortex encounters based a feedforward disturbance compensation and its analysis in offline and pilot-in-the-loop investigations as well as in flight tests.

[58] Hahn (2002), Paper describing the impact of wake vortices on aircraft and the possibility to reduce this impact by means of a suitable control system.

[59] Fock, Hahn, and Schwarz (2006), DLR institute report about the analysis of a pilot assistance system for wake vortex encounters with different forward-looking sensors.

[60] Hahn and Schwarz (2008), Paper about the analysis of a control system using a forward-looking lidar sensor for the alleviation of the impact of gusts and wake vortices.

[61] Hahn et al. (2010), Paper about the development and analysis of a wake encounter flight control assistance system based on the processing of forward-looking lidar measurements.

[62] Kloidt (2007), Dissertation about the development of a flight control system for the alleviation of the impact of wake vortices.

[63] Held (2003), Diploma thesis about the analysis of a flight control system for the reduction of the hazard potential of wake vortices in the approach phase.

[64] Fischenberg (2010), Paper presenting a method to validate wake vortex encounter models on the basis of flight test data.

[65] Hahn (2002), Paper describing the impact of wake vortices on aircraft and the possibility to reduce this impact by means of a suitable control system.

[66] Hahn, Schwarz, and Friehmelt (2004), Paper about the development of a simplified hazard area prediction model.

larger than 1, *Kloidt (2007)*[62] suggests different preview control approaches. The first concept is an anticipatory disturbance rejection, which considers the wake disturbance over a longer time interval. In order to compensate for a roll disturbance exceeding the aircraft's roll control authority, the flight control system already starts to command countervailing roll control deflections before the wake vortex encounter has actually started. It aims to compensate for the average wake-induced rolling moment over a distinct time interval ranging from the current moment to an instant of time in the future. Concerning the length of the time interval *Kloidt (2007)*[62] analyzed different approaches with fixed time spans as well as with variable time spans, for which the optimal length is constantly adapted by a receding horizon strategy. As the upcoming wake vortex disturbance is unknown to the pilot and the flight control commands are thus not comprehensible for him, the pilot's authority is set to zero during this wake vortex flight control mode in order to prevent undesired pilot intervention.

In addition to the direct disturbance compensation, *Kloidt (2007)*[62] also presents two concepts of wake vortex control which comprise the design of the complete aircraft control system including the feedback gains. The first approach is related to *Prokop and Sharp (1995)*[67] and aims at the compensation of the limited bandwidth of the pilot-aircraft system. It stores information about future disturbances in a shift register and includes the stored preview information about the disturbance moments in the linear system of equations which is solved by conventional linear control methods. The resulting controller possesses feedback gains for the states of the aircraft and feedforward gains incorporating the preview information about the disturbance. The second approach for a design of the overall control system in *Kloidt (2007)*[62] is a receding horizon strategy using model predictive preview control. This is a comprehensive linear-quadratic-based model predictive control strategy that also allows for the consideration of nonlinear boundary conditions. A sequential quadratic programming algorithm solves a resulting quadratic programming problem, in which the current preview-vector of the disturbance is included.

A problem that has not particularly been addressed in the work of Kloidt is the question how the relevant information about the wake vortex is extracted from the measurement of the sensor. Kloidt bases the disturbance rejection directly on the wake-induced rolling moment and does not detail how this disturbance moment was derived from the sensor lidar measurements. The early works of Hahn et al.[57,59,60] assume that the sensor would be able to measure the full vector of wind velocities. This assumption does not seem accomplishable for suitable sensors of the near future. The most promising sensor to be used for the remote measurement task is a Doppler lidar sensor. This sensor can, however, usually only detect the velocity component in the direction of the measurement beam, the so-called Line-of-Sight (LoS) direction. For the wake impact alleviation control approach pursued by Hahn et al. the vertical velocity component of the wake vortex with respect to the aircraft trajectory is most relevant. In encounter scenarios with small relative encounter angles between the flight path of the follower aircraft and the wake vortex, this velocity component is nearly completely lost in a LoS measurement. *Hirschberger (2013)*[68]

[67] Prokop and Sharp (1995), Paper presenting a refined approach for the implementation of preview control in discrete time.

[68] Hirschberger (2013), Dissertation about the simulation and analysis of lidar measurements for the determination

studied different concepts to derive the vertical velocity component of a backscatter lidar without using the Doppler effect from the 2D shift of two subsequent measurements. Even though this concept is very promising, Hirschberger states that it is not mature for the application to active flight control yet. Schönhals presents the approach to apply filter fusion technologies for the fusion of wake vortex parameters obtained from a lidar measurement and a prediction model such as the P2P.[69,70] In this case, the author presumes that the output of the lidar sensor directly comprises the circulation and the position of the wake cortex. She does not give any details about the processing steps in which the lidar sensor determines these parameters from the LoS measurements. As the underlying measurement setups in Schönhals' work are always ground-based applications where the lidar measures perpendicular to the vortex centerline, the determination of the wake vortex parameters is much simpler than in the case of an airborne lidar measurement on an aircraft flying behind another aircraft. In the latter case it cannot be assumed that a lidar sensor of the near future will be able to provide the vortex circulation and position as output parameters. An alternative approach, suggested in *Hahn et al. (2010)*[71] and *Fischenberg (2013b)*[72], is to apply a special identification algorithm to derive a wake vortex model from the measured LoS velocities and use this information as a basis for the wake impact alleviation control system. The application of a wake vortex model has the additional advantage that it is not limited to specific measurement locations but can provide information about the flow field at any desired positions. This makes it even more attractive than the direct use of measurements, even if the measurements could provide vertical wind components. The realization and analysis of this combination of a lidar-based wake identification and a wake impact alleviation control system has, however, not been studied in detail before and will be subject of this thesis.

1.3 Objectives of this Thesis

The purpose of this thesis is to contribute to the development of a wake impact alleviation control system. This control system should minimize the influence of a wake vortex disturbance on the aircraft dynamics. It thus reduces the pilots' workload, increases the safety during the encounter, and might represent a possibility to contribute to an improvement of the airspace capacity by allowing reduced separation minima while maintaining at least the same safety standards. The concept to be studied is the idea to combine a wake identification algorithm and wake identification control system. Although the basic approach has already been suggested in *Hahn et al. (2010)*[73] and *Fischenberg (2013b)*[72], its detailed realization, limits and benefits have not been investigated before and represent the objective of the present work. To analyze these

of the wind flow field in front of aircraft.

[69] Schönhals (2015), PhD thesis about the coupling of prediction and detection methods for wake vortices.

[70] Schönhals, Steen, and Hecker (2011), Paper about the application of fusion filter technologies for wake vortex detection and prediction.

[71] Hahn et al. (2010), Paper about the development and analysis of a wake encounter flight control assistance system based on the processing of forward-looking lidar measurements.

[72] Fischenberg (2013b), Patent of an online wake identification algorithm.

[73] Hahn et al. (2010), Paper about the development and analysis of a wake encounter flight control assistance system based on the processing of forward-looking lidar measurements.

issues, the following scientific questions shall be answered in this thesis:

- **How can a lidar-based wake identification algorithm and a wake impact alleviation control system be combined and integrated into the flight control architecture of modern aircraft?**
  The first step for the analysis of the wake impact alleviation system is to investigate how the information of a wake identification algorithm can effectively be used for a wake impact alleviation system. This comprises the integration of the identification module in an online airborne application and the definition of an interface between the wake identification and the impact alleviation controller. Furthermore, the entire wake vortex control system has to be integrated into the flight control architecture of the aircraft. As it can be assumed for modern aircraft that they possess an automatic control system, a sensible way to combine both control systems should be found. It should be investigated how a wake identification and impact alleviation system can be added to the existing control system of the aircraft such that both systems work effectively together and do not interfere unfavorably with each other.

- **What is the realistic potential of a lidar-based wake impact alleviation system to reduce the aircraft reaction during wake vortex encounters?**
  The central question of this thesis is to analyze the overall potential of the wake impact alleviation system based on the combination of lidar-based wake identification and impact alleviation under realistic conditions. For this purpose it shall, on the one hand, be investigated how far the disturbance rejection approach is able to mitigate the wake-induced aircraft response under the assumption that the wake identification can perfectly characterize the disturbance and delivers ideal information about the wake vortex. This analysis provides an insight of the theoretical limits of the control concept and reveals the maximum benefit that could be achieved. On the other hand, the realistic potential of the overall system should be studied by including the wake identification in the alleviation system and analyzing the entire system performance. As the success of the wake identification and thus the potential of the complete alleviation system is strongly dependent on the measurement quality, the performance of the complete system is assessed for different sensor characteristics. The analysis covers various encounter scenarios with different encounter geometries and vortex ages.
  The term “realistic potential”, in this context, expresses that the analysis is based on realistic assumptions and boundary conditions with regard to the sensor capacities, the aircraft dynamics and the flight control system. Due to the complex interdependencies of the different modules, such as the sensor, the wake identification, the wake alleviation control functions, the basic control system, and the aircraft dynamics, a comprehensive analysis of the potential of the alleviation system is only possible using a fully coupled simulation environment covering all these interdependencies as well as a full flight dynamics model including flight control laws. Such a simulation environment is developed during the course of this thesis and is used as a basis for the analysis of the wake impact alleviation system. The analysis can thus be performed on an overall system level and is not limited to an analysis of the separate components.

- **What requirements in terms of sensor characteristics can be derived as a prerequisite for a successful application of the lidar-based wake impact alleviation system?**
  To date airborne Doppler lidar sensors have only been applied in flight tests and are not regularly available on civil aircraft yet. The sensor technology is still under development such that the exact characteristics of these sensors are not yet defined. The sensor system has a large range of design parameters and their influences on the measurement quality and finally on the performance of the alleviation system are very complex and strongly nonlinear. The benefit of the wake identification and impact alleviation system thus strongly depends on the available characteristics of the lidar sensor. The purpose of the analysis in this work is to investigate the influence of the different design parameters of the sensor system and to provide the necessary knowledge to derive sensor requirements that allow a satisfactory wake impact alleviation performance.

1.4 Structure of the Thesis

Chapter 2 and 3 of this thesis provide an overview of the physical background of the wake vortex phenomenon and the Doppler lidar sensor technology. Chapter 2 describes the basic processes of wake vortex formation and evolution and presents different established models, which allow the simulation and analysis of wake vortices. The impact of wake vortices are briefly discussed for different encounter scenarios. Chapter 3 illustrates the measurement principle of Doppler lidar sensors including a brief outline of the different technologies, the basic influences on measurement uncertainty and the state of the art of the application of Doppler lidar sensors for the detection of wake vortices and atmospheric turbulence.

Chapter 4 clarifies the setup of the simulation environment, in which the wake identification and impact alleviation is analyzed, before chapter 5 presents the wake impact alleviation concept itself. This includes a detailed description of the realization of the online wake identification algorithm and the control system functions alleviating the impact of wake vortices as well as the investigation of the interaction between the wake impact alleviation controller and the basic control system and the presentation of an improved combination of both systems.

The application and analysis of the wake impact alleviation system is covered in chapters 6 and 7. Chapter 6 presents the analysis of the performance of the wake impact alleviation controller for the ideal case that the wake vortex disturbance is ideally known. The online wake identification is thus not included in this analysis but assumed to provide a perfect model of the wake vortex. Based on this assumption the theoretically achievable wake impact alleviation is investigated for different encounter scenarios with varying encounter geometry and vortex strength. Furthermore, the influence of the accuracy of the different parameters of the wake vortex model provided by the wake identification is investigated with respect to the alleviation performance. In chapter 7 the realistic performance of the wake impact alleviation system including the online wake identification is analyzed. For this purpose the system is applied with various lidar sensor configurations, in several encounter scenarios and with wake vortices of different vortex ages.

The main findings of the analysis of the wake impact alleviation system are highlighted in special boxes in the text. The overall summary of the present work as well as an outlook on additional aspects that could be part of future investigations are finally presented in chapter 8.

2 Physical Background of Wake Vortices

2.1 Basic Principles of Wake Vortices

Wake vortices inevitably develop whenever an aircraft generates lift. The Kutta-Joukowski lift theorem states that a rotating flow around a wing generates lift. The lift is the result of the pressure difference of the upper (suction) and lower (pressure) side of the wing. Due to the Kutta condition the flow cannot circulate around the sharp trailing edge of a wing. This defines the circulation on the wing. The circulation varies along the wing and has its maximum at the wing root and is zero at the wing tip. Figure 2.1 shows the circulation for an elliptical lift distribution[1]. According to the third Helmholtz vortex theorem, vortex tubes cannot end inside the fluid. They can only end at a solid boundary or form a closed loop. The vortex on the wing, which is also called bound vortex, can consequently not end at the wing tips, but is continued in form of two trailing vortices (also called free vortices) in the wake of the wing, as illustrated in Fig. 2.1. The detached vorticity in the wake rolls up and forms the so-called tip or trailing vortices. The starting vortex (not shown in Fig.2.1) connects the two trailing vortices at a long distance behind the wing such that the vortex tube is closed and fulfills the third Helmholtz vortex theorem. For a steady flight condition the starting vortex can be assumed to be located infinitely far away and be neglected. The bound and the trailing vortex form a horseshoe vortex, which ends at infinity in this case.

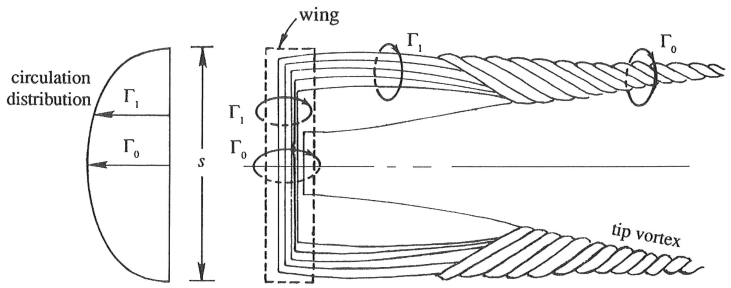

Figure 2.1: Circulation on the wing and in its wake[2]

A simplified but very descriptive explanation for the development of wake vortices is that the pressure difference between the upper and lower surface of the wing provokes a flow around the wing tip, which rolls up in two counter-rotating vortices behind the wing, called wake vortex. For more detailed descriptions of the aerodynamics of the wing and the formation of wake vortices refer to aerodynamic reference books such as *Kundu and Cohen (2008)*[3] or *Schlichting and Truckenbrodt (2001a)/Schlichting and Truckenbrodt (2001b)*[4].

[1] The lift distribution is often assumed to be elliptical. This represents the ideal case, which generates minimum drag and is therefore pursued in the wing design. The assumption of an elliptical lift distribution is usually a valid approximation for the lift distribution of realistic wings.

[2] Kundu and Cohen (2008), p. 696, Reference book of fluid mechanics.

[3] Kundu and Cohen (2008), Reference book of fluid mechanics.

[4] Schlichting and Truckenbrodt (2001a)/Schlichting and Truckenbrodt (2001b), Reference books of aerodynamics of the aircraft, part 1 and 2, publication of first edition in 1959.

The evolution of a wake vortex consists of three main phases: the wake formation, a stable phase and the vortex decay. Figure 2.2 shows these different phases, whereupon the unstable wake zone and the wake breakdown zone form the vortex decay.

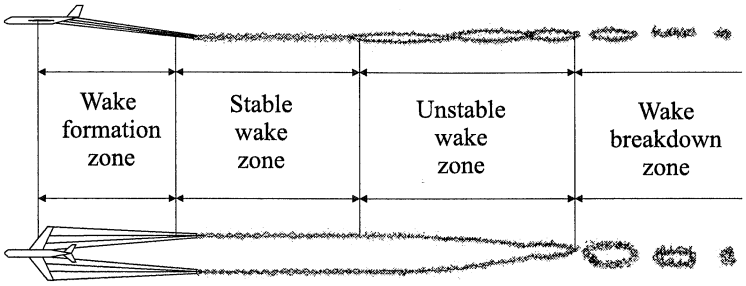

Figure 2.2: Evolution of the wake vortex behind the aircraft[5]

The formation zone is the near-field region behind the wing of the generating aircraft up to the point where the vortices are completely rolled up in a pair of two counter-rotating vortices. This region ranges usually between 15 and 20 wing spans behind the aircraft. After the wake vortex is rolled up, the wake consists of a stable structure of two approximately straight, parallel vortex tubes. The length of this zone depends on the atmospheric conditions and can range up to 150 wing spans. In the far-field region behind the stable zone the wake vortex loses its straight form and starts to decay. The so-called Crow Instability[6] provokes a sinusoidal motion of the vortex centerline in lateral direction, which, under certain atmospheric conditions, ends up in vortex rings, before they breakdown completely. The so-called core bursting represents an unstructured decay process, which is initiated by the collision of two pressure waves inside the wake vortex. After the breakdown no defined wake structure exists anymore and the wake vortex can no longer be distinguished from the surrounding atmospheric turbulence.

Right after the vortex roll-up the circulation of the wake vortex has its largest value. This initial circulation Γ_0 can be approximated for horizontal flight (with the simplification that the total lift L is equal to the weight mg) using the Kutta-Joukovsky lift theorem:

$$\Gamma_0 = \frac{L}{\pi/4 \rho b V} = \frac{mg}{\pi/4 \rho b V}, \tag{2.1}$$

whereupon the factor $\pi/4$ is valid for the assumption for an elliptical lift distribution. The parameters b, ρ, and V represent the wing span of the generator aircraft, the air density, and the airspeed of the generator aircraft respectively.

The typical wind profile for a young wake vortex shortly after roll-up is illustrated in Fig. 2.3. The fine lines describe the induced vertical velocities of the left (dashed line) and the right (fine solid line) vortex. The bold solid line represents the resulting vertical velocity, i.e. the sum of the velocities of the two counter-rotating vortices.

[5] Ginevsky and Zhelannikov (2009), p. 5, Monograph about the modeling of wake vortices behind aircraft.
[6] Crow (1970), Paper describing the instability during the decay process of wake vortices.

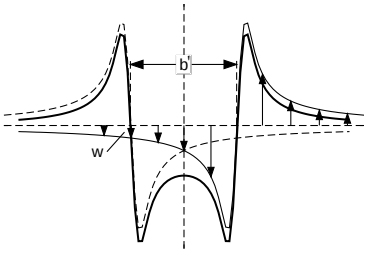

Figure 2.3: Schematic presentation of the vertical velocity profile of a wake vortex pair with the vortex separation b' (based on *Holzäpfel (2005)*[7])

The parameter b' denotes the distance between the two vortex cores, which is often called vortex separation. The corresponding initial value b'_0 right after the vortex formation can, under the assumption of an elliptical lift distribution, be derived from the generator wing span b as follows:

$$b'_0 = \frac{\pi}{4} b. \tag{2.2}$$

The induced vertical velocity provokes a downward motion of the wake vortex because each vortex core affects the induced vertical velocity

$$w = \frac{\Gamma}{2\pi b'} \tag{2.3}$$

at the core of the other vortex. The wake vortex thus descends with the velocity w of equation 2.3. The initial descent speed w_0 is used to define the reference time t_0, often applied to normalize the vortex age in the context of wake evaluation:

$$t_0 = \frac{b'_0}{w_0} = \frac{2\pi (b'_0)^2}{\Gamma_0}. \tag{2.4}$$

For commercial aircraft the typical descent speed lies in the range of 1 to $2\,\mathrm{m/s}$ and the wake vortex can sink up to distances of more than $300\,\mathrm{m}$.[7] Under atmospheric conditions with very stable stratification, however, the wake vortex can also rebound again. Besides the inherent, self-induced downwards motion of the wake vortex with respect to the surrounding air, the wake can also be transported with respect to the earth-fixed reference frame by the wind.

When the wake vortex sinks close to the ground the so-called ground-effect occurs. At an altitude of about $1.5\,b_0$ above ground the two vortices start drifting apart from each other. The divergence results from mutual velocity induction of the vortices due to the vorticity layer (boundary layer), which the vortices induce at the solid ground. At approximately $0.7\,b_0$ secondary vortices develop, which lead to a rebound as well as to an accelerated decay of the wake vortex.[8] The altitude at which secondary vortices are formed also depends on the directions and

[7] Holzäpfel (2005), p. 2, Habilitation treatise about the evolution and prediction of wake vortices.

[8] Holzäpfel and Meiko (2007), Figure 13, Paper about the evolution of wake vortices in ground effect including the analysis of field measurement data of 288 wake vortex pairs at Frankfurt Airport.

strength of crosswinds.[9] Lidar measurements at Munich Airport suggest, however, that these effects can already start at much higher altitudes as well.[10]

2.2 Wake Deformation and Decay

After its roll-up the wake vortex has its strongest circulation. From this point on the wake vortex starts to decay and the circulation decreases continuously. During this decay process the shape of the wake vortex first remains approximately the same (stable zone in Fig. 2.2), whereupon the main change consists of an increase of the core radius and a reduction of the circulation. Later during the decay process the wake vortex also loses its straight form and starts to meander (unstable zone in Fig. 2.2).

The decay of the circulation progresses in two phases. The first phase is the diffusion decay and results from internal diffusion in the wake vortex and a stretching of the secondary vortices. The atmospheric conditions hardly influence the diffusion decay such that this process under all conditions proceeds approximately the same way. The second decay phase is called rapid decay. During this phase the decay is dominated by turbulent friction processes and progresses faster than in the first phase. The point when the rapid decay starts depends on the environmental conditions. The main influence factors on the rapid decay are the temperature stratification and the turbulence in the atmosphere. The stratification is usually described by the normalized Brunt-Väisälaä frequency

$$N^* = \sqrt{\frac{g}{\Theta_0}\frac{d\Theta}{dz}}t_0, \tag{2.5}$$

with g = gravity constant,
Θ = potential temperature,
z = vertical position,
t_0 = reference time, in which the wake vortex sinking distance of the wake vortex corresponds to the initial vortex separation b_0 (cf. equation 2.4).

The turbulence is often specified by the eddy dissipation rate, denoted by EDR or ϵ, which describes the rate at which energy dissipates in the atmosphere. For the characterization of the effects of turbulence on wake vortices, the normalized eddy dissipation rate ϵ^* is often used.

$$\epsilon^* = \frac{(\epsilon b_0')^{\frac{1}{3}}}{w_0} \tag{2.6}$$

[9] Holzäpfel and Meiko (2007), Figure 14, Paper about the evolution of wake vortices in ground effect including the analysis of field measurement data of 288 wake vortex pairs at Frankfurt Airport.

[10] Holzäpfel, Stephan, and Körner (2014), Figure 6, Paper about the evolution of wake vortices during approach and landing and the influence of plate lines on this evolution.

A high stratification and turbulence level lead to an early start of the rapid decay and cause a faster reduction of the vortex circulation. Figure 2.4 shows the effects of different degrees of turbulence and stratification on the decay of the circulation. $\Gamma_{5\text{-}15}$ denotes the average circulation of radii between $5\,\mathrm{m}$ and $15\,\mathrm{m}$ and t^* is the normalized time t/t_0. The two phases of the decay process can clearly be distinguished by the different gradients of the circulation reduction. For combinations of low values of N^* and ϵ^* (i.e. low turbulence and weak stratification) the steep gradient of the rapid decay phase occurs significantly later.

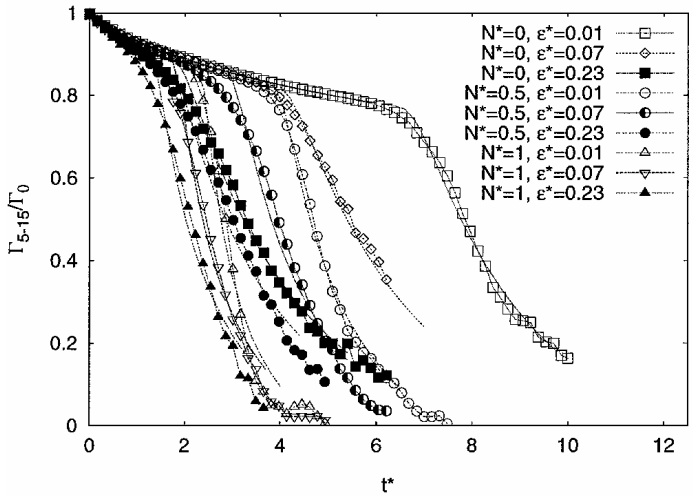

Figure 2.4: Decay of vortex circulation for different degrees of turbulence and stratification[11]

The stratification also influences the sink rate of the wake vortex. A normalized Brunt-Väisälaä frequency of 1 represents, according to *Holzäpfel (2005)*[12], the threshold above which rebounding of wake vortices can occur. In a very stably stratified atmosphere with $N^* = 1.4$ the wake vortex only sinks about one vortex spacing and afterwards rebounds up to the flight level of the generator aircraft again. The circulation has, however, strongly decreased by the time the wake vortex reaches the flight level again.[13] Besides the decline of the circulation another important influence during the vortex aging is the influence of the Crow instability[14] that influences the shape of the wake vortex. Crow investigated the decay process of wake vortices and identified symmetric and asymmetric, stable and unstable, sinusoidal modes. The dominant symmetric instability has a wavelength[15] λ_{Crow} of $8.6\,b_0$ and leads to symmetric, sinusoidal oscillations of the vortex centerlines in lateral direction. With increasing vortex age the amplitude of the two opposing oscillations increases and the two vortex lines can link to vortex rings. The evolution of the Crow instability and the lifespan of the wake vortex strongly depend on the atmospheric turbulence and meteorological conditions.[16]

[11] Holzäpfel (2003), Figure 2, Paper describing the probabilistic two-phase wake vortex decay and transport model developed at DLR.

[12] Holzäpfel (2005), p. 7, Habilitation about the evaluation and prediction of wake vortices.

[13] Holzäpfel (2005), p. 8, Habilitation about the evaluation and prediction of wake vortices.

[14] Crow (1970), Paper describing instability during the decay process of wake vortices.

[15] for a ratio of the core radius and the initial vortex spacing of 0.095, *Hennemann (2010)* (PhD thesis about deformation and decay of wake vortices in a turbulent and stratified atmosphere)

[16] Crow and Bate (1976), Paper about the investigations of the lifetime of wake vortices in turbulent atmosphere.

2.3 Wake Vortex Models

Different approaches of varying complexity exist to model wake vortices. The most complex and realistic way to model wake vortices consists of numerical simulations such as Large Eddy Simulations (LES). These computationally expensive computations can generate very accurate wake vortex flow fields including realistic modeling of the vortex topology and deformation. For fast simulations simpler models of reduced complexity can be used. These models can be divided into two categories: models describing the transport and decay of wake vortices as well as flow field models providing wind velocities induced by the wake vortex.

Examples of 2D wake transport and decay models are the deterministic two-phase model (D2P) and probabilistic two-phase model (P2P) developed at DLR.[17-19] These models predict the wake circulation and position based on the prevailing wind, turbulence, stratification, and ground proximity. The D2P model provides the deterministic solution, whereupon the P2P model also contains probabilistic components and has been adapted to provide the best possible match with LES results and experimental measurements. Alternative real-time models for the prediction of the vortex position and circulation are the model of Sarpkaya[20], which is part of the NASA Aircraft Vortex Spacing System AVOSS, the deterministic and probabilistic wake vortex model (DVM/PVM) of UCL, which is integrated in the simulation environment WAKE4D for the prediction of wake vortex evolution[21], and the TASS Driven Algorithms for Wake Prediction (TDAWP)[22].

For the simulation of wake vortex encounters a series of simple analytical wake vortex models has been developed, which model the two-dimensional wake vortex flow field perpendicular to the wake vortex axes by means of the tangential velocities. This approach allows to model straight wake vortices after roll-up. The vortex age can only be considered by using reduced values for the circulation. The tangential velocities are computed by analytical formulas for the port and starboard vortex and superimposed to provide the resulting flow field of the vortex pair. Commonly used analytical wake vortex flow field models have been developed by Rankine[23],

[17] Holzäpfel (2003), Paper describing the probabilistic two-phase wake vortex decay and transport model developed at DLR.

[18] Holzäpfel (2004), Paper presenting the application and assessment of the probabilistic two-phase wake vortex decay and transport model developed at DLR.

[19] Holzäpfel (2006), Paper about further developments, applications and assessments of the probabilistic two-phase wake vortex decay and transport model developed at DLR.

[20] Sarpkaya (2000), Paper about a wake decay and transport model and its comparison with lidar measurements in Memphis and Dallas-Fort worth Airports.

[21] De Visscher et al. (2010), Paper presenting the 3D model for the prediction of wake vortex transport and decay developed at UCL.

[22] Proctor, Hamilton, and Switzer (2006), Paper about the description of wake transport and decay prediction model TASS Driven Algorithms for Wake Prediction (TDAWP) and its validation with field data.

[23] Gerz, Holzäpfel, and Darracq (2002), Overview paper about the European view on wake vortices of commercial aircraft.

Lamb and Oseen[24], Burnham and Hallock[25] as well as Rosenhead[26], Proctor[27], Winkelmanns[28], and Jacquin[29]. The analytical model that is used in this work is the Burnham-Hallock model. It is identical to the model proposed by Rosenhead. The tangential velocity V_Θ at a given distance r from the vortex core is computed by

$$V_\Theta(r) = \frac{\Gamma}{2\pi} \frac{r}{r_c^2 + r^2}, \tag{2.7}$$

whereupon r_c represents the core radius.

The corresponding formulas of the other models are shown in appendix C. Despite the different analytical equations the resulting wind profile is very similar for all of these models as shown in Fig. 2.5[30]. Only the peak velocities vary slightly for the different analytical models. Good overviews of the different vortex models are provided in *Gerz, Holzäpfel, and Darracq (2002)*[31] and *Luckner (2012)*[32].

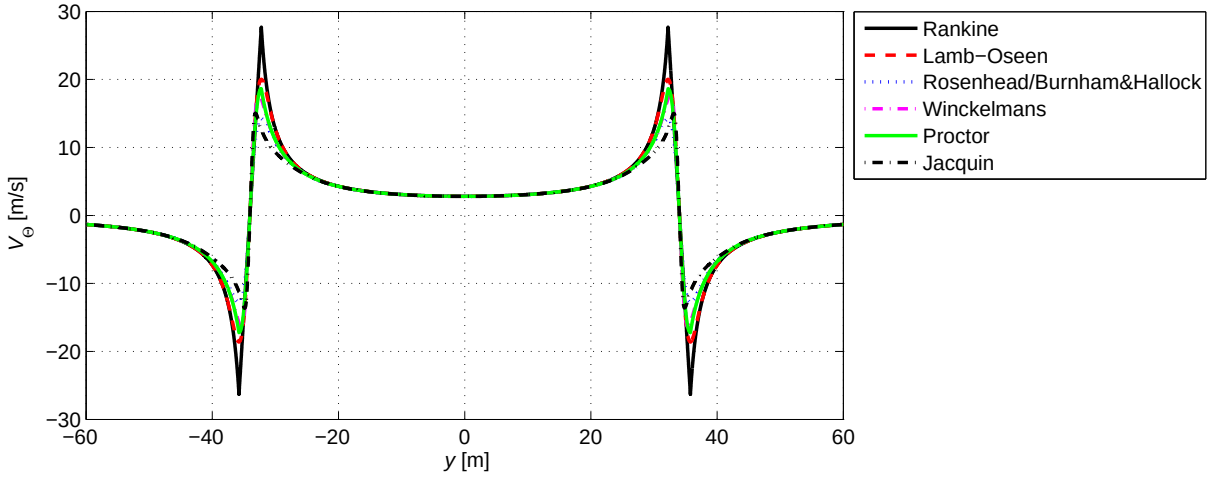

Figure 2.5: Tangential velocities of different analytical wake vortex models, based on *Gerz, Holzäpfel, and Darracq (2002)*[31] and *Luckner (2012)*[32]

[24] Lamb (1932), Reference book about dynamics of liquids and gases.
[25] Burnham and Hallock (1982), Technical report about measurements of the strength and decay of wake vortices at Chicago's O'Hare International Airport.
[26] Rosenhead (1932), Paper about the formation of vortices.
[27] Shen et al. (1999), Paper about 3D LES simulations of wake vortices.
[28] Winckelmans, Thirifay, and Ploumhans (2000), Presentation about parametric wake vortex models and their comparison with CFD studies.
[29] Fabre and Jacquin (2004), Paper about the short-wave cooperative instabilities in vortices of different aircraft.
[30] The wake vortex models are displayed for a core ratio of $r_c = 0.052 b_0$, which results implicitly from the model suggested by Winkelmanns.
[31] Gerz, Holzäpfel, and Darracq (2002), Overview paper about the European view on wake vortices of commercial aircraft.
[32] Luckner (2012), Overview paper about the modeling and simulation of wake vortex encounters.

2.4 Impact of Wake Vortices on Encounter Aircraft

For subsequent aircraft entering into to wake of a preceding aircraft, the wake vortex flow field represents a disturbance that can have serious impacts. The type of the impact depends on the relative flight path of the generator and the encountering aircraft. Figure 2.6 illustrates the main effects depending on the encounter position and angle.

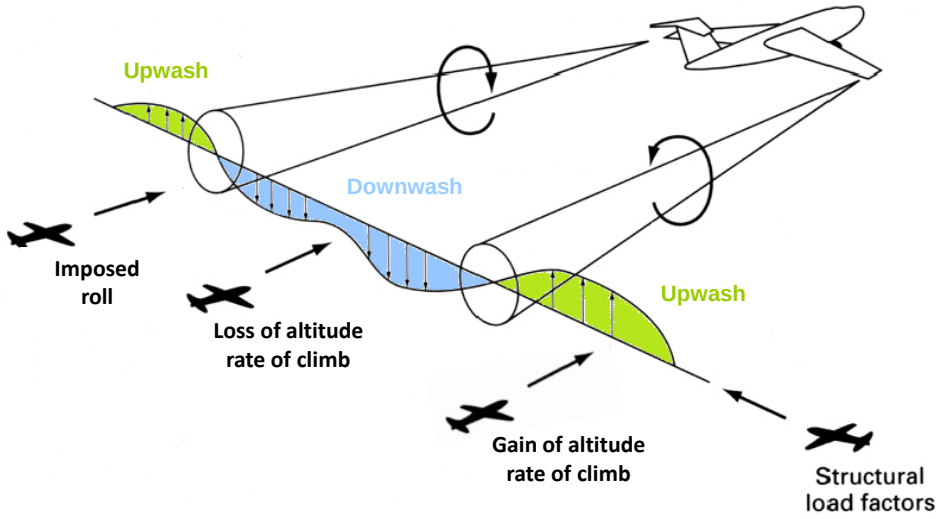

Figure 2.6: Impact of a wake vortex on the encountering aircraft (based on *Rossow et al. (1996)*[33])

If the aircraft flies directly behind the generator aircraft and stays between the two vortex cores, both wings are located in the downwash area of the wake vortex (unless the aircraft is much larger than the generating aircraft) and the aircraft experiences an altitude loss or reduced rate of climb. For an aircraft flying on the right- or left-hand side outside of the wake vortex cores (i.e. with both wings on the same side of the vortex cores), the upwash leads to a gain of altitude rate of climb. This effect can be used in formation flight and allows a horizontal flight with reduced fuel burn. If the rear aircraft flies with a small lateral offset behind the generator aircraft or crosses the wake vortex with a small encounter angle, one wing experiences an upwind whereupon the other wing is exposed to a downwash. The result is an imposed rolling motion of the encountering aircraft. This represents the most common case of wake vortex encounters during approach and departure because the aircraft usually fly closely behind each other with small relative angles between their flight paths in this flight phase. During encounters with very large encounter angles, the encountering aircraft crosses the wake vortex almost perpendicularly such that both wings simultaneously experience a change between upwind and downwash. This poses mainly structural loads on the aircraft. The duration of the encounter is rather short in this scenarios and the disturbance velocities act successively in opposing directions such that no strong flight path deviations occur.

[33] Rossow et al. (1996), Figure 1, Paper presenting measurements of the wake vortices of two 0.03-scale models of a B-747 and a DC-10.

3 Doppler Lidar Sensor

Doppler LIDAR (LIght Detection And Ranging) sensors represent a possible way to measure wind velocities. Their characteristics make them an attractive candidate for remote wind measurements on aircraft. The following sections shall give a brief overview of the main aspects of prevalent lidar technologies. It is, however, not the purpose of this work to go very deeply into the details and realization of the sensing technologies. The lidar sensor is rather considered in a generic way as a mean to provide the required velocity measurement in front of the aircraft. Profound descriptions of the lidar technology can be found e.g. in *Reitebuch (2012)*[1] and *Weitkamp (2005)*[2]. A good overview of airborne remote wind measurement can be found in *Bogue and Jentink (2004)*[3] and a special focus on measurements of turbulence and wake vortices is given in *Vrancken (2016)*[4] and *Wolkensinger (2010)*[5].

3.1 Measurement Principle

Doppler lidar sensors function similarly to RADAR (RAdio Detection And Ranging) sensors but operate at shorter wavelengths. Both sensors emit radiation, which is backscattered from small elements in the atmosphere, and determine the velocity of these elements relative to the sensor by means of the Doppler shift between the emitted and backscattered radiation. Radar sensors operate with electromagnetic radiation in the microwave frequency domain. The frequently used Doppler radar in X-band needs hydrometeors in the air, such as rain droplets or clouds, from which the radiation is reflected. Lidar sensors, in contrast, use a laser (Light Amplification through Stimulated Emission of Radiation) source to emit light of much shorter wavelength from infrared (IR) to ultraviolet (UV) domain. The light is backscattered by much smaller targets in the air such as suspended aerosols or by the air molecules themselves. Different lidar sensor technologies have been developed for the purpose of airflow measurement in the recent years. They vary, for instance, concerning the emission rate, the wavelength of the emitted light, and the applied light scattering. The advantage of using a laser as a light source is that the light has a narrow bandwidth and can be narrowly collimated or focused. The laser light can be emitted in continuous waves or pulses. If the laser has a good coherence, this characteristic can be favorable for the detection of the velocity of molecules and aerosols in the air. The type of laser may vary for different lidar sensors and can be gas (often CO_2), solid state (also including all fiber lasers), or diode lasers. Examples of suitable lasers can be found in table 2 of *Bogue and Jentink (2004)*[6].

The Doppler Effect, as a basis for the measurement of Doppler lidar sensors, describes the fact

[1] Reitebuch (2012), Description of principle of Doppler lidars and their applications for atmospheric measurements.
[2] Weitkamp (2005), Reference book with broad overview over Doppler lidar technology.
[3] Bogue and Jentink (2004), Overview of airborne optical air flow measurement techniques.
[4] Vrancken (2016), Overview of airborne forward-looking lidar measurements of atmospheric turbulence.
[5] Wolkensinger (2010), Comparison of airborne technologies for measurements of atmospheric disturbances.
[6] Bogue and Jentink (2004), p. 38, Overview over airborne optical air flow measurement techniques.

that the frequency of waves is modified if the transmitter and the receiver of the signal move relative to each other such that the length of the path between them is varied. If the source and the observer move towards each other, the frequency is increased (blue shift). A relative motion apart from each other leads to a reduced frequency of the received signal (red shift). As a lidar sensor emits light and detects the reflected light from particles in the air, the frequency shift is doubled in the received signal. The ratio of the frequency shift Δf (between the emitted and backscattered light) and the relative velocity v (i.e. the rate of change of the distance covered by the wave) between the lidar sensor and the particle, the light is backscattered from, is

$$\Delta f = 2f\frac{v}{c} = 2\frac{v}{\lambda}, \tag{3.1}$$

whereupon f and λ describe the frequency and the wavelength of the emitted light and c is the speed of light. The relative velocity thereby only covers the velocity in direction of the sensor measurement axis. This is called the line-of-sight velocity and usually denoted as V_{LoS}. It corresponds to the projection of the velocity vector of the reflecting particle with respect to the lidar sensor onto the measurement axis of the lidar:

$$V_{LoS} = \vec{V}_{wind} \cdot \vec{u}_{LoS}, \tag{3.2}$$

with $\vec{u}_{LoS}$ = unit vector in line-of-sight direction.

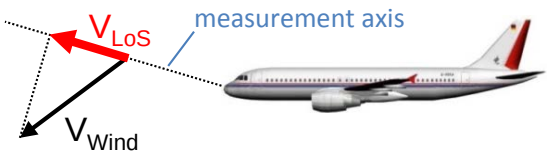

Figure 3.1: Line-of-sight measurement[7]

Along the measurement axis the measurement volume has to be defined, in which the velocity is determined. Different mechanisms can be used to specify the measurement region. Which mechanism can be used depends on the emission mode (continuous-wave or pulsed, cf. section 3.1.2). For short distances focusing and masking represent suitable methods to determine the measurement volume. For longer distances range gating can be used. This is only applicable with pulsed lidars but has the advantage that several measurement volumes can be defined along one measurement axis. A detailed description of the different approaches for the measurement volume definition can be found in section 3.1.2. Depending on the way the measurement volume is determined the backscattered signal from different locations is weighted differently. In a simplified approach the measurement volume is often called measurement point. This simplified expression describes a three-dimensional measurement volume, which is assigned to a

[7] Ehlers and Fezans (2015b), Presentation of a wake impact alleviation control concept based on Doppler lidar measurements and wake identification including first insights of suitable lidar sensor configurations.

single point in space, denoted as measurement point (cf. appendix B).

If the lidar sensor shall determine the wind velocity at different measurement axes, a scan mechanism has to be used. This allows a variation of the direction of the measurement axis and thus provides the possibility to get information about the wind velocities of broader regions. The scan patterns realized by moving the measurement axis can vary depending on the requirements of the measurement task and the ability of the realization of the optical scan mechanism. Possible scan patterns could for instance be:

- subsequent measurements at separated measurement axes (Fig. 3.2a), whereupon each measurement axis is defined by a specific vertical and lateral scan angle,
- measurements around a cone (Fig. 3.2b), whereupon the measurement axis is permanently rotated,
- measurements along a Lissajous pattern (Fig. 3.2c).

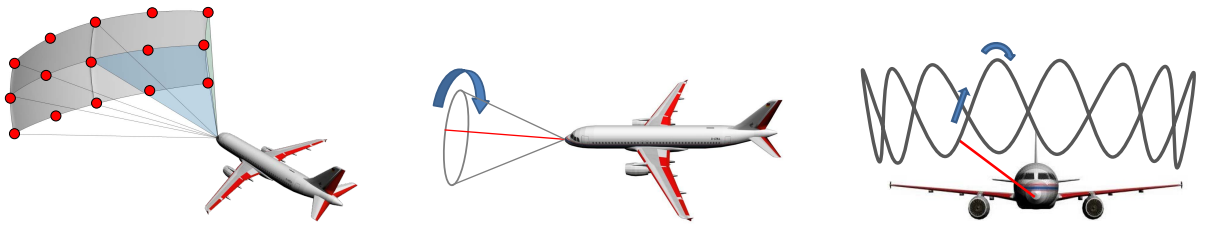

(a) separate measurement axis (b) measurement along cone (c) measurement along Lissajous pattern

Figure 3.2: Different lidar scan patterns

3.1.1 Direct Detection and Coherent Doppler Lidars

Based on the general measurement principle, deploying the Doppler Effect as described above, two main sensor realizations can be distinguished: the coherent Doppler lidar and the direct detection Doppler lidar. The differences of these two lidar technologies are their detection techniques, which use different scattering types. The coherent Doppler lidar uses the so-called Mie scattering. The emitted laser beam is thereby backscattered from aerosols. These are small particles suspended in the air such as e.g. dust, water droplets or ice crystals. Their typical sizes range from $10\,\text{nm}$ to $10\,\mu\text{m}$. The backscattered signal of the aerosols exhibits a narrow spectral line (cf. Fig. 3.3), which allows determining the Doppler shift by mixing the reference laser beam of a local oscillator with the backscattered light (heterodyne measurement). A prerequisite for this detection principle is that the laser light has good coherence characteristics. These sensors usually work in the infrared (IR) wavelength domain due to the favorable backscatter cross-section at longer wavelengths.[8] Typical wavelength are 1.5 - $1.6\,\mu\text{m}$, $2\,\mu\text{m}$ and $10.6\,\mu\text{m}$[9].

[8] The backscatter coefficient of aerosols is approximately proportional to the wavelength.
[9] Vrancken (2016), Overview of airborne forward-looking lidar measurements of atmospheric turbulence.

Direct detection Doppler lidars can also be used with Mie scattering, but in contrast to the coherent measurement they are not limited to conditions in which aerosols are present but can also be applied with light backscattered directly by the molecules of the air, the so-called Rayleigh scattering. The intensity of the Rayleigh scattering depends on the molecule content in the air and the wavelength.[10] The backscatter spectrum is significantly broadened due to the Brownian thermal motion of the molecules (cf. Fig. 3.3). As a consequence, heterodyne measurement based on the coherence property of the laser (as it is used for coherent lidars) is not applicable in this case. Instead interferometry approaches with fringe imaging or double edge techniques can be applied in order to determine the Doppler shift of the backscattered signal. The direct detection Doppler lidars generally require more laser power than coherent lidars and usually operate in the ultraviolet (UV) regime. The Rayleigh backscatter coefficient declines with the laser wavelength to the power of four. So lasers with short wavelength are used. A typical wavelength, used in different realizations[11,12], is for instance 355 nm, the third harmonic of the well-proven Nd:YAG laser.

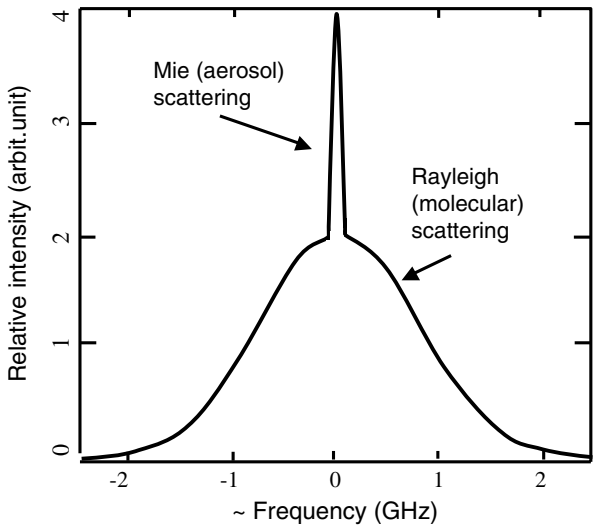

Figure 3.3: Frequency spectrum of Mie and Rayleigh scattering[13]

The higher power consumption represents a drawback of direct detection lidars compared to coherent lidar sensors. The great advantage of the direct detection measurement is, however, the fact that they are not dependent on aerosols in the air. Close to the ground the aerosol density is usually high such that an aerosol-based measurement with coherent lidars also delivers a good measurement quality. With increasing altitude, in particular above the boundary layer, the aerosol concentration decreases significantly though, as shown in Fig. 3.4. This effect is

[10] The backscatter coefficient of molecules is proportional to the wavelength to the reciprocal of the wavelength approximately to the power of 4: $\lambda^{\frac{1}{4}}$.

[11] Rabadan et al. (2010), Paper about forward-looking lidar measurements for clear turbulence detection and alleviation.

[12] Cézard et al. (2009), Paper about lidar systems for airflow measurements including comparison of Rayleigh and Mie scattering.

[13] Rabadan et al. (2010), Figure 4, Paper about forward-looking lidar measurements for clear turbulence detection and alleviation.

even more distinct in some geographical regions such as the tropical pacific. Specific atmospheric conditions such as rainfalls, which wash out the particles in the air, can also reduce the aerosol density. Further details on the distribution of aerosols in the atmosphere can be found in *Petzhold and Kärcher (2012)*[14]. The concentration is thus often too low to allow a successful coherent measurement. In order get a reliable velocity measurement in all flight conditions a direct detection Doppler lidar is therefore considered as the preferable sensor technology for airborne wind sensing of wake vortices. The combined application of Mie and Rayleigh scattering is favorable because this joins the advantages of both scattering types. In low altitudes or in clouds, when enough aerosols are present, the good signal-to-noise ratio of the Mie scattering can be exploited and in regions with low aerosol density such as clear air and high altitudes the Rayleigh scattering of the molecules can be used.

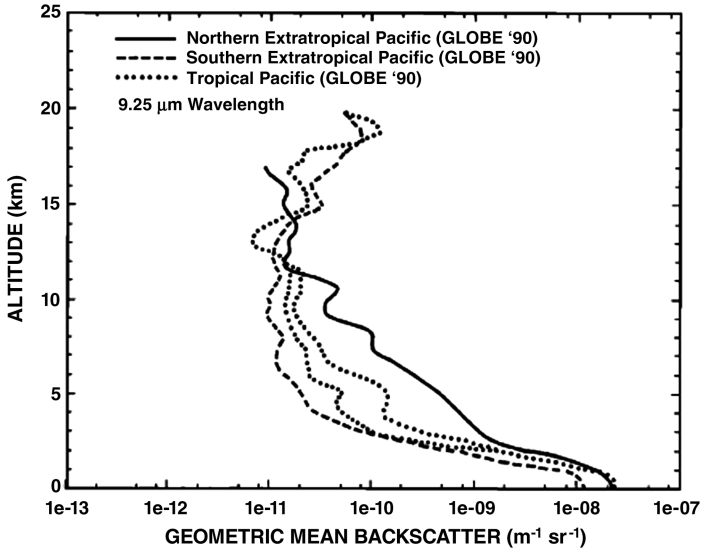

Figure 3.4: Variation of aerosol density with altitude in different geographic regions[15]

3.1.2 Emission and Focusing Methods

Besides the detection method another general difference between different lidar sensor technologies is the emission of the laser beam. It can be distinguished between Continous-Wave (CW) and pulsed lidars. CW lidars continously emit the laser light. It provides a very good accuracy of the velocity measurement and has the benefit of reduced complexity and costs.[16] A drawback is the fact that no information about the measurement distance is available. Due to the constant laser beam it is no possible to measure the transit time between the emitted

[14] Petzhold and Kärcher (2012), Overview of atmospheric aerosols including basic definitions, properties and spatial distribution in atmosphere.

[15] Menzies and Tratt (1997), Figure 5, Results of NASA Global Backscatter Experiment (GLOBE) airborne field campaigns in 1989 and 1990 with measurements of tropospheric and lower stratospheric aerosol backscatter.

[16] Harris et al. (2002), Paper presenting ground-based vortex measurements with coherent lidar sensors including results of campaigns of DLR, Onera and QinetiQ and the potential for on-board detection and reduced-scale studies.

and received laser signal. This can be overcome by focusing as mentioned in *Hill and Harris (2010)*[17] and *Bogue and Jentink (2004)*[18], which effect that the received signal mainly consists of the backscatter of a volume at a specified distance. These focusing techniques are, however, limited to rather short-range applications. For airborne applications with typical practical lens diameter of approximately $10\,\text{cm}$ the usage of focusing is limited to short range applications with measurement ranges below about $150\,\text{m}$.[18] If only very short measurement ranges of less than $20\,\text{m}$ are considered, masking represents another alternative to define the measurement volume. It only works for sensors where the receiver is positioned separately from the light source and considers the measurement region from a different axis. The overlapping of the field of view of the receiver and the illuminated volume define the measurement region in this case. For ground-based applications the distance information of the measurement can also be derived by means of triangulation methods.[19] CW lidar sensors are usually used for short range measurements and are thanks to their good velocity resolution well suited for wake characterization.

Pulsed lidars emit short laser pulses with durations in the order of a few tens of nanoseconds. This lidar technology allows precise range resolution of the measurement by means of range gating techniques. The measurement distance can be defined by capturing the emitted laser signal after the time period the emitted pulse needs to travel to the desired measurement region and back. The minimum range resolution is thereby limited by the pulse length and the needed SNR in one range gate. By considering separate time segments of the emitted pulse, the wind velocity can be measured at several range gates (i.e. bins) along the measurement axis with the same transmitted laser pulse. A further advantage is the possibility to realize long measurement ranges.[20] A disadvantage is the lower velocity resolution resulting from a broadened spectrum in case of very short pulses.[16]

Theoretically, both emissions methods, continuous-wave and pulsed, could be realized as coherent as well as in the form of direct detection lidars. In practice, however, CW lidars are usually realized as coherent lidars whereas pulsed emission is used with both coherent and direct detection lidars. A comparison of a ground-based application of wake vortex measurements with a CW and a pulsed laser can be found in *Köpp et al. (2005)*[21].

3.2 Measurement Uncertainty

The velocity measurement provided by any kind of sensor generally only represents an approximation of the exact velocity. It always contains some degree of measurement uncertainty, such that the result of the measurement deviates from the exact value of the parameter to be mea-

[17] Hill and Harris (2010), Detailed description of Doppler lidar measurement principle with main focus on CW lidars and short discussion of pulsed lidar sensors.
[18] Bogue and Jentink (2004), p. 22, Overview of airborne optical air flow measurement techniques.
[19] Köpp et al. (2003), Paper about multiple-lidar triangulation approach for wake vortex characterization purposes.
[20] Bogue and Jentink (2004), p. 21, Overview of airborne optical air flow measurement techniques.
[21] Köpp et al. (2005), Comparison of the DLR pulsed and Onera/QinetiQ CW lidar for wake measurement in field trials at Tarbes airfield.

sured. According to *Taylor and Kuyatt (1994)*[22] measurement uncertainties can be grouped into the "component of uncertainty arising from a random effect" and the "component of uncertainty arising from a systematic effect". It is suggested in *Taylor and Kuyatt (1994)*[22] to express each component of uncertainty by an estimated standard deviation. The standard deviation σ of the measurement in general increases if the Signal-to-Noise Ratio (SNR) decreases, whereupon the SNR depends on the characteristics of the detector in the case of a lidar measurement. This general trend of increasing standard deviation with decreasing SNR is, however, limited by a lower bound resulting from the detector resolution. The detector resolution induces a measurement error which cannot be compensated even if the measurement signal is further increased (cf. lower bound of standard deviation in the lidar model in section 4.3). The exact relationship of the standard deviation and the SNR depends on the algorithm applied to post-process the backscattered laser signal. The work in this thesis uses a generic approach. It is based on the assumption of a reciprocally proportional relationship, as it is suggested by empirical investigations of lidar sensors such as the sensor presented in *Herbst and Vrancken (2016)*[23], with a dependency of the standard deviation of the measurement signal on the signal-to-noise ratio according to

$$\sigma \sim \frac{1}{\mathrm{SNR}}, \tag{3.3}$$

with SNR = S/N, whereupon S is the signal, i.e. the collected energy or number of photons per pulse per range gate, and N is the noise level of the detector. Assuming a Poisson distribution for the collected photons, the noise N is the square root of the signal

$$N = \sqrt{S}. \tag{3.4}$$

Combining equation 3.3 and 3.4 provides

$$\sigma \sim \frac{1}{\sqrt{S}}. \tag{3.5}$$

Besides the standard deviation the measurement result can also exhibit a constant offset with respect to the true velocity. This can be represented by indicating a mean value for the uncertainty. Systematic uncertainties can, for instance, result from an error in the alignment of the laser beam, from uncertainties in the laser frequency or in the time delays in the processing chain, or from the design of the detector itself. If the sensor system is well designed these uncertainties can be assumed to be small compared to uncertainties due to random effects. In many cases they can also be compensated via calibration. The random or statistic uncertainties thus play the more important role in the context of Doppler lidar sensors. They can result from various sources and their quantification is strongly dependent on the exact sensor type and configuration. Some examples and trends of relevant effects concerning the random uncertainties are given in the following.

[22] Taylor and Kuyatt (1994), NIST technical note with guidelines for the determination and description of measurement uncertainties.

[23] Herbst and Vrancken (2016), Paper presenting a concept for the design of a monolithic Michelson interferometer for an airborne, UV, direct-detection Doppler wind lidar receiver.

One of the most important influences on the measurement uncertainty is the density of aerosols and molecules in the air, which declines significantly with altitude. How strong the influence of this density is depends on the sensor type, i.e. whether direct direction or coherent measurement is applied. But in both cases the signal-to-noise ratio decreases with lower aerosol and molecule density because the backscatter is reduced. Further atmospheric conditions that influence the measurement quality are the temperature, clouds and sunlight. A higher temperature provokes a broadening of the molecular backscatter and this increases the uncertainty. Clouds have, on the one hand, the beneficial effect that they increase the backscatter. On the other hand, the extinction is very large in clouds and scattering into other directions than the measurement direction provokes a mitigation of the energy of the laser light, which, in turn, reduces the SNR. Sunlight can deteriorate the measurement accuracy because the sensor does not only receive backscattered light from the measurement volume but additional light either directly from the sun or scattered sunlight from the atmosphere. It could be shown in flight tests[24] that the influence of sunlight can be nearly completely precluded by appropriate daylight filters and gating of the detector sensitivity. However, in particular cases, e.g. with low signals, sun noise can be critical. For applications with very large measurement ranges sun noise is the most important uncertainty source.

Besides these atmospheric influences, the characteristics of the sensor also influence the uncertainty of the measurement. A long measurement distance increases the measurement uncertainty because less backscatter reaches the receiver. The signal reduction is approximately proportional to the square root of the range

$$S \sim \frac{1}{\text{range}^2}. \tag{3.6}$$

Considering equation 3.5 this delivers approximately a linear dependency of the standard deviation of the measurement on the measurement range

$$\sigma \sim \text{range}. \tag{3.7}$$

In reality the uncertainty increases slightly stronger than linearly with increasing range due to extinction in the atmosphere. This can, however, be neglected as a first approximation.

All variations of lidar parameters that influence the signal of the received photons proportionally provoke a square-root-dependent change of the standard deviation of the measured line-of-sight velocity. If the dimensions of the measurement volumes are increased, for instance, the received signal is increased because in the larger measurement domain more particles backscatter the light. If a cylindrical measurement volume is assumed an increase of the length of the measurement volume (i.e. an increased blur depth, cf. appendix B) reduces the uncertainty approximately according to

$$\sigma \sim \frac{1}{\sqrt{\text{blur depth}}} \quad \text{because } S \sim \text{blur depth}. \tag{3.8}$$

[24] Rabadan et al. (2010), Paper about forward-looking lidar measurements for clear turbulence detection and alleviation.

For very inhomogeneous flow fields, such as wake vortices for instance, the possible increase of the measurement volume is limited, however, because the information of local velocity differences is lost as the measurement result represents the average velocity of the whole measurement volume. Hence, a larger blur depth induces a loss of spatial resolution.

An obvious mean to reduce the measurement uncertainty is to increase the signal by an increase of laser power. This directly raises the energy in the emitted laser light and thus in the backscattered signal .

$$S \sim \text{laser power} \quad \rightarrow \quad \sigma \sim \frac{1}{\sqrt{\text{laser power}}} \tag{3.9}$$

A similar effect can be achieved by improving the sensitivity of the receiver, i.e. the detector. This increases the number of generated photo-electrons and thus improves the measured signal.

$$S \sim \text{receiver sensitivity} \quad \rightarrow \quad \sigma \sim \frac{1}{\sqrt{\text{receiver sensitivity}}} \tag{3.10}$$

The measurement result provided by a pulsed lidar usually contains backscattered signals of several pulses that are combined in a post-processing step in order to reduce the uncertainty by means of averaging. If the application demands a higher update rate, the signals of fewer pulses can be averaged such that the uncertainty increases. An increase in update rate[25], while maintaining the same average laser power, raises the standard deviation approximately according to

$$\sigma \sim \frac{1}{\text{number of averaged pulses}} \quad \rightarrow \quad \sigma \sim \text{update rate}. \tag{3.11}$$

If several range gates along one measurement axis are considered the effect of the uncertainty depends on the way the signal is detected. If each range gate requires a separate receiver, the energy of the emitted signal is split between the backscattered signals of the different range gates. That means the energy per range gate is lower and the uncertainty thus higher. The standard deviation increases approximately according to

$$\sigma \sim \sqrt{\text{number of range gates}}. \tag{3.12}$$

More advanced technologies allow a simultaneous detection of all range gates along one measurement axis with the same receiver. In this case the number of range gates does not influence the measurement uncertainty.

The presented influences on the standard deviation of the lidar measurement only represent a very simplified approach of describing the influences on the measurement uncertainty. In reality the system is much more complex and numerous additional aspects influences the measurement uncertainty such as, for instance, the resolution and saturation of the detector, the analysis of the interferences, or diffraction in the optics. As the detailed dependencies of these influences are, however, not relevant for the analysis in this thesis, they are not further discussed here.

[25] The term update update rate, in this case, refers to the update rate of a single measurement axis.

3.3 State of the Art of Doppler-lidar-based Wake Vortex and Turbulence Detection

In the past good progress could be achieved in the developments of Doppler lidar technology and sensors have been developed for many different applications. Various applications exist for different types of wind measurement in aviation such as the determination of the true airspeed of aircraft[26] and helicopters [27] or the detection of atmospheric winds, but also in other domains outside aviation such as for instance wind measurements at wind turbines[28,29]. In the following some examples for lidar sensors will be given, which were applied for wake vortex and turbulence detection.

In different field experiments lidar sensors have been established in ground-based applications for wake detection and monitoring purposes close to airports. At Tarbes airfield pulsed and continuous-wave Doppler lidar sensors have been applied during the EU project C-Wake for the detection and characterization of wake vortices of large transport aircraft[30] The pulsed lidar was a $2\,\mu$m pulsed Doppler lidar from DLR. It is based on a Tm:LuAG laser and has a measurement range 500 - 1100 m. Details on the laser parameters can be found in *Köpp et al. (2005)*[21] and *Harris et al. (2002)*[16]. The CW lidar systems of Onera and QinetiQ were $10\,\mu$m continuous-wave Doppler lidar sensors, which are based on CO_2 laser sources and described in detail in *Harris et al. (2002)*[16]. Both sensors are coherent lidar systems. At Toulouse airport ground-based axial detection of wake vortices was carried out with a $2\,\mu$m coherent pulsed Doppler lidar in March 2000 during the EU project MFLAME (Multifunction Future Laser Atmospheric Measuring Equipment).[31] The sensor was placed under the glide slope and measured the wake vortices of approaching aircraft in axial direction. It had a two dimensional sinusoidal scanner and measurement ranges between 400 m and 2 km. 20 range gates with a length of 75 m are considered for the estimation of the mean radial velocity. Onera developed a 1.5 μm pulsed fiber lidar. It was applied during the EU project CREDOS (Crosswind - Reduced Separations for Departure Operations) at Frankfurt airport field in February and March 2007 for ground-based lateral wake vortex measurements of departing aircraft. The lidar during that field experiment was equipped with a 50 μJ/15 Hz MOPA (Master Oscillator Power Amplified) laser source and had a measurement range of 400 m.[32]

[26] Spuler et al. (2011), Paper about NCAR's development of an air motion sensor for their Gulfstream GV research aircraft.

[27] Matayoshi, Asaka, and Okuno (2007), JAXA's flight test for a lidar based true airspeed measurements of a helicopter.

[28] Schlipf (2013), Description of a concept for wind turbine control based on lidar measurements.

[29] Hill and Harris (2010), Detailed description of Doppler lidar measurement principle with main focus on CW lidars and short discussion of pulsed lidar sensors.

[30] Köpp, Rahm, and Smalikho (2004), Results of characterization of wake vortices of large transport aircraft based on lidar measurements with DLR $2\,\mu$m pulsed lidar at Tarbes airfield.

[31] Keane et al. (2002), Paper about ground-based axial wake vortex detection at Toulouse airport in March 2000 including sample results of Airbus A340- and Airbus A320-generated wake vortices.

[32] Dolfi-Bouteyre et al. (2009), Paper about $1.5\,\mu$m fiber laser developed by Onera and several applications of this lidar with different laser sources.

Airborne applications of lidar measurements represent a special challenge because the sensor system has to fulfill additional constraints such as e.g. weight restrictions and because the dynamics of the aircraft during the flight make the measurements more difficult. Furthermore, the particle density is lower at higher altitudes than close to the ground, which reduces the signal-to-noise ratio of the measurement. No standardized lidar sensor for onboard wake vortex measurements exists to date, but a few lidar systems have been developed and applied for test purposes. During the European AWIATOR (Aicraft Wing with Advaned Technology OpeRation) project the DLR $2\,\mu$m lidar, which had already been used for the ground-based wake vortex monitoring at Tarbes airfield, was mounted on the DLR research aircraft Falcon 20 for vertical wake vortex measurements.[33] The wake generating aircraft was the DLR research aircraft ATTAS. A Falcon 20 flew at a certain distance above the generator aircraft and measured the wake vortex of the ATTAS with a downward-looking lidar sensor.

If the lidar measurements shall be used for the flight control of the encounter aircraft, either to warn the pilot to fly the aircraft around the disturbance or to use automatic flight control assistance to alleviate the flight through the disturbance a forward-looking measurement is required. During the EU project I-Wake airborne axial wake measurements have been performed with a coherent pulsed lidar with measurement ranges up to $2360\,$m. The light source of the sensor was a $2\,\mu$m diode-pumped Tm:LuAG laser.[34] The lidar system was installed on the NLR Citation II aircraft. One of the windows on the side of the aircraft were modified with a special protruding fairing such that the lidar could measure in forward direction with a small angle offset of $9°$ to the right-hand side and downwards from the body-fixed longitudinal axis of the aircraft. Onera developed a fiber lidar for airborne axial wake vortex measurements. For this purpose, the $1.5\,\mu$m fiber lidar of Onera was applied with a $120\,\mu$J/ $12\,$KHz MOPA laser. The sensor was successfully tested during ground-based measurements at Orly airport, where wake vortices were detected up to $1.2\,$km range. Airborne tests have not been conducted so far. JAXA developed and tested different lidar systems for long-range airborne wind measurements with the purpose to generate early warnings of atmospheric disturbances. The lidar systems consist of an all fiber $1.5\,\mu$m pulsed lidar, which was combined with different laser sources. The first prototype had a measurement range of $1\,$NM.[35] By increasing the laser output the measurement range was extended to $3\,$NM.[36] This sensor was flight-tested with the JAXA Beechcraft Model 65 research aircraft. The airspeed could be measured with very low standard deviations of $0.63\,$m/s at ranges of $450\,$m - $600\,$m and $0.7\,$m/s at ranges of $900\,$m - $1050\,$m. A further increase of the laser power enabled a further extension of the measurement range to $9\,$NM. This lidar sensor was tested in flight test with a Gulfstream II at high altitudes[37] and allowed the successfully

[33] Rahm, Smalikho, and Köpp (2007), Paper about flight tests with vertical wake vortex measurements with the DLR lidar during the AWIATOR project.

[34] Douxchamps et al. (2008), Paper presenting results of airborne lidar measurements of wake vortices in axial direction.

[35] Kameyama et al. (2007), Paper about the development of a $1.5\,\mu$m all-fiber pulsed coherent Doppler lidar system.

[36] Inokuchi, Tanaka, and Ando (2008), Development and flight tests of the $1.5\,\mu$m all-fiber coherent lidar of JAXA.

[37] Inokuchi, Tanaka, and Ando (2010), Paper about the development and flight tests of the JAXA 1.5 μm lidar with 5 NM range.

detection of clear air turbulence[38]. Further flight tests for clear air turbulence measurements with a long-range forward looking lidar have been performed during the EU project DELICAT (DEmonstration of LIdar based Clear Air Turbulence detection)[39,40]. The lidar sensor was a pulsed UV lidar based on a Nd:YAG laser and had a range of 15 km. The measurement principle was different here, as it was not the line-of-side velocity that was measured in this case but the density fluctuations, which are associated with the vertical movements of turbulent air masses.

Flight tests with lidar measurements for the purpose to provide input for an automatic turbulence control system have been performed during the AWIATOR project.[41] The main focus was on clear air turbulence. The sensor war a direct-detection Rayleigh/Mie UV lidar with a measurement range of 50 m and four measurement directions, which were updated with 60 Hz. The lidar was installed on an Airbus A340-300 aircraft and measured the airspeed at a cruise altitude at 39000 ft in four measurement directions in a rectangular measurement pattern. Measurements were successful under different atmospheric conditions including clear air, clouds, rain and ice. Standard deviations of 1 - 1. 5 m/s could be achieved for the line-of-sight velocity. Figure 3.5 exemplary illustrates lidar measurements in the four measurement directions, which were obtained during these AWIATOR flight text campaign. The figure demonstrates the promising potential of the lidar measurements since the measurements adequately reproduce the true airspeed. The four measurement directions were used to reconstruct the full velocity vector of the airspeed.

Based on the developments and results of the AWIATOR project, the project Green-Wake (Demonstration of lidar based Wake Vortex Detection System incorporating an Atmospheric Hazard Map) had the objective to develop a lidar system for the particular purpose of airborne wake vortex detection and the mitigation of wake vortex effects on aircraft by specific control systems. The requirements that were defined in the project for such a lidar sensor are summarized in table 3.1. The measurement locations are assumed to be located along a Lissajous pattern.

[38] Inokuchi, Furuta, and Inagaki (2014), Airborne CAT detection with the JAXA 1.5 μm lidar with 5 NM range.
[39] Vrancken et al. (2010), Report about the development of a long-range lidar for airborne clear air turbulence detection in the DELICAT project.
[40] Veermann, Vrancken, and Lombard (2014), Paper about the flight test campaign for lidar-based clear air turbulence detection in the DELICAT project.
[41] Rabadan et al. (2010), Paper about forward-looking lidar measurements for clear turbulence detection and alleviation.
[42] Rabadan et al. (2010), Figure 17, Paper about forward-looking lidar measurements for clear turbulence detection and alleviation.
[43] Rees (2014), p. 13, Presentation of the results of the Green-Wake project.

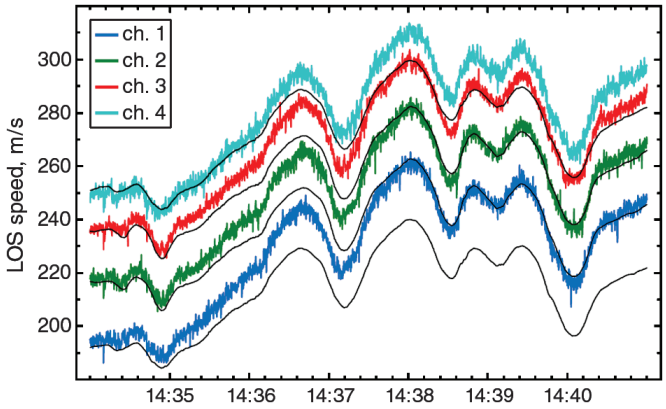

Figure 3.5: Exemplary lidar measurements during AWIATOR flight test campaign (noise curves: lidar measurements in four LoS directions, shifted upwards by 20m/s for better visibility; smooth curves: aircraft reference speeds in the same LoS directions, also shifted by 20m/s, before optical aberration compensation)[42]

Table 3.1: Required system parameters for lidar sensor specified in the Green-Wake project[43]

Parameter	**Value**
minimum range	50 m
maximum range	200 m
minimum number of measurement points	100
scanning area	120 m x 50 m
range resolution	2 range gates
full field-of-view update rate	2. 5 Hz
required LoS velocity accuracy in a single integration	1 m/s
operating altitude (max)	flight level 400
maximum atmospheric density	all conditions
range of velocities	+/-25 m/s
receiver optics	200 mm

4 Simulation Environment

This chapter provides an overview of the simulation framework for the analysis of the wake impact alleviation system. The alleviation performance of this system is evaluated during simulated wake vortex encounters. The underlying simulation setup comprises models of the wake vortex, the encountering aircraft, and the lidar sensors. These modules as well as the definition of the encounter scenarios will be described in detail in the following sections. Furthermore, a short discussion about a suitable assessment metrics for the evaluation of the alleviation performance is provided at the end of this chapter.

4.1 Model of Encountering Aircraft

4.1.1 Dynamic Aircraft Model

The dynamic aircraft model of the encountering A320 aircraft is a 6-DoF model of the DLR research aircraft ATRA (Advanced Technologies Research Aircraft), which has been developed at the DLR Institute of Flight Systems during the last years. The aircraft model is based on the nonlinear equations of motion for a rigid body and includes a landing gear model, a propulsion model of the IAE V2500 engines, an aerodynamic model, sensor and actuator models as well as an automatic flight control system. The model has been validated with flight test data from the ATRA and can be considered to provide acceptable accuracy for scientific purposes.[1]

The aerodynamic model is realized as a derivative model with stability and control derivatives, derived from available simulator data and handbook formula and identified on the basis of flight test data. Nonlinear corrections, in terms of the Prandtl-Glauert-factor, are included in order to account for dynamic pressure and Mach number effects. Furthermore, the aerodynamic model involves a nonlinear stall model and a ground effect model. Details about the aerodynamic model can be found in *Raab (2010a)*[2]. The actuators of the control surfaces are modeled as simple second order systems with time delays. The sensor models comprise an air data system with pressure and temperature sensors, wind vanes, etc., an inertial reference system and navigation sensors such as ILS, DME and VOR, as well as a radio altimeter. The engine model is realized as a nonlinear first order system, whereupon the data for the stationary behavior such as thrust, pressure ratios and rotational speeds are based on datasets of the PEP (Performance Engineers Programs) software packages.

The flight control system of the ATRA simulation model includes an autopilot as well as manual control laws. The control system is designed according to the Airbus flight control system philosophy and includes the corresponding A320 flight modes and logics. For the wake encounter simulations in this thesis, the autopilot is always disengaged and only the manual control laws

[1] Raab (2012), DLR institute report about the validation of ATRA flight dynamics simulation model with flight test data.

[2] Raab (2010a), DLR institute report describing the aerodynamic model of the ATRA flight dynamics simulation model.

are used. The manual control system in the ATRA simulation model contains a direct, alternate and normal law. However, only the normal law, which represents the regular control mode in manual flight, is used during the simulations in this thesis. The applied normal law is not the original Airbus normal law, but should behave very similarly and can be considered as a representative manual control system. In the pitch axis, the control system uses a load factor command system with a control law structure according to *Favre (1994)*[3]. The roll control loop is a roll rate command / bank angle hold system and a sideslip angle command is used in the yaw axis, whereupon the sideslip angle is estimated on the basis of the lateral acceleration measurements. The design of the lateral control system, consisting of the roll and yaw control loops, comprises a decoupling of the roll and yaw motion in presence of external disturbances according to *Farineau (1989)*[4].

4.1.2 Aerodynamic Interaction Model

The basic aerodynamic model of the ATRA can only cover homogenous flow fields. In order to model the effects of inhomogeneous flow fields such as wake vortices on the aircraft dynamics additional models are required. In the present thesis, this is an Aerodynamic Interaction Model (AIM), which uses the so-called strip method. This strip model is based on lifting line theory and calculates the induced delta forces and moments resulting from wake vortex disturbance velocities. The different components of the aircraft are divided into strips as illustrated in Fig. 4.1.

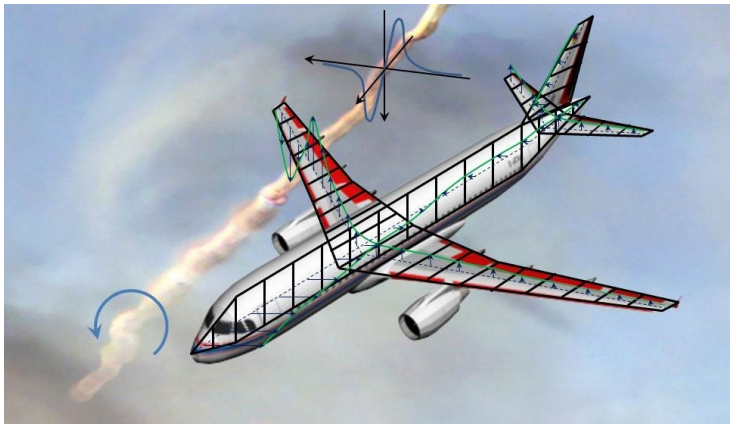

Figure 4.1: Strip model of Aerodynamic Interaction Model (AIM)[5]

For each strip the additional lift (for the wing and horizontal tail) or side force (for the fuselage and vertical tail) resulting from the wake-induced angles of attack and sideslip is computed and summed up with an elliptical weighting along the wings to form the overall wake-induced forces. A multiplication of the induced forces of each strip with the corresponding lever arms delivers the wake-induced moments. A simple stall model is included in the AIM that limits

[3] Favre (1994), Paper giving an overview of the characteristics of the Airbus fly-by-wire control laws.
[4] Farineau (1989), Paper about the Eigen structure assignment technique for lateral flight control laws of civil aircraft.
[5] Vechtel (2016), Paper about the analysis of wake vortex encounters with straight and deformed wake vortices.

the maximum and minimum values of the angles of attack and sideslip. Drag changes due to the local vortex flow velocities are not modeled in the AIM such that the applied AIM covers the wake effects in five degrees of freedom and does not include a wake-induced x-force. The wake-induced delta forces and moments determined by the AIM are added to the forces and moments of the basic aerodynamic model and fed into the equations of motion of the dynamic aircraft model. Further details about the AIM and its validation with flight test data can be found in *Fischenberg (2010)*[6] and *Jategaonkar, Fischenberg, and Gruenhagen, v. (2004)*[7].

4.2 Wake Vortex Model

A wake vortex represents a complex, inhomogeneous wind field, which can be modeled by different approaches, as shown in section 2.3. For the analyses in this thesis an analytical wake vortex model as well as LES wake vortices will be considered. In both cases the generator aircraft is an Airbus A340-300 with a mass of $190\,\mathrm{t}$ and a wing span of $60.3\,\mathrm{m}$. The applied analytical wake vortex model is the Burnham-Hallock model (cf. equation 2.7). The decay of the wake vortex is, in this case, only modeled by the reduction of the vortex circulation, which is set to $70\,\%$ of the initial circulation in the present case. This corresponds to a vortex age of approximately $80\,\mathrm{s}$ for an atmosphere with moderate turbulence and neutral thermal stratification ($N^* = 0$, $\epsilon^* = 0.23$) and a distance of approximately $3\,\mathrm{NM}$ between the generator and follower aircraft for an approach speed of the generator of $70\,\mathrm{m/s}$.[8] These conditions can, according to *Frech et al. (2007)*[9], be considered as realistic atmospheric conditions for the lower layer of the atmosphere. In a worst case scenario (i.e. atmospheric conditions without turbulence and neutral stratification, $N^* = 0$, $\epsilon^* = 0.01$, leading to the slowest possible decay) this would correspond to a vortex age of about $200\,\mathrm{s}$ and $7.6\,\mathrm{NM}$ separation distance. The core radius of the Burnham-Hallock wake vortex is set to $0.035 \cdot b_0$ (with an initial vortex spacing b_0 estimated as $\pi/4$ of the generator wing span), which was identified from flight test data[10].

The LES wake vortex flow fields used in the analysis were generated by the DLR Institute of Atmospheric Physics during the DLR-internal project "Wetter & Fliegen" (Weather and Flying)[11] and comprise wake vortices of different ages between $16\,\mathrm{s}$ and $136\,\mathrm{s}$. Details about the flow fields can be found in *Hennemann (2010)*[12].These flow fields include a realistic modeling of the deformation and decay of the wake vortices and range from almost straight wake vortices

[6] Fischenberg (2010), Paper presenting a method to validate wake vortex encounter models on the basis of flight test data.

[7] Jategaonkar, Fischenberg, and Gruenhagen, v. (2004), Paper presenting an overview of the system identification activities at DLR.

[8] This distance is less than the minimum separation of a MEDIUM aircraft such as the Airbus A320 behind a HEAVY aircraft such as the Airbus A340 according to ICAO, which would be $5\,\mathrm{NM}$, and still less than the corresponding minimum separation of RECAT-EU of $4\,\mathrm{NM}$.

[9] Frech et al. (2007), Paper about the production and analysis of a weather database for the terminal area Frankfurt airport.

[10] Fischenberg (2002), Paper about the identification of wake vortex models from flight test data.

[11] Gerz and Schwarz (2012), Research report of DLR project "Wetter & Fliegen" (Weather and Flying).

[12] Hennemann (2010), PhD thesis about deformation and decay of wake vortices in a turbulent and stratified atmosphere.

to vortex rings. The atmospheric conditions underlying the Large Eddy Simulations were moderate turbulence and neutral thermal stratification ($N^* = 0$, $\epsilon^* = 0.23$). These conditions were selected because they lead to relatively symmetrical deformation and avoid a too fast decay of the vortices, which would occur in atmospheric conditions with strong turbulence and stable thermal stratification. As already mentioned, they can furthermore be considered as realistic for approach according to *Frech et al. (2007)*[9]. The airspeed of the generator aircraft is 72 m/s and the assumed air density is $1.168\,\mathrm{kg/m^3}$, which corresponds to the air density of the standard atmosphere of 12°C at 500 m above sea level.[13]

The resulting wind velocities of the wake vortex flow field, computed either by the analytical Burnham-Hallock model or by Large Eddy Simulations, are on the one hand fed into the AIM of the flight dynamics aircraft model to simulate the impact of the wake vortex on the aircraft. On the other hand, the same flow field is passed to the lidar simulation model, which measures the wind velocities for the wake impact alleviation system.

4.3 Lidar Simulation Model

The sensor simulation model used in this work is a generic Doppler lidar sensor. It does not have the purpose to represent the sensor physics in a very profound manner but to cover the main principles and provide measurements that are representative at the scales of interest and can be used as an input for the wake characterization algorithm. These measurements usually consist of the ideal measurement and an error term. The ideal measurement corresponds to the signal which a perfect sensor with no inaccuracies arising from sensor hardware or signal processing would theoretically provide. It results from the measurement geometry, defining the angle of the measurement beam and the measurement location, as well as from the wind velocities at these measurement locations. The error term incorporates the fact that practical applications cannot achieve this ideal measurement and models the deviation from the perfect measurement. Sources for errors can, among many others, for instance be an inaccurate determination of the Doppler shift, basic noise in the detector, imprecise positioning of the laser beam, and uncertainties in the signal processing. The characteristics and performance of Doppler lidar sensors vary strongly depending on the technological realization of the sensors. The different sensor types described in section 3.1 such as direct detection and coherent lidar sensors, for example, lead to very different dependencies of the sensor performance. The applied model is roughly based on the technology of pulsed direct detection Doppler lidar sensors. However, the generic manner of the sensor model effects that the model is not restricted to any particular sensor type but only provides a general measurement signal resulting from the specified measurement geometry and a simple error model. Figure 4.2 shows the workflow of the applied sensor simulation model.

The sensor simulation model consists of three main parts: the determination of the locations at which the wind is measured, the calculation of the ideal line-of-sight velocities and the computation of the measurement error, which is added to the ideal LoS velocity to form the measured

[13] The encounter simulations in the present thesis are performed at an altitude of 2000 ft. Marginal deviations in the air density are assumed have no significant effect on the shape of the wake vortices.

LoS velocity provided as a sensor output. The measurement geometry determines the positions of the measurements and the direction of the measurement beam, the so-called line-of-sight velocity. It is defined by a series of parameters specifying the geometry of the measurement screen, as shown in Fig. 4.3, as well as by the full screen update rate, the installation of the lidar sensor with respect to the aircraft, and the aircraft position and orientation.

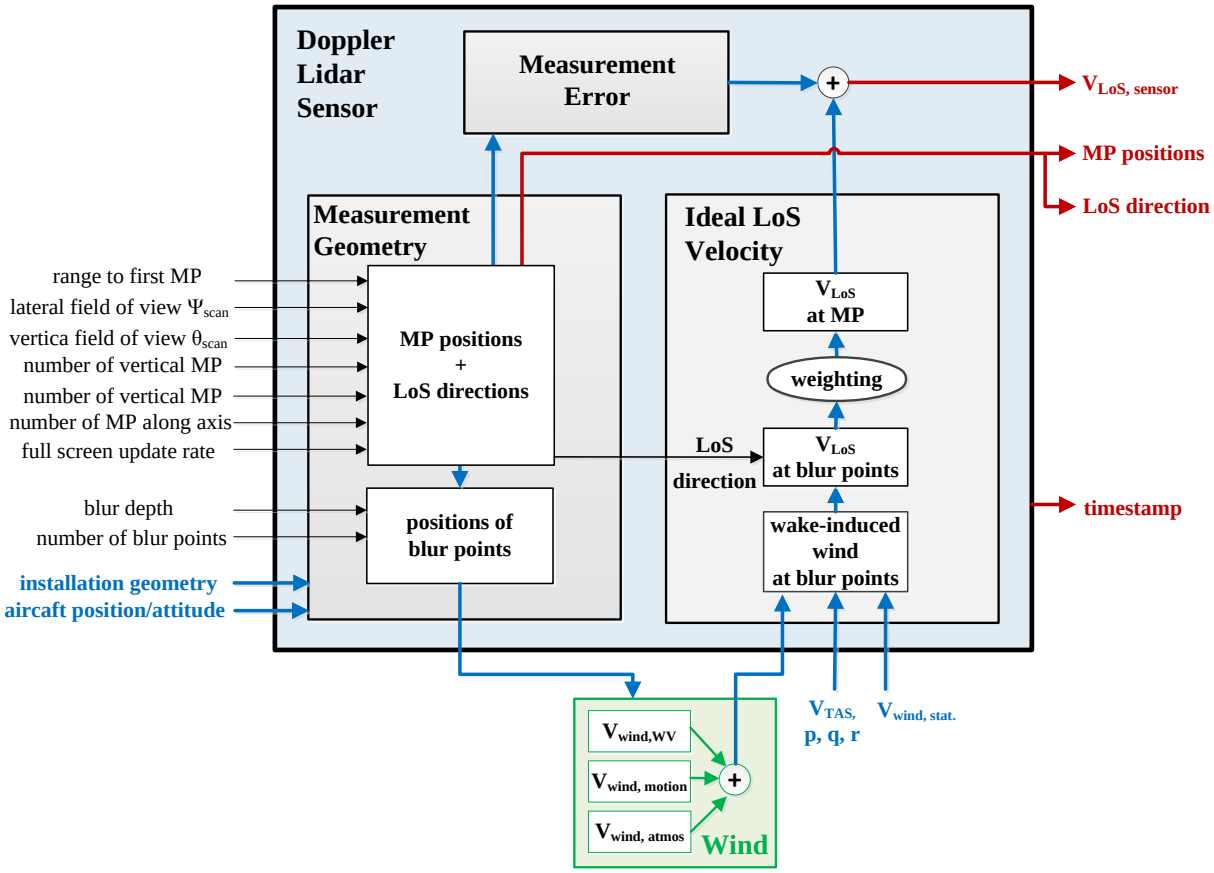

Figure 4.2: Structure of Doppler lidar simulation model

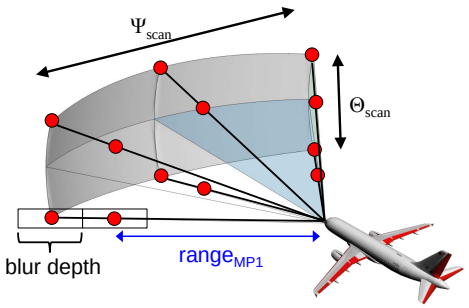

Figure 4.3: Parameters of measurement screen

The red circles in Fig. 4.3 mark reference points for different measurements. For reasons of

simplicity they are called “measurement points” even though each measurement point physically corresponds to a measurement volume. The measurements are arranged in a regular grid defined by regular steps of the lateral and vertical scan angle $\Delta\Psi_{\text{scan}}$ and $\Delta\Theta_{\text{scan}}$. The size of the scan angle steps results directly from the overall field of view specified by the parameters Ψ_{scan} and Θ_{scan}, as shown in Fig. 4.3, and the number of vertical and lateral measurement points. Along each measurement axis there can be several measurement points. The measurement point located closest to the sensor has the range defined by the parameter $\text{range}_{\text{MP1}}$. Further measurement points are subsequently placed in the distances of the blur depth behind the previous measurement point. All measurements along one axis are updated simultaneously. The different measurement axes are updated successively. The full screen update rate defines the frequency with which all measurement axes are updated. If the full screen update rate is for example $10\,\text{Hz}$ and the sensor has six measurement axes, the update rate for a new measurement is $60\,\text{Hz}$ and all measurements are refreshed after $0.1\,\text{s}$.

This kind of scan pattern represents only one option to distribute the measurements and many other arrangements would be possible as mentioned already, for instance, in Fig. 3.2. The regular grid is selected as a basis for the analyses here because it allows an easy and relatively independent variation of the different parameters and thus helps to get first insights of the required spatial resolution of measurements for the application for wake impact alleviation purposes. Especially for sensor configurations with many measurement axes the scan mechanism might be challenging. Once the requirements for the spatial resolution are determined, different arrangements can be derived that provide a similar spatial resolution but are easier to realize by optical scan mechanisms.

For each measurement point the sensor model computes a measurement volume belonging to this designated reference point. As the diameter of the laser beam is small compared to the axial measurement dimension, the cross dimensions are neglected and the measurement domain is modeled as a series of measurements along the laser beam direction. The length of the measurement domain is defined by the parameter blur depth. Within this blur domain the wind is measured at the specified number of nodes along the line-of-sight direction. These nodes are called “blur points” here (cf. appendix B). In order to determine the wind at the blur points, the computed positions have to be transformed into a global inertial coordinate system by considering the current position and attitude of the aircraft as well as the position and orientation of the lidar sensor with respect to the aircraft reference frame. It is assumed in this work that the lidar sensor is installed at the aircraft nose. The reference axis, from which the scan angles Ψ_{scan} and Θ_{scan} are defined, is tilted $5°$ downwards in order to broadly compensate for the aircraft’s angle of attack such that the sensor is approximately aligned with the flight path of the aircraft.

The wind, which is measured by the sensor, consists of three portions. The first component is the wake-induced wind velocity. This is the relevant part of the wind, for which the lidar sensor shall be used as a measurement device. In the simulation it is modeled by a vortex model (cf. section 4.2). The wind component denoted as “$V_{\text{wind,motion}}$” in Fig. 4.2 is the wind resulting from the motion of the aircraft relative to a inertial reference frame. It can be decomposed into the wind velocity arising from the translatory airspeed of the aircraft and the movement of the measurement positions due to the rotatory motion of the aircraft. The third wind component, called

"$V_{wind,atmos}$" in Fig. 4.2, covers atmospheric wind of other origins than the wake vortex such as for instance stationary wind or atmospheric turbulence. The sum of these three wind components represents the resulting wind at the blur points (i.e. at the positions of the different nodes) and is returned to the sensor. As the wind component of interest for the application in this work is only the wake-induced wind, the lidar sensor is modeled in that way that it provides only this wind component. The sensor itself always measures the entire wind. It is, however, assumed in this thesis that a post-processing removes additional wind components (other than the wake-induced wind components) from the measured wind and that the sensor output only contains the wake-induced wind velocities.[14] The sensor model thus determines the wake-induced wind by subtracting the wind components resulting from the aircraft motion and atmospheric wind of other origin than the wake vortex. The computation of the wake vortex wind components are based on sensor data of the true airspeed and the rotational rates as well as an onboard estimation of stationary wind. Errors in the sensor data as well as atmospheric turbulence (other than the wake vortex turbulence) lead to errors in the measurement of the wake-induced velocities. As a first approach, ideal sensor data is assumed for the true airspeed and rotatory velocities and no other atmospheric wind but the wake-induced wind is considered. The input wind vectors of the sensor model thus correspond to the ideal wake-induced velocities at the blur points. Future studies should analyze the influence of sensor errors and different atmospheric winds on the system performance.

As a real Doppler lidar sensor only measures the line-of-sight wind velocities, the wake-induced wind velocities in the sensor simulation model are reduced to the line-of-sight component of the full wind vector. At each blur point the projection of the wind vector on the corresponding LoS direction is computed according to equation 3.2 to get the LoS velocity. In a next step, the measurements at the different blur points are merged to the resulting line-of-sight velocity at the respective measurement points by means of a weighting function (cf. appendix B). The weighting function models the different backscatter energy from different positions along the laser beam. The form of the function depends on the sensor type and its exact settings. Different weighting functions can be selected for the sensor simulation model such as e.g. a constant weighting of the velocities measured at all blur points or a cosine-shaped weighting function giving more weight to measurements located in the center of the measurement domain. The output of the weighting function represents the ideal LoS velocity at the corresponding measurement point.

The measurement error is computed by a very simple error model. Measurement uncertainties are only modeled for the sensor parameters measurement range, length of the measurement volume, update rate, and number of measurements along one measurement axis. These parameters influence the measurement geometry and lead to different spatial resolutions and/or values of the ideal LoS velocity. The relative variation of the measurement uncertainty with these pa-

[14] For realistic applications it is more likely that the sensor provides the measurement based on the entire wind and that the extraction of undesired wind components is part of the processing in the modules the measurement is used in, like the OWIDIA system in this case. This could easily be realized in the OWIDIA system. For reasons of simplicity, however, it is assumed in this thesis, that the sensor already provides the desired wake-induced wind velocities.

rameters influences how well a wake vortex can be detected and characterized and is thus very important for the analysis of the potential of the wake impact alleviation system. In reality numerous further parameters, such as e.g. the laser power or the sensitivity of the detector, influence the measurement uncertainty as well, but do not change the measurement geometry of the lidar sensor. The effects of these parameters are not covered in the simple error model used in this thesis. Their impact can be considered as a shift of the overall error. The resulting absolute level of uncertainty is considered as a kind of generic technology factor that can be adjusted by the sensor design and is strongly dependent on future developments in the sensor technology.

For the parameters considered in the error model, the measurement error is modeled as a random number with a specified standard deviation. The sensor is assumed to have no bias, such that the mean value of the measurement uncertainty is set to zero. The values and dependencies of the standard deviation on the different parameters are derived on the basis of the exchange with lidar experts and experiences from flight tests with airborne lidar sensors in the projects AWIATOR[15] and DELICAT[16,17]. The reference configuration for the determination of the standard deviation of the measurement uncertainty is a sensor with $100\,\mathrm{m}$ range, $15\,\mathrm{m}$ blur depth, one range gate and an update rate of a single measurement axis of $150\,\mathrm{Hz}$. It is assumed that this sensor configuration has a standard deviation of $1\,\mathrm{m/s}$. This standard deviation corresponds to the value assumed in the Green-Wake project[18]. The other sensor parameters are set to comparable values[19] as defined in Green-Wake (cf. section 3.3) or are even prone to lead to a lower standard deviation.[20] In the flight tests performed in the AWIATOR project the lowest standard deviation, which was achieved, was $1\text{-}1.5\,\mathrm{m/s}$ and thus slightly higher than the $1\,\mathrm{m/s}$ assumed for the reference configuration in this thesis.[15]. On the one hand the measurement range and update rate had smaller values of $50\,\mathrm{m}$ and $60\,\mathrm{Hz}$ in these flight test, which were more advantageous for the achievement of a low measurement uncertainty. On the other hand the clear air and the high altitude represent challenging conditions for a good signal-to-noise ratio. In the long range measurements at very low altitudes, performed by JAXA (cf. section 3.3 and *Inokuchi, Tanaka, and Ando (2008)*[21]) standard deviations even below $1\,\mathrm{m/s}$ ($0.63\text{-}0.7\,\mathrm{m/s}$) could be demonstrated with a $3\,\mathrm{NM}$ lidar. It is, hence, assumed that a sensor with $1\,\mathrm{m/s}$ standard deviation in approach altitudes could be feasible with the given parameter combination.

[15] Rabadan et al. (2010), Paper about forward-looking lidar measurements for clear turbulence detection and alleviation.

[16] Vrancken et al. (2010), Report about the development of a long-range lidar for airborne clear air turbulence detection in the DELICAT project.

[17] Veermann, Vrancken, and Lombard (2014), Paper about a flight test campaign for lidar-based clear air turbulence detection in the DELICAT project.

[18] Rees (2014), Presentation of the results of Green-Wake project.

[19] The measurement distance lies between the minimum and maximum values specified in Green-Wake.

[20] In case of the reference configuration for the determination of the standard deviation of the measurement uncertainty in this thesis, only one range gate is considered compared two range gates in Green-Wake. Depending on the receiver technology (cf. section 3.2) a lower number of range gates might reduce the standard deviation. The single axis update rate is lower than the 250 Hz (100 measurement axes with $2.5\,\mathrm{Hz}$ full screen update rate) assumed in Green-Wake, which should also reduce the standard deviation. An altitude of $40000\,\mathrm{ft}$ is assumed in Green-Wake. At lower altitudes in approach a lower measurement uncertainty can be expected due to the higher aerosol and molecule density.

[21] Inokuchi, Tanaka, and Ando (2008), Development and flight tests of the 1.5 μm all-fiber coherent lidar of JAXA.

On the basis of this standard deviation for the reference sensor configuration the standard deviation is varied as a function of the range, update rate, number of range gates and blur depth. The dependencies of the standard deviation are modeled on the basis of the equations 3.7, 3.8, 3.11, and 3.12 of section 3.2. Regardless of the parameter values a lower bound of $0.63\,\mathrm{m/s}$ is specified for the standard deviation. It is presumed that this represents the minimum uncertainty level a lidar sensor is able to provide because the detector resolution induces a measurement error that cannot be compensated by an increase in the measurement signal. Concerning the range gates it is assumed here that each range gate requires a separate receiver (cf. section 3.2) such that a higher number of range gates leads to a SNR that is equivalent to the SNR of a sensor with a laser power that is by the factor of the number of range gates lower. The dependencies of the standard deviation are considered as uncertain and must be adjusted for any given real sensor. However, they are expected to model the general trends of the measurement uncertainty as a function of the parameter variations.

Once the measurement error is determined in accordance with the error model it is added to the ideal LoS velocity. In more complex error models the uncertainty could also be modeled as a function of the ideal LoS velocity itself. This effect is not covered in the applied very basic error model though. The sum of the ideal LoS velocity and the error represents the output of the lidar sensor as shown in Fig. 4.2. In addition, the sensor also provides the corresponding position, line-of-sight direction, and timestamp of each measurement.

4.4 Encounter Scenarios

Wake vortices can occur during all flight phases. However, they are very likely during approach[22,23] because the aircraft fly closely behind each other and with similar flight paths during this flight phase. The approach thus represents an important element for wake vortex research. This thesis hence analyzes and optimizes the wake impact alleviation system for the approach flight phase. Due to the similar flight paths of the aircraft during approach the encounter scenarios are usually characterized by shallow lateral and vertical encounter angles. The definitions of the geometric parameters describing the encounters are illustrated in Fig. 4.4. The lateral encounter angle between the wake vortex and the flight path of the encountering aircraft is denoted as $\Delta\Psi_{\mathrm{WV}}$, the corresponding vertical angle is $\Delta\Theta_{\mathrm{WV}}$. A positive lateral encounter angle ($\Delta\Psi_{\mathrm{WV}} > 0$) means that the follower aircraft penetrates the wake vortex from the right. A positive vertical encounter angle ($\Delta\Theta_{\mathrm{WV}} > 0$) means that the follower aircraft encounters the wake from the top. The vertical offset between the wake vortex and the center of gravity of the encountering aircraft is called ΔH_{WV} and is defined positive for the case that the wake vortex is located above the aircraft. If the vertical encounter angle is nonzero the vertical distance is defined at the intersection point of the projection of the wake vortex and the follower aircraft flight path into the horizontal plane.

[22] Münster and Schwarz (2010), Report about the analysis of the ASRA database concerning wake vortex incidents in the US.

[23] Viellette (2002), Paper presenting the analysis of wake vortex accidents and incidents in the USA from 1983 through 2000.

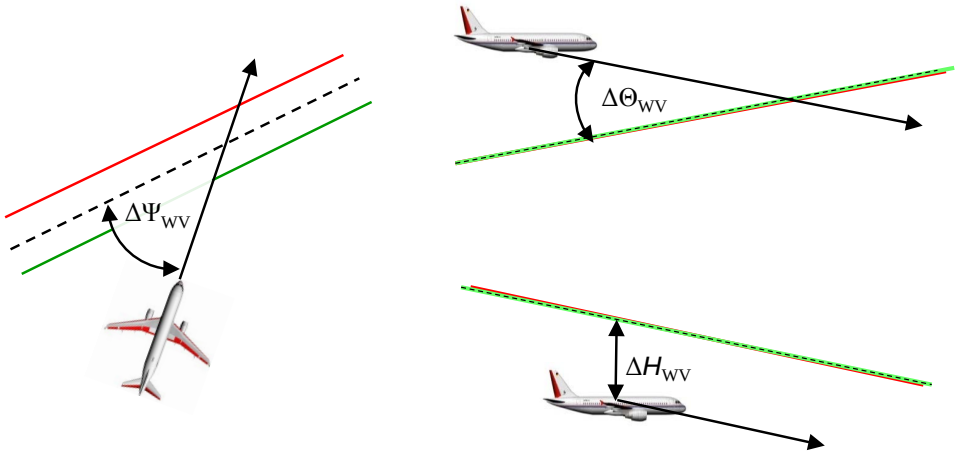

Figure 4.4: Definition of geometric parameters of wake vortex encounters

Unless stated otherwise, the encounter scenarios in this thesis always corresponds to the A320 ATRA, described in section 4.1.1, encountering the wake vortex of an Airbus A340 (either modeled as a Burnham-Hallock or as a LES wake vortex, cf. section 4.2) during approach at an altitude of 2000 ft and with an airspeed of 150 KIAS. The encountering aircraft flies in normal law with the autopilot disengaged and the pilot makes no control inputs throughout the entire encounter. The reference encounter scenario, which is used for most of the investigations, is a horizontal encounter with 0° vertical and 10° lateral encounter angle. Deviations from this encounter setup are particularly denoted in the text.

4.5 Assessment Metrics for Wake Impact Alleviation

A wake vortex influences an aircraft in various ways and results in different disturbances such as translatory and rotatory accelerations, attitude changes or flight path deviations. So far, no commonly accepted criterion exists for the evaluation of wake vortex encounter, such that the method to evaluate and quantify the benefit of a wake impact alleviation system is not self-evident. In the literature different criteria for the assessment of wake vortex control systems are mentioned. A very common approach is to evaluate the maximum bank angle occurring during the encounter. This parameter has been used by many authors in the past to assess the perfor-

mance of their control systems.[24-30] Especially during shallow encounters, the wake-induced rolling motion is the most relevant effect. The wake-induced bank angle excursion thus definitely represents one of the most relevant parameters for evaluation of these encounters.

Other studies included additional parameters besides the maximum bank angle in their evaluation of the alleviation performance. The authors of the wake impact controllers of *Hahn et al. (2010)*[25], *Schwarz and Hahn (2011)*[26] and *Horn, Niedermeier, and Ehlers (2002)*[31], for instance, considered the maximum lateral or lateral and vertical deviation from the original flight path in addition to the maximum bank angle to assess their control systems. *Rafi and Steck (2013)*[32] applied the maximum bank angle, the maximum altitude loss and the maximum airspeed loss as evaluation criteria. *Kloidt (2007)*[24] considered the maximum values of the glideslope and localizer deviation, bank and yaw angle, roll rate, and vertical load factor for the assessment of his control systems in simulator trails. The application of the parameters used for the control system performance assessment in these studies is justifiable as well. Accelerations such as the roll rate and vertical load factor, for instance, strongly influence the pilots' perception, which might, in worst case, cause undesired control actions, as well as the passenger comfort. Flight path deviations are critical in particular in final approach close to landing and might impede a successful landing. At low altitudes especially an altitude loss can be very dangerous and might imply the risk of ground collision. In cruise or during holding in contrast, deviations of the flight path in vertical or lateral direction are not very critical.

The problem of the evaluation of the control performance by means of multiple parameters is to compare the system performance of two cases with different performances with regard to these different parameters and to define priorities. It is for instance not evident if an encounter with a larger lateral flight path deviation is more or less critical than another encounter with a smaller lateral flight path but a larger vertical load factor excursion. *Held (2003)*[33] and *Kloidt (2007)*[24]

[24] Kloidt (2007), Dissertation about the development of a flight control system for the alleviation of the impact of wake vortices.

[25] Hahn et al. (2010), Paper about the development and analysis of a wake encounter flight control assistance system based on the processing of forward-looking lidar measurements.

[26] Schwarz and Hahn (2011), Paper about a control system for wake vortex encounters based a feedforward disturbance compensation and its analysis in offline and pilot-in-the-loop investigations as well as in flight tests.

[27] Looye, Lombaerts, and Kier (2012), Paper describing the design of feedback control laws for wake vortex encounters and the assessment of the control system in flight tests.

[28] Tinling (1977), Technical memorandum about the analysis of the effectiveness of automatic control for the alleviation of wake-induced roll excursions.

[29] Johnson, Teper, and Rediess (1974), Paper about the analysis of the effectiveness of a control system in alleviating wake vortex upsets.

[30] Hahn (2002), Paper describing the impact of wake vortices on aircraft and the possibility to reduce this impact by means of a suitable control system.

[31] Horn, Niedermeier, and Ehlers (2002), Paper about the analysis of wake impact alleviation control systems and the requirements for forward-looking sensors used for these systems.

[32] Rafi and Steck (2013), Paper about the development and testing of a flight control system for wake vortex encounters including an envelope protection scheme.

[33] Held (2003), Diploma thesis about the analysis of a flight control system for the reduction of the hazard potential of wake vortices in the approach phase.

applied a comprehensive assessment metrics to their wake impact control system, which consists of cost functions including multiple flight dynamic parameters. However, the selection and weighting of these parameters is based on engineering judgment only and has not been analytically derived or verified with pilot evaluations. The development of a substantiated assessment metrics, which comprises all relevant influences and defines the priorities between them, thus still needs further research, but is not part of the present thesis.

This thesis will instead use the simple but meaningful evaluation criterion of the maximum bank angle, which has also been commonly used in studies in the past. As the analysis in this thesis focuses on the approach flight phase, the encounter scenarios usually consists of shallow encounters, during which excursions in the roll axis represent the most relevant effect (cf. section 2.4). The attainable mitigation of the maximum bank angle during the encounter is thus considered as a suitable measure for the performance of the wake impact alleviation system here.

An aspect that is not covered in thesis is the consideration of the structural loads occurring during the encounter. Due to the rigid body model, used for the simulations in this thesis, an analysis of the loads is not possible. The present thesis only focuses on the alleviation of wake-induced aircraft reactions and especially on roll excursions. Nevertheless, structural loads could be a relevant aspect during wake vortex encounters as well and should be analyzed in different studies.

5 Concept for the Alleviation of Wake Vortex Impacts on the Basis of Remote Lidar Measurements

The present chapter gives an overview of the way the wake impact alleviation control system is realized. This includes a presentation of the overall concept as well a detailed description of the different components and the way they are realized and optimized.

5.1 The OWIDIA Concept for Wake Impact Alleviation

The approach taken here to alleviate the aircraft response during a wake vortex encounter consists in measuring the wake vortex disturbance in a short distance in front of the aircraft with an appropriate wind sensor and using this information to generate control surface deflections to countervail that disturbance. For this approach the aircraft is equipped with a forward-looking wind sensor as shown in Fig. 5.1 and a specific alleviation system, which processes the sensor measurements and generates the required control commands.

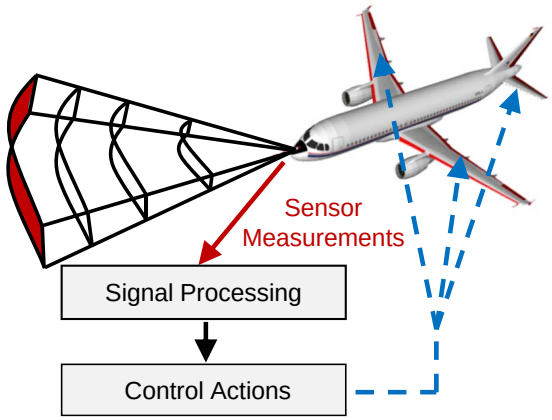

Figure 5.1: Wake impact alleviation approach[1]

Figure 5.2 gives an overview of the general workflow of the wake impact alleviation approach. The wind field is measured in a short distance ahead of the aircraft. The remote wind sensor applied to measure the wind velocities could be realized as different sensor types. For this application a Doppler lidar sensor as described in section 4.3 is used. The measured wind velocities at different positions in front of the aircraft are then passed to the specific wake vortex control system called Online Wake IDentification and Impact Alleviation (OWIDIA). The OWIDIA system consists of two modules: the Online Wake Identification (OWI) and the Wake Impact Alleviation Control (WIAC). The online wake identification module is required

[1] Ehlers and Fezans (2015b), Presentation of a wake impact alleviation control concept based on Doppler lidar measurements and wake identification including first insights of suitable lidar sensor configurations.

because the measurement from the lidar sensor does not provide very much information about the vortex flow flied and cannot be used directly as an input for a simple controller. The OWI uses the information from the lidar measurement to detect and identify a wake vortex model describing the measured flow field. On the basis of the identified wake vortex model the wake impact alleviation controller derives control commands to countervail the detected disturbance. The different modules of the system will be described in more detail in the subsequent sections.

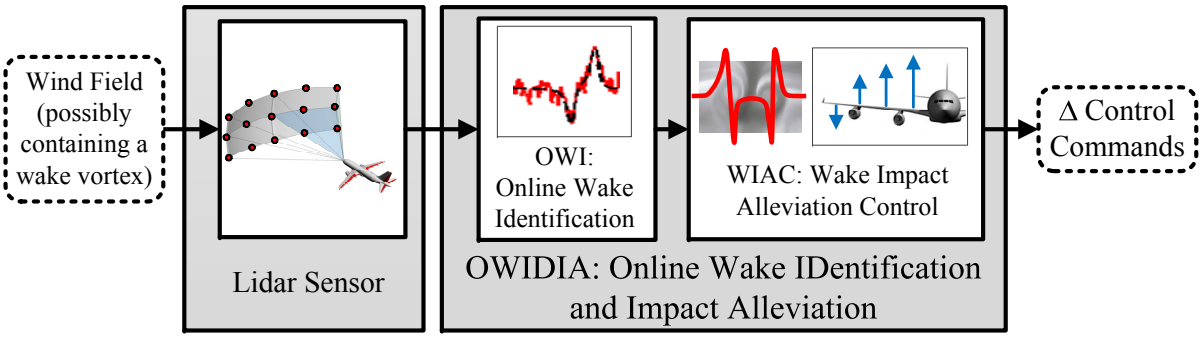

Figure 5.2: Workflow of wake impact alleviation[2]

5.2 Online Wake Identification

The fact that a Doppler lidar sensor can only measure in the direction of the measurement beam, the so-called Line-of-Sight (LoS) direction, implicates that most of the information is lost if the wind velocity vector has a large relative (i.e. almost perpendicular) angle with respect to the measurement direction of the sensor. Encounter scenarios with wake vortices perpendicular to the flight direction and thus to the measurement direction are encounters with small encounter angles. These encounters are, however, very relevant due to fact that they can be seen as worst cases in terms of roll reaction. The approach taken here to reconstruct the missing information is to apply an Online Wake Identification (OWI) algorithm that identifies a wake vortex model from the measured wind velocities. This wake vortex model allows deriving the full velocity vector of the wake-induced wind velocity at any desired location. The general principle of the OWI is to set up a wake vortex model and to compare the simulated line-of-sight measurement of the wind velocities of this model with the actual line-of-sight measurements of the lidar sensor as shown in Fig. 5.3. The parameters of the wake vortex model are estimated such that the cost function comparing the actual LoS velocities and the LoS velocities based on the model is minimized.

The general principle of the online wake identification was developed by Fischenberg[3,4] and is

[2] Ehlers and Fezans (2015a), Paper about results of sensitivity study of suitable lidar sensor parameters for wake characterization and alleviation.

[3] Fischenberg (2013a), Development of concept for an online wake identification algorithm which uses forward looking lidar sensor measurement to detect and characterize wake vortices.

[4] Fischenberg (2013b), Patent of online wake identification algorithm.

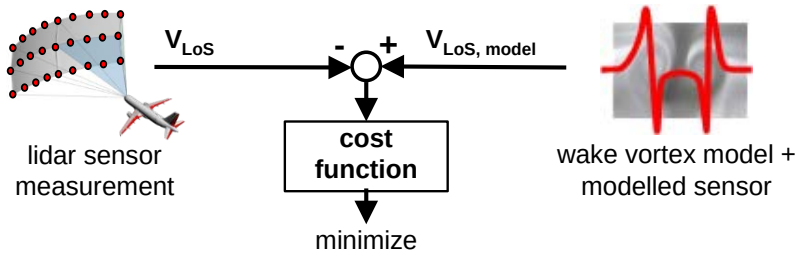

Figure 5.3: Principle of online wake identification[1]

extended for a fully integrated implementation in the OWIDIA system within the full 6-DoF simulation framework in *Ehlers and Fezans (2015a)*[2]. Figure 5.4 shows the detailed workflow of the OWI.

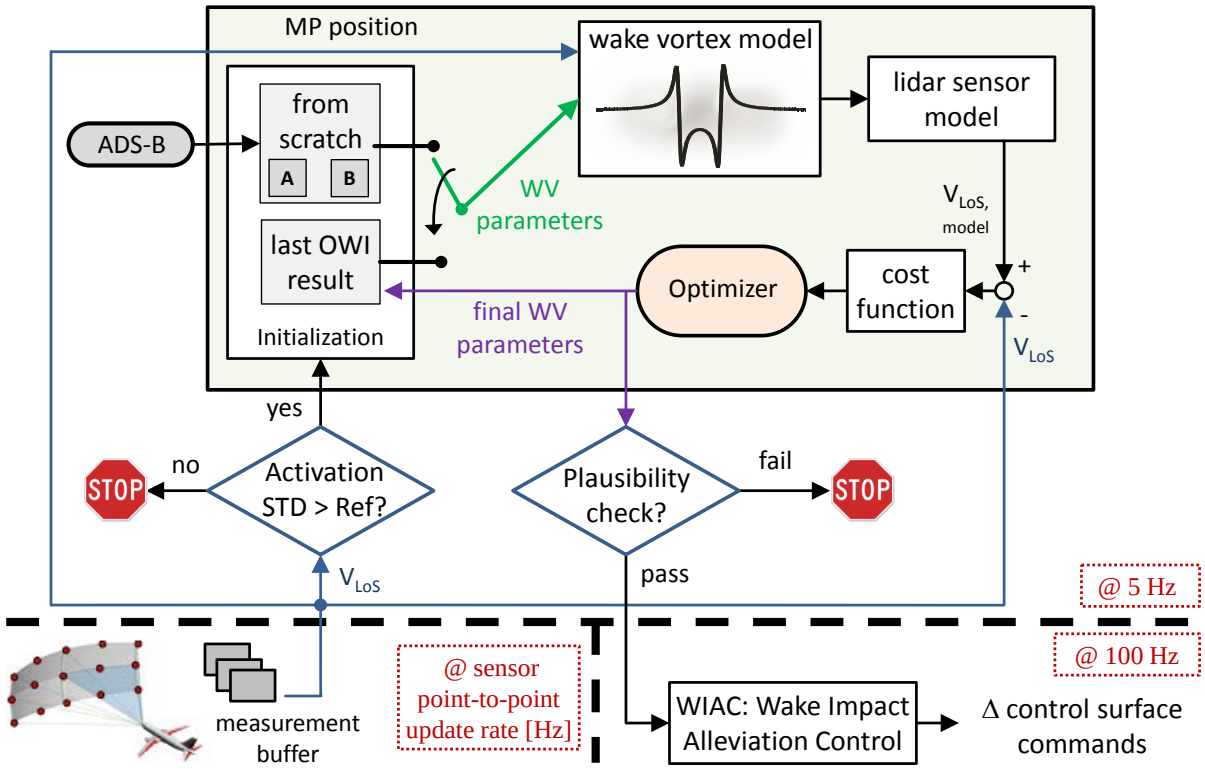

Figure 5.4: Workflow of online wake identification[2]

The buffering of the measurements uncouples the execution of the OWI (with respect to the execution time) and the update of the measurements from the lidar sensor. This decoupling allows the instantaneous consideration of several measurements at different locations for the identification in opposition to a recursive scheme based on updates of the current estimate using each new measurement only. As a first approach for the sizing of the buffer, the buffer size is specified in that way that it contains measurements over a time frame of 2 s. This corresponds to measurements ranging over about 160 m in flight direction for an encounter scenario in approach with an airspeed 150 KIAS (i.e. approximately 80 m/s true airspeed for an altitude of

2000 ft). The idea behind the definition of the buffer size is that a significant portion of the potential wake vortex should be represented by the stored measurements but that the percentage of measurements outside of the range of the wake vortex is not too large. If the data buffer contains measurements over a too long time frame this increases the risk that the majority of the stored data are measurements outside of the region where the wake vortex is located. This would reduced the SNR average over all stored measurements, which would, in turn, impair the satisfaction of the activation criterion (cf. section 5.2.1). Furthermore, a large buffer is disadvantageous in terms of computation time and implies the risk that the older measurements might be obsolete because the wake vortex has changed in the meantime.

The measurement buffer is updated every time when new measurements are available according to the principle first-in-first-out. The measurement positions stored in the buffer are continuously propagated because the relative position with respect to the aircraft changes when the aircraft moves relative to the surrounding air. The coordinate system used to define the measurement positions is a north-east-down (NED) system originated at the center of gravity of the aircraft. The advantage of this aircraft-carried coordinate system is that it evades the influence of stationary wind. In an earth-fixed coordinate system both, the wake vortex and the aircraft, are shifted parallelly but the relative distance, which is relevant for the impact of the wake vortex on the aircraft, is not influenced by the wind if stationary wind is present. The position of the measurement points stored in the data buffer thus does not have to be adapted in the presence of stationary wind. The change of the relative position between the measurement points and the aircraft resulting from the motion of the aircraft with respect to the surrounding air is adjusted at the frequency, at which the airspeed is available (i.e. at 100 Hz). The measurement positions are shifted by the change of the aircraft position relative to the surrounding air. The latter is approximated by the multiplication of the true airspeed of the aircraft with the sample time Δt_s of the dynamic aircraft model:

$$\begin{bmatrix} x_\mathrm{MP} \\ y_\mathrm{MP} \\ z_\mathrm{MP} \end{bmatrix}_\mathrm{new,NED} = \begin{bmatrix} x_\mathrm{MP} \\ y_\mathrm{MP} \\ z_\mathrm{MP} \end{bmatrix}_\mathrm{old,NED} - \begin{bmatrix} u_\mathrm{TAS} \\ v_\mathrm{TAS} \\ w_\mathrm{TAS} \end{bmatrix}_\mathrm{old,NED} \cdot \Delta t_\mathrm{s}, \tag{5.1}$$

with Δt_s = sample time [s]

$\begin{bmatrix} u_\mathrm{TAS} \\ v_\mathrm{TAS} \\ w_\mathrm{TAS} \end{bmatrix}_\mathrm{NED}$ = components of true airspeed in NED coordinates.

The vector of the true airspeed is derived from the magnitude of the true airspeed V_TAS and the aerodynamic angles of attack α_A and sideslip β_A, which define the orientation of the true airspeed with respect to the body-fixed frame. The transformation into the NED coordinate system then provides the required components $u_\mathrm{TAS,NED}$, $v_\mathrm{TAS,NED}$, $w_\mathrm{TAS,NED}$:

$$\begin{bmatrix} u_\mathrm{TAS} \\ v_\mathrm{TAS} \\ w_\mathrm{TAS} \end{bmatrix}_\mathrm{NED} = \underline{M}_\mathrm{NED,b} \cdot V_\mathrm{TAS} \begin{bmatrix} \cos\alpha_\mathrm{A} \cdot \cos\beta_\mathrm{A} \\ \sin\beta_\mathrm{A} \\ \sin\alpha_\mathrm{A} \cdot \cos\beta_\mathrm{A} \end{bmatrix} \tag{5.2}$$

whereupon

$$\underline{M}_{\text{NED,b}} = \begin{bmatrix} \cos\Psi\cos\Theta & \cos\Psi\sin\Theta\sin\Phi - \sin\Psi\cos\Theta & \cos\Psi\sin\Theta\cos\Phi + \sin\Psi\sin\Theta \\ \sin\Psi\cos\Theta & \sin\Psi\sin\Theta\sin\Phi + \cos\Psi\cos\Theta & \sin\Psi\sin\Theta\cos\Phi - \cos\Psi\sin\Phi \\ -\sin\Theta & \cos\Theta\cos\Phi & \cos\Theta\cos\Phi \end{bmatrix}. \tag{5.3}$$

As the update of the measurement positions is based on the motion of the aircraft relative to the stationary surrounding air, the aerodynamic angles of attack α_{A} and sideslip β_{A} as well as the true airspeed V_{TAS} used in equation 5.1-5.3, should also be parameters relative to the stationary surrounding air. The values provided by the aircraft sensors, however, contain unsteady wind components of the wake vortex. It is assumed that the measurement signals are low-pass-filtered to remove turbulences such that they correspond to the values relative to the stationary surrounding air.

For the wake identification all measurements stored in the data buffer are considered for each execution of the OWI. For state or parameter estimation problems various recursive schemes are often used (e.g. Kalman filter and its variants). However, the strong nonlinearity of the relationship between the measurements and the parameters to be estimated in the present case cannot be handled well with these techniques. Furthermore, it also seems unlikely that a well-performing recursive formulation could be defined due to the fact that the information (LoS velocity measurements and corresponding metadata[5]) reused from one execution of the OWI to the next one[6] is significantly richer than the parameter estimates from the previous execution and theirs estimated covariances[7]. Instead a "one-shot" estimation process is applied, as described in further detail in *Fezans, Schwithal, and Fischenberg (2015)*[8].

The OWI is executed every $0.2\,\text{s}$ in the simulation and the result is assumed to be available $0.2\,\text{s}$ after starting the algorithm. In the current implementation the identification algorithm is not running that fast yet and is therefore not real-time capable yet. So far it was not optimized for this purpose. However, it is expected to be able to be run with $5\,\text{Hz}$ in real-time if the code is parallelized and optimized.
Each time the OWI is called an activation criterion is executed first. Only if this activation criterion is satisfied the actual optimization algorithm it started, which estimates the wake vortex parameters providing the best fit with the measured velocities. After the estimation process has converged the result is checked for physical plausibility. If the parameters of the wake vortex model lie within the bounds of the plausibility check, they are passed to the wake impact alleviation control module. Details of the different steps of the OWI are given in sections 5.2.1 to 5.2.5.

[5] The metadata comprise the location and orientation of the measurement here.
[6] I.e. the portion of the buffer that is kept between two successive executions.
[7] This would typically be the information reused by a Kalman filter during the following step.
[8] Fezans, Schwithal, and Fischenberg (2015), Paper about application of remote sensing technologies for active load alleviation of gusts and turbulence and wake impact alleviation.

5.2.1 Activation Criterion

The purpose of the activation criterion is to avoid the execution of the optimization algorithm if there is no wake vortex present. This is the case during most of the flight time. By only running the optimization if there are strong hints of the possible presence of a wake vortex, an additional safety net for the most common situation of no wake vortex is introduced. The activation criterion is based on the standard deviation of all line-of-sight measurements stored in the measurement buffer and checks if this standard deviation reaches a threshold value. The threshold is specified as $120\,\%$ of the reference standard deviation of the sensor. If the noise characteristics of the lidar sensor are reliably known the reference standard deviation can be specified beforehand. In the current implementation the reference standard deviation of the LoS velocity is determined as the standard deviation of all wind measurements in the data buffer when it is filled for the first time, assuming that there is no wake vortex at the very beginning of the simulation. If the current standard deviation of the LoS velocities in the measurement buffer gets larger than $120\,\%$ of this reference value, the actual identification algorithm of the OWI is started.

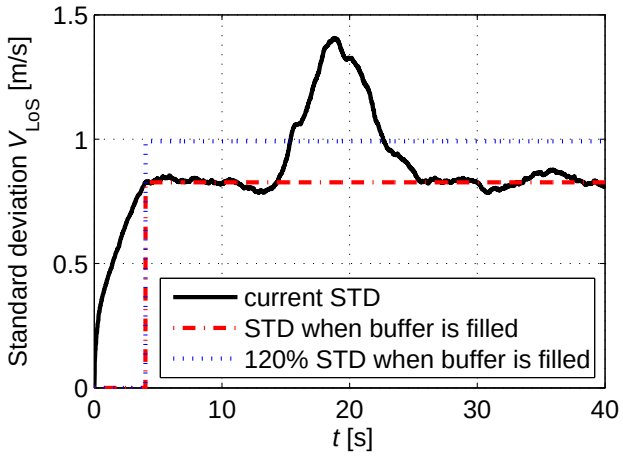

Figure 5.5: Example of LoS velocity trigger for a $15°$ lateral encounter

Figure 5.5 gives an example of the time history of the standard deviation of the LoS velocities in the measurement buffer. The reference standard deviation is $0.83\,$m/s here. When the wake vortex is contained in the measurements, approximately in the time period between $15\,$s and $25\,$s, a significant increase in the standard deviation can be noticed. Between $15.4\,$s and $22.6\,$s the current standard deviation is larger than $120\,\%$ of the reference value and the identification algorithm is executed.
If the measurement noise is very high, as shown exemplarily in Fig. 5.6, the signal-to-noise ratio[9] is so low that the $120\,\%$ threshold of initial standard deviation is never reached. In this

[9] The SNR in this context must not be confused with the SNR mentioned in section 3.2. In section 3.2 the signal-to-noise ratio referred to the ratio of the energy or number of photons per pulse per pulse per range gate received by the lidar sensor in relation to the detector noise. In conjunction with the OWI or in particular with the activation criterion the SNR describes the ratio of the line-of-sight wind velocity and the measurement noise level.

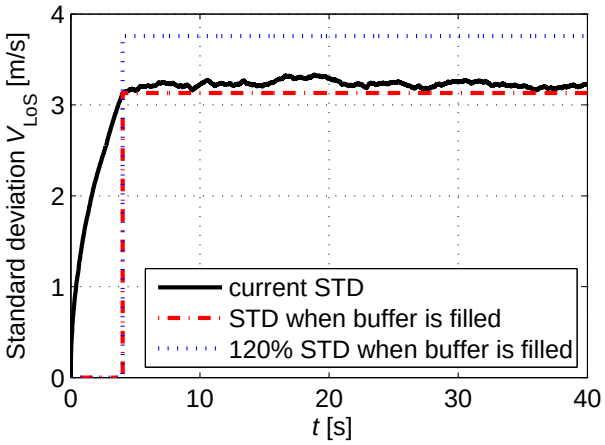

Figure 5.6: Wake vortex encounter with very high measurement noise: no activation of optimization algorithm

case the OWI is never activated during the encounter because the activation criterion is not passed. This very simple activation criterion thus exhibits the deficit that is does not detect all possible wake vortices. For weak wake vortices with low circulation it is not critical that the OWI is never activated because these cases are not very relevant as the aircraft response is very low anyway. However, cases with high measurement noise levels, in which even comparably strong wake vortices do not stand out with respect to the reference standard deviation of the lidar sensor, might be interesting to consider with the OWI. Especially if the sensor has a high noise level but also a high spatial resolution, a successful wake identification might still be possible. In order to study these cases a more complex activation criterion would have to be used.

5.2.2 Maximum Likelihood Estimation of Wake Parameters

When the activation criterion is satisfied the actual optimization algorithm is started. The goal of the optimization is to estimate the values of the parameters of a wake vortex model which provide the best possible fit between the predicted LoS velocities derived from the identified wake vortex model and the measured LoS velocities. This corresponds to a maximum-likelihood problem which can be solved with different classical optimization algorithms, as explained for instance in *Fischenberg (2013b)*[10]. The algorithm applied here has been developed and used during several projects at the Institute of Flight Systems at DLR.

The estimation process considers all measurements stored in the data buffer and compares these velocities to the LoS velocities resulting from the wake vortex model with the estimated parameters at the measurement locations stored in the buffer. As the measurements are not grouped in any way during the optimization the maximum-likelihood cost function is equivalent to a nonlinear least square fitting problem. This is solved with a Broyden-Fletcher-Goldfarb-Shanno

[10] Fischenberg (2013b), Patent of online wake identification algorithm.

algorithm[11-15]. The line search step thereby consists of a nonstandard algorithm combining different approaches from the classical line search algorithms depending on the particular situation. Other algorithms could be applied for this optimization problem here but have not been studied in this work.

5.2.3 Identification Model

The wake vortex model used in the optimization process is the Burnham-Hallock model[16] (cf. section 2.3). Other analytical wake vortex models such as e.g. the Lamb-Oseen model[17] could be used as well. The particular selection of the model type among the classical analytical wake vortex models has negligible influence on the success of the maximum likelihood parameter estimation procedure. Neither do they have any impact on the convergence rate. However, a simple model is preferable since the fact that the wake vortex model is evaluated for each measurement in the data buffer entails that the evaluation of the wake vortex model represents the largest portion of the computation time of the parameter estimation procedure.

The parameters of the wake vortex model which are passed to the wake impact alleviation control module (cf. section 5.3) are:

- vortex circulation Γ,
- distance between the two vortex cores b',
- wake elevation Θ_{WV},
- wake azimuth Ψ_{WV},
- lateral distance between cortex centerline and center of gravity of the aircraft Δy_{WV},
- vertical distance between cortex centerline and center of gravity of the aircraft Δz_{WV}.

Figure 5.7 illustrates the geometry of these parameters.

A disadvantage of these parameters is that the position parameters are strongly coupled. This impedes the convergence of the wake identification algorithm because the change of one identification parameter influences other identification parameter. Figure 5.8 illustrates that a change

[11] Broyden (1970), Paper about the analysis of a class of double-rank minimization algorithms.
[12] Fletcher (1970), Paper presenting a new approach to variable metric algorithms.
[13] Goldfarb (1970), Paper presenting new variable-metric methods.
[14] Shanno (1970), Paper presenting approximating matrices of quasi-Newton methods and their conditioning for function minimization.
[15] Shanno and Kettler (1970), Paper about optimal conditioning of quasi-Newton methods.
[16] Burnham and Hallock (1982), Technical report about measurements of the strength and decay of wake vortices at Chicago's O'Hare International Airport.
[17] Lamb (1932), Reference book about dynamics of liquids and gases.
[18] Ehlers, Niedermeier, and Fischenberg (2015), Paper presenting an airborne, lidar-based wake identification algorithm and a control system to alleviate the detected wake vortex.

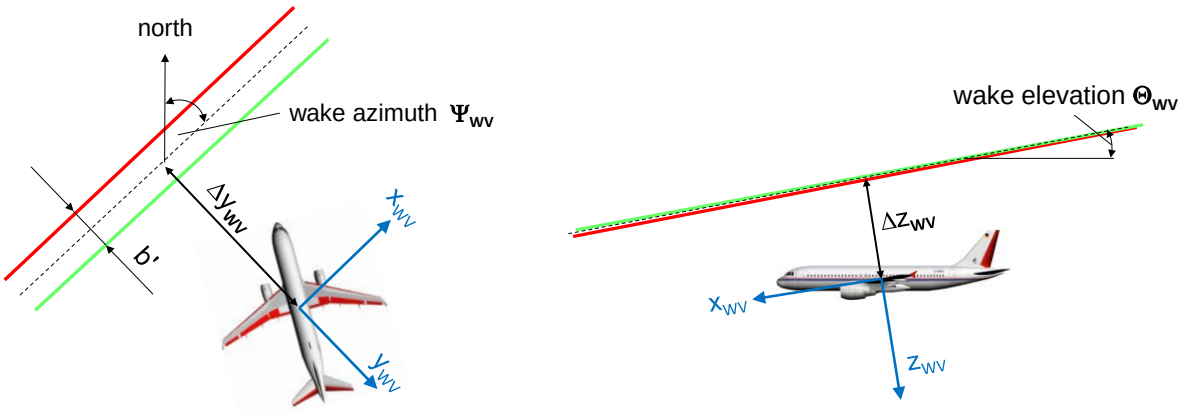

(a) top view (b) sideview

Figure 5.7: Geometry of OWI output parameters[18]

of the wake azimuth leads to a different lateral position Δy_{WV} of the vortex centerline relative to the aircraft. As the coordinate system, in which the vortex position is defined, is aligned with the vortex centerline, the coordinate system itself varies as well when the orientation of the wake is changed during the iterations of the optimization.

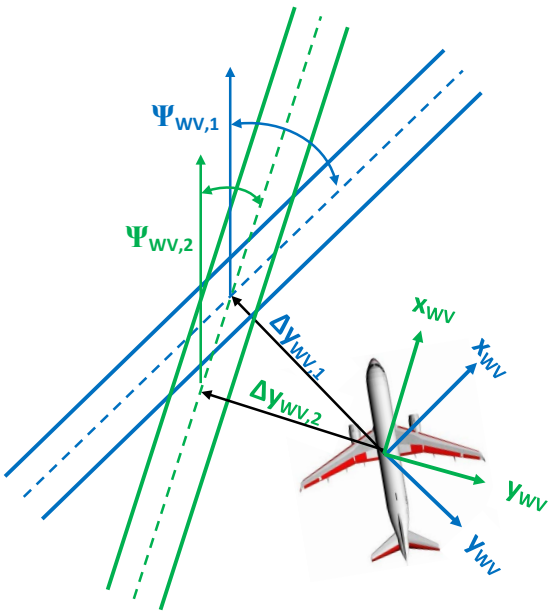

Figure 5.8: Wake azimuth and y-position of vortex centerline in wake coordinate system

The consequence of this coupling is that the OWI is very sensitive to these two parameters. If the initial values of these parameters are not selected suitably, the OWI often does not converge to a successful result. In the first implementation of the OWI[19], the initial values of the lateral wake vortex position Δy_{WV} was specified in dependence of the initial value for the wake

[19] Fischenberg (2013a), Development of concept for an online wake identification algorithm which uses forward looking lidar sensor measurement to detect and characterize wake vortices.

azimuth in order to respect the coupling between these two parameters. To handle the strong sensitivity of the identification algorithm to these two parameters, a multi-start of the optimization routine was implemented. The OWI was called five times with different initial values for the wake azimuth and for the lateral position Δy_{WV} accordingly. The initial wake azimuth was varied by 3° and 6° in both directions of the generator track angle provided via ADS-B. The corresponding initial lateral position was derived from each wake azimuth angle by geometric correlations.
Concerning the wake elevation and the vertical position of the wake vortex centerline Δz_{WV} an equivalent coupling exists. But in the longitudinal axis, the changes of the wake elevation are smaller and the initial parameter is known more precisely. This coupling is thus less critical for the OWI and a multi-start of the wake elevation is not necessary.
The procedure with a multi-start with different initial wake azimuth angles robustly provides successful OWI results even if the ADS-B track angle of the generator aircraft is inaccurate e.g. due to wind influences. The drawback of this approach is the additional computation time because the OWI is executed five times staring with each inital value of the azimuth angle.

In order to avoid this unfavorable coupling of the wake vortex parameters, different parameters are used within the internal optimization process to define the geometric position and orientation of the wake vortex. A so-called identification (ID) coordinate system is introduced, which is located in the horizontal plane at a fixed distance Δx behind the aircraft. Its base vector x_{ID} is colinear to the vector obtained by projecting the body-fixed x-axis onto the horizontal plane. The z_{ID}-axis is oriented downwards and the y_{ID}-axis complements the $(x_{\mathrm{ID}}, y_{\mathrm{ID}}, z_{\mathrm{ID}})$ basis such that it is right-handed, as illustrated in Fig. 5.9. In this coordinate system two points P_1 and P_2 on the vortex centerline define the relative position of the wake vortex with respect to the aircraft and its orientation. Point P_1 is the point where the vortex centerline and the projections of the body-fixed x-axis of the aircraft onto the horizontal plane intersect. The y_{ID}-position of P_1 is zero by definition. Point P_2 is defined as the position of the vortex centerline for $x_{\mathrm{ID}} = 0$. The coordinates x_1, z_1, y_2 and z_2 of the points P_1 and P_2 thus uniquely describe the location and orientation of the wake vortex.

Whereas variations of the wake orientation lead to a rotation of the coordinate system in case of the the wake vortex coordinate system, the ID coordinate system remains fixed if the wake orientation is varied during the parameter estimation process in order to find a best fit for the wake vortex model (cf. Fig. 5.8 and 5.10). The intersection of the aircraft flight path and the wake vortex stay unaffected of variations of the wake orientation, as illustrated in Fig. 5.10. The coordinate x_1 is thus independent of the wake azimuth. The azimuth change can be expressed by varying the lateral distance y_2 to point P_2 for a constant distance x_1. This makes the initialization of the identification parameters for the wake vortex easier.

Additional advantages of the identification parameters illustrated in Fig. 5.9 are the avoidance of a periodicity of the solution and a possibly better numerical conditioning. If angles are used to define the wake orientation this implies a periodicity of the 2π, which is unfavorable for the estimation process. This periodicity is prevented by describing the wake orientation by means of two points on the vortex centerline. The numerical conditioning might be better in case of the new ID-parameters than in case of the old WV-parameters of Fig. 5.7 because the values of

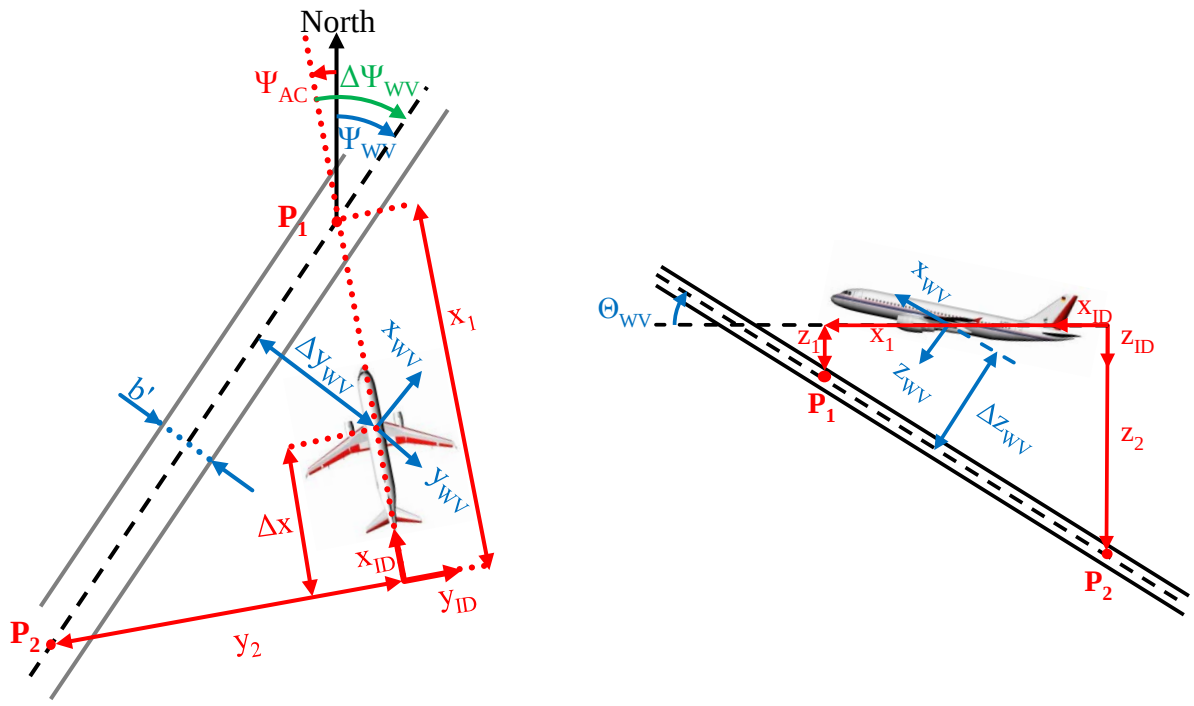

(a) top view (b) sideview

Figure 5.9: Identification parameters for OWI[2]

the coordinates of P_1 and P_2, which are defined in meters, are larger than the values of the angle Ψ_{WV} and Θ_{WV} expressed in radian. The angles in radian are significantly smaller than the other parameters that have to be estimated such as the lateral distance y_{WV} and the vortex circulation Γ. This can lead to numerical problems during the estimation process. Possible benefits resulting from the better numerical conditioning due to the using the coordinates of P_1 and P_2 in the ID-coordinates have not been particularly investigated in this thesis though.

A drawback of the new identification parameters in the ID-coordinate is the fact that the geometric identification parameters x_1 and y_2 tend to zero when the vortex centerline reaches the point (x_{ID},y_{ID})=(0,0). This singularity would not occur if the old wake vortex parameters with Ψ_{WV} and Θ_{WV} were used. However, problems due to this singularity can easily be avoided by locating the origin of the ID-coordinate system a defined distance Δx behind the center of gravity of the aircraft. This way the singularity does not occur when the vortex centerline crosses the center of gravity of the aircraft, where the wake vortex would have a strong influence on the aircraft dynamics, but far aft behind the aircraft, where the influence of the wake vortex is not relevant anymore. In the current implementation the origin of the ID-coordinate system is located 200 m behind the center of gravity of the aircraft.
The resulting parameters that are now used for the internal optimization process in the OWI are:

- the vortex circulation Γ,
- the lateral vortex separation b',
- the x-position of point 1 on the vortex centerline in ID-coordinates x_1,

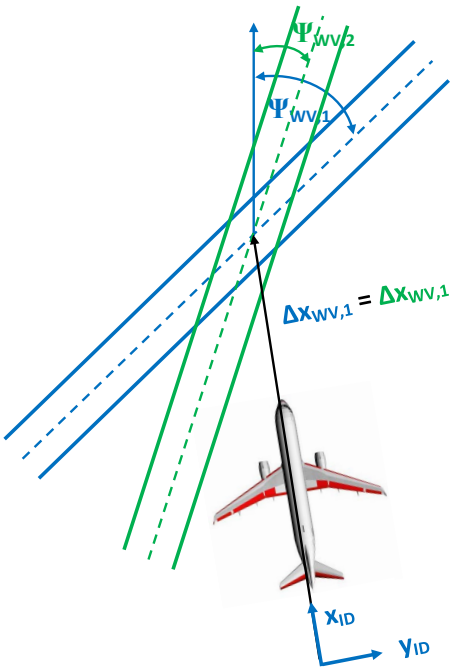

Figure 5.10: Wake azimuth and x-position of vortex centerline in identification coordinate system

- the z-position of point 1 on the vortex centerline in ID-coordinates z_1,
- the y-position of point 2 on the ortex centerline in ID-coordinates y_2,
- the z-position of point 2 on the vortex centerline in ID-coordinates z_2.

The geometric parameters x_1, z_1, y_2 and z_2 are shown in red in Fig. 5.9. The transformation of these parameters to the more intuitively interpretable wake vortex parameters based on wake angles and the lateral distance from the aircraft center of gravity illustrated in blue in Fig. 5.9 can be found in appendix D.

The chosen approach for the identification parameters, which describe the wake vortex geometry on the basis of the points P_1 and P_2, reaches its limits for encounter scenarios with almost perpendicular lateral encounter angles. To identify a relative lateral encounter angle $\Delta\Psi_{\mathrm{WV}}$ of $90°$ or -90° the y-position y_2 of points P_2 must become very large in magnitude. If the relative encounter angle varies slightly and crosses the perpendicular line of $90°$ or $-90°$ the identification parameter y_2 has to jump from a large negative value to a large positive value or vice versa. The OWI might thus provide imperfect azimuth angles for nearly perpendicular lateral encounters. This limitation is, however, not harmful for the overall performance of the OWIDIA system because, on the one hand, such steep encounters do not lead to large aircraft responses because they pass very fast. On the other hand, counteracting flight control commands cannot be realized fast enough to achieve significant alleviations during almost perpendicular encounters.

The goodness of fit of the estimated parameters of the wake vortex model is evaluated by comparing a predicted line-of-sight measurement of its wake-induced velocities with the actual

measurements of the wake vortex stored in the measurement buffer. For the simulated measurement a simplified sensor model is applied in the OWI. The simulated sensor simply determines the line-of-sight components of the wake-induced wind velocities of the wake vortex model at the positions of the true measurements. In order to capture the effect that the true measurements are not confined in space but cover a measurement volume (cf. section 3.1) the simulated measurement in the OWI also comprises a simple blur model. The LoS velocities of the wake vortex model are not only determined at the exact measurement positions of the measurements in the data buffer but along a small blur depth around the nominal measurement point. The length of this blur volume is adapted to the blur depth of the true lidar sensor in the aircraft. The number of blur points, at which the LoS velocities for the wake vortex model are computed, is constantly set to 11 points. Larger numbers of blur points of the simulated sensor in the OWI would strongly increase the computation costs of the optimization. As the wake vortex model in the OWI does not include any turbulence, it is not necessary to model a very large number of blur points.
The simulated measurements at the different blur points are accumulated to one measurement, which is provided by the sensor for the nominal measurement position. In order get one resulting measurement the LoS velocities at the different blur points are weighted with a cosine-function. The resulting LoS measurements for the nominal measurement points can then be compared to the corresponding measurements stored in the data buffer. The parameters of the wake vortex model in the OWI are varied until the best fit of the simulated and stored measurements is found.

5.2.4 Initialization of the Parameter Estimation Procedure

In order to start the iterative optimization algorithm of the OWI, initial values of the identification parameters are required. If the optimization algorithm is started in a case in which no wake vortex has recently been identified, the initial values of the identification parameters are specified on the basis of the current aircraft dynamics and information of the generator aircraft provided by Automatic Dependent Surveillance - Broadcast (ADS-B) or by means of fixed reference values. For the vortex circulation and the lateral vortex separation the initial values[20] $\Gamma_0 = 250\,\mathrm{m}^2/s$ and $b_0^{'} = 40\,\mathrm{m}$ are used for all wake encounter scenarios as suggested in *Fischenberg (2013a)*[21]. The parameter x_1, i.e. the x_{ID} position of point P_1, is initialized in consideration of the measurement range of the lidar sensor. The basic idea behind the initialization of x_1 is the assumption that the OWI is able to detect the wake vortex for the first time when the point P_1 is approximately located at the center of the lidar measurement screen. Based on this assumption, the initial x-position of point P_1 is derived from the average body-fixed x-component of the measurement range of all stored measurement points $x_{\mathrm{mean,lidar}}$, as described in equation 5.5, transformed into ID-coordinates:

$$x_{1,0} = x_{\mathrm{mean,lidar}} \cdot \cos\Theta_{\mathrm{AC}} + \Delta x, \tag{5.4}$$

[20] The initial values of the identification parameters are indicated by the the index 0.
[21] Fischenberg (2013a), Development of concept for an online wake identification algorithm which uses forward looking lidar sensor measurement to detect and characterize wake vortices.

whereupon

$$x_{\text{mean,lidar}} = \sum_{i=1}^{N_{\text{MP}}} \frac{\left(r_{x,\text{MP,b}}\right)_i}{N_{\text{MP}}}, \tag{5.5}$$

with $\left(r_{x,\text{MP,b}}\right)_i$ = body-fixed x-component of measurement range of current measurement point[22],
N_{MP} = number of stored measurement points.

This value provides a good initial guess for x_1 if the aircraft flies directly through the wake vortex and the lidar sensor consequently measures significant wake vortex velocities. In order to increase the robustness for cases with no or only a small influence of the wake vortex, the optimization algorithm is executed with two different initializations of x_1. In the second run a large distance of $500\,\text{m}$ is added to equation 5.4.

$$x_{1,0} = x_{\text{mean,lidar}} \cdot \cos\Theta_{\text{AC}} + \Delta x + 500\,\text{m}, \tag{5.6}$$

In cases with no remarkable wake vortex influence the second initial value of x_1 according to equation 5.6 leads to a lower cost function value of the OWI result such that this OWI result is selected.

The initial value for the vertical position of point P_1 is derived from the mean lidar x-measurement distance. Under the assumption that the tilt of the lidar reference axis is small, the initial value of z_1 is estimated as the sine component of $x_{\text{mean,lidar}}$:

$$z_{1,0} = -x_{\text{mean,lidar}} \cdot \sin\Theta_{\text{AC}}. \tag{5.7}$$

The initial guess of the position of point P_2 is determined by means of external input data via ADS-B. It is assumed that the generator aircraft is equipped with standard ADS-B and transmits its current flight path azimuth and angle of climb. These data are used to derive the initial values for the lateral and vertical position of Point P_2 from the position of point P_1.

$$y_{2,0} = -x_{1,0} \cdot \tan\left(\chi_{\text{ADS-B}} - \Psi_{\text{AC}}\right) \tag{5.8}$$

$$z_{2,0} = z_{1,0} + \sqrt{x_{1,0}^2 + y_{2,0}^2} \cdot \tan\gamma_{\text{ADS-B}} \tag{5.9}$$

[22] This corresponds to the body-fixed x-position of the measurement point at the time when it is stored. As time goes on the body-fixed x-position of the measurement points stored in the measurement buffer is adopted by the relative motion between the aircraft and the measurement point. But for the computation of $x_{\text{mean,lidar}}$ only the x-distance at the moment of the measurement is considered.

The described way of initializing the identification parameters is used whenever there is no OWI result available of an identification run shortly before. If a former run of the OWI has provided an identification result, however, the initialization of the identification parameters is not performed from scratch, as described above, but the identified wake vortex parameters of the previous successful OWI call are selected as initial values for the next optimization process. While the aircraft is encountering the same wake vortex, this initialization approach usually provides a better initial guess than estimated values on the basis of ADS-B data. The parameters of the OWI output are directly used as initial values. Only the initial values of the wake position are corrected by the motion of the aircraft since the last OWI call. Due to the relatively low update rate of the OWI the aircraft moves significantly between two subsequent calls of the OWI. If the airspeed is $150\,\mathrm{kt}$ during approach and OWI call rate is $5\,\mathrm{Hz}$, as it is currently implemented, the aircraft moves approximately $15\,\mathrm{m}$ between two OWI calls. The identified wake vortex position of the previous OWI call is corrected by this distance, equivalently to a "propagation step" of Kalman or particle filters.

If the result of a previous successful OWI call is used for the initialization of the successive OWI call, the initial values are usually relatively exact already such that a second run of the optimization algorithm with a different set of initial values is not performed in this case. A problem with this initialization procedure of using the result of the last OWI call could only occur if the aircraft has passed the wake vortex. If the aircraft encounters the wake vortex of different generator aircraft the previously identified parameters of the old wake vortex are obviously no good choice for the initial values of the identification parameters because the new wake vortex can have totally different characteristics. To avoid this problem, the last result is only remembered for a period of up to $4\,\mathrm{s}$ and after this time the initial OWI parameters are initialized from scratch with the help of ADS-B data again, as described above, in order to allow the identification of a potential new wake vortex.

5.2.5 Plausibility Check

When the optimization algorithm has converged and found the parameters of the wake vortex model that provide the best fit between the modeled and actually measured LoS wind velocities, which it could determine, this identification result is not directly used for the wake impact alleviation but checked for physical plausibility before. This plausibility check has the function of an additional safety net, which prevents that inappropriate identification results are used to generate control commands in the WIAC module. It evaluates if the identified wake vortex is physically possible and likely for the considered scenario. Available information about the generator aircraft received over ADS-B is included in this evaluation process. The following six criteria are applied to check the plausibility of the strength, dimensions, position and orientation of the identified wake vortex:

1. **Limits for circulation:** $\mathbf{100\,m^2/s < \Gamma < 700\,m^2/s}$
   The limits for the identified vortex circulation have the function to filter out results with very low circulation caused by atmospheric turbulence without the presence of wake vortices as well as unrealistically high results. For first investigations they were set to

$100\,\mathrm{m}^2/\mathrm{s}$ and $500\,\mathrm{m}^2/\mathrm{s}$ as suggested in *Fischenberg (2013a)*[23]. However, for the application of the OWI with LES wake vortices (cf. section 7.5) it turned out that the upper limit for the vortex strength should be increased because the true circulation of the LES vortices at young vortex ages is already close to $500\,\mathrm{m}^2/\mathrm{s}$. The upper limit for the vortex circulation is thus set to $700\,\mathrm{m}^2/\mathrm{s}$.

2. **Limits for wake elevation:** $\mathbf{-10^\circ < \Theta_{WV} < 20^\circ}$
   The limits for the wake elevations that are considered as physically plausible are derived from the estimated maximum descent and climb rate of the generator aircraft as suggested in *Fischenberg (2013a)*[3]. The lower limit for the wake elevation in addition to the maximum descent rate of the generator aircraft also considers the estimated maximum descent rate of the wake vortex itself and is set to -10°. The upper limit for the plausible wake elevation is specified as 20°.

3. **Limits for wake azimuth:** $\mathbf{|\Psi_{WV} - \chi_{ADS\text{-}B}| < 15^\circ}$
   In order to evaluate the plausibility of the identified wake azimuth the course angle of the generator aircraft, which is available via standard ADS-B is taken into account. It is assumed that atmospheric influences such as wind or errors in the transmitted ADS-B signal do not cause larger deviations from the actual wake azimuth than 15°. This value is thus selected as the limit for plausible identification results.

4. **Plausibility check for vertical position of wake vortex centerline**
   The underlying assumption concerning the evaluation of the plausibility of the position of the vortex centerline is that a wake vortex can only be realistically identified if its area of influence intersects with the measurement domain of the lidar sensor. In vertical direction this is assessed by checking if the vortex centerline between P_1 and P_2 plus an additional vertical tolerance $\Delta z_{\text{tolerance}}$ of $37.5\,\mathrm{m}$ crosses the vertical range of the locations of the stored measurement points, as illustrated in Fig. 5.11.

   The additional tolerance is added in order to take account of the fact that the wake vortex not only affects the encountering aircraft if it passes right through the vortex centerline but also represents a significant disturbance at a certain distance below and above its centerline. Figure 5.12 shows the decrease of the influence of a wake vortex on encountering aircraft with increasing distance from the vortex cores. The black circles indicate the vortex cores. The influence on the encountering aircraft is expressed in terms of the required roll control ratio (RCR_{req}), which describes the ratio of the roll control power needed to compensate for the wake-induced rolling moment with respect to the maximum available roll control power of the encountering aircraft. According to *Hahn and Schwarz (2007)*[24] the wake vortex disturbance can be considered as uncritical outside the so-called simplified hazard area (red box in Fig. 5.12) where the required roll control ratio does not get larger than 0.2. The tolerance $37.5\,\mathrm{m}$, used for the plausibility check here, is coarsely derived from the area with required roll control ratios of more than 0.3. This corresponds

[23] Fischenberg (2013a), Development of concept for an online wake identification algorithm which uses forward looking lidar sensor measurement to detect and characterize wake vortices.

[24] Hahn and Schwarz (2007), Derivation of safe limits for wake penetration from pilot ratings during flight simulator studies and in-flight simulations.

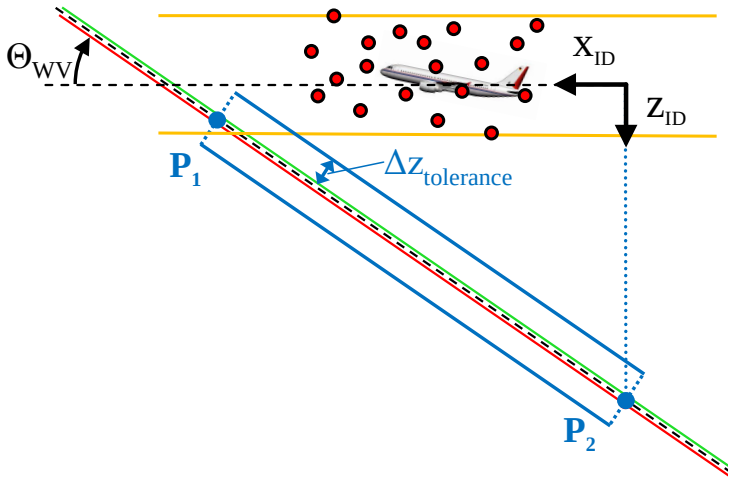

Figure 5.11: Plausibility check of vertical position of vortex centerline: verification if at least one blue lines (i.e. vortex centerline between P_1 and P_2 + $\Delta z_{tolerance}$) intersects with vertical range of the stored measurement points

to approximately $75\,\%$ of the lateral core distance. If an average value of $50\,\mathrm{m}$ is assumed for the lateral core distance, this delivers a tolerance of $37.5\,\mathrm{m}$.

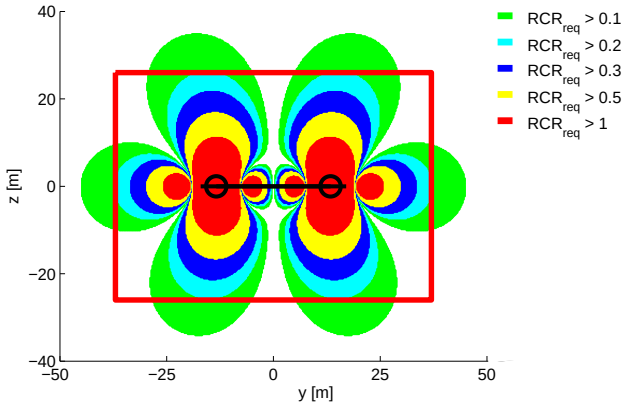

Figure 5.12: Wake-induced required roll control power at different locations around the wake vortex[24]

5. **Plausibility check for lateral position of wake vortex centerline**
   For the lateral position of the wake vortex a similar plausibility check as in vertical direction is applied. It verifies if the projection of the vortex centerline plus a tolerance of $37.5\,\mathrm{m}$ intersects with the lateral range of the stored measurement points. For the assessment of this criterion, a rectangle is defined in body-fixed coordinates which encloses the projection of all stored measurement points onto the horizontal plane, as shown in Fig. 5.13. The rectangle (orange box in Fig. 5.13) ranges from the minimum to the maximum body-fixed x- and y-positions of the stored measurement points. The plausibility check is passed if the blue lines, which correspond to the cortex centerlines plus the lateral tolerance of $37.5\,\mathrm{m}$, intersect with the rectangle enclosing the stored measurement points.

The tolerance of 37.5 m is selected as the same value as the vertical tolerance. The exact value is not crucial for the application. It only needs to be in the order of magnitude of the area of influence of the wake vortex.

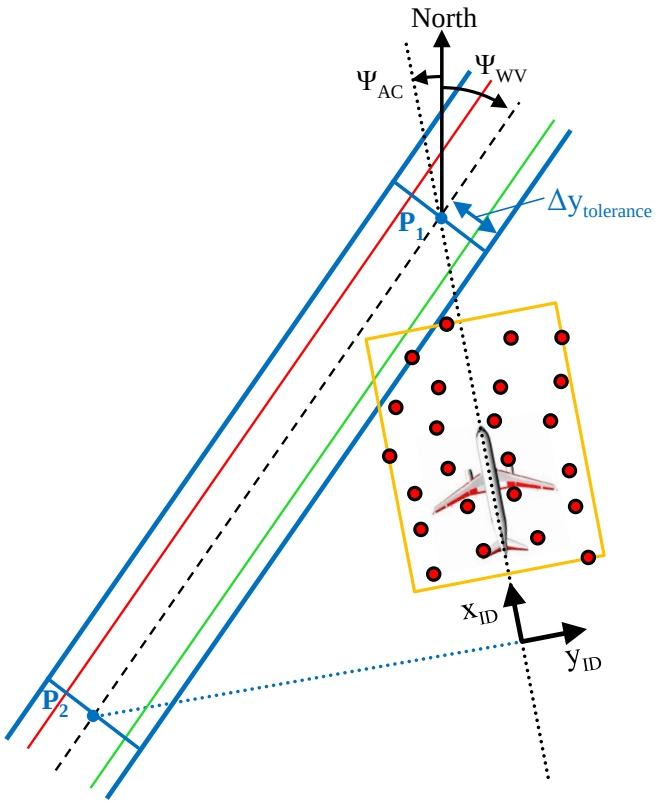

Figure 5.13: Plausibility check of lateral position of vortex centerline: verification if blue lines (i.e. vortex centerline + $\Delta y_{\text{tolerance}}$) intersects with orange rectangle (enclosing the stored measurement points)

Only if the identified wake vortex fulfills all of these six criteria, the parameters of the wake vortex are passed to the wake impact alleviation control module. If the OWI result does not pass the plausibility check no output is passed to the WIAC module and the control command generation is either based on the last available OWI output or not applied at all if no wake vortex has previously been identified.

5.3 Wake Impact Alleviation Control

5.3.1 Initial WIAC Design

The wake impact alleviation control (WIAC) module of the OWIDIA system computes the control commands necessary to compensate for the wake-induced aircraft reaction. This computation is based on the wake vortex model provided by the OWI described above and has the purpose to generate exactly those control surface deflections which provoke the countervailing

moments to the wake-induced moments. Fig. 5.14 gives an overview of the workflow of the WIAC module.

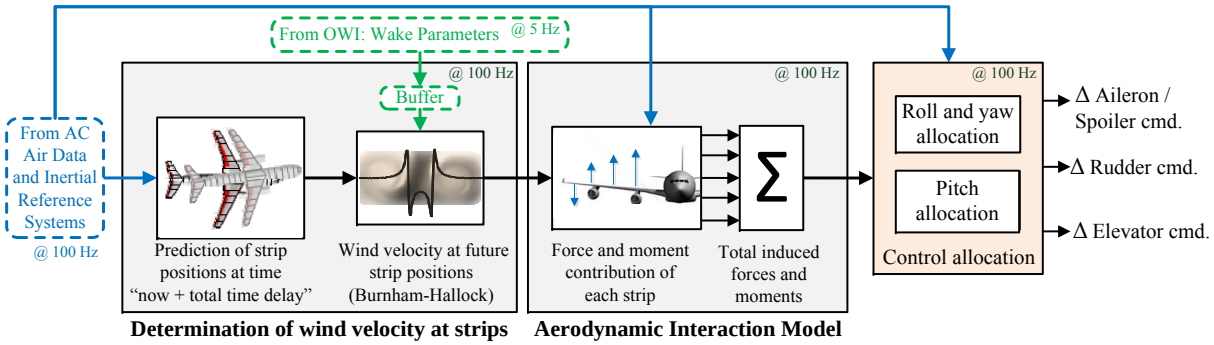

Figure 5.14: Workflow of wake impact alleviation control command generation[25]

The WIAC module receives input from the OWI and the Air Data Inertial Reference Unit (ADIRU) of the aircraft. The information from the ADIRU comprises data of the aircraft's attitude and motion as well as data about the current aerodynamic and atmospheric conditions such as Mach number, incident angles and air density. The input data from the OWI are the parameters of the wake vortex model including the vortex strength Γ, the orientation of the wake vortex defined by Θ_{WV} and Ψ_{WV} as well as the position of the wake vortex defined by the vertical (Δz_{WV}) and lateral (Δy_{WV}) distance of the vortex center line from the center of gravity of the aircraft, and the distance between the vortex cores b (cf. section 5.2.3). In contrast to the input data from the ADIRU, which is available at $100\,\text{Hz}$, the data of the OWI is only provided with a much lower frequency of $5\,\text{Hz}$. If no new OWI result is available - either because the OWI was not executed due to a non-fulfillment of the activation criterion (cf. section 5.2.1) or because the result of the estimation process has not been considered as valid by the plausibility check (cf. section 5.2.5) - the wake vortex parameters received from the OWI can also be updated with less than $5\,\text{Hz}$. The input of the OWI consequently needs to be buffered in order to use it for the wake impact alleviation control, which runs with $100\,\text{Hz}$. The update of the wake vortex position relative to the aircraft is performed equivalently to the update of the position of the lidar measurements in the measurement buffer (cf. section 5.2).

The stored wake vortex parameters represent the basis for the determination of the wake-induced forces and moments acting on the aircraft. The computation of these forces and moments is done by means of an Aerodynamic Interaction Model (AIM), as described in section 4.1.2. The aircraft is divided into strips, at which the wake-induced wind is assessed. In order to account for the time delay due to processing time and actuator delays, not the current position of each strip is considered for the computation of the wake-induced wind, but its estimated position when the command control surface deflection will actually be reached (i.e. after the time delay). These strip positions are determined by predicting the aircraft position and

[25] Ehlers and Fezans (2015a), Figure 7, Paper about results of sensitivity study of suitable lidar sensor parameters for wake characterization and alleviation.

attitude after this time delay on the basis of the current translational and rotational velocity:

$$\begin{bmatrix} \Phi \\ \Theta \\ \Psi \end{bmatrix}_{\text{pred}} = \begin{bmatrix} \Phi \\ \Theta \\ \Psi \end{bmatrix} + \begin{bmatrix} \dot{\Phi} \\ \dot{\Theta} \\ \dot{\Psi} \end{bmatrix} \cdot \Delta t_{\text{delay}}, \tag{5.10}$$

$$\begin{bmatrix} \Delta x \\ \Delta y \\ \Delta z \end{bmatrix}_{\text{NED}} = \begin{bmatrix} u_{\text{TAS}} \\ v_{\text{TAS}} \\ w_{\text{TAS}} \end{bmatrix}_{\text{NED}} \cdot \Delta t_{\text{delay}}, \tag{5.11}$$

with Δt_{delay} = considered time delay between control deflection command generation and command realization.

At each predicted strip position the wake-induced velocity is determined by applying a Burnham-Hallock wake vortex model with the identified wake vortex parameters stored in the data buffer. On the basis of the wind velocities at each strip the AIM can derive the wake-induced delta forces and moments, as described in detail in section 4.1.2 and *Fischenberg (2010)*[26]. The wake-induced velocities provoke additional angles of attack and sideslip at the different strips, which in turn generate additional forces and moments. For the strips at the wing and the horizontal tail only the wake-induced angle of attack and the resulting local lift are considered. For strips at the vertical tail and the fuselage only the wake-induced sideslip angle and the resulting local side force are included. Drag is not considered. The roll, pitch and yaw moment result from the multiplication of the forces at each strip with the corresponding lever arm. In the next step all forces and moments of the separate strips are summed up to provide the overall wake-induced forces and moments.

The goal of the control allocation is to compensate these forces and moments by adequate control surface deflections, which generate exactly the opposite forces and moments such that any wake-induced aircraft reaction is avoided. As common aircraft only use ailerons, elevators and rudder as control surfaces, they can only control the three degrees of freedom roll, pitch and yaw. A simultaneous compensation of disturbances in all six degrees of freedom is thus not possible. The approach taken here is to compensate for the wake-induced moments only. In the lateral-directional axes the wake-induced roll and yaw moment represent the main disturbance anyway. The influence of the wake-induced side force does not cause strong aircraft reactions. In the longitudinal axis, however, the vertical disturbance due to the wake-induced vertical force is not negligible. If an aircraft exhibited any kind of direct lift control such as e.g. symmetrically deflected control surface on the right and left wing, this would allow a simultaneous compensation of the wake-induced disturbance in the vertical and pitch axis and therefore significantly improve the wake impact alleviation in the longitudinal axis. As this is to date not common for commercial transport aircraft, this approach is not further considered in this work. Instead only the wake-induced pitching moment is compensated with appropriate elevator commands.

[26] Fischenberg (2010), Paper presenting a method to validate wake vortex encounter models on the basis of flight test data.

The most suitable control strategy in the longitudinal axis (i.e. if the wake-induced pitching moment is indeed more critical than the wake-induced vertical force and should therefore be the disturbance to be compensated or if a compensation of the vertical force or a combination of both disturbances would be more beneficial) should still be analyzed in detail in the future but is out of the scope of this work.

The required control surface deflections to counteract the wake-induced moments are derived by analytically inverting the aerodynamic control surface efficiency matrix of the aircraft. This provides the following equation for the computation of the aileron and rudder deflections:

$$\begin{bmatrix} \Delta\delta_{\text{ail}} \\ \Delta\delta_{\text{rud}} \end{bmatrix} = -\frac{s}{\bar{q}\cdot S}\cdot \begin{bmatrix} \left(C_{l,\delta_{\text{ail}}} + \sum_{i=2}^{5} K_{\delta_{\text{ail}}\delta_{\text{SP}}}\cdot C_{l,\delta_{\text{SP},i}}\right) & C_{l,\delta_{\text{rud}}} \\ \left(C_{n,\delta_{\text{ail}}} + \sum_{i=2}^{5} K_{\delta_{\text{ail}}\delta_{\text{SP}}}\cdot C_{n,\delta_{\text{SP},i}}\right) & C_{n,\delta_{\text{rud}}} \end{bmatrix}^{-1} \begin{bmatrix} L_{\text{WV}} \\ N_{\text{WV}} \end{bmatrix}. \quad (5.12)$$

The A320 aircraft model considered here possesses five pairs of spoilers. Spoilers 2 to 5 are applied as roll spoilers so that they have to be included in equation 5.12. Their deflection is defined as the deflection difference of each left and right spoiler pair and connected to the aileron deflection by the fixed factor $K_{\delta_{\text{ail}}\delta_{\text{SP}}}$. This factor is assumed to be identical for each spoiler pair. For the determined aileron deflection $\Delta\delta_{\text{ail}}$ the wake impact alleviation control system thus commands the following additional spoiler deflections:

$$\begin{bmatrix} \Delta\delta_{\text{SP,2,L-R}} \\ \dots \\ \Delta\delta_{\text{SP,5,L-R}} \end{bmatrix} = \begin{bmatrix} K_{\delta_{\text{ail}}\delta_{\text{SP}}} \\ \dots \\ K_{\delta_{\text{ail}}\delta_{\text{SP}}} \end{bmatrix} \Delta\delta_{\text{ail}}. \quad (5.13)$$

To compute the required elevator deflection not only the wake-induced pitching moment but also the contribution of the spoiler deflection to the pitching moment needs to be considered because the spoiler deflections significantly influence the overall pitching moment. The required elevator deflection thus results in:

$$\Delta\delta_{\text{elev}} = -\frac{l_\mu}{\bar{q}\cdot S\cdot C_{m,\delta_{\text{elev}}}}\cdot\left(M_{\text{WV}} + M_{\text{SP}}\right). \quad (5.14)$$

For the determination of the required control surface deflection in equations 5.12 and 5.14 it is assumed that these control allocation equations are linear in the control surface deflections. The control surface efficiencies $C_{l,\delta_{\text{ail}}}$, $C_{l,\delta_{\text{rud}}}$, $C_{n,\delta_{\text{ail}}}$, $C_{n,\delta_{\text{rud}}}$ and $C_{m,\delta_{\text{elev}}}$ are in general nonlinear functions of further parameters. In the given aircraft model of this work they depend on the angle of attack, the Mach number and the aircraft configuration (in terms of high-lift devices).

The determined control surface commands of the aileron, roll spoilers, rudder and elevator, shown in equations 5.12 and 5.14, represent the output of the wake impact alleviation control system and are added to the control surface deflections commanded by the regular flight control system.

5.3.2 Interaction of WIAC with Basic Control System

The developed wake impact alleviation control system has the particular purpose to minimize wake-induced aircraft reactions and is only active during the wake vortex encounter. For modern aircraft it can be assumed that the aircraft is equipped with a automatic flight control system,

which influences the flight dynamics of the aircraft and improves its flying qualities. This flight control system will be called “basic control system” here and is usually active during the whole flight. In manual flight a basic control system such as the normal law described in section 4.1.1 supports the pilot. When the aircraft flies with autopilot, the control system is usually designed as a cascade system, whereupon the outer control loops control the flight path of the aircraft. In this work only the manual flight mode is considered (cf. section 4.4). The basic control system thus corresponds to the normal law of section 4.1.1.

Assuming that the normal law is permanently active and the wake impact alleviation control is activated during a wake encounter, the question arises how these two control system should be combined. In the first implementation of the wake impact alleviation controller, the basic control system and the wake impact alleviation controller are implemented as two separate elements of the overall control system, which are simultaneously active during the encounter. The control commands generated by the basic control system and the wake impact alleviation controller are summed up and handed to the actuators.

Figure 5.15 illustrates the system behavior using this implementation concept. It displays a comparison of the alleviation of the aircraft attitude deviation occurring during a 10° horizontal wake vortex encounter when the wake impact alleviation control system is active with the same wake vortex encounter without the wake impact alleviation control system. In both cases, the basic control system is active and there are no additional inputs from a pilot or any other outer loop control system such as an autopilot. In this simulation, it is assumed that the wake vortex is perfectly known. This corresponds to the theoretical case that the OWI provides an ideal model of the external disturbance, such that the wake vortex model used within the wake impact alleviation control system is identical to the wake vortex actually affecting the aircraft. Although this case will never be reached in practice, it represents a revealing analysis case and shows the maximum performance of the system under idealized conditions. To point out that no wake identification is included in the following analysis but the perfectly known wake disturbance is used as the basis for the control command generation, the encounter with active wake impact alleviation is denoted by “WIAC”[27] in the Fig. 5.15.

As the disturbance is ideally known in this case, it would be expected that the wake impact alleviation could almost perfectly eliminate the wake-induced aircraft response. In Fig. 5.15, however, there are still significant deviations in the Euler angles when the wake impact alleviation is active. Two obvious, possible explanations can be found, which prevent a perfect elimination of the wake-induced aircraft even if the wake vortex disturbance is perfectly reconstructed:

- **Actuator dynamics and limits**
  Realistic actuators always exhibit actuator dynamics with certain limits. Due to their deflection, rate and acceleration limits as well as their dynamic behavior defined by the

[27] in contrast to OWIDIA, which is the name of the entire wake identification and impact alleviation system including the online wake identification module

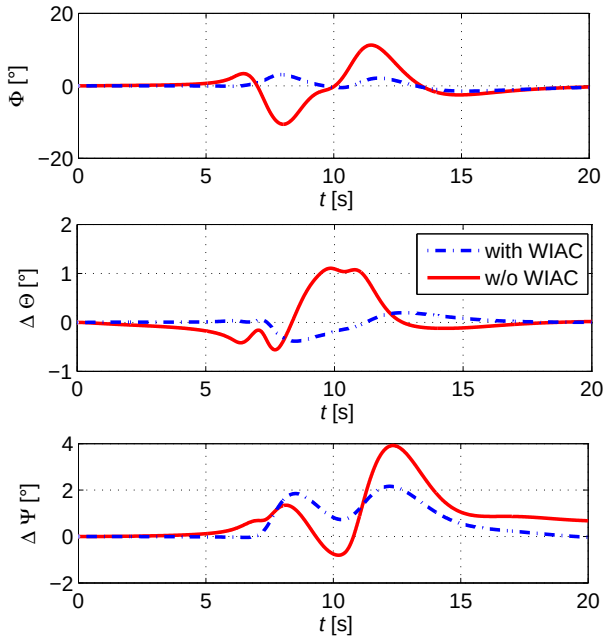

Figure 5.15: Wake impact alleviation during a $10°$ lateral encounter with separate implementation of WIAC and the basic control system

particular damping, eigenfrequency and delay of each actuator, the control surfaces cannot follow all commands of the flight control system instantaneously. Even though the control commands of the WIAC might perfectly compensate for the disturbance, the control surfaces do not exactly realize these commands and the disturbance is not completely eliminated. An average delay of the actuators is compensated within the WIAC because the disturbance forces and moments are always predicted for a moment when the control surfaces will have reached their commanded position. In case of the present implementation, however, a constant delay of $0.1\,\mathrm{s}$ is assumed. This approximates the average delay of the actuators but does not respect the particular dynamics.
Nevertheless, the actuator dynamics and limits are not the limiting factors for the considered wake encounter because the commanded dynamics are not too demanding during this encounter scenario. Figure E.1 in appendix E demonstrates this by presenting the same encounter, again with and without WIAC, for the theoretical case that there were no limits for the maximum and minimum deflection, rate and acceleration of the control surfaces. The actuator dynamics are replaced by a constant delay of $0.1\,\mathrm{s}$, which corresponds to the delay used within WIAC for the determination of the disturbance forces and moments. The aircraft responses in Fig. 5.15 and E.1 do not show significant differences, which confirms that the actuator dynamics and limits are not the explanation for the suboptimal wake impact alleviation of the WIAC system.

- **Control surfaces to control three degrees of freedom only**
  As already explained in section 5.3.1, it is not possible to compensate the full wake vortex disturbance because common aircraft only possess control surfaces (aileron, rudder, and elevator) to control three axes whereas the wake vortex usually disturbs all six de-

grees of freedom.[28] A conflict arises particularly in the longitudinal axis because the wake-induced vertical force and pitching moment both significantly disturb the aircraft motion and the elevator cannot compensate for the wake-induced disturbance in both axis simultaneously. This issue will be considered in further detail in section 5.3.3. In the lateral axis, the conflict between the translational and rotational disturbances is less crucial because the wake-induced side force is by orders of magnitude smaller than the wake-induced yawing and rolling moment. Especially the comparably large remaining peaks in the roll response of the aircraft with an active wake impact alleviation in Fig. 5.15 cannot be explained solely by the uncompensated wake-induced side force.

So although a perfect wake impact alleviation cannot be achieved even in the case of ideal knowledge of the disturbance, at least in the roll axis, a better wake impact alleviation would be expected than it can be seen in Fig. 5.15. The reason for the impeded performance of the wake impact alleviation control system can be found in a suboptimal interaction of WIAC with the basic control system. The wake impact alleviation approach presented in section 5.3.1 computes the control surface deflections required to compensate for the wake-induced roll, pitch and yaw moment and assumes that these control surface commands are completely realized by the corresponding control surfaces. However, as the basic control system may also generate control surface commands, which are added to the commands of WIAC, the resulting control commands may differ from the commands for the sole wake vortex disturbance rejection. Figure 5.16 displays the control commands of the basic control system, of WIAC and the actual deflection of the control surfaces, which result from the summation of both commands.

The figure shows that the control surface deflections, which are commanded by WIAC and would countervail the wake-induced disturbance moments, do not correspond to the actual control surface deflections because the basic controller also reacts to the wake-induced disturbance with control commands that conflict with the commands of the WIAC. The reasons for the conflicting commands of both control system modules are the following:

- **Conflict in pitch axis**
  In the longitudinal axis, the wake impact alleviation controller and the basic control system pursue different goals. WIAC aims at the compensation of the wake-induced pitching moment whereas the basic control system tries to prevent deviations of the vertical load factor. The elevator deflections to achieve these goals are obviously not the same. Nevertheless, the summation of both commands provides good alleviation results, as shown in Fig. 5.15. One possible explanation is that the two control systems work at different frequencies. The WIAC works at high frequencies, whereas the nz-law of the basic control system operates in the low frequency regime.

- **Conflict in roll axis**
  In the roll axis the basic control system and the wake impact alleviation on principle

[28] The Aerodynamic Interaction Model (AIM) applied here does not model the wake-induced x-force. In this case the wake vortex thus only acts in five degrees of freedom. Nevertheless, it cannot be fully compensated with control surfaces available in three degrees of freedom only. The sixth degree of the disturbance in the x-axis is usually comparably small but exists, of course, in reality.

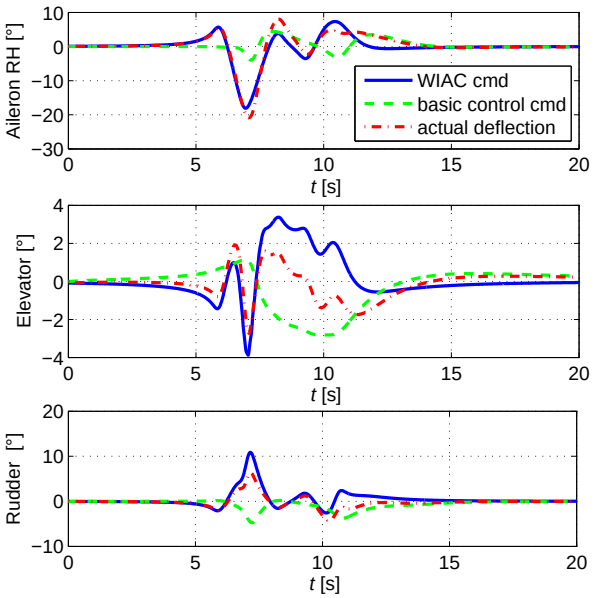

Figure 5.16: Control commands of WIAC and the basic control system as well as actual control surface deflections during a $10°$ lateral encounter with separate implementation of WIAC and the basic control system

pursue the same goal. Both control systems have the main objective to minimize any undesired rolling motion of the aircraft. The control commands of WIAC are designed to countervail the wake-induced rolling moment. The roll control module of the basic control system aims to follow the roll control command, which is usually a rate command attitude hold, like in the case of the control system considered in this work, or a commanded roll rate. That means it also tries to keep the roll rate equal to zero if there is no pilot input. It might thus seem unexpected that the basic control system commands aileron deflections opposing the WIAC commands in the second half of Fig. 5.16.
The remaining peak of the bank angle at $8.5\,\mathrm{s}$, when the wake impact alleviation controller is applied, results from the fact that the basic control system commands an aileron deflection opposing the WIAC aileron command. This aileron command originates from the lateral control design of the specific control system applied in this work, which includes a decoupling of the roll and yaw axis responses to external disturbances. For this purpose the roll controller of the basic control system includes a sideslip angle feedback signal. This feedback modifies the natural coupling of the roll and yaw axis, which can be attributed to the aerodynamic sideslip-angle-induced rolling moment coefficient $C_{l\beta}$. A feedback of the sideslip angle to the roll control command with an appropriate feedback gain allows an artificial cancellation of the natural aerodynamic coupling between the sideslip angle and roll response of the aircraft. In the case of a sole disturbance of the sideslip angle, the roll controller thus commands an aileron deflection to overturn the natural sideslip-induced roll response and the aircraft recaptures the target sideslip angle by a pure yawing motion.
The problem with this control architecture of the basic control system in combination with the wake impact alleviation controller is that the WIAC in the current implementation generates its control commands based on the assumption that the natural yaw-roll-

coupling of the aircraft would still exist. The aileron command of WIAC thus contains a component to compensate for the roll response induced by the sideslip disturbance of the wake vortex. As this coupling, however, does not exist anymore due to the sideslip feedback of the roll controller of the basic control system, the WIAC roll command oversteers in the roll axis.

- **Conflict in yaw axis**
  In the yaw axis it is more evident than in the roll axis that the basic control system and the wake impact alleviation control system command conflicting control surface deflections because both control modules pursue opposing goals. The basic control system tries to follow the reference sideslip angle commanded by the pedal input of the pilot. In most cases, the pilot does not command any sideslip angles, such that the basic controller aims to eliminate any sideslip excursions. In case of lateral wind, this supports the natural weathercock stability, which effects that the aircraft yaws into the wind. The wake impact alleviation system, in contrast, commands control surface deflections which countervail the wake-induced yaw moment and prevent a yawing motion of the aircraft. These different goals of preventing either an excursion of the sideslip angle or a yawing motion of the aircraft obviously lead to conflicting control surface commands because WIAC tries to keep the aircraft nose straight whereas the basic control system supports the aircraft's tendency to turn its nose into the wind. A simple summation of the control commands of both controllers thus represents a suboptimal way to combine these control modules.

A simple summation of the control surface commands of the wake impact alleviation controller and the basic control system leads to a suboptimal wake impact alleviation performance because the two control systems exhibit unfavorable interactions in some respects.

- In the pitch axis, the basic control system and the wake impact alleviation controller pursue different goals (i.e. minimizing the deviation of the vertical load factor in case of the basic control system and reducing the pitch motion in case of the wake impact alleviation controller) but the combined application of both system still leads to a good reduction of the wake-induced pitch reaction.
- In the roll axis, both control system principally pursue the same goal. However, in the original implementation of the control systems, the sideslip-angle-induced rolling moment of the wake vortex is compensated by both control systems, which leads to a slight oversteering in the roll axis.
- In the yaw axis, the basic control system and the wake impact alleviation controller pursue conflicting goals by minimizing the sideslip angle (in case of the basic control system) and the yaw rate (in case of the wake impact alleviation system) such that they work against each other and impair the alleviation performance.

5.3.3 Improved Combination of WIAC and Basic control System

As the simple summation of the control commands of WIAC and the basic control system without consideration of the behavior of the basic control laws showed an impairment of the achiev-

able wake impact alleviation, an improved integration of the WIAC into the overall control architecture is suggested in the following. The presented approach corresponds to the concept in the patent DE 10 2013 112 059[29].

The main wake impact alleviation performance impairment occurs due to the double consideration of the wake-induced rolling moment component resulting from the wake-induced sideslip angle in both control systems. To avoid an overcompensation of this component of the rolling moment it should only be considered in one of the control systems. One solution to this problem would be a modification of the control laws of the basic control system. By removing the feedback of the sideslip angle in the roll controller the artificial decoupling of the roll and yaw motion could be repealed. This would lead to an improved wake impact alleviation in the roll axis because the wake-induced rolling moment component resulting from the wake-induced sideslip angle would only be considered in the WIAC module then. However, cutting the sideslip angle feedback in the basic control law would also influence the overall behavior of the basic control system and thus the dynamic aircraft behavior throughout the flight. Another solution is not to consider the sideslip-angle-induced rolling moment for the command generation in the WIAC module. This approach does not modify the basic control laws and the general dynamic behavior of the aircraft and is therefore selected here.

The entire wake-induced rolling moment is calculated by means of the AIM (cf. section 4.1.2). The sideslip-angle-induced component of the moment can be determined by means of the aerodynamic sideslip-angle-induced rolling moment coefficient $C_{l\beta}$ and the equivalent wake-induced sideslip angle β_{WV} and is subtracted from the entire wake-induced rolling moment.

$$\Delta L_{\mathrm{WIAC,cmd}} = \Delta L_{\mathrm{AIM}} - C_{l\beta} \cdot \beta_{\mathrm{WV}} \cdot S \cdot s \cdot \overline{q} \tag{5.15}$$

The wake-induced sideslip angle β_{WV} is a fictitious parameter. It describes an equivalent sideslip angle at the center of gravity, which would cause the same resulting forces and moments as the inhomogeneous wind field of the wake vortex. It can be derived from the wake-induced forces and moments provided by the AIM by inverting the aerodynamic model of the aircraft. It is approximated[30] here as

$$\beta_{\mathrm{WV}} = \frac{\Delta Y_{\mathrm{AIM}}}{C_{Y\beta} \cdot \beta_{\mathrm{WV}} \cdot S \cdot \overline{q}}. \tag{5.16}$$

Figure 5.17 illustrates the improvement of the wake impact alleviation if the sideslip-angle-induced rolling moment component is not considered in WIAC for an exemplary wake vortex encounter with 10° lateral encounter angle[31]. Both implementations of the wake impact alleviation control system (blue dash-line and green dash-dot-line) show a good reduction of the wake-induced Euler angles compared to the encounter without the application of the wake impact

[29] Schwithal and Niedermeier (2017), German patent for a procedure for the reduction of the influence of airstream turbulence on aircraft with consideration of the aircraft control unit.

[30] The influence of the sideslip angle on the roll and yaw moment as well as the interaction with the longitudinal axis are neglected here such that β_{WV} can be easily derived only from the wake-induced side force. The resulting error of the wake-induced sideslip angle has been found to be small.

[31] A320 encountering the wake of A340 aircraft during approach with 10° lateral and 0° vertical encounter angle; wake vortex located 2 m above the aircraft, no pilot inputs, autopilot disengaged.

alleviation system (red solid line). However, it can also be noticed that, if the sideslip-angle-induced rolling moment component is not considered twice, the bank angle and heading are further reduced. When the sideslip-angle-induced rolling moment component $C_{l\beta} \cdot \beta_{\mathrm{WV}} \cdot S \cdot s \cdot \overline{q}$ is not considered in the WIAC control command generation (blue dash-dot-line) especially the wake-induced bank angle is very successfully alleviated and there is almost no bank angle deviation during the encounter.

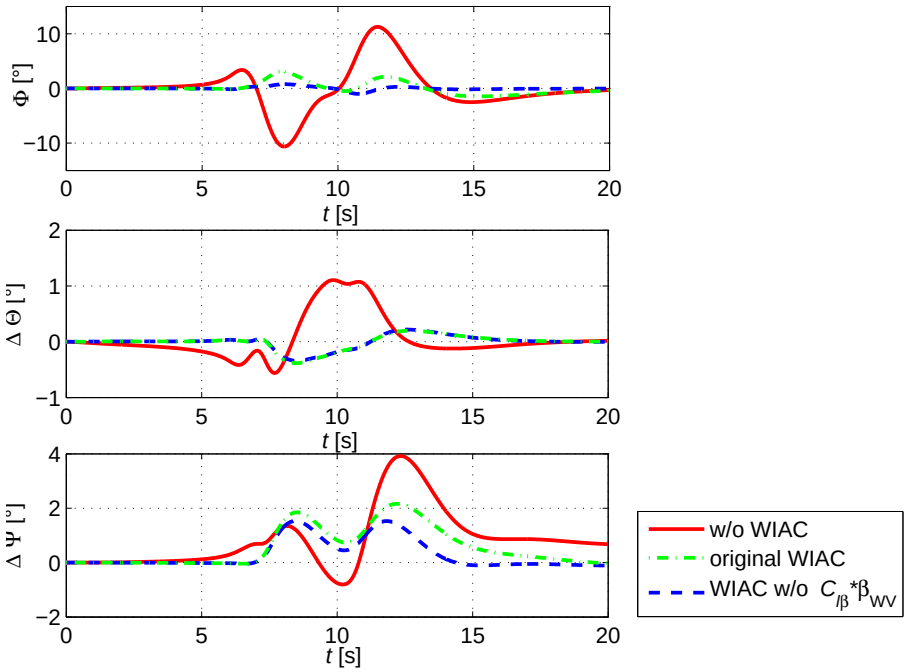

Figure 5.17: Reduction of wake-induced Euler angles for different implementations of WIAC: no WIAC (red solid line), WIAC with compensation of entire wake-induced rolling moment (green dash-dot line) and WIAC with compensation of rolling moment without sideslip-angle-induced component (blue dashed line)

A further improvement of the wake impact alleviation performance can be achieved by an improved combination of the WIAC and the basic control system in the directional axis. The conflict in the yaw axis of conflicting goals of the two control systems can be solved by adapting the command value of the yaw controller of the basic control system. In the normal implementation the basic yaw control system receives the pedal commands as the desired input value for the sideslip angle. The yaw controller thus tries to follow the sideslip angle command of the pilot, which is usually zero during flight[32], and minimizes occurring sideslip angle deviations. To achieve the desired behavior during a wake vortex encounter that the aircraft does not turn into the wind but performs as little yawing motion as possible, the wake-induced sideslip angle is added to the command value of the yaw controller as shown in Fig. 5.18. This way the yaw controller of the basic control system aims to keep the prevailing sideslip angle resulting from the wake vortex wind velocities in addition to the sideslip angle command by the pilot. If there is no pedal input, the yaw controller tries to keep the aircraft nose straight and to prevent any

[32] except for some special conditions such as e.g. a decrab maneuver at landing

yawing motion. This corresponds to the goal of the wake impact alleviation control system and the basic controller and WIAC do not interact unfavorably anymore.

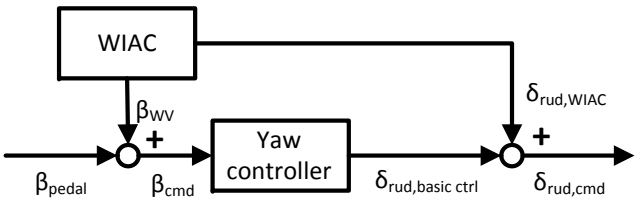

Figure 5.18: General concept for modification of yaw controller command value

The concept for the modification of the yaw controller command value presented in Fig. 5.18 assumes that the yaw controller is designed without a separate feedforward gain for the commanded sideslip angle as it would be the case for a simple P- or PI-control structure for the sideslip angle. The basic control system considered in this work, however, contains a separated feedforward gain, which is tuned to adjust the aircraft response to pedal inputs to the pilots' expected perception. This gain is higher than the gain of the proportional sideslip angle feedback. During the wake encounter the desired behavior is just that the basic controller maintains the wake-induced sideslip angle that affects the aircraft in that moment. The aircraft shall not capture a new commanded sideslip angle as it is the case for a pedal input. The wake-induced sideslip angle should thus not be applied with the feedforward gain tuned for an appropriate response to pedal inputs. Instead the wake-induced sideslip angle is only considered for the control of the error between the commanded sideslip angle and the corresponding feedback value of the estimated sideslip angle[33] β_{est}, as shown in Fig. 5.19. If there are no pedal inputs, the only difference between the wake-induced sideslip angle β_{WV} and the estimated sideslip angle β_{est} is the flight path sideslip angle β_{K}. So the basic controller aims to eliminate β_{K}, which corresponds to the desired behavior during a wake vortex encounter.

Figure 5.20 shows the influence of the modification of the yaw controller command value on the wake impact alleviation performance. If the wake-induced sideslip angle is added to the yaw control command value the heading deviation of the aircraft is further reduced. As the heading deviation is much smaller in magnitude than the roll excursion during a wake vortex encounter, the overall benefit of the adaptation of the yaw command value of the basic control system is smaller than the gain in roll performance thanks to the adaptation of the WIAC roll control command. So the more important aspect for an improved combination of the wake impact alleviation and the basic control system is to exclude the sideslip-angle-induced rolling moment component in the computation of countervailing control commands of WIAC.

The improvement of the wake impact alleviation performance for an improved combination of WIAC and the basic control system can also be seen by comparing the wake-induced moments and the commands produced by the control surfaces of the aircraft. Figures 5.21 to 5.22 show

[33] As described in section 4.1.1, the sideslip angle is estimated on the basis of the lateral acceleration measurements.

[34] The parameters x_p and x_r describe the integrated error of the bank angle deviation and the sideslip angle deviation from their command values respectively.

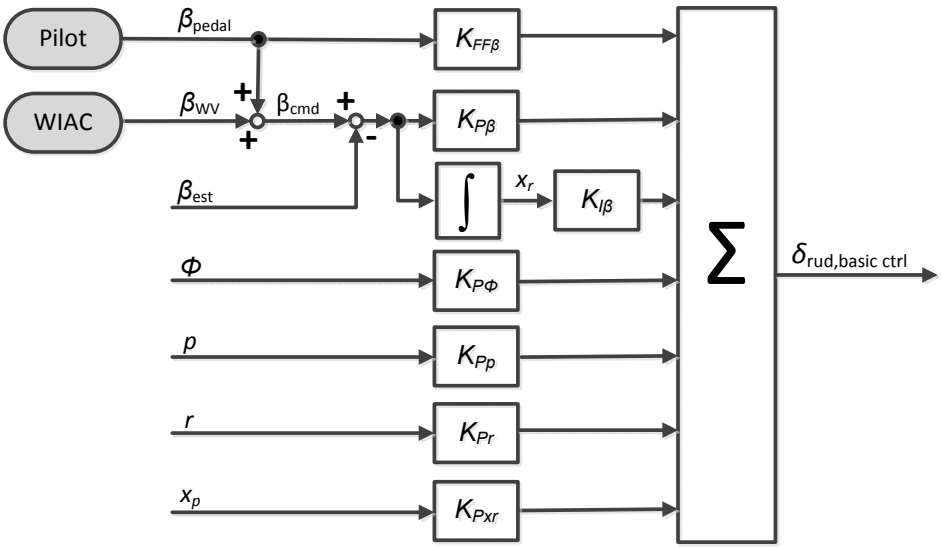

Figure 5.19: Detailed implementation of modification of yaw controller command value in basic control system[34]

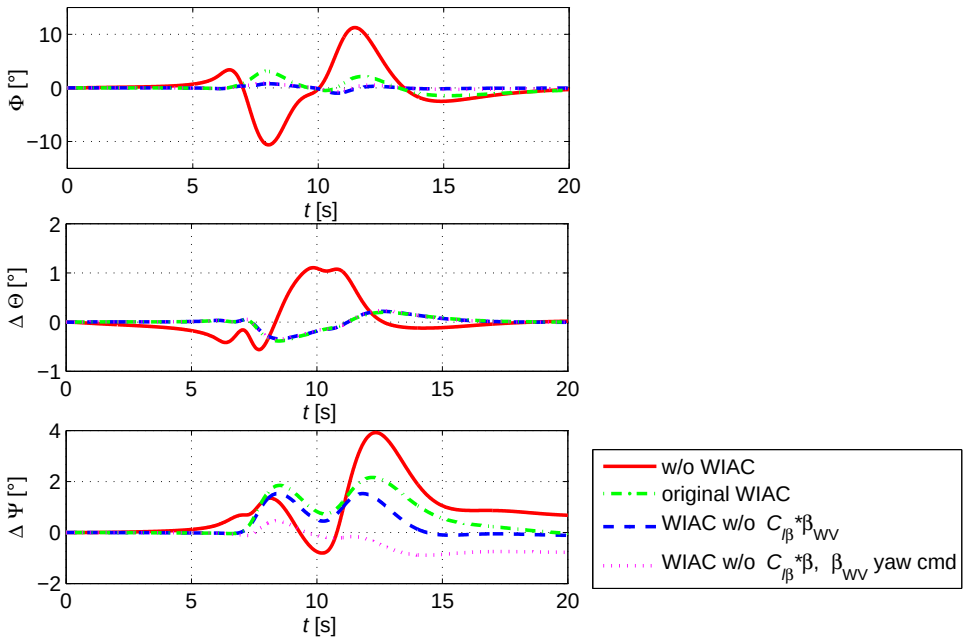

Figure 5.20: Reduction of wake-induced Euler angles for different implementations of WIAC: no WIAC (red solid line), WIAC with compensation of entire wake-induced rolling moment (green dash-dot line) and WIAC with compensation of rolling moment without sideslip-angle-induced component with regular yaw control command value (blue dashed line) and modified yaw command value (magenta dotted line)

this comparison for the different implementations of the wake impact alleviation control system in the overall control architecture for the 10° lateral encounter also shown in Fig. 5.20 and 5.17. The black solid lines depict the wake-induced moments. As we consider the case here that the wake vortex is ideally identified, these moments also correspond to the moments detected by WIAC and represent the basis for the determination of the control surface deflections commanded by the wake impact alleviation control system.[35] The red dashed line shows the negative of the moment produced by the control surfaces of the aircraft. The control surface deflections result from the commands of the WIAC and the basic control system as described above. If the negative moments produced by the control surface deflections correspond exactly to the wake-induced moments this means that the wake vortex disturbance can be perfectly compensated for.[36]

The comparison of Fig. 5.21 and Fig. 5.22 shows that the match of wake-induced rolling moment with the countervailing control surface deflections is improved if the sideslip-angle induced roll moment component is not considered twice. If the command value of the basic yaw controller is additionally adapted by adding β_{WV} to the pedal command, the match of the yaw moment can also be improved and the wake-induced rolling moment is almost ideally met by the moment of the control surfaces, as shown in Fig. 5.23.

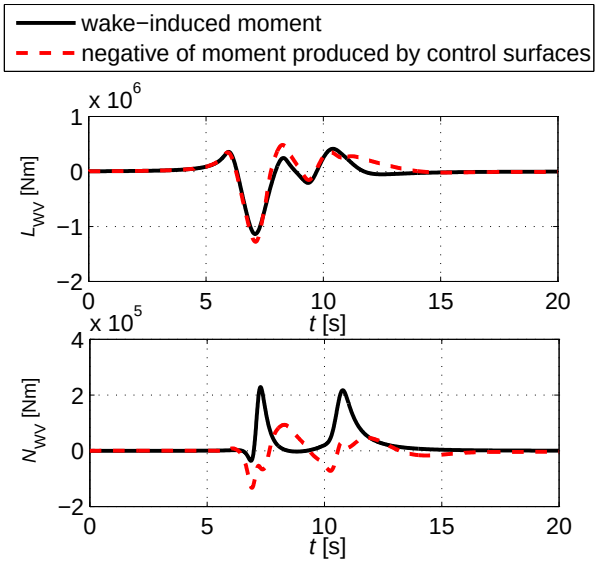

Figure 5.21: Comparison of moments resulting from wake vortex and control surface deflections for original WIAC implementation

[35] Minimal deviations can only occur due to the prediction of the strip position and the approximation of a fixed actuator delay of 0. 1 s, but the influence is negligible.

[36] under the assumption that there are no pilot inputs as it is the case here

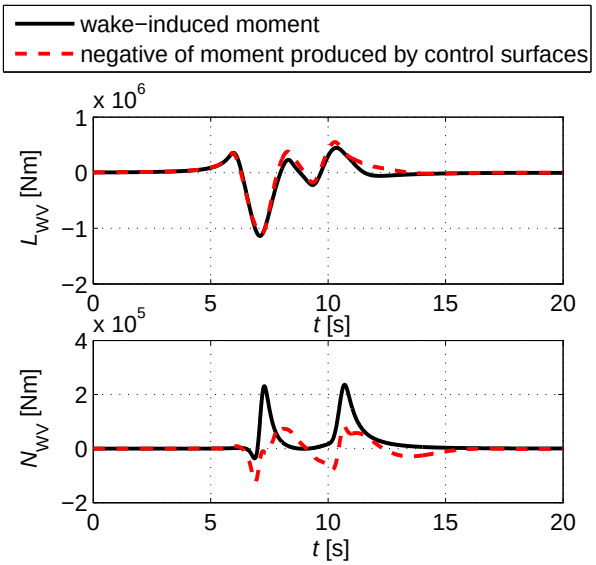

Figure 5.22: Comparison of moments resulting from wake vortex and control surface deflections for WIAC with compensation of rolling moment without sideslip-angle-induced component (regular yaw control command value for basic control system)

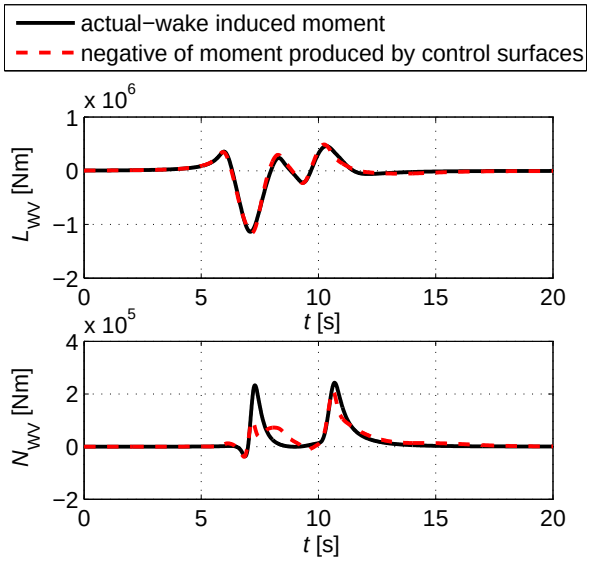

Figure 5.23: Comparison of moments resulting from wake vortex and control surface deflections for WIAC with compensation of rolling moment without sideslip-angle-induced component and modified yaw control command value for basic control system

The results show that the wake impact alleviation performance of the WIAC system is significantly improved if it is appropriately integrated into the overall flight system architecture. In order to improve the interaction of the wake impact alleviation and the basic control system

- the sideslip-angle-induced rolling moment component is excluded from the roll command computation of the WIAC module because it is already compensated by the basic control system,
- the wake-induced sideslip angle is used as a reference value for the yaw controller of the basic control system in order to prevent that the latter supports the natural weathercock of the aircraft, which turns the aircraft nose into the direction of the wind.

5.3.4 Further Possible Improvements for the Combination of Wake Impact Alleviation and Basic Control System

Section 5.3.2 showed that the wake impact alleviation and the basic control system pursue different goals in the longitudinal axis as well. This suggests a potential for an improvement of the wake impact alleviation by an enhanced combination of the two control systems in the longitudinal axis also. As the current work focuses on the lateral dynamics during the wake encounter, which are much stronger during encounters with small lateral encounter angles (cf. section 2.4), the combination of WIAC and the basic controller in the longitudinal axis is not further optimized in this work. Furthermore, Fig. 5.15 shows that the current combination works acceptably well and that the overall pitch disturbance is small anyway.

Another potential improvement could be achieved by a modification of the basic control system itself. Wake vortex encounters are currently not considered in the design of the control law of the basic control system. An adequate adaptation of the feedback gains during the encounter could improve the disturbance rejection of the basic controller and thus additionally alleviate the wake impact. If the feedback control has to react to the disturbance, this is always slower than a feedforward disturbance compensation such as the wake impact alleviation controller presented in section 5.3.1. Nevertheless, a significant wake impact alleviation performance improvement can be expected by an increase of the feedback gains. Especially the combination of increased feedback gains and the current disturbance rejection approach of the OWIDIA system seems to be a very promising approach that should be studied in future investigations. In this context, it should be considered that the increase of the feedback gains also implies stronger loads in the aircraft structure. The ideal solution would thus be to avoid a feedback controller with permanently increased gains but to adapted the feedback gains during the wake encounter only. In combination with the OWIDIA system this can easily be realized because the OWIDIA system includes the detection of a wake vortex and could trigger the gain adaptation in the basic control system. The design and analysis of such a combination of the OWIDIA system and the adaptation of the basic control system go beyond the focus of this thesis but should be investigated in future studies.

6 Separate Performance Analysis of Wake Impact Alleviation Control Module

The OWIDIA system consists of several modules and many elements with complex interdependencies. The overall performance of the system in terms of wake impact alleviation is not trivial to analyze and depends on a large number of parameters with usually nonlinear influences and also on the scenario of the wake vortex encounter itself. The purpose of the present and the following chapter is to provide insight in the overall system performance and its sensitivities. In order to deal with the complexity of the system, the problem is broken down and different aspects are analyzed separately as a first approach. In the present chapter the performance of the wake impact alleviation control (WIAC) module is investigated separately. In chapter 7 the performance of the whole OWIDIA system (including the wake identification by the OWI module) is analyzed.

6.1 Analysis of WIAC Performance with Ideal Wake Vortex Model

The main aspect influencing the performance of the OWIDIA system is expected to be the correct detection and characterization of the wake vortex. Only if the detected wake vortex corresponds well to the actual disturbance the control commands commanded by the WIAC system can successfully alleviate the wake-induced aircraft reaction. Note, however, that a perfect knowledge of the wake vortex does not guarantee a perfect compensation of the disturbance. As partly mentioned already in section 5.3.2, there are several reasons why a perfect wake impact alleviation is not achievable even in the case of an ideal wake vortex detection and characterization:

- Conventional control surface architectures with ailerons, rudder and elevators can only control three degrees of freedom whereas the disturbance occurs in all six degrees of freedom.
- The actuators of the control surfaces have maximum deflection limits and cannot be deflected instantaneously but exhibit dynamics with delays and rate limits.
- The prediction of the strip positions after the time delay between the control command generation and realization is usually imperfect since they are computed under the assumption of steady motion neglecting aircraft accelerations.
- The Aerodynamic Interaction Model (AIM) does not perfectly model the impact of the wake vortex on the aircraft.

The uncertainties in the AIM lead to uncertainties in the prediction of the wake-induced aircraft response and, hence, possibly to an impaired WIAC performance. The analysis of flight data suggests that the current version of the AIM shows an acceptable match with the true influence

of the wake vortex on the aircraft.[1] The error due to uncertainties in the AIM is thus expected to be small and will be neglected for the following analysis. The AIM applied within the wake impact alleviation control system and the AIM used in the simulation framework to model the impact of the wake vortex on the aircraft are identical. It has to be kept in mind that this represents a simplification and additional penalties of the wake impact alleviation performance may occur in real fight if an inaccurate AIM is used.

Figure 6.1 shows the encounter, already analyzed in sections 5.3.2 and 5.3.3, with a lateral encounter angle of $10°$ and a vertical encounter angle of $0°$.[2] For all encounters considered in the following, the improved WIAC[3] integration into the flight control architecture[4] is used and it is assumed that no autopilot or manual control inputs of the pilot are applied. Only the normal law and the WIAC system are active. The left hand side of Fig. 6.1 depicts the Euler angles of the aircraft during the encounter with and without the wake impact alleviation controller. This corresponds to the red solid and magenta dotted lines in Fig. 5.20. The right hand side of Fig. 6.1 demonstrates the deviation from the trimmed flight path during the encounter with and without WIAC.

Although an ideal wake impact alleviation cannot be expect for the reasons given above, the wake-induced attitude deviation as well as the lateral flight path deviation are significantly reduced thanks to the WIAC system. The vertical deviation from the trimmed flight path, however, increases when the wake impact alleviation controller is active. The maximum flight path angle deviation is increased from $-2.3°$ to $-3°$ and the maximum altitude deviation is increased from $6\,\mathrm{m}$ to $10\,\mathrm{m}$. As z_{NED} is defined positive downwards, the increase of the z-position means that the aircraft loses altitude, which is undesired and might, especially in approach close to ground, be critical. The absolute increase of $4\,\mathrm{m}$ is, however, still relatively small and thus not too critical in this case. The reason for the stronger altitude loss when WIAC is active can be explained by considering the wake-induced pitching moment and vertical force during the encounter, shown in Fig. 6.2.

A possible explanation for a larger flight path deviation could theoretically be a change in the wake-induced force and moment in the longitudinal axis resulting from a different flight evolution through the wake vortex when WIAC is active. When the same encounter scenario is considered with and without WIAC only the initial aircraft state and relative position and orientation between the wake vortex and the aircraft are identical in both cases. The evolution of the encounter is not the same because the mitigation of the wake-induced aircraft response by means of WIAC leads to a different flight path through the wake. It would thus be imaginable

[1] Fischenberg (2010), Paper presenting a method to validate wake vortex encounter models on the basis of flight test data.

[2] Generator aircraft is an Airbus A340. The wake vortex is located 2 m above the center of gravity of the aircraft.

[3] The expression WIAC is again used to emphasize that not the complete OWIDIA system including the online wake identification (OWI) is applied here, but only the WIAC module, which computes the control commands on the basis of the ideally known wake vortex disturbance in this case.

[4] I.e. WIAC does not consider the rolling moment component resulting from the wake-induced sideslip angle and the wake-induced sideslip angle β_{WV} is added to the pedal command value for the yaw controller of the basic flight control system, as described in section 5.3.3

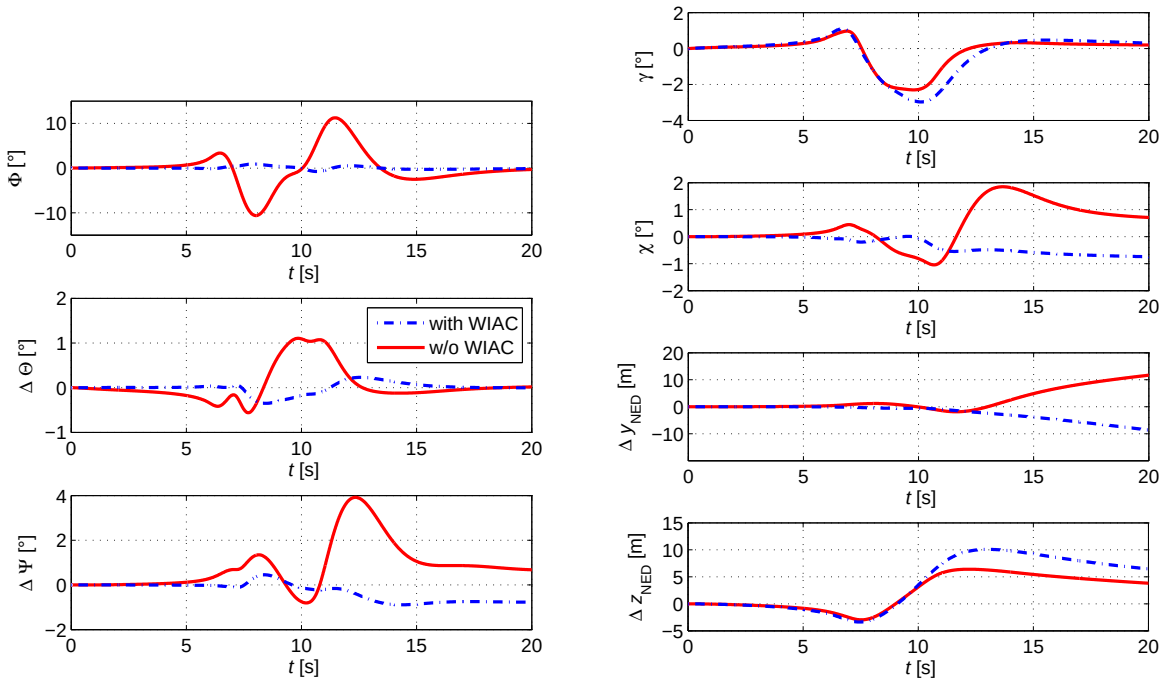

Figure 6.1: Comparison of Euler angles and flight path with and without WIAC for a 10° lateral encounter with ideally known wake vortex

that the different relative position between aircraft and wake leads to a considerably different wake-induced pitching moment and vertical force provoking a stronger longitudinal flight path deviation. However, Fig. 6.2 shows that the wake-induced disturbances M_{WV} and Z_{WV} are very similar in both cases.

Instead the reason for the increased altitude loss with WIAC can be attributed to the fact that only one control device is available and that it is not possible to compensate for both disturbances, pitching moment and vertical force, simultaneously. Concerning the vertical flight path deviation the wake-induced pitching moment and vertical force have partly compensating influences. The vertical force is positive and thus pushes the aircraft down, whereas the wake-induced pitching moment mainly leads to a pitch-up motion of the aircraft and this way counteracts the altitude loss. If the wake-induced pitch-up motion is reduced by the wake impact alleviation system, the aircraft sinks further down.

Whether the used alleviation strategy of compensating the pitch disturbance instead of the vertical disturbance is the optimal solution and to what extent an increase in altitude loss is acceptable in favor of a reduced pitch reaction, still needs to be investigated in a separate study. This thesis assumes that the rotational disturbance is most critical for the pilots and thus only pursues the approach of alleviating the wake-induced moments. An adaption of the alleviation strategy to vertical disturbances (if required) would, however, be possible as well.

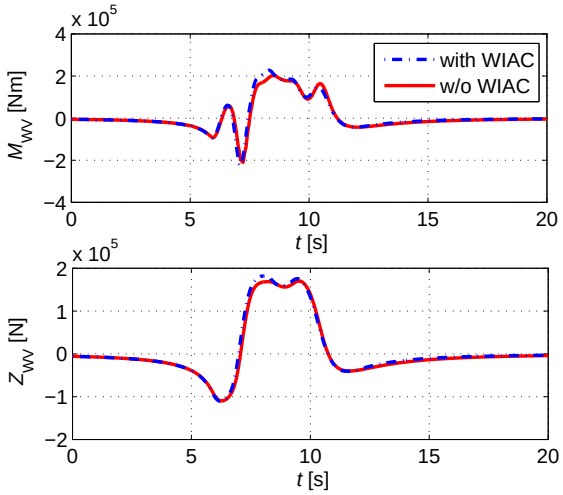

Figure 6.2: Wake-induced pitching moment and vertical force with and without WIAC for a 10° lateral encounter with ideally known wake vortex

The subplot of the lateral flight path deviation Δy_{NED} on the right-hand side of Fig. 6.1 shows that this lateral position error constantly increases even though the wake impact alleviation system is active. This results from the fact that the WIAC system does not contain any component that corrects the flight path (such as an autopilot for instance). The WIAC system only minimizes the wake-induced attitude deviations. If the heading and bank angle deviation is not perfectly compensated during the encounter and the aircraft flies into a different direction after the wake encounter, the WIAC system does not influence this flight path in any way. Such small flight path deviation can easily be corrected by the pilot in real flight. If an automatic correction of the wake-induced flight path deviations was desired, outer control loops could be added to the WIAC system. This is, however, not considered in this thesis.

In summary the wake impact alleviation control system can, under ideal conditions with a perfectly known wake vortex, almost perfectly alleviate the wake induced rolling and yawing motion during shallow wake vortex encounters. The wake-induced pitching motion is significantly reduced and generally small for shallow lateral encounter angles.
Due to the reduction of the wake-induced pitch-up moment without a simultaneous mitigation of the wake-induced vertical force the flight path deviation in downwards direction is larger with WIAC than without the wake impact alleviation control system. The need for a different alleviation strategy in the longitudinal axis for encounters very close to the ground should be investigated in future studies.

6.1.1 Influence of Encounter Geometry

The geometric setup of a wake vortex encounter, defined by the relative position and orientation of the wake vortex and the flight path of the aircraft, significantly influences the aircraft reaction during the encounter. As already described in section 4.4, only shallow encounter angles between the wake and the encountering aircraft, which are dominated by large aircraft reactions, are considered here. Encounter geometries with almost perpendicular encounter angles between

the flight path of the generator and follower aircraft, which mainly lead to structural impacts, are not assessed. However, even for relatively shallow encounter angles the aircraft reaction may vary markedly with varying encounter scenarios.

The lateral encounter angle mainly influences the duration of the wake vortex impact on the aircraft. A shallower encounter angle means that the aircraft remains longer under the influence of the wake vortex, which usually leads to larger aircraft reactions if no counter control actions are taken. Figure 6.3 shows the comparison of the wake-induced rolling moment for $5°$, $10°$, $15°$ and $30°$ lateral encounters of an A320 aircraft with an A340-size aircraft with no vertical encounter angle and $2\,\mathrm{m}$ altitude offset between the two aircraft (wake vortex above aircraft).

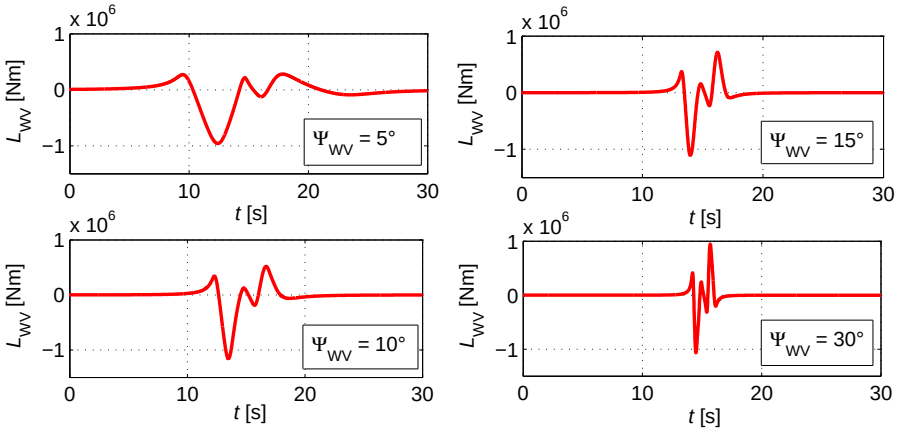

Figure 6.3: Wake-induced rolling moment for different lateral encounters with no vertical encounter angle and altitude offset

The wake-induced rolling moment has almost the same shape[5] for all four encounters but the frequency of the disturbance increases with increasing lateral encounter angle. The disturbance acts in a shorter time at larger encounter angles. This applies to the wake-induced forces and moments in all axes. Consequently the resulting aircraft motion is similar for all lateral encounter angles as well but smaller for steeper lateral encounters due to the reduced time it is exposed to the wake. So the steeper the lateral encounter angle the less critical is the wake-induced attitude change. This effect can be observed in Fig. 6.4. In the $5°$ lateral encounter angle case the maximum bank angle deviation without the WIAC system is $-12°$. Noticeable attitude changes occur already at $t = 5\,\mathrm{s}$ and last up to $t = 30\,\mathrm{s}$ here. In the $\Psi_{\mathrm{WV}} = 40°$ case the maximum angle is only $-2°$ and the attitude deviations are limited to the time between $t = 13\,\mathrm{s}$ and $t = 20\,\mathrm{s}$.

At the same time the wake impact alleviation control system becomes less effective when the lateral encounter angle increases. The reason for the performance reduction lies in the actuator dynamics. Due to their time delays as well as rate and deflection limits, the actuators are not able

[5] Slight deviations in the shape and amplitude of the disturbance result from the different flight paths through the encounter. At shallower encounter angles the aircraft deviates stronger from its trimmed flight path than for steeper encounters with shorter endurance. It thus meets slightly different disturbance velocities.

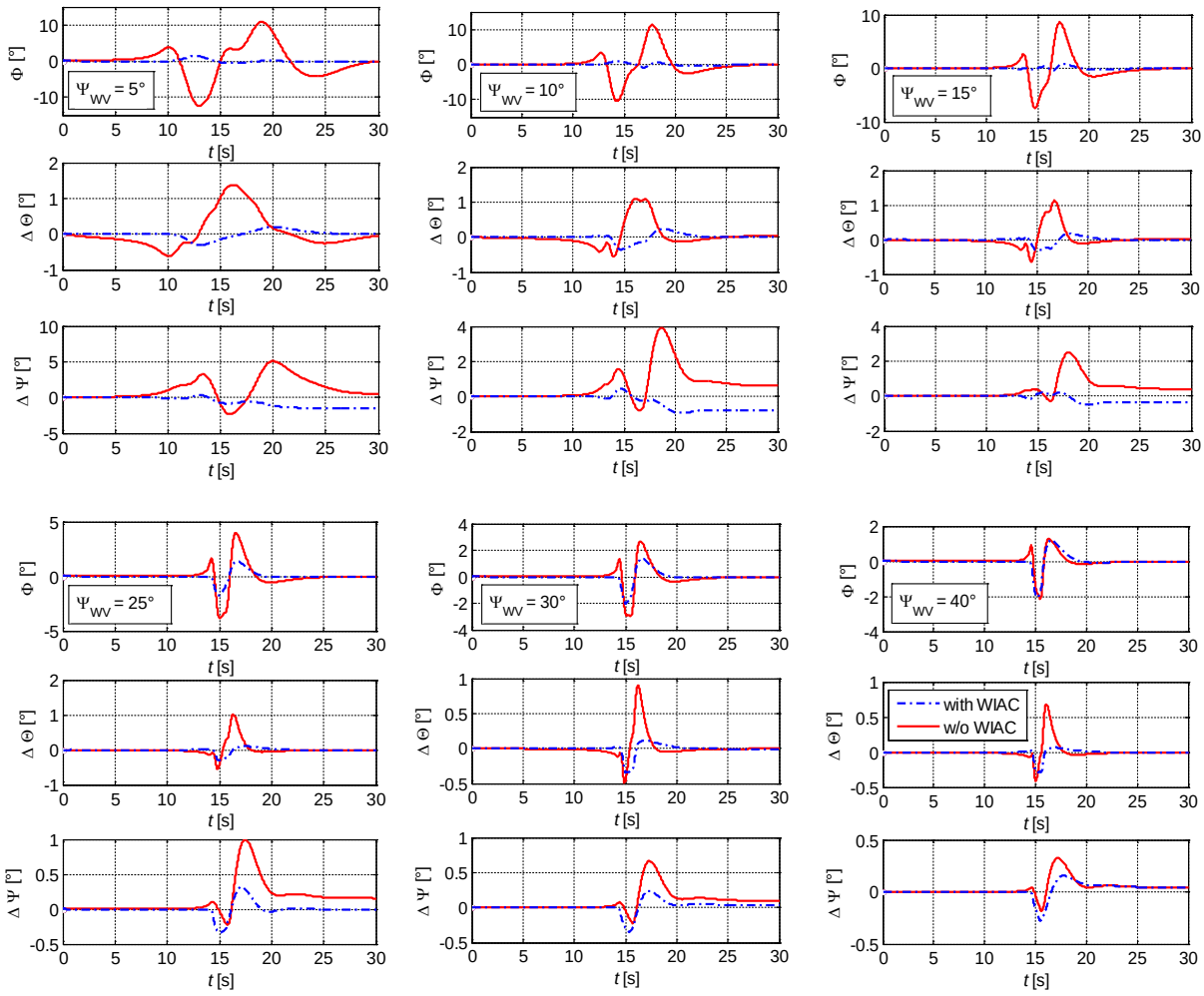

Figure 6.4: Comparison of Euler angles with and without WIAC for different lateral encounter angles

to perfectly follow any arbitrary movement commanded by the control system. When the disturbance moments change very rapidly during steep encounters and the WIAC thus commands very dynamic control surface deflections, these commands cannot be followed. Figures 6.5 to 6.7 depict the aileron, elevator and rudder deflections and their first derivatives for $10°$, $15°$ and $30°$ lateral encounters. The red dashed lines indicate the corresponding actuator limits. The limits represent typical values for modern transport aircraft such that the results obtained here can be considered as representative trends for other civil transport aircraft as well. At $10°$ lateral encounter angle the deflection rate stays well below the limits and the actuators can easily realize the commanded control surface deflections. At $\Psi_{WV} = 15°$ the rate limits of the elevator and aileron are sometimes reached. But the comparison with Fig. 6.4 shows that the performance of the WIAC system is hardly impaired. At $\Psi_{WV} = 30°$, however, the actuators frequently hit their rate limits. This leads to a significantly reduced mitigation of the wake-induced Euler, as shown in Fig. 6.4. At $\Psi_{WV} = 30°$ the relative reduction of Euler angle is much lower than in cases with shallower lateral encounter angles. The maximum bank angle is only reduced by $32\,\%$ compared to the same encounter without WIAC. At $\Psi_{WV} = 40°$ the WIAC system has no benefit anymore. The maximum bank angle cannot be reduced compared to the case without WIAC because the changes in the disturbance are too rapit. As the occurring attitude changes are generally only very small in magnitude, an additional reduction by WIAC is not necessary here such that the impaired performance of the system at steep encounter angles is uncritical.

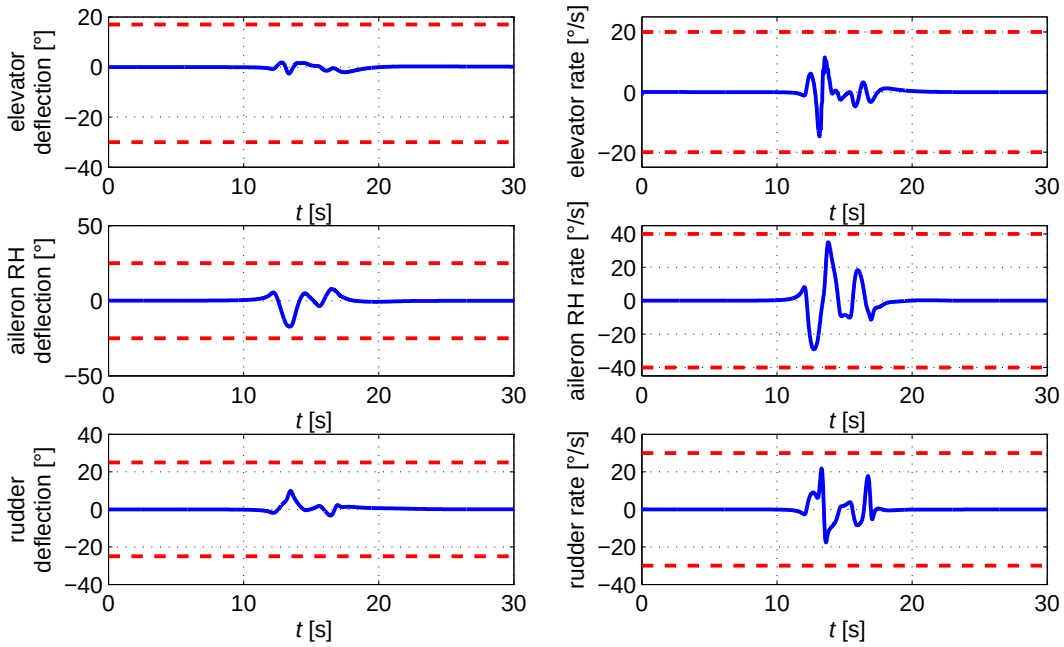

Figure 6.5: Control surface deflections and rates (blue solid linies) with corresponding actuator limits (red dashed lines) for a $10°$ lateral encounter

Other parameters of the geometric setup of the encounter such as the vertical encounter angle Θ_{WV}, the vertical offset between the wake vortex and the aircraft, and the lateral offset have only minor influence on the shape of the aircraft reaction. If the vertical encounter angle is

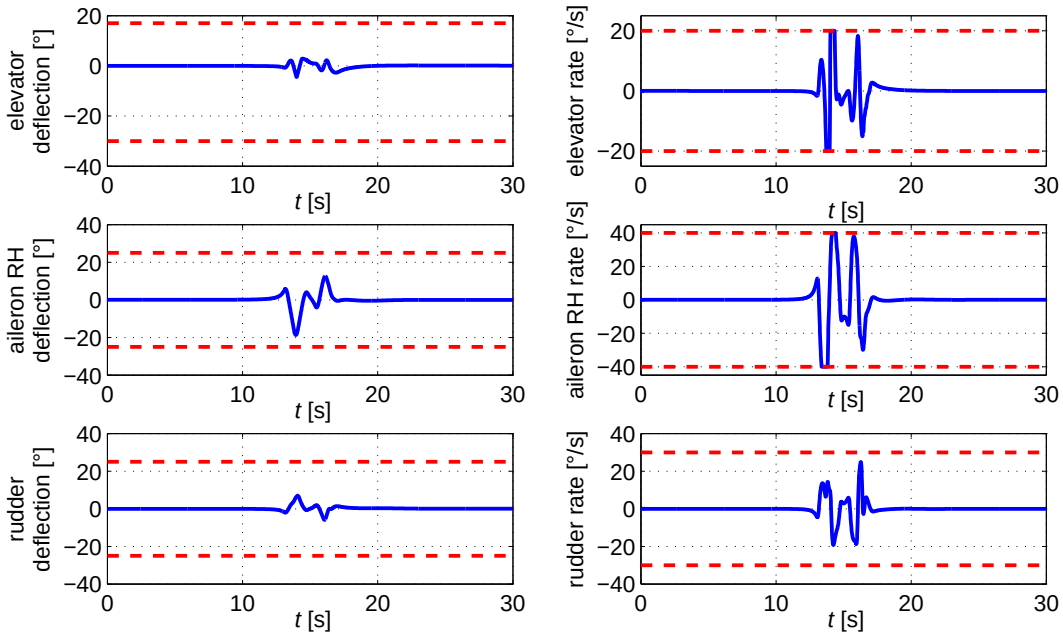

Figure 6.6: Control surface deflections and rates (blue solid linies) with corresponding actuator limits (red dashed lines) for a 15° lateral encounter

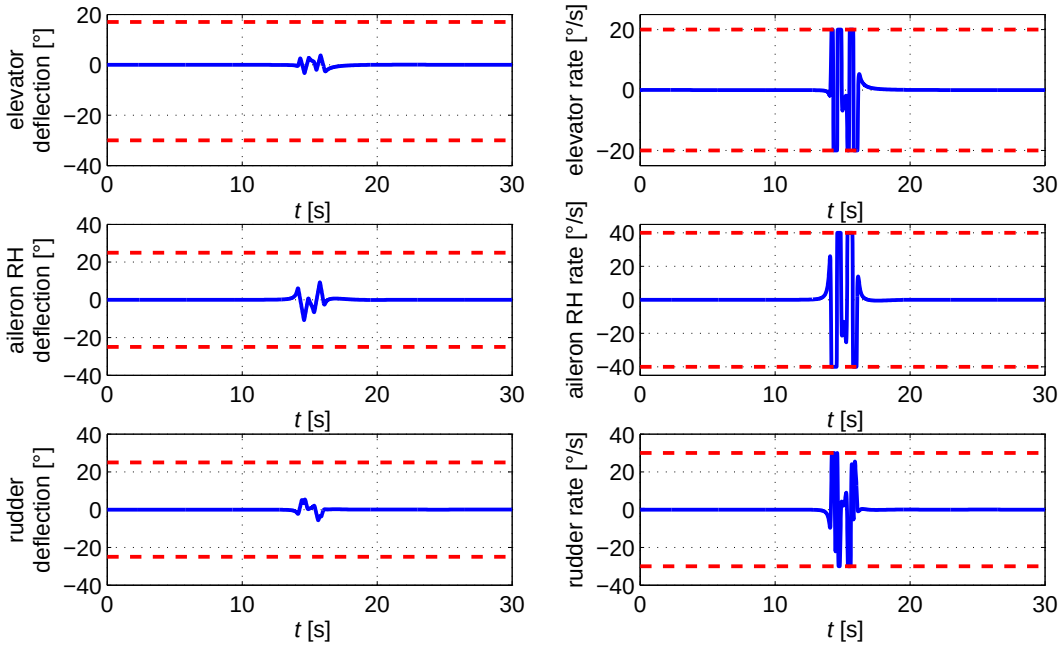

Figure 6.7: Control surface deflections and rates (blue solid linies) with corresponding actuator limits (red dashed lines) for a 30° lateral encounter

nonzero the magnitude of the attitude deviation declines because the time period during which the aircraft is close to the wake vortex is shorter. Similarly to the lateral axis, the effect becomes stronger for steeper vertical encounter angle. Only a comparably small negative vertical encounter angle such as -3° can increase the wake-induced attitude change. The wake-induced aircraft movement in downwards direction leads to the effect that the aircraft flies almost parallelly to the wake for a certain time and is hence influenced by it for a longer period of time. Very large vertical encounter angles are very unlikely and not considered any further. As usual flight procedures of regular transport aircraft do not include very strong climb or descent maneuvers, the vertical flight path angle between two different aircraft and consequently the relative vertical encounter angle between an aircraft and the wake of another aircraft is not expected to be extremely large.

The vertical and lateral offset between the aircraft and the wake vortex influence mainly the magnitude of wake-induced aircraft response. In principle, a larger distance from the vortex centerline leads to a reduction of the wake-induced wind velocities and consequently of the wake-induced aircraft motion. In the lateral axis, however, the distance between the two vortex cores has to be considered as well. If the main part of the aircraft is influenced by the port vortex and parts of the aircraft (such as e.g. one wing) reach into the area of the wind velocities of the counter rotating starboard vortex (or vice versa), the impact of the wake on the rotational aircraft motion is reduced.

The wake impact alleviation performance of the WIAC system is not significantly influenced by the vertical encounter angle or the vertical offset between the wake and the aircraft. As long as the lateral encounter angle does not become too steep the WIAC system performs well independently of the other geometric parameters of the encounter.

The analysis shows that the lateral encounter angle has a strong influence on the achievable wake impact alleviation performance.

- For steep lateral encounter angles the rate limits of the aileron actuators are reached such that the bank angle reduction by the WIAC system is impaired.
- For the analyzed A320 aircraft the wake impact alleviation system has no real benefit anymore from lateral encounter angles of 30° on and becomes ineffective with respect to the bank angle alleviation at 40° lateral encounter angle. For other civil transport aircraft, the lateral encounter angles at which the wake impact alleviation system becomes ineffective can be expected at very similar values of the lateral encounter angle.
- The wake-induced bank angle during such steep lateral encounters, in which the wake impact alleviation does not work any more, are small and thus uncritical anyway.

6.1.2 Influence of Vortex Strength

The strength of a wake vortex mainly depends on the size and mass of generator aircraft as well as the vortex age. It is expressed by the vortex circulation Γ, which is directly proportional to the wake-induced tangential velocity at a given distance (cf. section 2.3). In the previous

sections the considered vortex has always been the wake of a A340-400 with a vortex strength of $70\,\%$ of its initial circulation Γ_0. Assuming atmospheric conditions with the slowest vortex decay (i.e. no turbulence in the atmosphere and neutral strification) this corresponds to a vortex age of $200\,\mathrm{s}$ and a distance of approximately $7.6\,\mathrm{NM}$ for a generator aircraft with a true airspeed of $70\,\mathrm{m/s}$. If the distance between the generator and the encountering aircraft decreases or the generator aircraft is heavier, the strength of the encountered vortex increases. In order to assess how an increase in vortex strength influences the wake impact alleviation performance the vortex circulation is artificially increased. Regardless of the physical origin of the circulation, such as e.g. a variation of generator mass or vortex age, the circulation itself is directly varied. Table 6.1 gives an overview of the vortex circulations considered in this section and the corresponding maximum roll control ratios RCR. The encounter scenario is always a horizontal encounter during approach with $10°$ lateral and $0°$ vertical encounter angle. The encountering aircraft is an Airbus A320 with flap configuration 3 and an airspeed $150\,\mathrm{KIAS}$ flying $2\,\mathrm{m}$ below the vortex cores. The first case with a circulation of $340.66\,\mathrm{m^2/s}$ corresponds to the encounter scenario analyzed in the previous sections with an A340-400 as generator aircraft and a circulation of $70\,\%$ of the initial vortex circulation.

The shown $\mathrm{RCR_{max}}$ is the maximum value of the roll control ratio that occurs during the wake vortex encounter with the denoted circulation and without the WIAC system. The $\mathrm{RCR_{max}}$ occurring when the WIAC system is active can slightly vary due to the different flight path with the reduced aircraft reaction, but the differences are small in the considered cases. For the computation of the RCR a maximum roll control power of $C_{l_{\xi_{\max}}}$ of -0.2094 is assumed. This value is relatively high compared to literature values of maximum roll control powers of different aircraft types, which are usually in the range of -0.05 to -0.15. The high $C_{l_{\xi_{\max}}}$ results from the fact that the roll spoilers, which have a high effectiveness, are applied. In this thesis it is assumed that the roll spoilers are always applied in order to get as much roll control power as possible. It has to be kept in mind that this might lead to large flap loads, which should be checked before the application in real flight. The aerodynamic effectiveness of the aileron and roll spoilers implemented in the A320 model, however, is not finally validated. The spoiler effectiveness is modeled linearly up to the maximum deflection of $35°$. Especially at very large deflection angles the roll effectiveness of the spoilers will probably be reduced in reality. The true RCR is thus expected to be a little higher than the values shown in table 6.1. The deployed values match with the aircraft model the simulations are based on and are thus the relevant numbers for the following results. These results should, however, be taken with caution because the roll control power of the encountering aircraft might be slightly overestimated.[6]

The circulation considered for the sensitivity analysis is increased up to comparably large values. A Boeing 747-400 with a maximum landing weight of $296\,\mathrm{t}$, a wing span of of $64.9\,\mathrm{m}$ and an approach speed of $81\,\mathrm{m/s}$ leads to an approximate maximum circulation of $550\,\mathrm{m^2/s}$ and an Airbus A380-800 with a maximum landing weight of $395\,\mathrm{t}$, a wing span of of $79.8\,\mathrm{m}$ and an approach speed of $71\,\mathrm{m/s}$ delivers a maximum circulation of about $680\,\mathrm{m^2/s}$ at the considered altitude of $2000\,\mathrm{ft}$, whereupon these values of the vortex circulation are only achieved

[6] There might be small deviations in the absolute values, however, the trend is modeled correctly.

right after the formation of the wake vortex and decrease with increasing vortex age.[7,8] So the largest circulation of table 6.1 with $850\,\mathrm{m}^2/\mathrm{s}$ exceeds the vortex strength that could be expected under realistic circumstances for this flight condition. In contrast to the roll control authority the values for the maximum vortex circulation are thus conservative.

Table 6.1: Values of circulation and corresponding maximum RCR for vortex strength sensitivity study

Circulation Γ [m^2/s]	**$\mathrm{RCR}_{\mathrm{max}}$**
340.66	0.74
450	0.94
550	1.08
650	1.18
750	1.27
850	1.33

Figure 6.8 shows the time histories of the Euler angles during the $10°$ lateral encounter with and without the wake impact alleviation system for the different vortex circulations. The red lines in Fig. 6.8 correspond to the Euler angles shown in Fig. 6.1. As expected, the wake-induced attitude deviation increases with rising circulation if the WIAC system is not active. The maximum Euler angles with an active WIAC system, arising from the imperfect alleviation of the WIAC, increase as well with rising circulation. Notice the different scales of the y-axes of the plots with and without WIAC in this context. In comparison to the increase of the maximum bank angle without WIAC, the relative increase of the maximum attitude deviations with WIAC is larger. This is particularly visible in Fig. 6.9, which illustrates the reduction of the maximum Euler angles with an active WIAC system relative to the maximum Euler angles without the WIAC system. When the circulation increases from $340.66\,\mathrm{m}^2/\mathrm{s}$ to $850\,\mathrm{m}^2/\mathrm{s}$, the maximum bank angle without WIAC rises from $11.3°$ to $19.0°$ and the bank angle with WIAC from $1.0°$ to $2.8°$. This denotes a reduction of the maximum bank angle by $91\,\%$ in case of a circulation of $340.66\,\mathrm{m}^2/\mathrm{s}$ and by only $85\,\%$ in case of the $850\,\mathrm{m}^2/\mathrm{s}$ circulation. Moreover the bank angle response with active WIAC system develops an additional minimum with increasing circulation. These two effects result from actuator limits that are reached when the vortex strength grows.

Figure 6.10 illustrates the respective control surface deflections and their first derivative during the encounters with different circulations when the WIAC system is active. The red horizontal lines mark the deflection and rate limits of the different control surfaces. For the rudder the red solid lines depict the maximum possible deflection. The effective deflection limit of the rudder depends on the current airspeed. It is marked by the red dashed lines in Fig. 6.10. As a stronger wake vortex with larger disturbances moments requires larger control surface deflections the risk to hit the actuator limitations increases with rising circulation. In case of $450\,\mathrm{m}^2/\mathrm{s}$ circulation the aileron rate limits are reached for a short time. This already leads to a reduction of the wake the wake impact alleviation performance, as can be seen in Fig. 6.9. As the circulation

[7] Airbus (2015), Section 3.5.0, Airbus A380 manual about aircraft characteristics.
[8] Boeing (2011), Table of aircraft data of different Boeing aircraft.

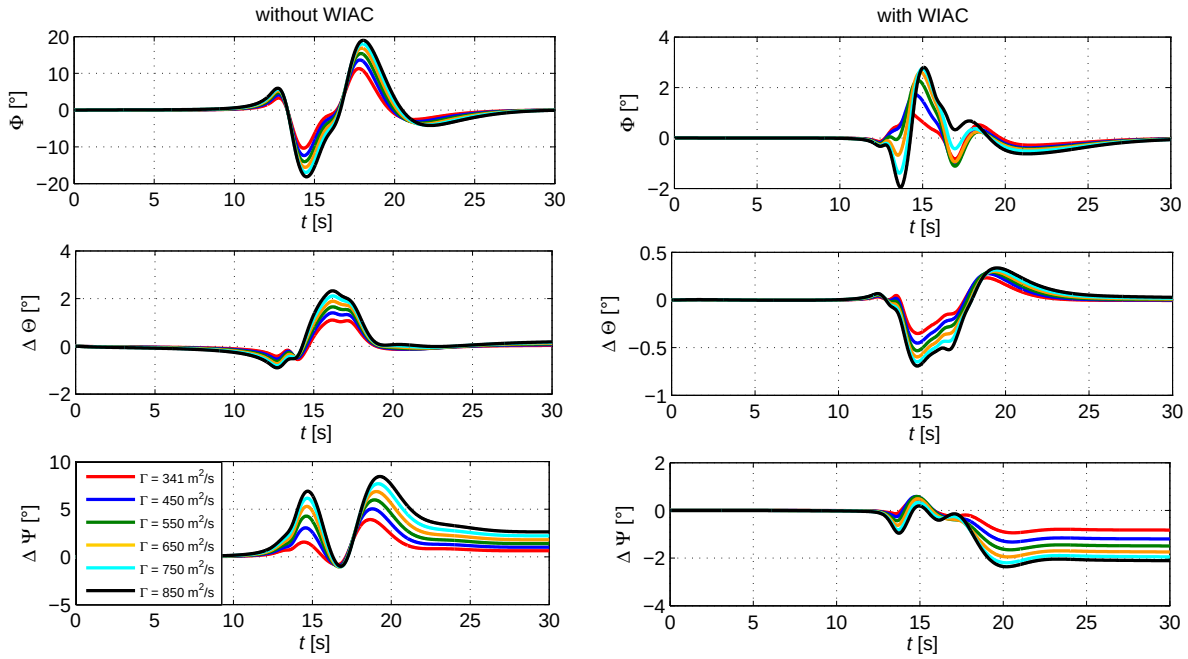

Figure 6.8: Euler angles during 10° lateral encounters with different circulations

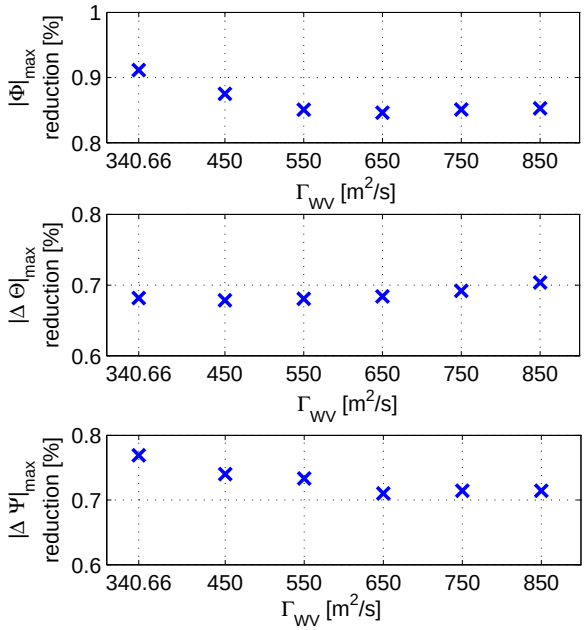

Figure 6.9: Relative reduction of maximum Euler angles with WIAC compared to maximum angles without WIAC during 10° lateral encounters with different circulations

is further increased the aileron rate limits further deteriorate the alleviation performance. For circulations of $650\,\mathrm{m}^2/\mathrm{s}$ and larger the aileron deflection limit is reached between $13\,\mathrm{s}$ and $14\,\mathrm{s}$. This is the reason for the additional negative bank angle deviation, which arises at about $14\,\mathrm{s}$ in the case with WIAC for circulation values larger than $450\,\mathrm{m}^2/\mathrm{s}$. An aileron deflection of more than +/-$25°$ would be needed to compensate for the negative wake-induced rolling moment. As this roll control power is not available the remaining disturbance moment causes the observed rolling motion to the left.

The elevator reaches neither its deflection nor its rate deflections. The wake impact alleviation performance is thus not reduced if the vortex strength is increased ($68\,\%$ bank angle reduction in case of $\Gamma = 341\,\mathrm{m}^2/\mathrm{s}$ and $70\,\%$ bank angle reduction in case of $\Gamma = 850\,\mathrm{m}^2/\mathrm{s}$). The rudder also increasingly hits its rate limits with increasing vortex circulation and in case of $\Gamma = 850\,\mathrm{m}^2/\mathrm{s}$ also slightly its deflection limits, which leads to an impairment of the reduction of the heading change from $77\,\%$ in case of $\Gamma = 341\,\mathrm{m}^2/\mathrm{s}$ compared to $71\,\%$ bank angle reduction in case of $\Gamma = 850\,\mathrm{m}^2/\mathrm{s}$.

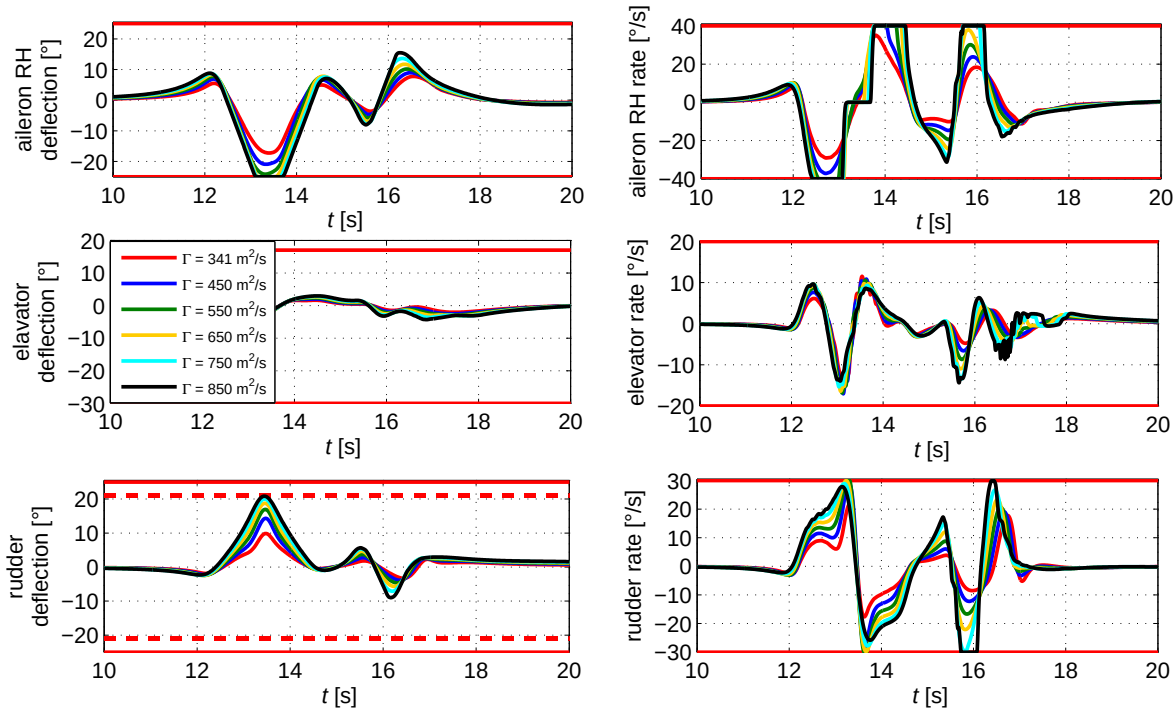

Figure 6.10: Control surface deflections during $10°$ lateral encounters with WIAC for different circulations

Even though an impairment of the reduction of the wake-induced attitude deviation can be noticed when the circulation is artificially increased, the overall alleviation performance is still very good ($85\,\%$ bank angle reduction and $88\,\%$ reduction of the heading change) even for strong vortices with a circulation of $850\,\mathrm{m}^2/\mathrm{s}$. As mentioned before these results and the absolute values of this study have to be considered with caution because the underlying roll control power of the aircraft might be too optimistic. Nevertheless, the analysis correctly models the trends for an increase of vortex circulation. If the encountering aircraft had a considerably lower

control power, obviously the wake impact alleviation would not work anymore at some point. It should thus always be pursued to apply as much roll control power as available (e.g. by using roll spoilers and all accessible roll control surfaces).

The alleviation performance of the WIAC system with varying vortex strength based on the considered A320 model works well up to very strong wake vortices with a circulation of $850\,\mathrm{m}^2/\mathrm{s}$ (which exceeds the vortex strength of modern large transport aircraft) and is not significantly impaired by the actuator deflection limits. However, this behavior is, of course, strongly dependent on the available roll control power of the encountering aircraft and could be worse for aircraft types with very poor roll control power.

6.2 Sensitivity of Wake Impact Alleviation Performance with respect to Wake Vortex Parameter Accuracy

If the wake impact alleviation is applied as a last step of the complete OWIDIA workflow it will be based on the wake characterization made by the OWI module and the wake vortex parameters will obviously never perfectly describe the actual wake vortex. Even in an artificial simulation framework, where the aircraft encounters an analytical Burnham-Hallock wake vortex, which is also used as a wake vortex model within the OWI, the estimated parameters will usually exhibit deviations from the actual wake vortex parameters because the wind measurements provided as input for the OWI contain measurement noise. Under real flight conditions, the wake vortex model including the estimated parameters of the OWI can be expected to match even less with the true wake vortex due to errors of the wake vortex model itself. A true wake vortex is never shaped perfectly such as an analytical Burnham-Hallock model. With increasing vortex age these differences increase because the wake vortex starts to deform and deviates even stronger from the straight vortex pair of the Burnham-Hallock model (cf. section 2.2).

Errors in the wake characterization obviously impair the wake impact alleviation performance of the OWIDIA system. To get insights of the dependency of the wake impact alleviation performance on the different parameters of the wake vortex model a sensitivity study is performed. The sensitivity study is very similar to the study presented in *Ehlers, Niedermeier, and Fischenberg (2015)*[9], but the former sensitivity study did not include the improved implementation of the WIAC module in the overall fly-by-wire control architecture yet (cf. section 5.3.3) and was performed for a different encounter angle. The general trends are, however, the same.

The sensitivity study shown hereafter considers a lateral encounter scenario during approach with 10° lateral and no vertical encounter angle. The generator aircraft is again an Airbus A340. The encountering aircraft is an Airbus A320 in manual flight condition with active normal law, autopilot disengaged and no pilot inputs during the encounter. During this encounter scenario the performance of the wake impact alleviation is analyzed for different errors of the parameters of the identified wake vortex. In this sensitivity study the errors of the different pa-

[9] Ehlers, Niedermeier, and Fischenberg (2015), Paper presenting an airborne, lidar-based wake identification algorithm and a control system to alleviate the detected wake vortex.

rameters are varied separately. In reality the estimation errors usually occur simultaneously. A separately variation analysis such as the present study cannot directly predict resulting effects of simultaneous errors. However, it can provide an impression of the main sensitivities of the wake impact alleviation concerning the errors of the estimated wake vortex parameters and give hints for the required accuracy of the identified wake vortex model. Figure 6.11 to 6.14 illustrate the sensitivity of the attainable reduction of the maximum bank due to WIAC with respect to varying errors of the different wake vortex parameters.

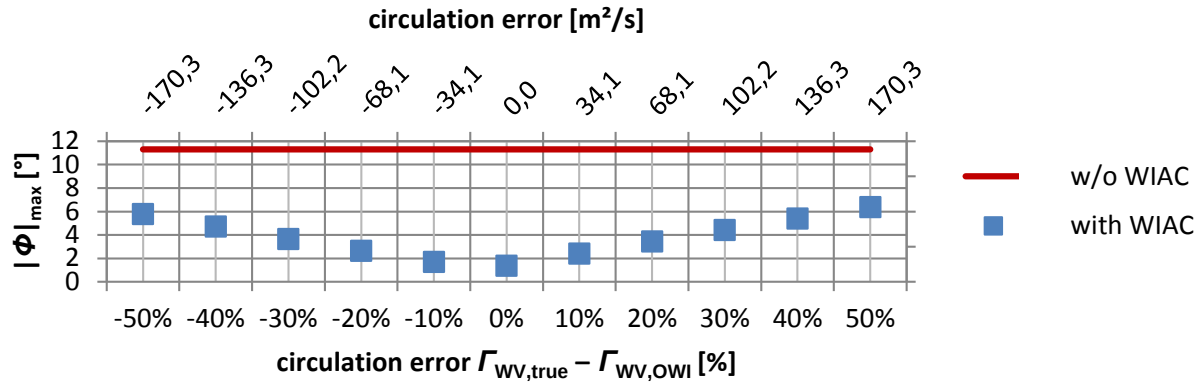

Figure 6.11: Impairment of the reduction of the maximum bank angle amplitude by the wake impact alleviation controller due to errors of the identified vortex circulation

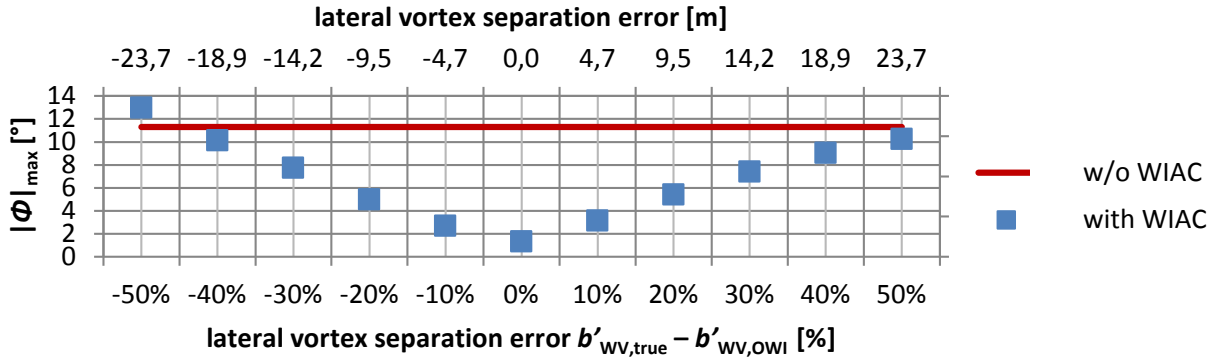

Figure 6.12: Impairment of the reduction of the maximum bank angle amplitude by the wake impact alleviation controller due to errors of identified the lateral vortex separation

The comparison of the influence of the errors of the identified vortex circulation in Fig. 6.11 and of the identified lateral separation of the vortex cores in Fig. 6.12 shows that the effect of deviations from the true vortex circulation concerning the attainable bank angle alleviation is comparably low. Errors of the vortex strength of +/-50 % still lead to a relatively small impairment of the reduction of the maximum bank angle, whereas 50 % deviation from the true lateral vortex separation already eliminates the benefit of the wake impact alleviation controller and $-50\,\%$ error of the lateral vortex separation even leads to an aggravation of the maximum bank angle during the encounter. The reason for the relatively low influence of errors of the

vortex circulation is that the circulation only modifies the strength of the disturbance velocities but does not influence the shape of the disturbance. Values of the vortex circulation that are estimated higher or lower than the true values effect that the WIAC commands too high or too low control surface deflections but still generates its commands at the correct point in time and in the correct deflection direction. If the lateral distance of the vortex cores is estimated too short or too long, in contrast, the shape of the disturbance moments is influenced and the temporal development of the disturbance affecting the aircraft does not stay the same. This can lead to the effect that WIAC can command control surface deflections which do not match to the disturbance time history. In the worst case it might command deflections into the incorrect direction and aggravate the maximum bank angle during the encounter.

Similarly to the lateral separation of the vortex cores, the precision of the identified position of the vortex centerline also has a strong influence on the success of the wake impact alleviation. Especially the lateral position of the vortex centerline needs to be estimated very accurately by the OWI in order to allow a good alleviation performance. Errors greater than +/-10 m already provoke an aggravation of the maximum bank angle (cf. Fig. 6.13). Control surface commands of incorrect signs occur very easily if the lateral position of the wake vortex is predicted incorrectly because this corresponds to a temporal shift of the detected wake-induced moments compared to the actual disturbance moments. For the considered lateral encounter with $10°$ encounter angle and an airspeed of 150 KIAS, 10 m lateral position error corresponds to a time shift of the disturbance of 0.75 s.

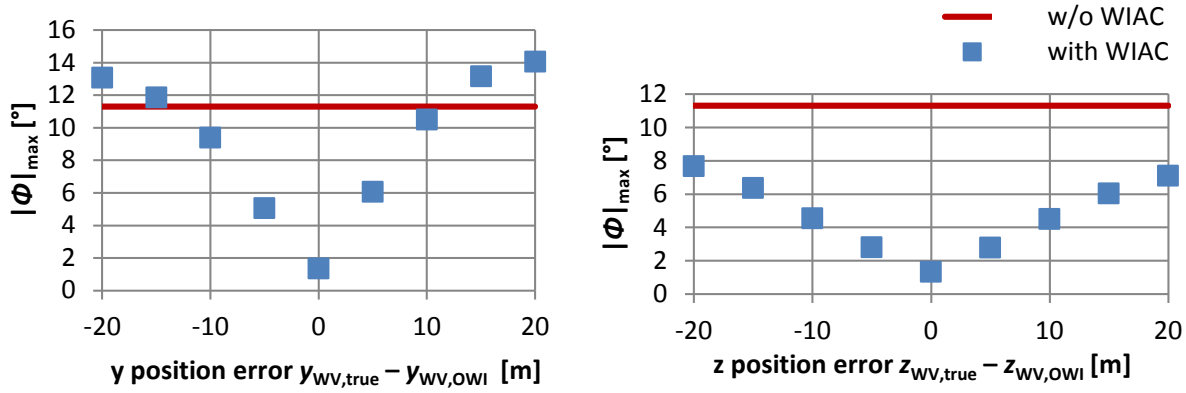

Figure 6.13: Impairment of the reduction of the maximum bank angle amplitude by the wake impact alleviation controller due to errors of the position of wake vortex centerline

Compared to errors of the identified lateral vortex separation, deviations of the lateral position of the vortex centerline lead to a stronger impairment of the alleviation performance of the WIAC. On the one hand, this results from the fact that errors of the lateral vortex separation are assigned to two vortex cores. An error of 10 m of the lateral vortex separation means that each vortex position is located 5 m besides its true position. An error of 10 m of the lateral position of the vortex centerline, however, means that each vortex core is shifted by 10 m compared to its actual location. On the other hand, the lateral position error of the vortex centerline provokes a complete temporal shift of the original disturbance, whereas the error of the lateral separation of the cores changes the shape of the disturbance because the sum of the wake-induced velocities

at each position varies if the distance of the vortex cores varies. In case of the temporal shift of the disturbance moments the risk of commanding aggravating control commands is even higher than in case of a modified distance shape.

In the vertical direction the alleviation performance of the WIAC is less sensitive to errors of the position of the vortex centerline. With +/-20 m error the WIAC can still reduce the maximum bank angle during the encounter. The lower sensitivity compared to errors in the lateral vortex positions results from the fact that the vertical position error does not provoke a time shift of the disturbance but again only influences the shape of the disturbance moments. The strongest influence occurs with respect to the yawing moment, which changes its sign if the vertical wake vortex position is identified on the opposite side of the aircraft. The rolling moment only varies in magnitude but keeps its original shape. As the wake-induced rolling moment is the main cause for the wake-induced rolling motion, this explains the lower impairment of the bank angle alleviation in case of errors of the vertical compared to the lateral wake position. However, it should be kept in mind that for encounter scenarios with very large vertical offsets between the wake vortex and the aircraft, a too closely detected vertical vortex position might provoke an overcompensation of the wake-induced rolling moment by too large control command deflections and thus lead to an increase of the bank angle compared to the case without the wake impact alleviation control.

The lateral and vertical distance between the aircraft and the wake vortex and the orientation of the wake vortex are parameters that are closely coupled as already explained in section 5.2.3. In the present analysis, the variation of the error of the lateral and vertical encounter angle is realized in that way that only the encounter angle is changed. The position of the vortex centerline is adapted such that the intersection of the trimmed flight path and the vortex centerline always stays at the same distance in the flight direction with respect to the point where the wake vortex has been detected. The effects of different errors in the identified wake elevation and azimuth are presented in Fig. 6.14.

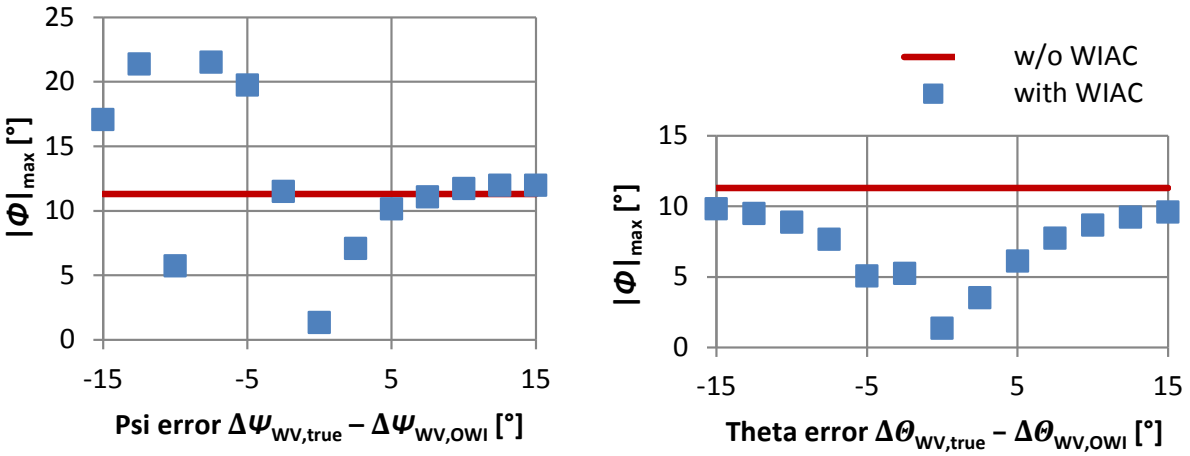

Figure 6.14: Impairment of the reduction of the maximum bank angle amplitude by the wake impact alleviation controller due to errors of the wake vortex orientation

As the orientation of the vortex centerline influences the lateral and vertical distance of the wake vortex relative to the aircraft, errors in the identified wake elevation and azimuth have similar effects as errors in the position of the vortex centerline. Equivalently to errors in the position of the cortex centerline, errors in the lateral wake vortex angle are also more critical than errors in the estimated wake elevation. For deviations up to +/-15° in the identified wake elevation the maximum bank angle during the encounter can still be reduced by the wake impact alleviation controller. A wake azimuth deviation of -2.5° already eliminates the benefit of the WIAC and larger negative deviation from the true wake azimuth provoke a serious impairment of the maximum bank angle. Only in case of an error of -10° the WIAC can alleviate the wake-induced bank angle. This represents the encounter scenario in which the identified wake vortex is located parallelly to the trimmed flight path of the aircraft. The detected wake-induced rolling moment is thus very small in this case because the wind velocities of the left and right vortex core compensate each other. The resulting roll control commands of WIAC are also small but still favorably influence the aircraft response. For the other negative deviations of the identified wake azimuth from its true values, the aggravation of the maximum bank angle is very strong because the relative lateral angle between the wake vortex and the aircraft is larger than it is actually the case. The incorrect control surface commands of WIAC thus act for a longer time. In case of positive errors of the identified wake azimuth a steeper encounter is assumed and the control commands act very fast such that their effect on the aircraft response is smaller. This explains why positive errors of the wake azimuth are less critical for the alleviation performance in this encounter scenario.

In summary the sensitivity study with respect to the errors of the identified parameters of the wake vortex model shows that a high accuracy of these parameters is essential for a successful alleviation of the wake-induced bank angle.

- The lateral position of the wake vortex with respect to the aircraft has the most sensitive influence on the wake impact alleviation performance. Large errors in the lateral position of the vortex centerline and the wake azimuth can cause serious aggravations of the maximum bank angle during the encounter and need to be avoided for a successful system performance.
- In vertical direction, identification errors are less critical. This includes the vertical position of the vortex centerline as well as the wake elevation.
- The vortex circulation is the least critical parameter concerning the precision of the wake identification. Even with relatively large errors of the identified circulation the attainable alleviation of the maximum bank angle is only reduced but the bank angle is not aggravated.

It has to be noticed that the presented sensitivity study considered comparably large errors of the identified parameters. It can be expected that the parameters identified by the OWI will not exhibit such large deviations from the true values. Identified wake vortex parameters with such strong errors (such as positions leading to rolling moments into the wrong direction for instance) would lead to large deviations of the measured LoS velocity and the predicted LoS

velocity of the OWI model such that is not very likely that the OWI would converge to these results. Furthermore, these results would most likely be caught in the plausibility check and not provided as a valid OWI result.

7 Wake Impact Alleviation Performance of Complete OWIDIA System

In chapter 6 the performance of the wake impact alleviation control system has been analyzed under the assumption that the wake vortex disturbance is ideally known and the sensitivities with respect to the accuracy of the different parameters of the wake vortex model, provided to the WIAC module, have been investigated. A transfer of the results of the sensitivity analysis of the identified wake vortex parameters to concrete requirements for the accuracy of the OWI result is not readily possible because the parameters of the wake vortex model used to determine the alleviating control commands in the complete OWIDIA system are permanently updated whenever a new OWI result is available. So the wake impact alleviation is not based on one set of fixed wake vortex parameters, as it is assumed for the sensitivity study in section 6.2, but always adapted to the latest OWI result. A very large error in one or more of the estimated parameters might thus not be very harmful if these parameters are only used for a very short time. This is one of the reasons why, in contrast to the WIAC module, a separate analysis of the OWI module is not very meaningful and the OWI module should be considered in the complete framework of the OWIDIA system. A second reason is the fact that the wake identification can be impaired by large attitude changes during the encounter. In encounters, during which only the OWI but not the WIAC module is active, the attitude changes of the aircraft can be expected to be much larger. This can lead to the effect that the lidar measurements are located outside of the main wake vortex wind velocities. In this case, the OWI does not receive enough information about the wake vortex and cannot appropriately estimate its parameters. The quality of the OWI result in terms of its suitability for a successful wake impact alleviation is thus evaluated in the simulation framework of the complete OWIDIA system in the present chapter.[1] The following sections give an overview of the performance of the complete OWIDIA system under different conditions.

7.1 Examplarily Wake Impact Alleviation Performance of the OWIDIA System based on three Different Lidar Sensors

Figure 7.1 displays the reduction of the bank angle during a 10° lateral wake vortex encounter[3] thanks to the OWIDIA system (i.e. the combination of the OWI and the WIAC module) using three different lidar sensor configurations. Sensor 1 and 2 have 21 measurement axes arranged

[1] A separate analysis of the identification of wake vortex parameters, without a further usage within a wake impact alleviation control system, can be found in *Fischenberg (2012)*[2]. The OWI module is called O-ID in this application. However, the principle of the O-ID is very similar to the OWI in this thesis.

[2] Fischenberg (2012), Paper describing an analysis of a wake characterization approach using lidar measurements.

[3] 0° vertical encounter angle, wake vortex of A340 2 m above encountering A320 aircraft, no pilot inputs during encounter, normal law active, autopilot not engaged. This corresponds to the same encounter which has also been considered in the previous chapters, except for section 6.1.1.

in a rectangular grid with 3 vertical and 7 horizontal measurement axes. Sensor 3 has 15 measurement axes (3 vertical, 5 horizontal axes). The measurement range is 60 m in case of sensor 1, 90 m in case of sensor 2 and 75 m in case of sensor 3. The detailled characteristics of the Doppler lidar sensors can be found in appendix F. Figure 7.1 shows that the success of the bank angle alleviation is strongly influenced by the applied lidar sensor. Sensor 1 allows a very good alleviation of the wake-induced bank angle, which is similar to the alleviation performance of the OWIDIA system if the wake vortex was ideally known (cf. section 6.1). Sensors 2 and 3 lead to a comparably poor alleviation such that a larger bank angle response remains even if the OWIDIA system is active. Especially in case of the application in combination with sensor 3 the OWIDIA system reduces the bank angle only during the beginning of the encounter and has no benefit anymore during the rest of the encounter.

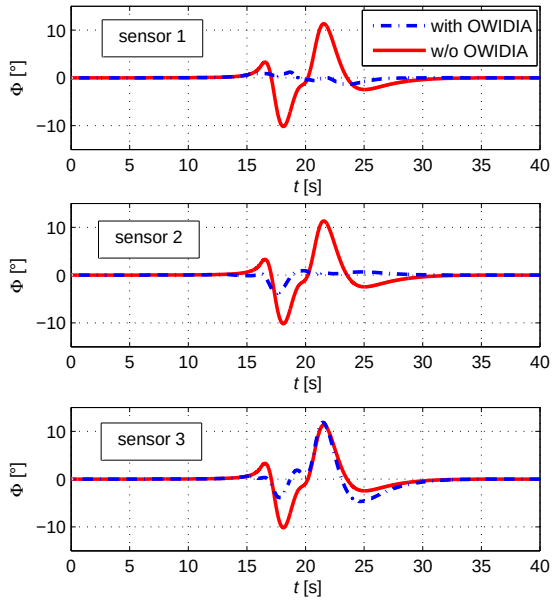

Figure 7.1: Bank angle reduction by the OWIDIA system in combination with different sensor configurations

Depending on the applied lidar sensor the measurement quality varies and makes the characterization of the wake vortex more or less challenging. If the identified parameters of the OWI exhibit a poor match with the actual wake vortex, this logically usually leads to a poor alleviation performance of the OWIDIA system. Figure 7.2 depicts the deviations of the identified wake vortex parameters from the true parameters of the wake vortex affecting the aircraft. The deviations are only displayed if a valid OWI result was available. The time periods during which this was the case (i.e. valid OWI output is one) are shown in Fig. 7.3 for all three sensors. If no OWI result is available (i.e. valid OWI output is zero) this is either because the identification was not activated or because the identification result did not pass the plausibility check (cf. section 5.2). The missing results (squares, crosses or diamonds) in Fig. 7.2 correspond to the times for which there was no valid results (i.e. zero in Fig. 7.3).

The time periods during which valid OWI results are available vary for the three different lidar

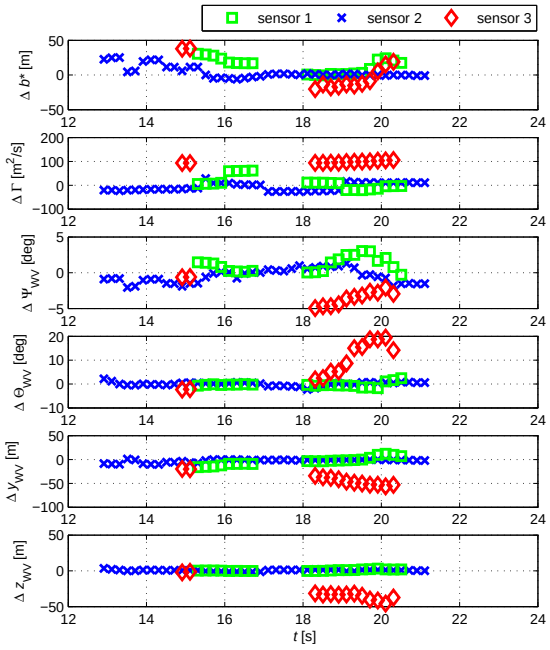

Figure 7.2: Deviations of identified wake vortex parameters from true values (Δ = identified value − true value)

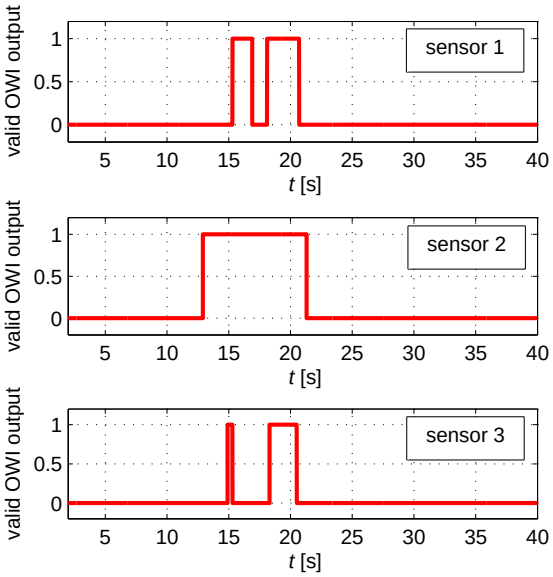

Figure 7.3: Availability of valid identification results during wake vortex encounter

sensors. With sensor 2 a valid OWI output is provided for a comparably long period of time, whereas sensor 1 and 3 only deliver valid identification results during shorter fractions of time of the encounter. During the time when no OWI result is available the WIAC module computes the control commands to compensate for the wake vortex disturbance on the basis of the last OWI result.

The error of the identified wake vortex parameters is not constant during the entire encounter but can vary for each OWI call. Each symbol in Fig. 7.2 corresponds to a new output of the online wake identification. It can be noticed that the errors of the identified parameters are generally larger when the OWIDIA system is applied in combination with sensor 3 than in case of the application in combination with sensor 1 or 2. This explains the worse bank angle reduction of the OWIDIA system with sensor 3 in Fig. 7.1. The errors of the OWI based on sensor 1 and 2 are in the same order of magnitude, even though sensor 2 leads to slightly larger errors. This again matches the observations of the bank angle alleviation in Fig. 7.1.

Although Fig. 7.2 gives an impression of the quality of the parameter estimation result of the OWI, it is difficult to evaluate the consequences of these errors on the alleviation performance. The different wake vortex parameters act in a rather coupled fashion such that the effects of the different errors on the match of the overall disturbance cannot be easily derived. For the success of the wake impact alleviation, it is not the match of the different wake vortex parameters that is most relevant but the resulting reconstruction of the disturbance moments. Figure 7.4 illustrates the comparison of actual wake-induced moments with the detected disturbance moments resulting from the identified wake vortex. The same trend of the influence of the sensor configurations as in the previous figures can be observed. The detected and actual wake-induced rolling moments match very well for the application in combination with sensor 1 and still fairly well with sensor 2. In case of the application of sensor 3 the determined disturbance rolling moment only broadly matches the true moment up to approximately $18\,\mathrm{s}$. After that the OWI determined a wake vortex which is located too far away from the aircraft. The wake-induced moments are thus almost zero and the WIAC does not command compensating control surface deflections anymore. This explains why the bank angle is almost the same during the second half of the encounter.

The results show that the OWIDIA system including the online wake identification can alleviate the wake-induced bank angle reduction almost as well as in the case of the ideally known wake vortex if an appropriate lidar sensor is available. In case of reduced quality of the lidar measurement, the wake impact alleviation performance can, however, be strongly impaired.

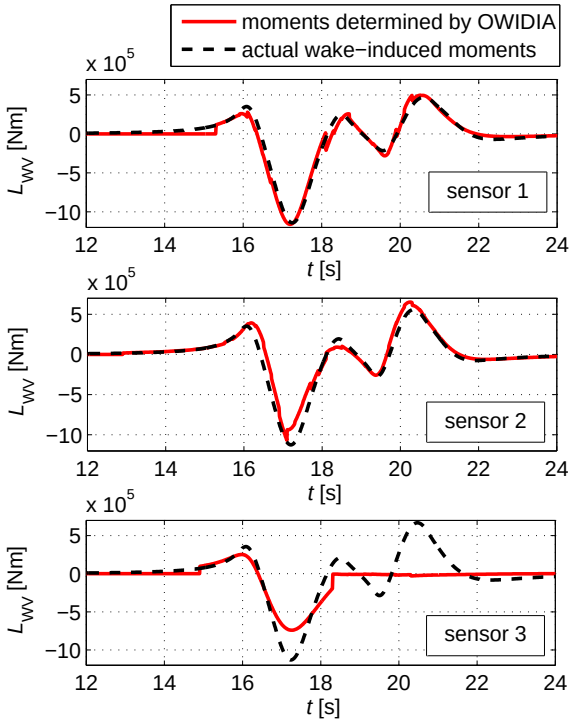

Figure 7.4: Match of actual wake-induced rolling moment with the disturbance rolling moment detected by the OWIDIA system

7.2 Performance Improvement by Increased Buffer Capacity

The wake characterization by the OWI always includes all measurements stored in the data buffer. As described in section 5.2, the OWI adapts the parameters of the wake vortex models such that the resulting line-of-sight velocities at the positions corresponding to the measurements stored in the data buffer provide the best possible match with the measured line-of-sight velocities. An increase of the data buffer consequently directly increases the computation time of the online wake identification. The first implementation of the OWIDIA system was realized with a data buffer that stores measurements over the last 2 s. This comparably small data buffer size was selected as a first guess to provide a good compromise of sufficient measurement information and reasonable computation time. The results presented in section 7.1 are generated with a buffer of 2 s. The analysis of the OWIDIA system showed that this buffer size provides a reasonable system performance for many encounter geometries. However, it turned out that especially for very shallow encounters the alleviation performance can be improved if the buffer size is increased such that all measurements of the last 4 s, instead of the last 2 s, are buffered.

Figure 7.5 shows the comparison of the maximum bank angle with and without OWIDIA during 5° lateral wake vortex encounters in different altitudes. The lidar sensor the OWIDIA system is

[3] The encountering aircraft is again an Airbus A320 flying with an airspeed of 150 KIAS into the wake of Airbus A340. The vertical encounter angle is 0°. The normal law is active, the autopilot turned off and no pilot

applied with has 3x3 measurement axes in vertical and horizontal direction, one measurement point along each axis, a measurement range of 75 m, 30 m blur depth, a field of view of +/-10° in vertical and +/-16° in lateral direction and a full screen update rate of 10 Hz. A positive altitude difference ΔH means that the wake vortex is located above the center of gravity of the aircraft. The buffer is sized that way that it contains all measurements of the last 2 s.

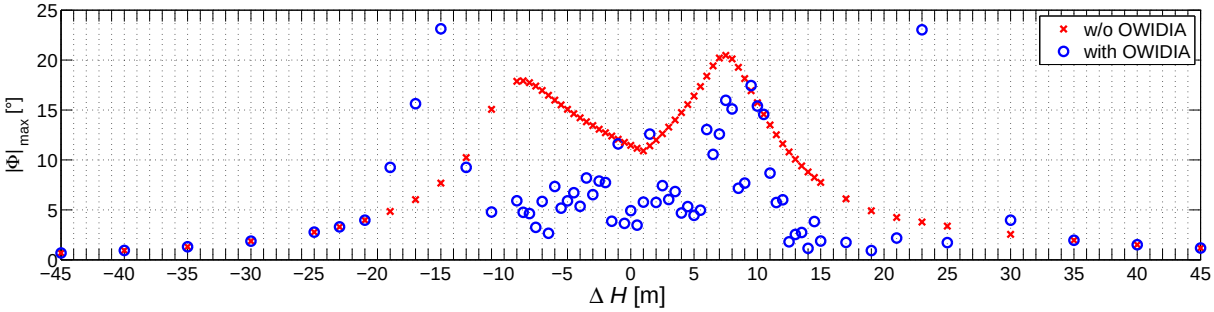

Figure 7.5: Reduction of maximum bank angle with OWIDIA using a lidar sensor with a grid of 3x3 measurement points for encounters with 5° lateral encounter angle and different relative wake altitudes[4]

Figure 7.6 shows the same encounter scenarios with the same lidar sensor for an OWIDIA system which has an extended buffer storing measurements over 4 s. It can be seen in both figures that the relative altitude between the wake vortex and the aircraft has a strong influence on the wake impact alleviation performance. At some altitude offsets the OWIDIA can significantly reduce the maximum bank angle compared to the maximum bank angle during same encounter without the OWIDIA system. At other altitude offsets the OWIDIA system has no benefit. This occurs especially in cases with large positive or negative altitude offsets, in which the sensor does not get much information of the disturbance flow field because the wake vortex is located comparably far below or above the aircraft. During encounters with smaller altitude offsets between the wake and the aircraft, the OWIDIA system works well during many encounters but in some cases aggravates the maximum bank angle. The overall system performance is thus not satisfactory yet because the aggravation of the aircraft response due to the OWIDIA system obviously needs to be prevented.[5] Nevertheless, the comparison of Fig. 7.5 and 7.6 is very interesting for the system design. It shows that the extended buffer of 4 s clearly improves the alleviation performance. The number of cases of bank angle increases as well as the magnitude of the increases are markedly lowered and the bank angle can be reduced to smaller values.

This analysis shows that for very shallow encounter angles such as the considered 5° lateral encounter angle a data buffer containing measurements over the last 2 s only is too small to provide enough information about the wake vortex. During these shallow encounters considering

commands are applied.

[4] Fezans, Schwithal, and Fischenberg (2015), Paper about application of remote sensing technologies for active load alleviation of gusts and turbulence and wake impact alleviation.

[5] Later on some lidar sensor configuration without such outliers will be shown.

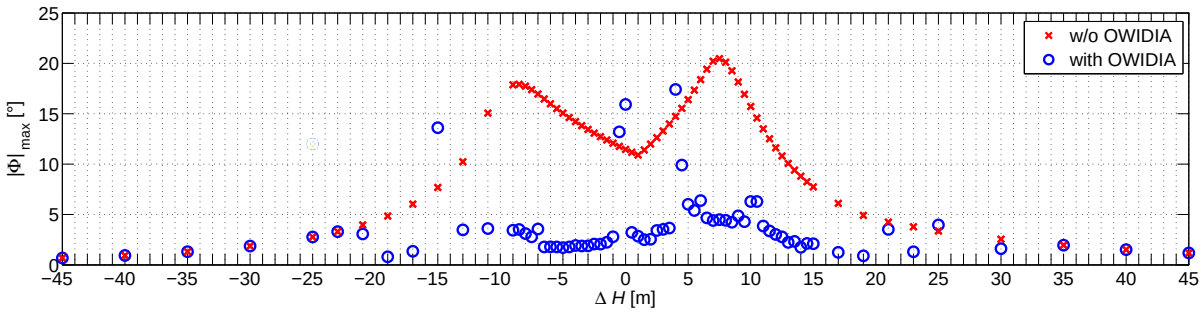

Figure 7.6: Reduction of maximum bank angle with OWIDIA a using lidar sensor with a grid of 3x3 measurement points and a **buffer of 4 s** for encounters with 5° lateral encounter angle and different wake altitudes

measurements over a longer timeframe allows the inclusion of more information about the wake vortex because the wake stays in the field of view of the sensor for a long time. In the following the OWIDIA system will thus be applied with an increased data buffer capacity that can store measurement points over a timeframe of 4 s.

For a successful wake identification it is important that the data buffer of the lidar measurements is large enough to provide sufficient information about the wake vortex for the online wake identification.

- A buffer capacity of measurements over 4 s is a good tradeoff of computation costs and information content for encounters during approach.
- A smaller data buffer containing measurements over the last 2 s only impairs the identification and thus the wake impact alleviation during shallow encounters (e.g. with a lateral encounter angle of 5° and a vertical encounter angle of 0°).

7.3 Sensitivity Study of Lidar Parameters

The results of sections 6.2 and 7.1 show that the performance of the wake impact alleviation system depends on the accuracy of the identification of the wake vortex disturbance. How well the wake vortex can be determined by the OWI depends on the quality of the lidar measurement in turn. Obviously the wake identification works better the more information about the wake vortex is provided by the lidar measurement. What exactly characterizes a good measurement quality is, however, not trivial to answer because the measurement setup can be influenced by a lot of different parameters with many complex interdependencies. It is generally desirable to achieve a high spatial resolution and a good signal-to-noise ratio with the measurement. Many sensor parameters have, however, conflicting influences on these two aspects. Increasing the update rate, number of measurement axes or number of measurement points along one axis, for instance, increases the spatial resolution but decreases the SNR. A smaller field of view increases the density of measurement points without influencing the SNR. On the other hand,

only a smaller portion of the wake vortex is covered by the measurements because the entire measurement domain is smaller. Furthermore smaller scan angles can reduce the information contained in the LoS measurement because the measurement axes have a steeper angle with respect to the wake vortex wind velocities[6] resulting in a smaller projection on the LoS direction.

In order to gain an insight into the dependencies of the different lidar parameters and the achievable wake impact alleviation performance a sensitivity study is performed, in which the lidar parameters are varied systematically. As the purpose is to identify possible parameter sets and to get an understanding of the general influences of the sensor settings, a wide range of lidar parameters but only a few encounter scenarios are considered. Once suitable sensor configurations have been identified these must be tested with further encounter geometries in order to verify their potential for a successful wake impact alleviation. For the lidar parameter sensitivity study only three different encounter scenarios are considered with a lateral encounter angle of $5°$, $10°$, and $15°$. The vertical encounter angle is $0°$ in all three scenarios and the wake vortex is always located 2 m above the center of gravity of the aircraft. This comparably small altitude offset between the wake and the aircraft is selected because it represents a favorable scenario since the wake vortex is positioned well within the field of view of the lidar sensor. As in all encounter scenarios in this work, the normal law of the basic control system is always active, the autopilot is disengaged and the pilot does not command any control inputs throughout the entire encounter. The different values of the lidar parameters considered in the sensitivity study are shown in table 7.1.

Table 7.1: Lidar parameters for sensitivity study

Parameter	**Range of values**
range of first measurement point, $\text{range}_{\text{MP1}}$ [m]	60; 75; 90
lateral scan angle range, Ψ_{scan} [°]	+/-16; +/-30; +/-40
vertical scan angle range, Θ_{scan} [°]	+/-10
# MP along measurement axis, N_{a} (2 in Fig. 7.7)	1; 3; 5
# horizontal MP axes, N_{h} (3 in Fig. 7.7)	3; 5; 7; 9
# vertical MP axes, N_{v} (3 in Fig. 7.7)	3
blur depth [m]	15; 30
full screen update rate [Hz]	5; 10

The lidar parameters correspond to the geometric parameters of the lidar model described in section 4.3. The field of view of the sensor is defined by the range of the lateral and vertical scan angles in negative and positive direction with respect to the lidar reference axis as shown in Fig. 7.7. The lidar reference axis is tilted $5°$ downwards with respect to the fuselage centerline in order to compensate for the aircraft angle of attack and to point approximately in the direction of the aircraft's flight path. The vertical scan angle range Θ_{scan} is set to +/-$10°$, which is slightly wider than the vertical field of view specified for a lidar sensor in the Green-Wake project (cf. table 3.1 in section 3.3, *Rees (2014)*[7]). The smallest lateral field of view configuration has a

[6] in case of small encounter angles as they are considered in this work

[7] Rees (2014), Presentation of the results of the Green-Wake project.

lateral scan angle range Ψ_{scan} of +/-16°, which corresponds to the Green-Wake specification. Besides that two broader lateral scan angle ranges of +/-30° and +/-40° are considered in the sensor parameter study as well. As described already in section 3.1, the simplified expression measurement point is used here to describe a measurement consisting of a defined measurement volume at a given position. The number of measurement points is defined by the number of vertical and horizontal measurement axes N_{v} and N_{h} as well as the number of measurement points along the axes N_{a} (i.e. the number of range gates). The position of the measurement points along the axis is thereby defined by the range of the first measurement point $\text{range}_{\text{MP1}}$, which is varied between 60 m, 75 m and 90 m, and the length of the measurement volume, the so-called blur depth. The closest measurement point is located at $\text{range}_{\text{MP1}}$ and subsequent measurement points are always positioned one blur depth behind the previous measurement point, as illustrated in Fig. 7.7. All measurements along one axis are updated simultaneously, whereupon the measurements at different axes are updated successively. The full screen update rate defines the rate with which all measurement axes are updated. The update rate with which a measurement axis is updated after another axis thus depends on the number of total measurement axes. If the full screen update rate is 10 Hz and the sensor has 9 measurement axes, for instance, the axis-to-axis update rate is 90 Hz.

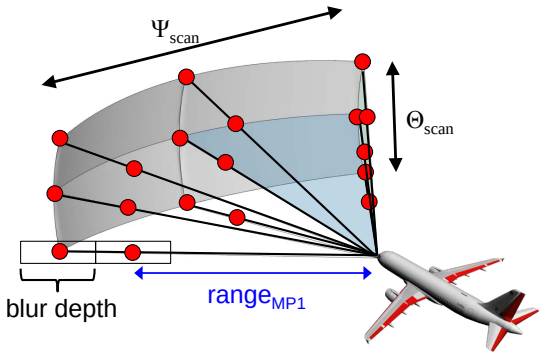

Figure 7.7: Examplary lidar sensor geometry of sensitivity study with 3 vertical and horizontal measurement points and 2 range gates

All possible combinations of sensor parameters shown in table 7.1 are tested for the three lateral encounter angles of 5°, 10°, and 15°. The performance of the OWIDIA system is evaluated by assessing the alleviation of the maximum bank angle occurring during the encounter. The bank angle is selected for the evaluation of the system performance because it represents the main disturbance during wake vortex encounters with shallow lateral encounter angles (cf. section 4.5).

Obviously the OWIDIA system can only influence the aircraft reaction during the wake vortex encounter if a wake vortex is identified by the OWI. Depending on the lidar measurement, the online wake identification does not always provide a valid identification result. If the SNR of the lidar measurement is so low that the activation criterion of the OWI (cf. section 5.2.1) is never fulfilled, the identification algorithm is not activated and no alleviating control commands are generated hence. If the activation criterion is fulfilled and the wake identification is executed, the WIAC might still not be activated because the OWI result does not pass the plausibility check (cf. section 5.2.5). Figure 7.8 shows the influence of the standard deviation of the lidar

measurements and the density of the measurement points on the execution of the OWI algorithm and the validity of its results. Red circles indicate that the activation criterion was not passed during the entire encounter and the OWI was never executed. Black crosses mark cases in which the activation criterion was passed for one or more times during the encounter but none of the OWI results passed the plausibility check. So in both cases (red circles and black crosses) the wake impact alleviation control is never active and the aircraft response is not influenced by the OWIDIA system. Encounters marked with a blue diamond or a green x represent cases in which the OWI algorithm provided between one and five (blue diamond) or more than five (green x) valid outputs that passed the plausibility check. In these cases the WIAC module commands control surface deflections in order to alleviate the disturbance. The control commands are always based on the last valid OWI result. So the WIAC stays active from the first valid OWI result on. If new identification results are provided by the OWI the command generation is based on the updated identified wake vortex (cf. section 5.3.1).

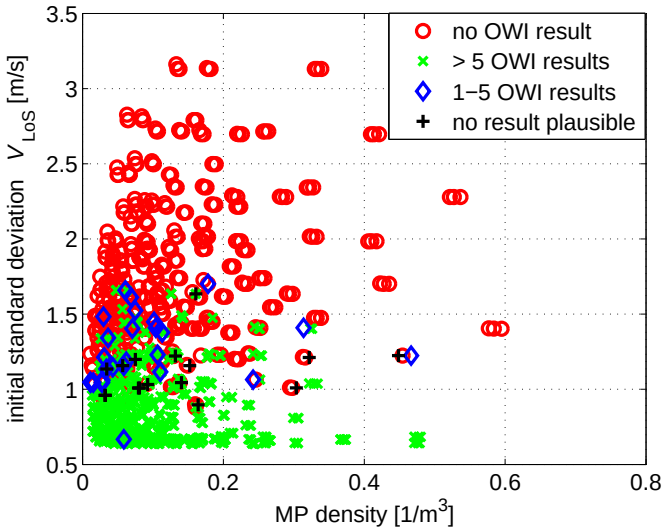

Figure 7.8: Influence of reference standard deviation and measurement point density on OWI execution and results

The density of the measurements does not show an obvious correlation with the execution of the OWI or the validity of its results. Concerning the reference standard deviation of the measured line-of-sight velocity, in contrast, a clear influence can be noticed in Fig. 7.8. The term reference standard deviation refers to the noise-related uncertainty of the lidar measurement. It is determined by computing the standard deviation of all measurements contained in the data buffer when the buffer is filled for the first time at the beginning of the encounter simulation. For a given lidar sensor configuration this value can be assumed to be known or be identified by an appropriate sensor calibration. It can be seen that an increase in the initial standard deviation impairs the successful wake identification. If the standard deviation becomes too high, the OWI is never executed because the activation criterion is never passed. Figure 7.8 shows that this is the case during some encounter scenarios for some sensor sets with an initial standard deviation of $0.87\,\mathrm{m/s}$ or higher. Above an initial standard deviation of $1.7\,\mathrm{m/s}$ only red circles remain, indicating that the OWI is never executed if the reference standard deviation is larger than $1.7\,\mathrm{m/s}$. This value has to be evaluated in relation to the strength of the wake

vortex because a stronger wake vortex implies higher LoS velocities and can thus still be detected although the sensor has a high reference noise level. Considering the vortex circulation of $341\,\mathrm{m}^2/\mathrm{s}$ of the present analysis, it can be concluded that the ratio of the vortex circulation and the reference standard deviation should not be lower than 200 (i.e. $341/1.7$) if the current activation criterion is applied. Concerning the activation criterion it is has to be kept in mind though that it is a very simple criterion and might also filter out cases in which the standard deviation is high but nevertheless a lot of information about the wake vortex is contained in the measurement signal (e.g. because the sensor has very many measurement axes) such that a successful identification might still be possible. An enhanced activation criterion should be developed for future applications in order to allow the use of a wider range of sensor configurations (including those with high noise but still high information about the disturbance). For reference standard deviations below 1 m/s the OWI provides more than 5 valid results in almost all cases. Only a few exceptions exist in which less than 5 valid results are available, none of the OWI results passed the plausibility check or the activation criterion was not satisfied.

For those cases with at least one valid OWI result the wake impact alleviation control is active and influences the aircraft response. The question to be answered is whether the identified wake vortex adequately describes the actual wake disturbance such that the commanded control surface deflection in deed lead to an alleviation of the wake-induced aircraft response. Figure 7.9 shows the maximum bank angle, which occurred during the wake encounter scenarios with $5°$, $10°$, and $15°$ lateral encounter angle[8] with an active OWIDIA system, for different sensor configurations. The red horizontal line indicates the maximum bank angle that occurred without the OWIDIA system. Only cases in which valid OWI results could be obtained and the WIAC is active are included in Fig. 7.9.

It can be observed in Fig. 7.9 that if the measurement point density is very low the OWIDIA system can lead to an increase of the maximum bank angle compared to the maximum bank angle that occurred without the OWIDIA system. This is obviously unacceptable and the corresponding lidar sensor configurations are not suitable for the present alleviation system. For measurement point densities larger than $0.15\,\mathrm{m/s}$ no aggravation of the maximum bank angle occurs anymore for the considered encounter scenarios, although for the 5° lateral encounter the maximum bank angle stays the same as without the OWIDIA system in some cases.

Nevertheless, a low measurement density does not automatically lead to bad alleviation performance. Many sensor configurations with a low measurement point density lead to a system performance with a significant reduction of the maximum bank. On the basis of Fig. 7.9, however, it is not possible to identify promising sensor configurations because not all sensor parameters such as the measurement range, the blur depth, the number of measurement axes and points along each axis and the full screen update rate can be distinguished in these figures. Even more importantly, it is not possible to identify which case of one encounter scenario corresponds to which case with another lateral encounter angle. It is for instance not possible to distinguish how well the sensor set corresponding to the lowest blue circle of the $5°$ lateral encounter scenario in Fig. 7.9 with a measurement point density of $0.19\,\mathrm{m/s}$, which allows a reduction of

[8] $0°$ vertical encounter angle, wake vortex located $2\,\mathrm{m}$ above aircraft, no pilot inputs and autopilot disengaged.

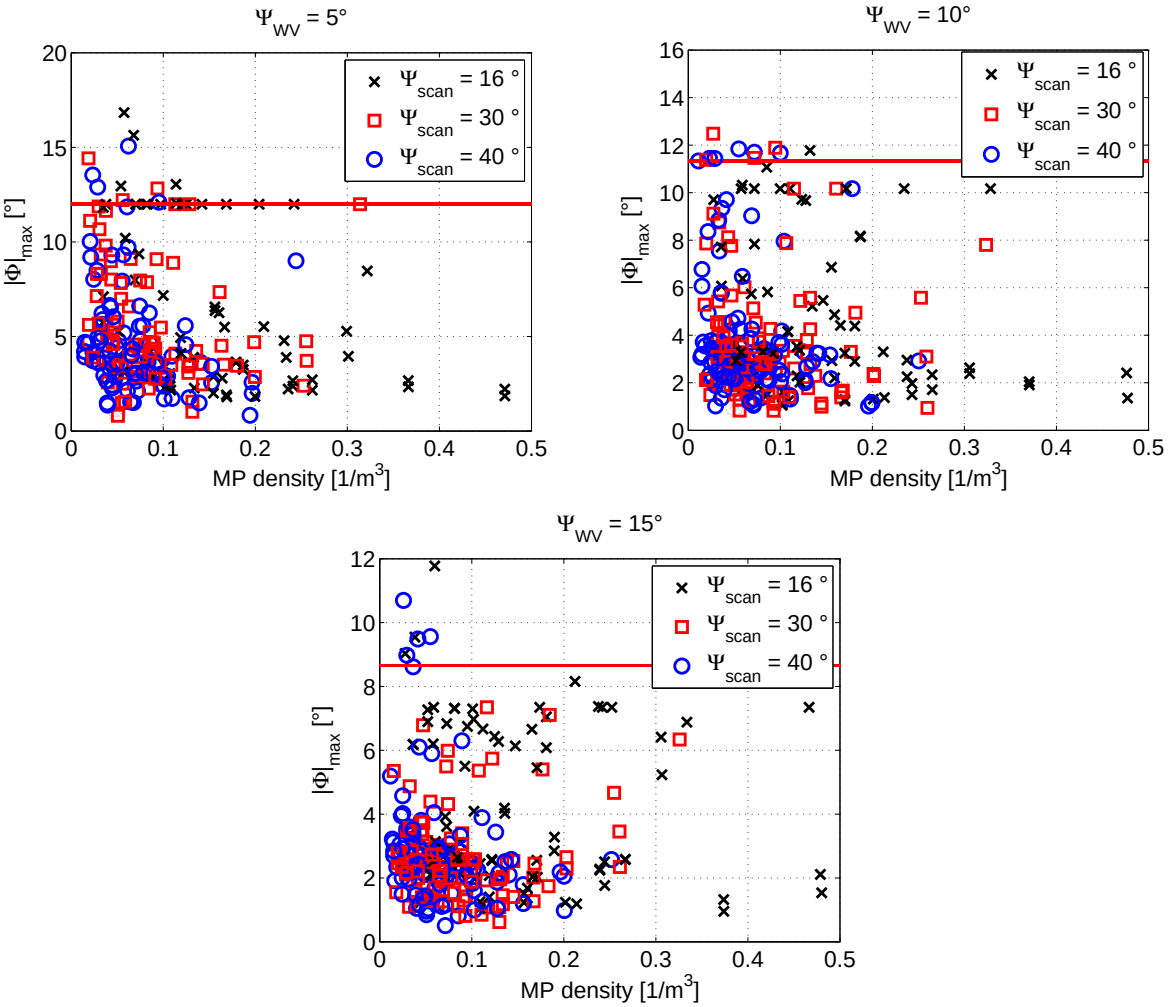

Figure 7.9: Maximum bank angle with OWIDIA during $5°$, $10°$, and $15°$ lateral encounter with different lidar sensor configurations

the maximum bank angle up to $0.8°$, worked for the $10°$ or $15°$ lateral encounters. As a sensor configuration must lead to a good performance for all encounter scenarios, Fig. 7.9 does not provide enough information for an adequate analysis of the sensor parameter sets. A more systematic representation is required that allows the comparison of the different sensor configurations for the three encounter scenarios. Figure 7.10 provides this systematic comparison of all sensor configurations for the three lateral encounter angles. It shows the relative reduction of the maximum bank angle due to the OWIDIA system with respect to the maximum bank angle occurring without wake impact alleviation for the different encounter angles and lidar settings. The uppermost plot illustrates the variations of the encounter angle Ψ_{WV}. The three encounter scenarios with lateral encounter angles of $5°$, $10°$, and $15°$ are grouped in one column for each sensor configuration. The three lowermost plots show the reduction of the maximum bank angle during the encounter by the OWIDIA system with respect to the maximum bank angle without the alleviation system for the three different measurement ranges of $60\,\mathrm{m}$, $75\,\mathrm{m}$, and $90\,\mathrm{m}$ to the first measurement point. The horizontal line at 1 signalizes the maximum bank angle during the wake encounter without the OWIDIA system. For different lateral encounter

angles the absolute value of the maximum bank angle without the OWIDIA system is different due to the different encounter geometry and varying exposure time of the aircraft to the wake. The maximum bank angles with the OWIDIA system are displayed as colored plus-symbols showing the relative change of the maximum bank angle during the encounter. A value of 0.7 corresponds to a reduction of the maximum bank angle by $30\,\%$ thanks to the OWIDIA system. Each plus-symbol represents a single simulation of a wake vortex encounter; whereupon the color of the plus-signs signalizes the combination of blur depth and full scan update rate. The lateral field-of-view angle Ψ_{scan} and the number of horizontal measurement axes N_{h} as well as the number of measurement points along each axis N_{a} are displayed in the second and third subplot of Fig. 7.10. The vertical scan angle Θ_{scan} and the number of vertical measurement axes N_{v} are in all simulations +/-$10°$ and 3 (cf. table 7.1).

If no plus-signs are visible in the lower three plots in Fig. 7.10 this means that the wake impact alleviation did not command any control commands because the OWI did not find a valid result during the entire encounter (either because the OWI was not executed or because the result did not pass the plausibility check). For each subplot of the different $\text{range}_{\text{MP1}}$ the three crosses in the same color in each column show the performance of one particular sensor configuration for the three lateral encounter angles. These three crosses always have to be considered in conjunction in order to evaluate each sensor setting. If one of the crosses is not displayed in one column the corresponding sensor configuration cannot be evaluated as suitable, even if it achieved a good bank angle reduction for the other two encounter angles, because the wake impact alleviation was not active during all encounter scenarios. The effect that the wake impact alleviation is not active occurs especially at sensor configurations with many measurement points. For the sensor settings with $N_{\text{h}}\text{x}N_{\text{a}}$ = 9x3, 5x5, 7x5, and 9x5 the wake impact alleviation is almost never active. The reason is the high measurement noise resulting from the high number of measurement points and the long measurement ranges of these cases. As these sensor sets exhibit several measurement points along their measurement axis, the range to the first measurement point $\text{range}_{\text{MP1}}$ is extended by the blur depth multiplied by the number of range gates. For a sensor configuration with 5 range gates, a blur depth of $30\,\text{m}$ and a $\text{range}_{\text{MP1}}$ of $75\,\text{m}$ the range to the furthest measurement point results in $275\,\text{m}$. The range to the furthest measurement point, which is relevant for the measurement noise, is thus strongly increased by raising the number of range gates. For an increasing $\text{range}_{\text{MP1}}$ the total range is shifted further away. This explains why for a $\text{range}_{\text{MP1}}$ of $75\,\text{m}$ and $90\,\text{m}$ more cases with no crosses occur than for a $\text{range}_{\text{MP1}}$ of $60\,\text{m}$. An increasing lateral field of view of the sensor is favorable for the wake identification because the sensor measures larger LoS component of the wake induced velocity in this case. Moreover, the domain in which information about the wake vortex is gathered is larger. So if the scan angle range is +/-$40°$, more sensor sets remain that provided valid OWI results and enable an application of the wake impact alleviation.

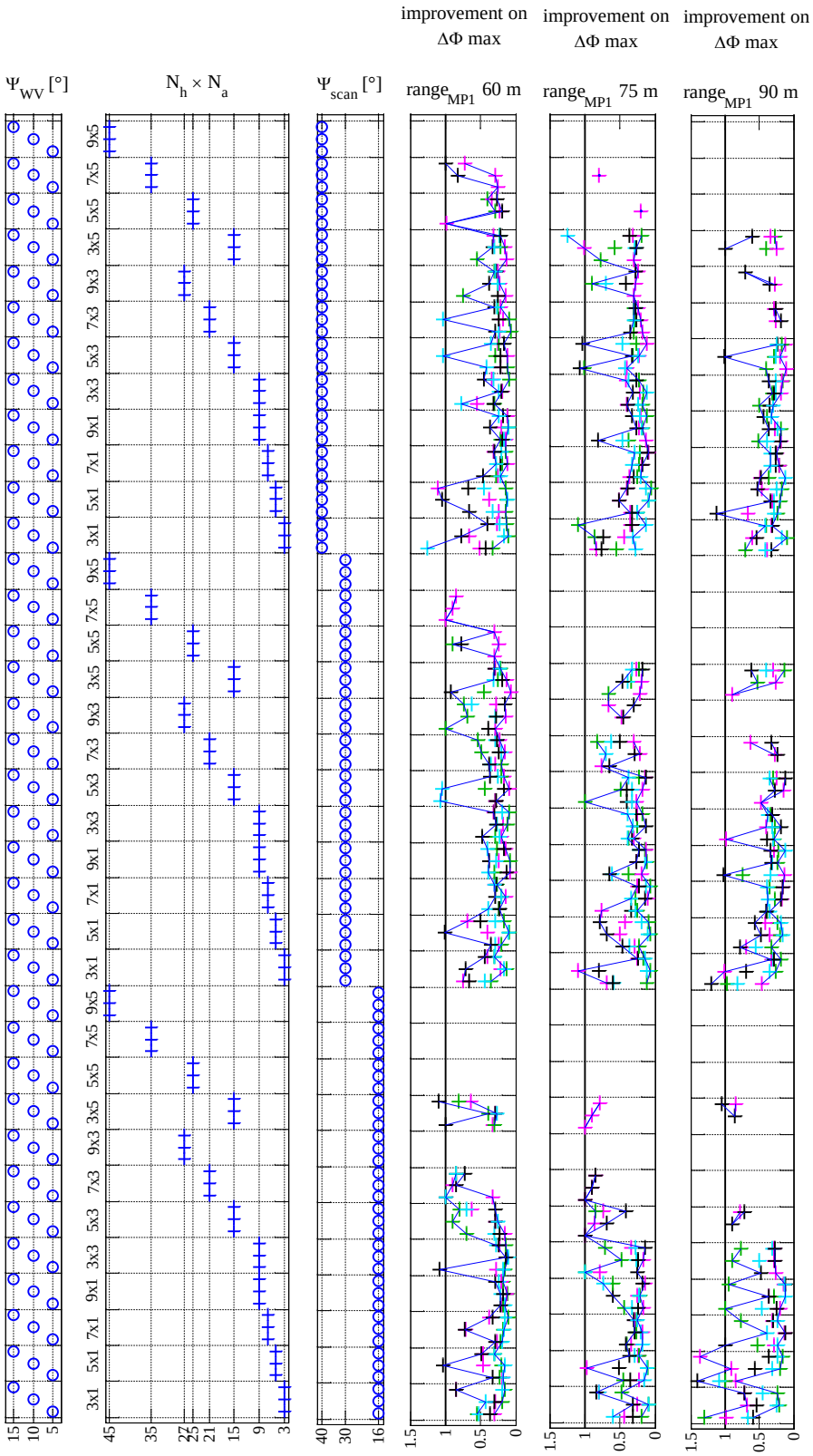

Figure 7.10: Alleviation performance for different encounter angles and lidar settings (+ blur depth 15 m and full scan update rate 5 Hz |+ 15 m and 10 Hz | + 30 m and 5 Hz | + 30 m and 10 Hz)

In order to improve the readability of the figure the sensor configurations with N_hxN_a = 9x3, 5x5, 7x5, and 9x5, which possesses no or only a few active cases with wake impact alleviation, are excluded for further analyses. Figures 7.11 to 7.13 show the same content as Fig. 7.10 separately for the three range$_{\mathrm{MP1}}$ without these sensor configurations in which the wake impact alleviation is hardly active. In addition to the information contained in Fig. 7.10, Fig. 7.11 to 7.13 also display the measurement point density and the reference standard deviation of the LoS velocity (i.e. the LoS velocity when the measurement buffer is filled up for the first time). The different columns comprising the three lateral encounter scenarios for the different sensor configurations are labeled with letters from A to X to allow an easier referencing of particular cases in the text.

It can be noticed in all three figures that the standard deviation often reaches the minimum value, i.e. for all combinations of blur depth and full scan update rate in columns A-D, I-L, and Q-T of Fig. 7.11, in columns A-B, I-J, and Q-R of Fig. 7.12 and in columns A, I, and Q of Fig. 7.13 as well as for some combinations of blur depth and full scan update rate in further columns.[9] In these cases variations of the sensor parameters that would usually influence both, the measurement uncertainty and the measurement point density, only change the measurement point density because the standard deviation of the LoS velocity (which corresponds to the measurement uncertainty) is already at its minimum. In the other columns with sensor configuration whose measurement noise level is generally higher the variation of the sensor parameters also influences the standard deviation of the LoS velocity according to its physical dependencies (cf. section 3.2).

Concerning the cases in which the wake impact alleviation is not active (i.e. no crosses visible) the same trends can be observed for the remaining sensor settings in Fig. 7.11 to 7.13 as in Fig. 7.10: For configurations with large range$_{\mathrm{MP1}}$ sets with several range gates the system is less often not active (no crosses shown) than with lower ranges of the first measurement point. Furthermore, an increased lateral field of view supports a successful wake identification and thus an application of the wake impact alleviation.

All three figures show cases in which the maximum bank angle is increased by the OWIDIA system compared to the case without the OWIDIA system, but also cases in which a remarkable reduction of the maximum bank angle can be achieved. Cases with an increased maximum bank

[9] Columns A, I, and Q in Fig. 7.11 to 7.13 exhibit some variations in the standard deviation for the different blur depth and full scan update rate combinations. This spread is not physically justified and arises from the fact that the standard deviation is determined by computing the standard deviation of the LoS velocity when the measurement buffer is filled for the first time during flight. The sensor configurations of A, I, and Q have comparably few measurement points. In these cases the computation of the standard deviation on the basis of these few values is not very precise. This spread is thus ignored for the further analysis.
Furthermore, in some columns such as e.g. columns V and W the standard deviation is higher for a lateral encounter angle Ψ_{WV} of $5°$ than for the other two lateral encounter angles. This effect is also not physically justified. In these cases there is already a small influence of the wake vortex present in the measurements stored in the buffer when it is filled for the first time. The moment for the standard deviation computation (i.e. the moment when the measurement buffer was filled for the first time) was thus too late during these simulations. The reference standard deviation should generally be determined under circumstances when the presence of a wake vortex can be excluded.

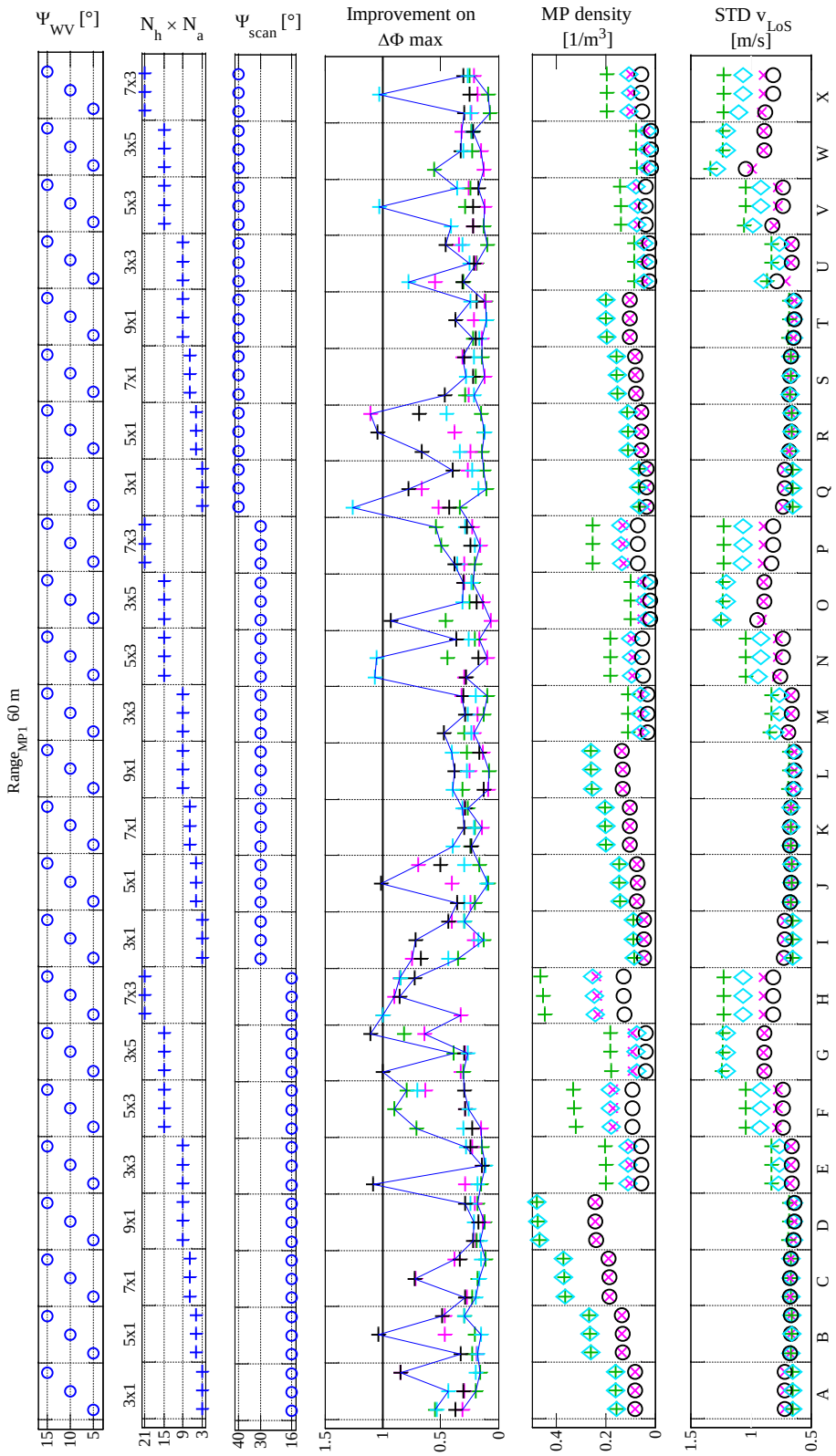

Figure 7.11: Alleviation performance for different encounter angles and selected lidar settings with 60 m range to first measurement point (+ blur depth 15 m and full scan update rate 5 Hz |+ 15 m and 10 Hz | + 30 m and 5 Hz | + 30 m and 10 Hz)

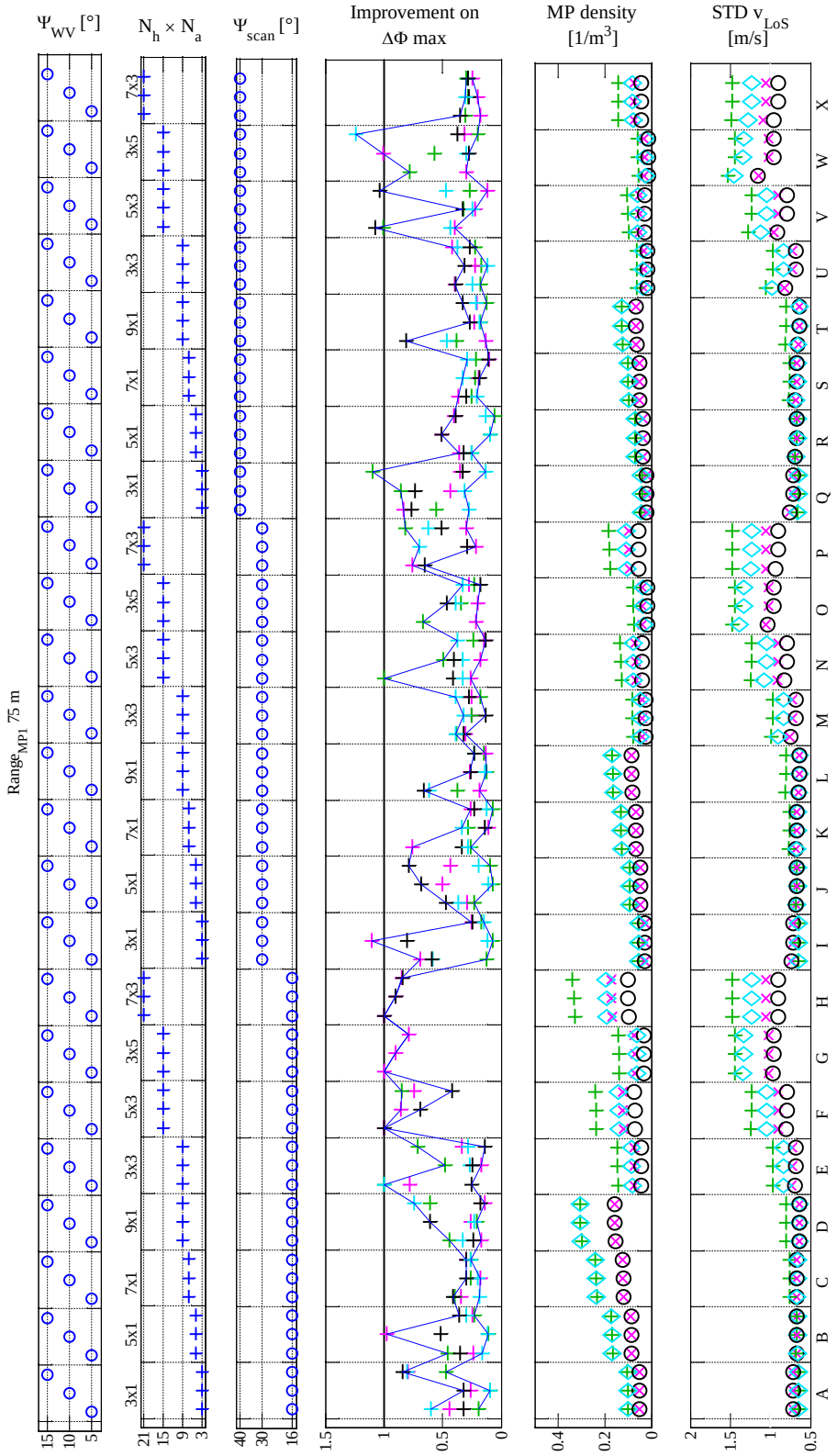

Figure 7.12: Alleviation performance for different encounter angles and selected lidar settings with 75 m range to first measurement point (+ blur depth 15 m and full scan update rate 5 Hz |+ 15 m and 10 Hz | + 30 m and 5 Hz | + 30 m and 10 Hz)

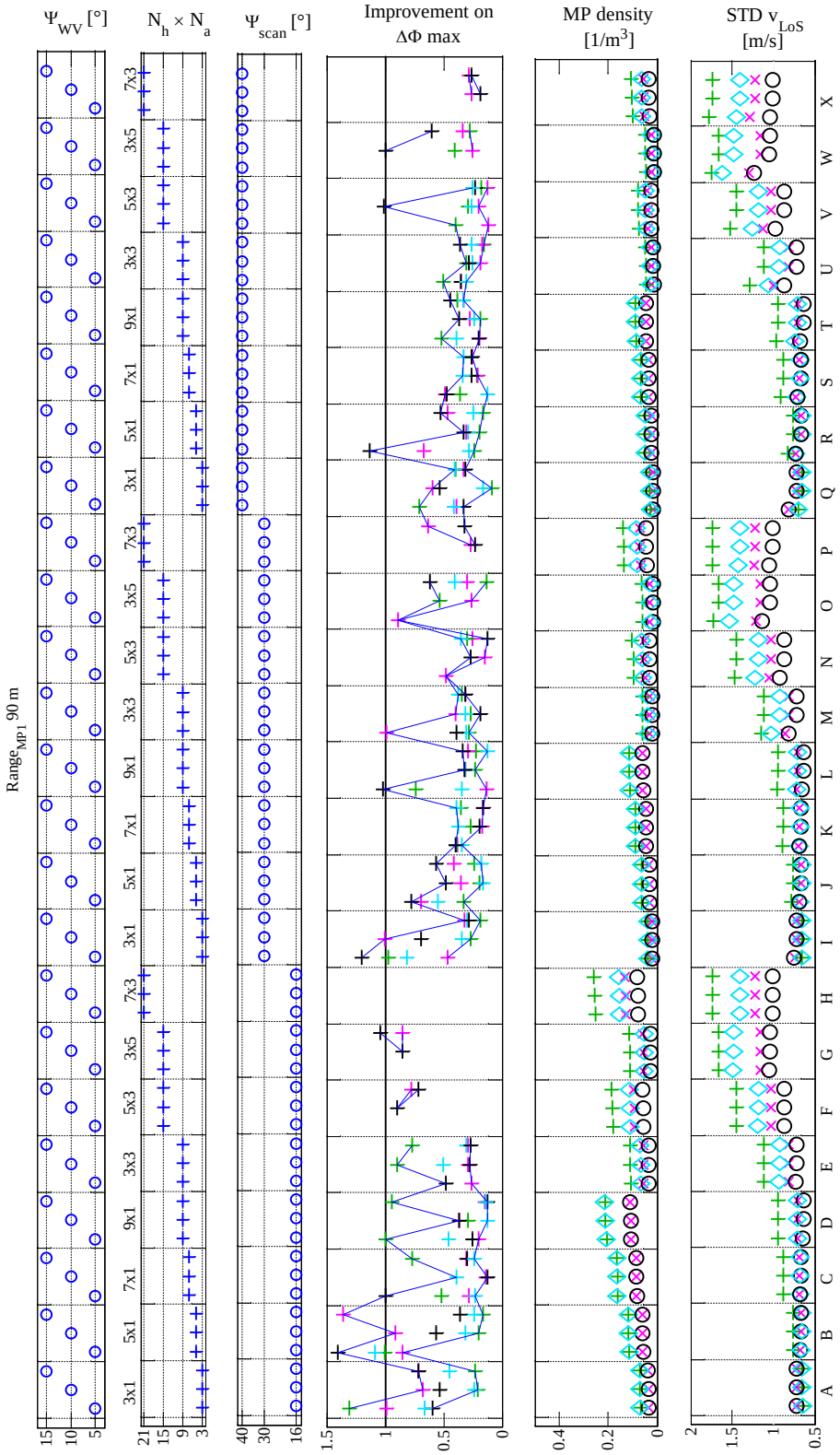

Figure 7.13: Alleviation performance for different encounter angles and selected lidar settings with 90 m range to first measurement point (+ blur depth 15 m and full scan update rate 5 Hz |+ 15 m and 10 Hz | + 30 m and 5 Hz | + 30 m and 10 Hz)

angle must obviously be avoided. They represent combinations of lidar sensor configurations and the OWIDIA system which are not suitable. The question to be answered is what sensor parameter combinations underlie the wake encounter simulations in which the OWIDIA system works well and significantly reduces the maximum bank angle.

The general observation from Fig. 7.11 to 7.13 is that a good tradeoff between a high spatial resolution of lidar measurements and a low measurement noise level provides a good basis for a precise wake identification and finally a successful wake impact alleviation. If a sensor set has too few measurement points, the spatial resolution is too low and the wake vortex cannot be identified well. If a sensor configuration has very many measurement points, the spatial resolution is usually very good but the measurement noise increases such that fewer valid wake identification results are provided and the valid results are often of bad quality.

The fact that a comparably short measurement range of $60\,\mathrm{m}$ is sufficient for a successful wake identification and impact alleviation in many cases might seem surprising at first sight because it might be expected that the aircraft is already influenced by the wake vortex disturbance before any control action can be taken by the OWIDIA system. However, at the beginning of the wake vortex encounter the effect of the wake vortex on the aircraft motion is still very small and can easily be compensated by the basic control system. It is thus not crucial if the wake impact alleviation control of the OWIDIA system only starts to be active when the aircraft is already partly in the influence zone of the wake vortex. The main benefit of the OWIDIA system occurs when the aircraft is exposed to the strong wake-induced disturbance moments close to the vortex cores. This result once more demonstrates the importance of a comprehensive, fully coupled simulation environment including all relevant modules (such as the combination with the basic control system in this case) in order to evaluate the realistic potential of the OWIDIA system for the wake impact alleviation.

The influence of the blur depth and the full scan update rate (distinguished by different color codes in each column) on the overall system performance is comparably low. An increased blur depth on the one hand reduces the measurement noise (cf. section 3.2), which is favorable for the wake identification. For the sensor configurations of the sensitivity study, however, this effect only becomes noticeable if the sensor configuration has several range gates or in the cases of a $\mathrm{range}_{\mathrm{MP1}}$ of $75\,\mathrm{m}$ and $90\,\mathrm{m}$ with many measurement axes because in the other cases the standard deviation is already so low that its minimum bound is reached. The present sensor is modeled in that way that a larger blur depth leads to an increased entire measurement range if more than one measurement point exists along the measurement axes because the measurement points are spaced one after another in the distance of the blur depth. This is the reason why a larger blur depth leads to a lower measurement density if the number of measurement points along the measurement axes is greater than one. Concerning the reduction of the maximum bank angle, however, no clear trend can be identified with respect to variations of the blur depth. The relevance of this parameter for the alleviation performance can thus be evaluated as comparably low.

The influence of the full scan update rate on the wake impact alleviation performance can be noticed more clearly. An increase of the full scan update rate raises both the spatial resolution of

the measurements in terms measurement point density as well as the measurement noise level. Depending on the measurement noise and spatial resolution resulting from the other sensor parameters either a lower or a higher update rate is more favorable for the sensor configuration. For sensor configurations leading to high measurement noise the wake impact alleviation is by trend better with 5 Hz full scan update rate. A higher update rate would further increase the measurement noise in these cases and a successful wake identification would not be possible anymore. In cases with a low spatial resolution of measurement points (i.e. few measurement axes and range gates) sensor sets with 10 Hz full scan update rate tend to deliver better performance because the high update rate increases the overall spatial resolution as the measurement points are spaced closer together in flight path direction.

A variation of the field of view influences the spatial resolution in two ways. On the one hand, a smaller field of view increases the measurement point density because the same number of measurements is located in a smaller measurement domain. On the other hand, the overall measurement volume is smaller such that the sensor sees a smaller portion of the wake vortex. The results of sensor parameter study in Fig. 7.11 to 7.13 show that a small field of view is unfavorable for sensor configurations with several range gates and many measurement axes such as in columns F, G, and H (N_hxN_a = 5x3, 3x5, 7x3). In these cases, the OWI often does not provide valid wake identification results and when the wake impact alleviation control is active, the alleviation performance is not very good. The corresponding sensor sets have high noise levels and the information about the wake vortex found in the small measurement field of view does not seem to be sufficient to allow a successful wake vortex identification.

For a $\mathrm{range}_{\mathrm{MP1}}$ of 60 m (Fig. 7.11) sensor sets with particularly good performance, independent of the blur depth and full scan update rate, can be found in columns D, K, L, S, and T. These sensor sets provide a good bank angle reduction for all combinations of blur depth and full scan update rate, which suggests a robust performance. They simultaneously fulfill the requirements of a high measurement point density and low standard deviation of the line-of-sight velocity. The sensor configurations displayed in columns B and C of Fig. 7.11 also exhibit a high measurement point density and a low measurement noise. However, the alleviation performance is, especially with 5 Hz full scan update rate, worse than in the cases mentioned before. The reason for this impairment is expected to originate from the small field of view. In combination with the lower number of measurement axes compared to sensor setups of column D the information about the wake vortex is not sufficient in some cases when the sensor configurations of columns B and C with 5 Hz full scan update rate are applied. Besides these sensor sets with high measurement density and low measurement noise the sensor configurations of column M in Fig. 7.11 also show a very good alleviation performance. This observation is surprising because these sensor sets have a comparably low measurement point density and a higher standard deviation of the LoS velocity than the other sensor configurations with good performance. In contrast to the other favorable sensor sets, which all only have one range gate, the sensor setup of column M has three measurement points along each measurement axis. This seems to provide a favorable distribution of the measurement points. Due to the small number of measurement axes the sensor setup still exhibits a relatively low measurement noise compared to other sensor setups with several range gates.

In case of a $\text{range}_{\text{MP1}}$ of 75 m (Fig. 7.12), similarly as for a $\text{range}_{\text{MP1}}$ of 60 m, the alleviation performance achieved with sensor configurations of columns M, K, L, S, and T is again good. The sensors displayed in column C lead to a better bank angle reduction than the sensor setups with a $\text{range}_{\text{MP1}}$ of 60 m. Due to the larger range of the sensors in Fig. 7.12 the measurement domain is larger for the same small scan angle range of +/-$16°$ such that the narrow scan angle range of the sensor is less critical if the measurement range is extended.

For a $\text{range}_{\text{MP1}}$ of 90 m (Fig. 7.13) the sensor setups of columns K, S, T, and U provide a good bank angle reduction. In these cases the measurement uncertainty is low again. The measurement point density is also not bad; however due to the larger measurement range, it is lower than for the equivalent sensor configurations with a $\text{range}_{\text{MP1}}$ of 75 m and 60 m. Additionally, the sensor sets of column U deliver a good alleviation performance for the $\text{range}_{\text{MP1}} = 90$ m case. Similarly to the sensor sets of column M for the cases with a $\text{range}_{\text{MP1}}$ of 75 m and 60 m, the parameter combination with nine measurement axes (three vertical and three horizontal axes) and three range gates seems to lead to a favorable distribution of the measurements in space.

Besides the mentioned sensor sets, specific combinations of blur depth and full scan update rate in many more columns lead to an excellent system performance with very large reductions of the maximum bank angle. Many of the analyzed parameter combinations of the lidar sensors allow a reduction of the maximum bank angle of more than $70\,\%$ for all lateral encounter angles and up to $90\,\%$ for some encounter angles.

The main findings of the sensitivity study of the lidar parameters can be summarized as follows:

- A good wake impact alleviation performance can be achieved with sensor configurations that provide a good tradeoff between the spatial resolution of the measurements and a low measurement noise level.
- With very many measurement points the measurement noise becomes too high to allow a successful wake identification such that the OWIDIA system is not active. If the ratio of the vortex circulation and the reference standard deviation of the LoS velocity is less than 200 (i.e. a reference standard deviation of the LoS velocity of more than 1.7 m/s in the present case with a vortex circulation of $341\,\text{m}^2/\text{s}$) the OWIDIA system was never active because the currently used simple activation criterion was never satisfied.
- The blur depth and full scan update rate have only minor influence of the wake impact alleviation performance. The update rate should be adjusted to get a favorable ratio of spatial resolution and measurement noise.
- Many sensor configurations allowed a very good wake impact alleviation with reductions of the maximum bank angle of 70 - $80\,\%$ for all three lateral encounter angle Ψ_{WV}.

7.4 Detailed Study of Selected Lidar Parameter Sets

The sensitivity study of section 7.3 covered a wide range of sensor parameter combinations and identified several favorable configurations. The next step is to analyze these promising sensor configurations in more encounter geometries in order to verify that they provide adequate performance in all encounter scenarios and not only for the few encounter geometries considered in the sensitivity study in section 7.3. Subsection 7.4.1 displays the sensor configurations that are selected for the detailed analysis and explains the methodology of the evaluation. As the relative altitude between the wake vortex and the aircraft has been shown to be an influential parameter for the success of the wake identification and alleviation, the selected sensor configurations, which supported a good alleviation for different lateral encounter angles at a favorable altitude offset of $2\,\mathrm{m}$, are analyzed for a wider altitude range in subsection 7.4.2. In subsections 7.4.3 to 7.4.5 additional variations of characteristics of the selected sensor configurations in terms of number of vertical measurement axes, vertical field of view, and measurement noise are considered, before further variations of the encounter geometry besides the shift of altitude offset are studied in subsection 7.4.6. The purpose of the section 7.4 is a detailed analysis of the OWIDIA system and the determination of suitable sensor configurations. The goal is thereby not only to present cases in which the system works well but also to identify challenging cases with impaired alleviation performance in order to improve the overall system performance.

7.4.1 Assessment Methodology

The sensor sets that will be considered in more detail and for more encounter geometries in the following subsections are highlighted in Fig. 7.14. The notation shown in Fig. 7.15 is introduced to describe the selected sensor configurations. The letter corresponds to the letters used in Fig. 7.14 defining the combination of the number of measurement points in horizontal direction and along the measurement axis as well as the lateral field-of-view angle. The red number next to the letter marks the number of vertical measurement axes. It is only included in the notation if the vertical number differs from 3 (as it is the case for the analysis with an increased number of vertical measurement axes in section 7.4.3). All sensor configurations shown in Fig. 7.14 have 3 vertical measurement axes such that the red number behind the letter is not used for the notation of these sensors. The first black number in the notation of the sensor configurations denotes the blur depth in meter, the second black number describes the full screen update rate in hertz, and the third black number indicates the range to the first measurement point $\mathrm{range}_{\mathrm{MP1}}$ in meter. The last number of the sensor notation in Fig. 7.14 is displayed in red again. It describes the range of the vertical field of view. Like the first red number, the last red number is also only used if the vertical field of view deviates from the values of +/-$10°$, which is the vertical scan angle range of all sensors shown in Fig. 7.14. Following this notation the selected sensor configurations of Fig. 7.14 and their detailed characteristics are summarized in table 7.2.

All of the investigations in the subsequent subsections comprise encounters with an extensive variation of the relative altitude between the wake vortex and the encounter aircraft. Figure 7.16 shows the reduction of the maximum bank angle with and without the OWIDIA system for $5°$ lateral encounters with different altitude offsets between the wake vortex and the aircraft exemplarily for the sensor parameter sets D-15-5-60, J-15-10-16 and K-30-10-90.

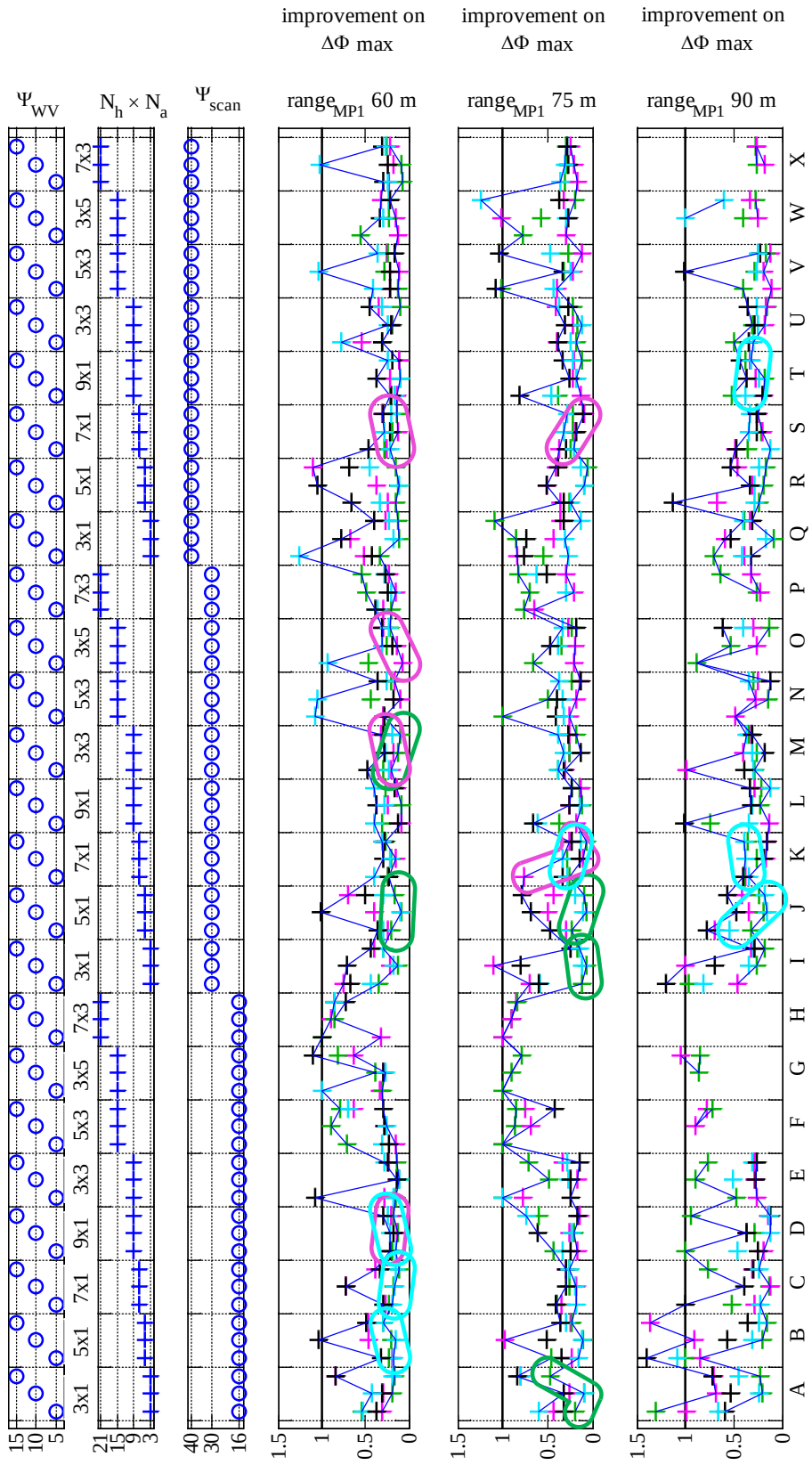

Figure 7.14: Selected lidar sensor configurations for analysis with more encounter altitudes (+blur depth 15 m and full scan update rate 5 Hz | + 15 m and 10 Hz | + 30 m and 5 Hz | + 30 m and 10 Hz)

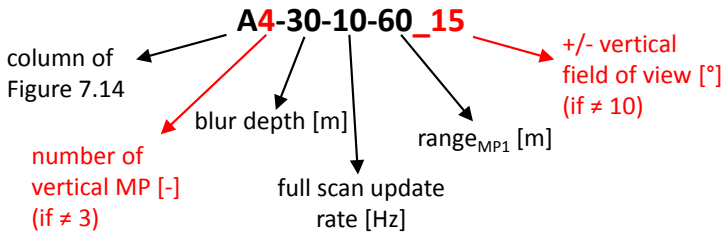

Figure 7.15: Notation of sensor configurations

Table 7.2: Selected sensor configurations for analysis with more encounter altitudes

Sensor configuration [-]	Number of vertical axes [-]	Number of horizontal axes [-]	Number of MP along axis [-]	Total number of MP [-]	range$_{MP1}$ [m]	Vertical field of view Θ_{scan} [°]	Lateral field of view Ψ_{scan} [°]	Blur depth [m]	Full scan update rate [Hz]	Single axis update rate [Hz]
B-30-10-60	3	5	1	15	60	+/-10	+/-16	30	10	150
C-30-10-60	3	7	1	21	60	+/-10	+/-16	30	10	210
D-15-5-60	3	9	1	27	60	+/-10	+/-16	15	5	135
D-30-10-60	3	9	1	27	60	+/-10	+/-16	30	10	270
J-15-10-60	3	5	1	15	60	+/-10	+/-30	15	10	150
M-15-5-60	3	3	3	27	60	+/-10	+/-30	15	5	45
M-15-10-60	3	3	3	27	60	+/-10	+/-30	15	10	90
O-15-5-60	3	3	5	45	60	+/-10	+/-30	15	5	45
S-15-5-60	3	7	1	21	60	+/-10	+/-40	15	5	105
A-15-10-75	3	3	1	9	75	+/-10	+/-16	15	10	90
I-15-10-75	3	3	1	9	75	+/-10	+/-30	15	10	90
J-15-10-75	3	5	1	15	75	+/-10	+/-30	15	10	150
K-15-5-75	3	7	1	21	75	+/-10	+/-30	15	5	105
S-15-5-75	3	7	1	21	75	+/-10	+/-40	15	5	105
J-15-10-90	3	5	1	15	90	+/-10	+/-30	15	10	150
J-30-10-90	3	5	1	15	90	+/-10	+/-30	30	10	150
K-30-10-90	3	7	1	21	90	+/-10	+/-30	30	10	210
T-30-10-90	3	9	1	27	90	+/-10	+/-40	30	10	270

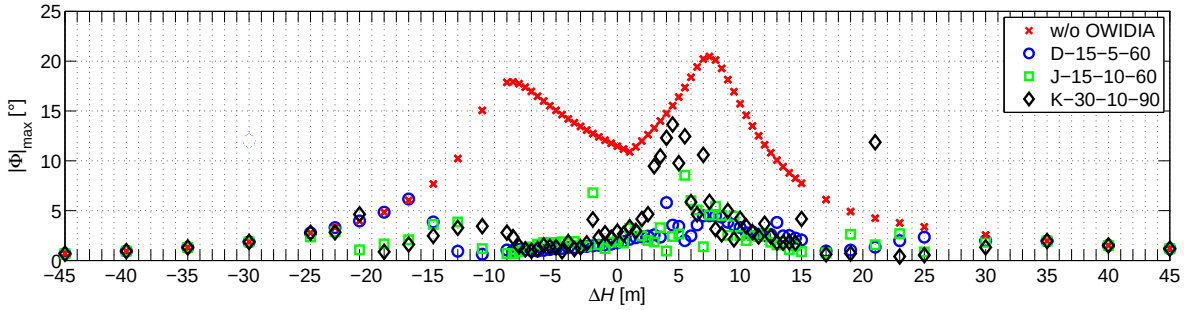

Figure 7.16: Bank angle with and without OWIDIA system for $5°$ lateral encounters with different altitude offsets (positive ΔH means that wake vortex is located above the aircraft)

This figure provides a good insight into the alleviation performance of the different sensor configurations. It shows, for instance, that sensor configuration D-15-5-60 allows a very good alleviation of the wake-induced bank angle, whereupon the maximum bank angle almost always stays below $5°$ when the system is active and can be reduced to values below $2°$ in cases with altitudes offsets between $\Delta H = -13\,\mathrm{m}$ to $0.5\,\mathrm{m}$. When the wake vortex is located relatively

far below or above the aircraft, the OWIDIA system is not active and the maximum bank angle stays the same as without the alleviation system. The applications of the OWIDIA system with the sensor configurations J-15-10-60 and K-30-10-90 show an lower alleviation performance. The remaining maximum bank angle with the OWIDIA system with both sensor configurations, J-15-10-60 and K-30-10-90, is larger than with the D-15-5-60 lidar. Especially with the K-30-10-90 lidar sensor the maximum bank angle is barely reduced at very small positive altitude offsets between the wake vortex and the aircraft. At an altitude offset of $21\,\mathrm{m}$, the maximum bank angle is even increased. The impairment of the maximum bank angle at $\Delta H = 21\,\mathrm{m}$ is so strong that the application of the OWIDIA system with this lidar sensor is not practicable.

For the comparison of a larger number of sensor configurations the representation of the alleviation performance of Fig. 7.16 is not very suitable though. Instead of this detailed graphical presentation of the maximum bank angles with and without the OWIDIA system at different encounter altitudes, several key performance parameters are defined, which summarize the alleviation performance of the OWIDIA system in combination with each sensor configuration over all considered encounter altitudes and thus allow a more systematic representation and an easier comparison of the sensors. These key performance parameters are:

- **average Φ_{max} reduction [%]**
  As an increase of the maximum bank angle due to the OWIDIA system is particularly critical and should be strictly avoided, the reduction and increase of the maximum bank angle occurring during the encounter are displayed separately. The average reduction of the maximum bank angle comprises those cases in which the maximum bank during the encounter with an active OWIDIA system is less or equal to the maximum bank angle during the encounter without OWIDIA. The average reduction is expressed in percent because the absolute value of the maximum bank angle varies for different altitude offsets between the aircraft and the wake vortex.

- **# Φ_{max} increases [-]**
  This parameter describes the number of cases in which the OWIDIA system leads to an increase of the maximum bank angle.

- **$\Sigma\Phi_{\mathrm{max}}$ increase [°]**
  In order to quantify the degree of the maximum bank angle increase, it is not the average relative increase, expressed in percent, that is displayed because the relative increase might be uncritical if it only occurs during encounter scenarios during which the absolute maximum bank angle is small. An increase from $1°$ bank angle to $3°$ maximum bank angle, for instance, would represent a relative increase of $200\,\%$ but the pilot would probably hardly be able to distinguish a difference. Instead the sum of the absolute maximum bank angle increases of all encounters ($\Sigma\Phi_{\mathrm{max}}$ increase) is used as a key performance parameter. The absolute numerical value of this parameter is meaningless but is allows a comparison between the different sensor configurations.

- **max Φ_{max} increase [°]**
  The maximum increase of the maximum bank angle is another informative parameter to consider because a single case with a strong impairment of the aircraft reaction might

make a sensor configuration unacceptable even if the increase of the maximum bank angle is low for most encounter scenarios.

- **# not activated [-]**
  The last key performance parameter is the number of encounters during which the wake impact alleviation control system was not active because the OWI did not find a valid identification result.

These key performance parameters are used in the following subsections in order to compare the alleviation performance of the OWIDIA system in combination with different sensor configurations.

7.4.2 Analysis of Selected Parameter Sets at Different Encounter Altitudes

The first step of the detailed analysis of the alleviation performance of the OWIDIA system in combination with promising lidar sensor configurations is the assessment of the sensor configurations shown in Fig. 7.14 and table 7.2 for encounters with different altitudes offsets between the wake vortex and the encountering aircraft. Figure 7.17 displays the key performance parameters for horizontal encounters with $5°$ lateral encounter angle and $0°$ vertical encounter angle and the range of altitude offsets shown in Fig. 7.16. In addition to the key parameters, the last two subplots provide information about the lidar sensor configuration by displaying the measurement point density and the standard deviation of the line-of-sight velocity of all measurement points when the data buffer is filled for the first time.

Figure 7.17 shows that most of the selected sensor configurations lead to a very good average reduction of the maximum bank angle of 60 - $70\,\%$. However, many of the selected sensor parameter sets, all of which allowed a successful bank angle reduction at an altitude offset of $\Delta H = 2\,\text{m}$ for all encounter angles, exhibit increases of the maximum bank angle at some encounter altitudes. Only the three sensor parameters sets D-30-10-60, J-15-10-60 and S-15-5-60, which are highlighted by red boxes in Fig. 7.17 never lead to an increase of the maximum bank angle. The lidar sensors D-15-5-60 and M-15-10-60, which are marked with dashed boxes in Fig. 7.17, exhibit only a minimal bank angle impairment of $0.1°$ and $1.0°$ at one encounter (i.e. at one altitude offset). This increase is negligible such that this sensor configuration can also be evaluated as suitable.

Except for the lidar sensor M-15-10-60, the favorable sensor configurations all have a very low standard deviation of the line-of-sight velocity. The parameter sets D-15-5-60 and D-30-10-60 have a very high measurement point density because they have many measurement points (9 horizontal x 3 vertical measurement points with 1 range gate) in a small field of view of +/-$10°$ x +/-$16°$. For the configuration J-15-10-60 and again for the sensor S-15-5-60 the measurement point density decreases in each case but the lateral field of view increases. These two sensor configurations exhibit fewer cases in which the wake impact alleviation control system is not active. Lidar sensor M-15-10-60 has a comparably low measurement point density and high measurement noise; but due to the fact that it has three range gates it has a larger measurement

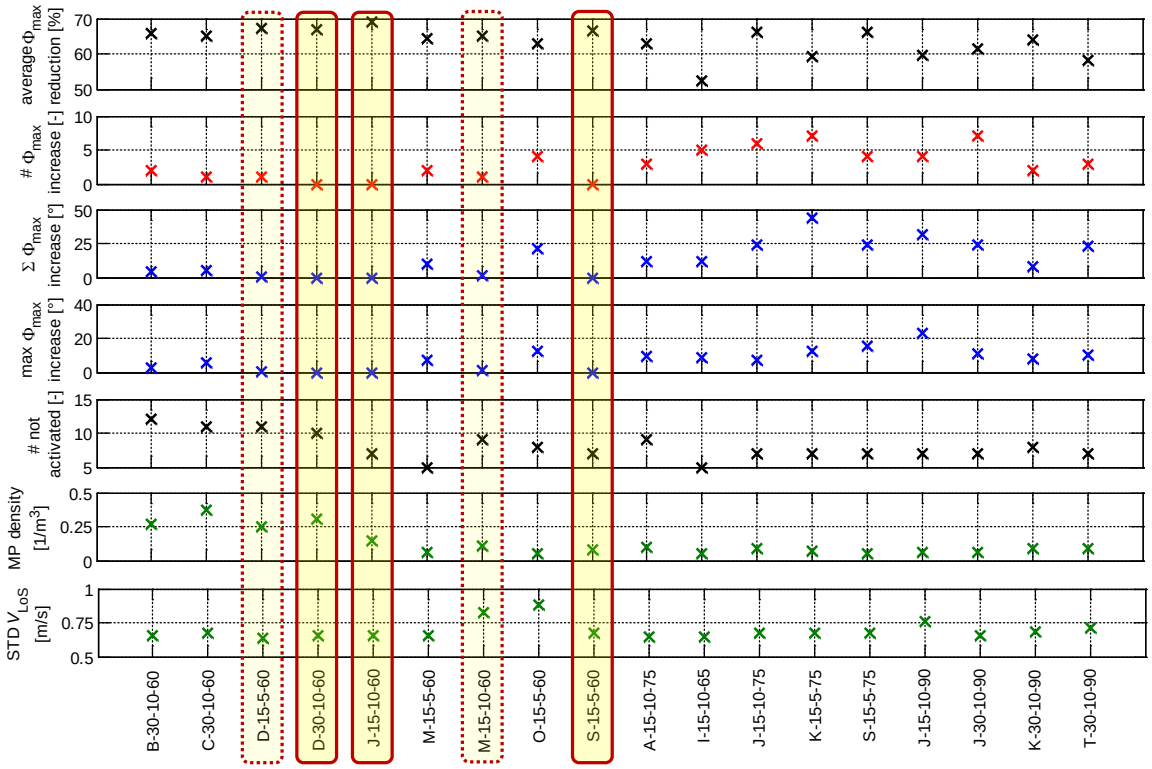

Figure 7.17: Summarized alleviation performance with selected sensor configurations for a large range of encounter altitudes with $5°$ lateral encounter angle

domain (because of the larger measurement range due to the additional range gates) and a good spatial distribution of measurement points in vertical direction, as explained in the next section. This seems to be favorable especially if many different altitude offsets of the wake vortex are considered.

Concerning the realizability of the lidar sensor the configuration M-15-10-60 is particularly favorable because it has only three measurement axes and a comparably low single axis update rate of only 90 Hz. Sensor S-15-5-60 with 15 measurement axes and 105 Hz single axis update rate is also attractive from the point of view of the sensor realization. The sensor configuration D-30-10-60, in contrast, has a significantly higher single axis update rate of 270 Hz and 27 measurement axes in total, which is likely to make this sensor more challenging and expensive to build.

7.4.3 Influence of an Increased Number of Vertical Measurement Axes on the Alleviation Performance

So far only lidar parameter combinations with three vertical measurement axes have been considered. One explanation for the observation that some sensor configurations allow a very good bank angle reduction for encounter scenarios with specific altitude offsets between the wake vortex and the aircraft and lead to a significantly poorer alleviation performance at other alti-

tude offsets could be that the spatial resolution of the measurement points in vertical direction is too low. With only three vertical rows of measurement points it is possible that the vertical position of the vortex lies unfavorably between the measurements, which impairs the wake identification. If the sensor configuration has only one measurement point along each axes, the vertical distance between the first measurement points is approximately $10\,\mathrm{m}$ for $\mathrm{range}_{\mathrm{MP1}} = 60\,\mathrm{m}$, $13.0\,\mathrm{m}$ for $\mathrm{range}_{\mathrm{MP1}} = 75\,\mathrm{m}$ and $16\,\mathrm{m}$ for $\mathrm{range}_{\mathrm{MP1}} = 90\,\mathrm{m}$. Compared to the core radius of the wake vortex of $2.4\,\mathrm{m}$, these vertical distances are relatively large. If the lidar sensor possesses several range gates, the spatial resolution in vertical direction is improved because the vertical distance between measurement points along each axis is smaller than the vertical distance between the measurement points of different axes.

The question thus arises if an increased number of measurement axes can improve the wake impact alleviation performance of the OWIDIA system. The previously analyzed sensor parameter sets of table 7.2 are thus extended in that way that they have four and five vertical measurement points respectively. The resulting sensor configurations are shown in table 7.3 and 7.4 and the corresponding alleviation performance data in Fig. 7.18 and 7.19. The notation of the sensor configurations is extended by an additional number directly behind the letter indicating the number of vertical measurement axes (cf. first red number in Fig. 7.15). Red boxes in Fig. 7.18 and 7.19 again highlight sensor configurations with no increase of the maximum bank altitude during any of the encounters. The red dashed boxes mark configurations with negligible increases of the maximum bank angle during only one encounter and with an absolute increase of less than $1°$.

Figure 7.18 and 7.19 show that an increase in the number of vertical measurement axes tends to result in an improved alleviation performance. The average reduction of the maximum bank angle is higher for most of the sensor parameter sets and reaches values of up to $76\,\%$ (compared to $68\,\%$ for the best sensor with 3 vertical measurement axes). The number of cases in which the OWIDIA system increases the maximum bank angle is significantly lower and the maximum and sum of the maximum bank angle increases over all altitudes is also reduced. The sensor sets with only three vertical measurement axes exhibit up to seven cases with an increased maximum bank angle, whereas at most four cases with increased bank angles occur if the sensor configurations are extended by a forth row of measurements. If the sensors have five vertical measurement axes, except for one sensor configurations, the sensor parameter sets exhibit at most two cases with increased bank angles. Both sensor extensions, with four or five vertical measurement axes, lead to noticeably more sensor configurations with no increase of the maximum bank angle (red solid boxes in Fig. 7.18 and 7.19) or only one increase with less than $1°$ (red dashed boxed in Fig. 7.18 and 7.19). These include sensor sets with a measurement range of $75\,\mathrm{m}$ and $90\,\mathrm{m}$ to the first measurement point. Among the sensor configurations with only three vertical measurement axes only those with a $\mathrm{range}_{\mathrm{MP1}}$ of $60\,\mathrm{m}$ had no or only one negligible increase of the maximum bank angle.

Table 7.3: Sensor configurations with four vertical measurement axes

Sensor configuration [-]	Number of vertical axes [-]	Number of horizontal axes [-]	Number of MP along axis [-]	Total number of MP [-]	$range_{MP1}$ [m]	Vertical field of view Θ_{scan} [°]	Lateral field of view Ψ_{scan} [°]	Blur depth [m]	Full scan update rate [Hz]	Single axis update rate [Hz]
B4-30-10-60	4	5	1	20	60	+/-10	+/-16	30	10	200
C4-30-10-60	4	7	1	28	60	+/-10	+/-16	30	10	280
D4-15-5-60	4	9	1	36	60	+/-10	+/-16	15	5	180
D4-30-10-60	4	9	1	36	60	+/-10	+/-16	30	10	360
J4-15-10-60	4	5	1	20	60	+/-10	+/-30	15	10	200
M4-15-5-60	4	3	3	36	60	+/-10	+/-30	15	5	60
M4-15-10-60	4	3	3	36	60	+/-10	+/-30	15	10	120
O4-15-5-60	4	3	5	60	60	+/-10	+/-30	15	5	60
S4-15-5-60	4	7	1	28	60	+/-10	+/-40	15	5	140
A4-15-10-75	4	3	1	12	75	+/-10	+/-16	15	10	120
I4-15-10-75	4	3	1	12	75	+/-10	+/-30	15	10	120
J4-15-10-75	4	5	1	20	75	+/-10	+/-30	15	10	200
K4-15-5-75	4	7	1	28	75	+/-10	+/-30	15	5	140
S4-15-5-75	4	7	1	28	75	+/-10	+/-40	15	5	140
J4-15-10-90	4	5	1	20	90	+/-10	+/-30	15	10	200
J4-30-10-90	4	5	1	20	90	+/-10	+/-30	30	10	200
K4-30-10-90	4	7	1	28	90	+/-10	+/-30	30	10	280
T4-30-10-90	4	9	1	36	90	+/-10	+/-40	30	10	360

Table 7.4: Sensor configurations with five vertical measurement axes

Sensor configuration [-]	Number of vertical axes [-]	Number of horizontal axes [-]	Number of MP along axis [-]	Total number of MP [-]	$range_{MP1}$ [m]	Vertical field of view Θ_{scan} [°]	Lateral field of view Ψ_{scan} [°]	Blur depth [m]	Full scan update rate [Hz]	Single axis update rate [Hz]
B5-30-10-60	5	5	1	25	60	+/-10	+/-16	30	10	250
C5-30-10-60	5	7	1	35	60	+/-10	+/-16	30	10	350
D5-15-5-60	5	9	1	45	60	+/-10	+/-16	15	5	225
D5-30-10-60	5	9	1	45	60	+/-10	+/-16	30	10	450
J5-15-10-60	5	5	1	25	60	+/-10	+/-30	15	10	250
M5-15-5-60	5	3	3	45	60	+/-10	+/-30	15	5	75
M5-15-10-60	5	3	3	45	60	+/-10	+/-30	15	10	150
O5-15-5-60	5	3	5	75	60	+/-10	+/-30	15	5	75
S5-15-5-60	5	7	1	35	60	+/-10	+/-40	15	5	175
A5-15-10-75	5	3	1	15	75	+/-10	+/-16	15	10	150
I5-15-10-75	5	3	1	15	75	+/-10	+/-30	15	10	150
J5-15-10-75	5	5	1	25	75	+/-10	+/-30	15	10	250
K5-15-5-75	5	7	1	35	75	+/-10	+/-30	15	5	175
S5-15-5-75	5	7	1	35	75	+/-10	+/-40	15	5	175
J5-15-10-90	5	5	1	25	90	+/-10	+/-30	15	10	250
J5-30-10-90	5	5	1	25	90	+/-10	+/-30	30	10	250
K5-30-10-90	5	7	1	35	90	+/-10	+/-30	30	10	350
T5-30-10-90	5	9	1	45	90	+/-10	+/-40	30	10	450

A larger number of vertical measurement points obviously increases the measurement point density because more measurement points are located in the same measurement volume. This effect is generally beneficial for a successful wake characterization and subsequent alleviation. At the same time, the increased number of measurement points also leads to a higher standard deviation of the measured line-of-sight velocities. Figure 7.18 and 7.19 show, however, that the increase in the measurement noise is not very large. Only if more than more range gate exist, as in the case of the sensor parameter sets of the category M and O, the raise of the standard deviation is significant. Concerning the practical realization of the lidar sensor an increase

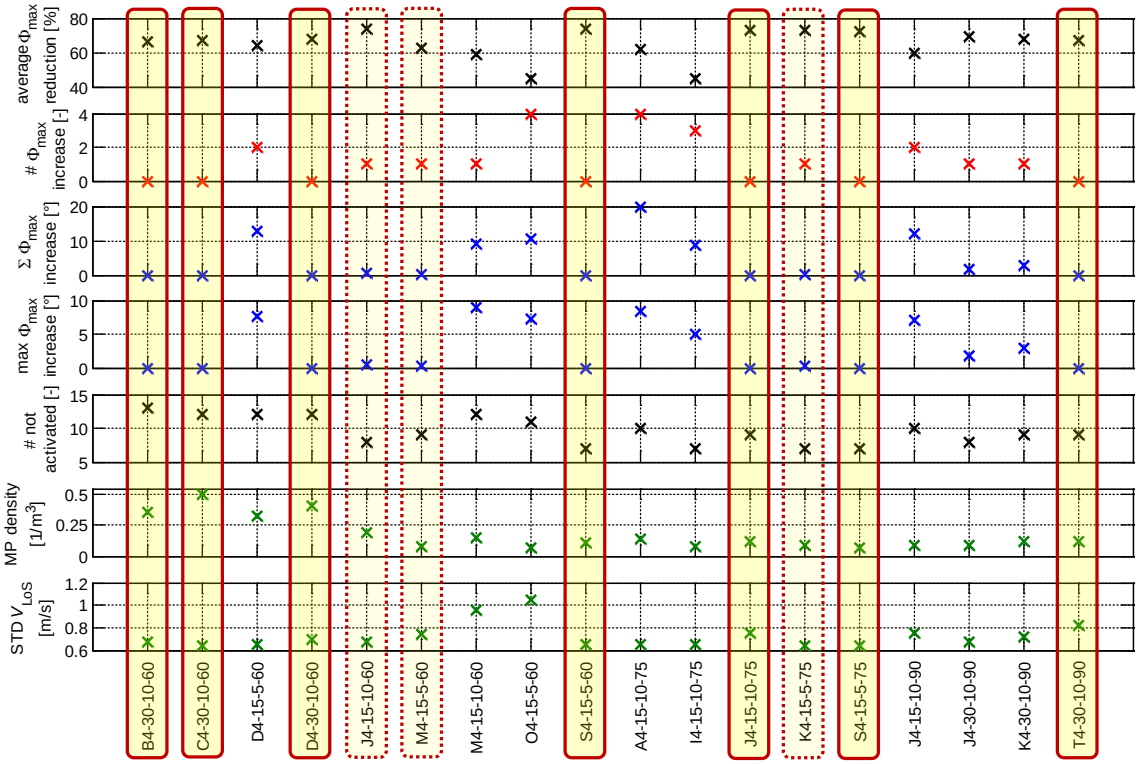

Figure 7.18: Summarized alleviation performance with sensor configurations with four vertical measurement axes for different encounter altitudes with $5°$ lateral encounter angle

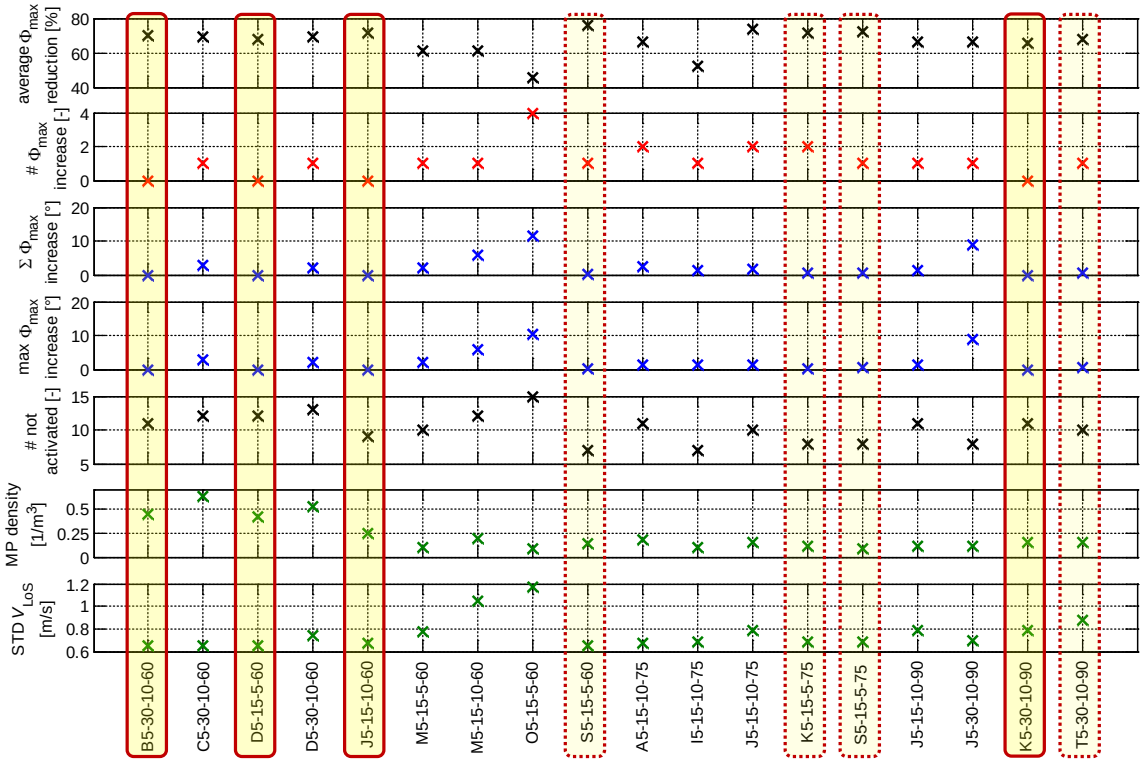

Figure 7.19: Summarized alleviation performance with sensor configurations with five vertical measurement axes for different encounter altitudes with $5°$ lateral encounter angle

of the measurement axes is unfavorable because it makes the sensor more complex and more challenging to build. Due to the large number of measurement axes the single axis update rate becomes very high with up to 360 Hz for sensors with four vertical axes and up to 450 Hz for some configurations with five vertical measurement axes (cf. table 7.3 and 7.4).

In summary an increase of the number of vertical measurement axes by trend improves the achievable alleviation performance as well as the robustness of the bank angle reduction for encounters at different altitude offsets between the wake vortex and the aircraft. Both sensor extensions with four and five vertical measurement axes provide many favorable sensor configurations, with which very good alleviation results could be achieved. An explicit improvement of the alleviation performance for an extension from four to five vertical measurement axes is in general not visible.

7.4.4 Influence of an Increased Vertical Field of View of the Lidar on the Alleviation Performance

Besides the number of vertical measurement axes, the vertical field of view is also not varied in the sensitivity study in section 7.3. It is thus analyzed in this section whether an increase in the vertical scan angle range Θ_{scan} can lead to an improved wake identification and alleviation. For this purpose, the previously analyzed sensor parameter sets are applied with an increased vertical field of view of +/-15° instead of +/-10°. The wake encounters are the same encounters with 5° lateral encounter angle and different altitude offsets between wake vortex and aircraft as in the previous sections 7.4.2 and 7.4.3. The summarized alleviation performance of sensor configurations with an increased vertical field of view (displayed as squares) compared to the sensor sets with the original +/-10° vertical field of view (represented as circles) for encounters at all altitudes is shown in Fig. 7.20 to 7.22. Sensor parameters for which the increased field of view leads to an improved alleviation performance are highlighted with green solid boxes. Green dashed boxes mark sensor configurations for which the increase in the vertical field of view improves the alleviation performance but the resulting performance is still not satisfactory.

The effect of an increased field of view in vertical direction is generally not very large. For sensor configurations with only three vertical measurement axes, it tends to impair the system performance. Almost all of these sensor configurations show a lower average bank angle and a rise in number of cases and magnitude of bank angle increases if the vertical scan angle range is increased to +/-15°. Only the sensor configuration O-15-5-60 shows a small improvement of the alleviation performance with a slightly higher average bank angle reduction and fewer encounters during which the OWIDIA system increases the maximum bank angle if the vertical field of view in increased. However, the magnitude of the largest increase of the maximum bank angle due to the OWIDIA system stays very high. With only three vertical measurement axes the distance between the vertical measurement points is comparably large. The extension of the vertical scan angle range further increases the vertical distance between the measurements, which impairs the wake characterization.

If the sensor configurations possess more than three vertical measurement axes, the increase in the vertical field of view is by trend more beneficial. With four or five vertical measurement

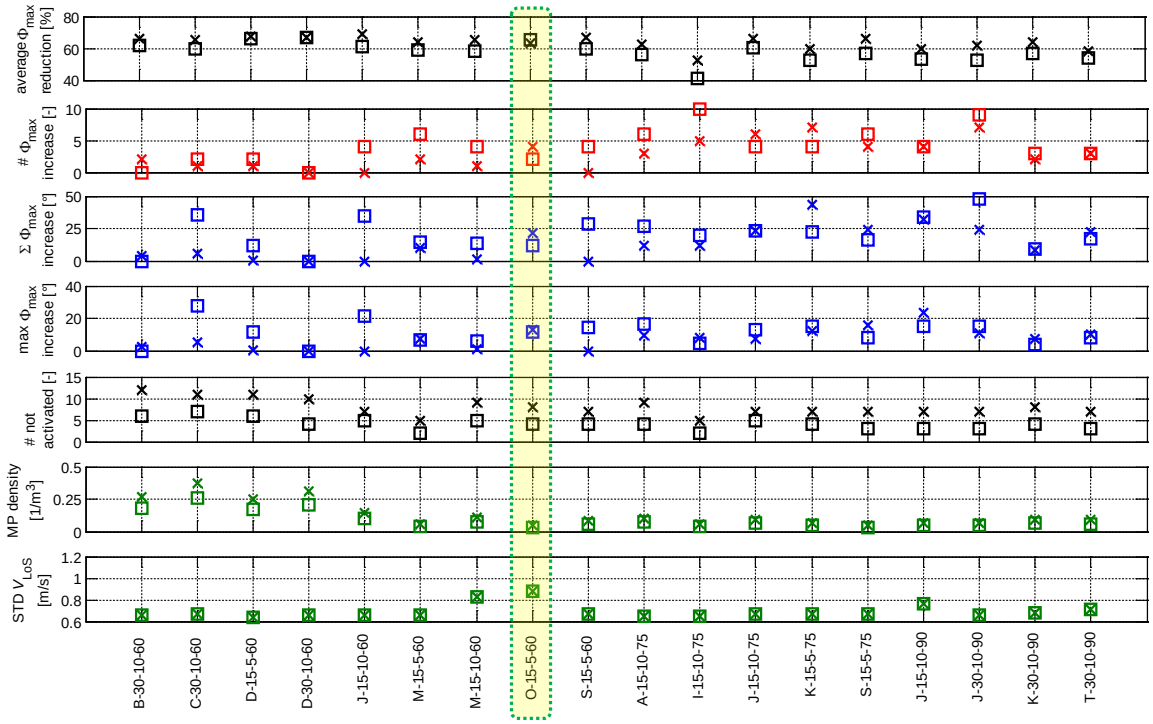

Figure 7.20: Comparison of summarized alleviation performance for sensor configurations with +/-10° (circles) and +/-15° (squares) Θ_{scan} and three vertical measurement axes

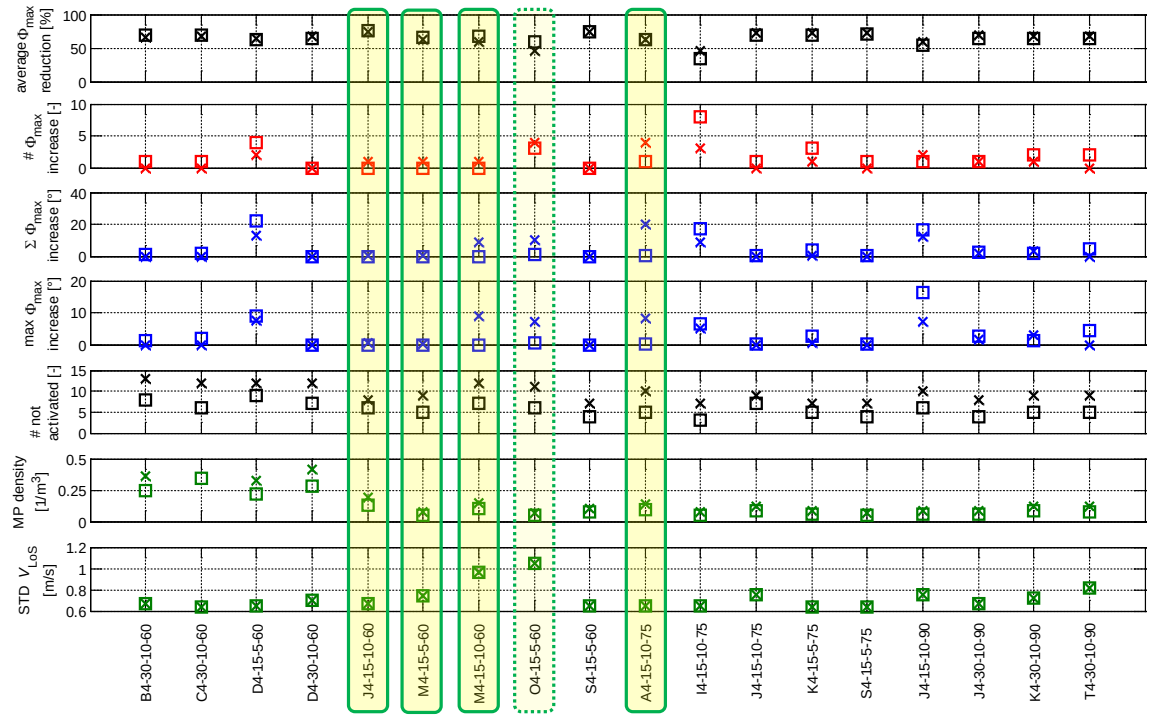

Figure 7.21: Comparison of summarized alleviation performance for sensor configurations with +/-10° (circles) and +/-15° (squares) Θ_{scan} and four vertical measurement axes

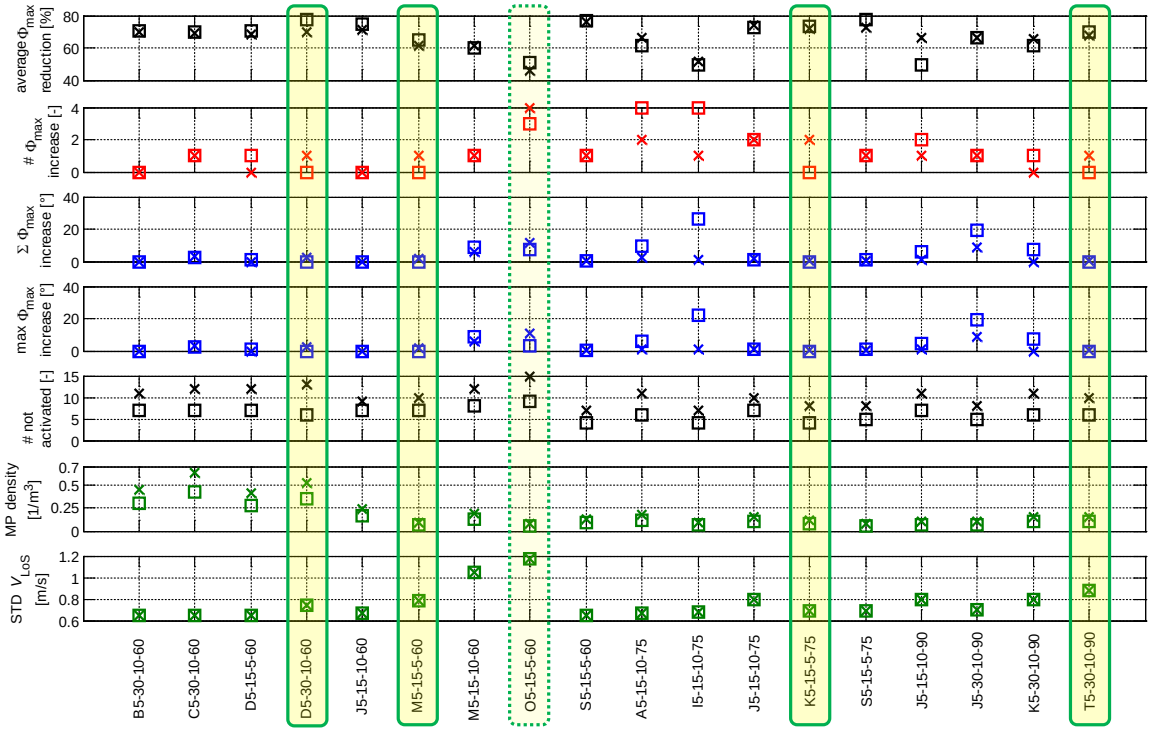

Figure 7.22: Comparison of summarized alleviation performance for sensor configurations with +/-10° (circles) and +/-15° (squares) Θ_{scan} and five vertical measurement axes

axes, more sensor configurations exist, for which the alleviation performance is improved due to the larger vertical scan angle range (cf. green boxes in Fig. 7.21 and 7.22). The vertical distance between the measurements is generally smaller for these sensor configurations than with only three vertical measurement axes. If the vertical scan angle range is increased the distance between neighboring measurements still allows a successful wake identification. At the same time the increased field of view leads to a larger entire measurement domain, which is additionally beneficial for the wake characterization.

In general, the increase of the vertical field of view helps especially for sensor configurations with more than one range gate to improve the alleviation performance. The additional measurement points along each measurement axis of theses sensors provide a comparably good vertical spatial resolution of the measurement. With a larger field of view the distance between the measurements is thus still small enough, whereupon the entire measurement domain is enlarged. It should be considered for future sensor studies to choose an irregular grid of measurement points in vertical direction. This might be a helpful mean to avoid the effect that important information about the wake vortex is lost due to too large spaces in between the lines of measurements.

For all considered sensor configurations the increase of the vertical field of view effects a reduction of the number of encounters during which the wake impact alleviation was not active (cf. fifth subplot of Fig. 7.20, 7.21, and 7.22). The larger measurement domain allows identifying wake vortices with larger vertical offsets. The OWIDIA system can thus still alleviate wake vortex encounters for wake vortices that are located comparably far above or below the

aircraft, as shown in Fig. 7.23. This effect also occurs if the overall alleviation performance is not improved due to the increase in the field of view, as can be seen in Fig. 7.24. Even though the maximum bank angle is less well reduced by the sensor with +/-15° vertical field of view during encounters with small altitude offsets, the bank angle alleviation still works for higher and lower vortex altitudes than in the case of the same sensor configuration with +/-10° vertical scan angle range. As the wake-induced aircraft reaction is not very strong at large altitude offsets between the aircraft and the wake vortex, however, the benefit of the OWIDIA system is not that large anymore during these encounters. It is more important that the OWIDIA system ensures good performance during encounters with small altitude offsets. If a sensor configuration leads to a poorer performance at small altitude offsets, it should not be used just because it permits the alleviation of the wake-induced aircraft response for very distant wake vortices.

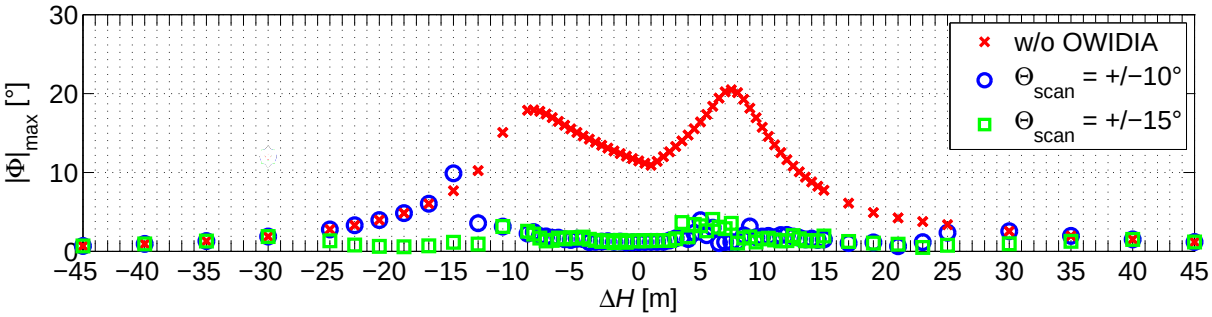

Figure 7.23: Comparison of the reduction of the maximum bank angle with sensor D5-30-10-60 with different vertical fields of view during encounters with 5° lateral encounter angle and various altitude offsets

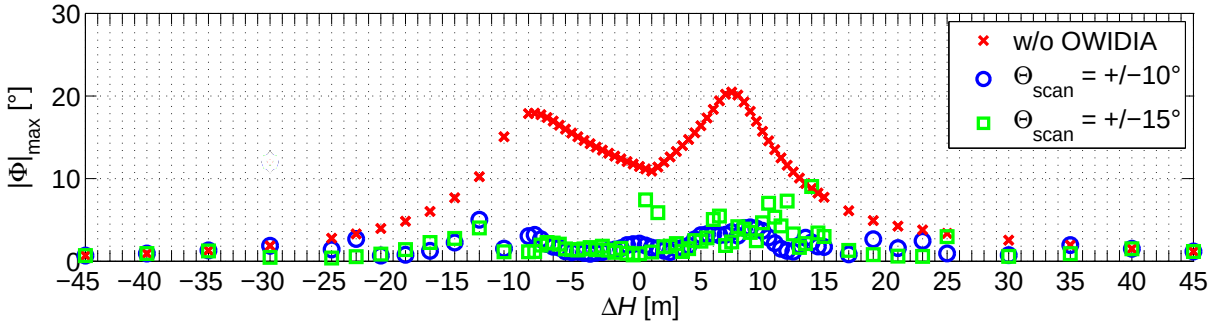

Figure 7.24: Comparison of the reduction of the maximum bank angle with sensor S4-15-5-75 with different vertical fields of view during encounters with 5° lateral encounter angle and various altitude offsets

In summary the benefit of the increase of the vertical field of view of the lidar sensor is not very large. For most of the sensor configurations, especially with three vertical measurement axes, the alleviation performance is worse if the sensor has a larger vertical field of view. For some sensor configurations, in particular with more than one range gate, the alleviation performance could be enhanced. The improvement is, however, not very strong.

7.4.5 Variation of Measurement Noise Level

The measurement uncertainty included in the lidar sensor model is a parameter that it very uncertainty itself. Its variation with sensor parameters such as the measurement range or the update rate is modeled according to the rough physical dependencies, as described in section 3.2. The absolute values of the measurement noise are, however, only an estimate and can vary significantly depending on the available technology level of the sensor. Improvements in the available laser power or receiver sensitivity can, for instance, essentially reduce the measurement noise. It shall thus be analyzed how strongly the results, obtained for the alleviation performance, depend on the specific values of the measurement noise. For this purpose the standard deviation of some of the previously analyzed sensor configuration is artificially varied whereupon the rest of the sensor parameters remain the same. As the assumptions for the measurement uncertainty in the applied sensor model are rather optimistic for current sensor technologies and a lower uncertainty level would be more favorable for the wake characterization, a further reduction of the standard deviation of the line-of-sight velocity is not analyzed but only an increase of the standard deviation is considered in the following.

For the sensor configurations D5-30-10-60_15, J4-15-10-75, and M4-15-5-60 the standard deviation of the line-of-sight velocity is increased to $120\,\%$, $150\,\%$, $175\,\%$, $200\,\%$ and $250\,\%$ of its nominal value (i.e. $100\,\%$). The resulting values for the standard deviation are displayed in table 7.5.

Table 7.5: Variation of measurement noise level of lidar sensor

Sensor configuration	$100\,\%$ STD V_{LoS} [m/s]	$125\,\%$ STD V_{LoS} [m/s]	$150\,\%$ STD V_{LoS} [m/s]	$175\,\%$ STD V_{LoS} [m/s]	$200\,\%$ STD V_{LoS} [m/s]	$250\,\%$ STD V_{LoS} [m/s]
D5-30-10-60_15	0.74	0.93	1.11	1.30	1.48	1.85
J4-15-10-75	0.75	0.94	1.13	1.31	1.59	1.88
M4-15-5-60	0.96	1.20	1.44	1.68	1.92	2.40

Figure 7.25 to 7.27 illustrate the reduction of the maximum bank angle with an active OWIDIA system compared to the maximum bank angle without OWIDIA during encounters with different altitude offsets between the wake vortex and the aircraft for varying measurement noise levels of the sensor configurations. As expected, an increase in the measurement noise impairs the wake impact alleviation performance of all sensor configurations. However, it can also be noticed that a small increase in the measurement noise level does not prohibit a successful application of the OWIDA system yet. If the standard deviation increases the same trend occurs for all three sensor configurations. With rising measurement noise level the altitude range in which the wake vortex can successfully be identified and alleviated decreases. In Fig. 7.25 to 7.27 this can be noticed by the fact that the same maximum bank angle with and without the OWIDIA occur at increasingly smaller altitude offsets between the wake and the aircraft if the measurement noise level rises. Furthermore, the bank angle reduction at moderate altitude offsets between the aircraft and the wake vortex becomes lower with higher standard deviations of the measured LoS velocity.

The development of the wake impact alleviation performance of the OWIDIA system applied with sensor J4-15-10-75 with increasing measurement noise, shown in Fig. 7.25, is especially desirable. The achieved bank angle reduction also decreases in these cases. However, expect for a negligible raise of the maximum bank angle during a single encounter with $200\,\%$ standard deviation, the maximum bank angle is never increased by the OWIDIA system. Even with comparably high standard deviations of $175\,\%$ and $200\,\%$, which corresponds to 1.31 m/s and 1.59 m/s, the OWIDIA system can still remarkably alleviate the wake-induced bank angle during many encounters. Only at a twice as high standard deviation of the LoS velocity compared the nominally assumed measurement noise, the wake impact alleviation is never active anymore.

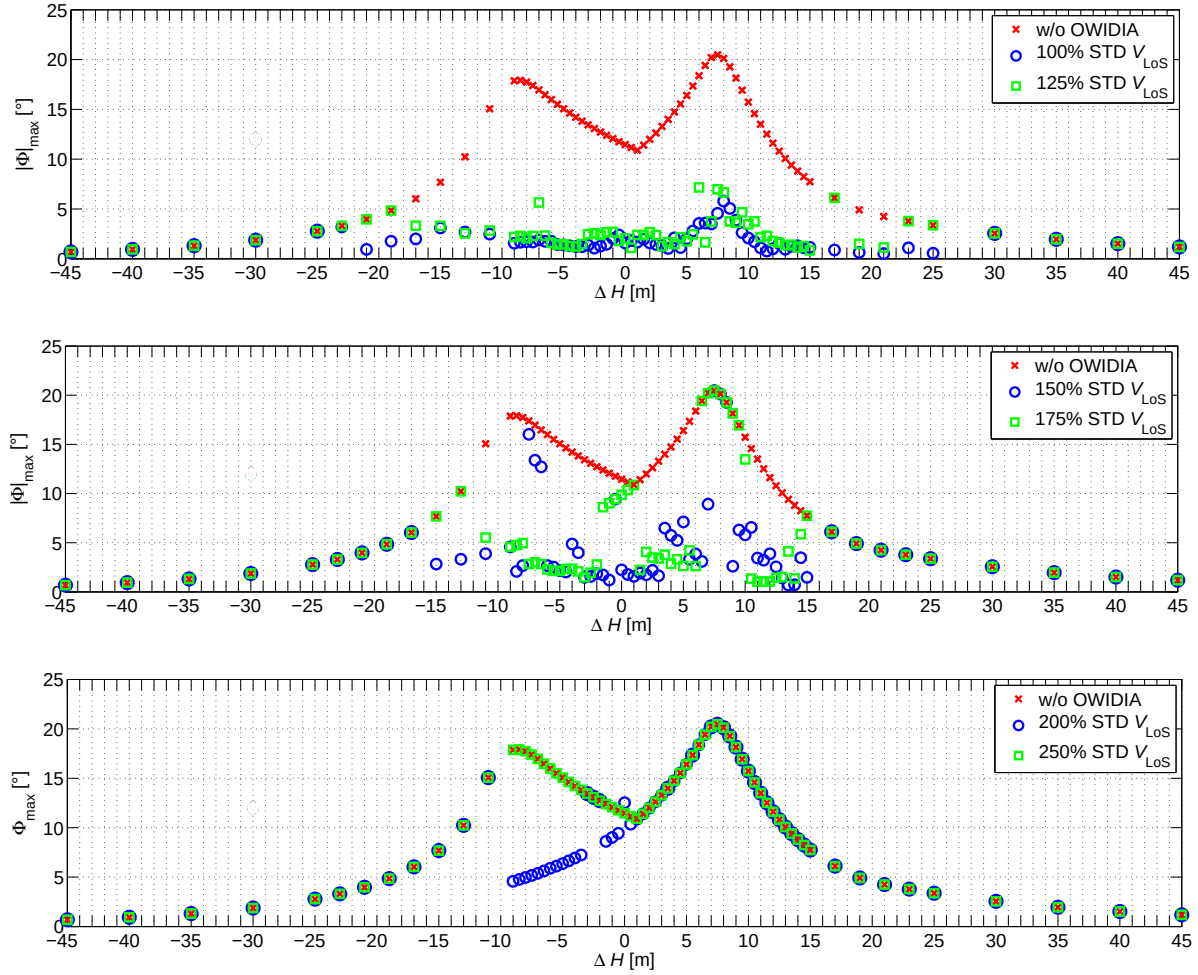

Figure 7.25: Variation of the wake impact alleviation performance at different encounter altitudes with increased standard deviation of the measured line-of-sight velocity of sensor J4-15-10-75

In case of the sensor M4-15-5-60 (cf. Fig. 7.26) the nominal measurement noise level is already comparably high. An increase of the standard deviation by $50\,\%$ already provokes a significant increase of the maximum bank angle during a few encounter scenarios. For this measurement noise level as well as further increased standard deviations, the sensor should not be used for the

OWIDIA system anymore. The maximum bank angle cannot be alleviated very well anymore and the occurring increases in maximum bank angle during many encounters are unacceptable.

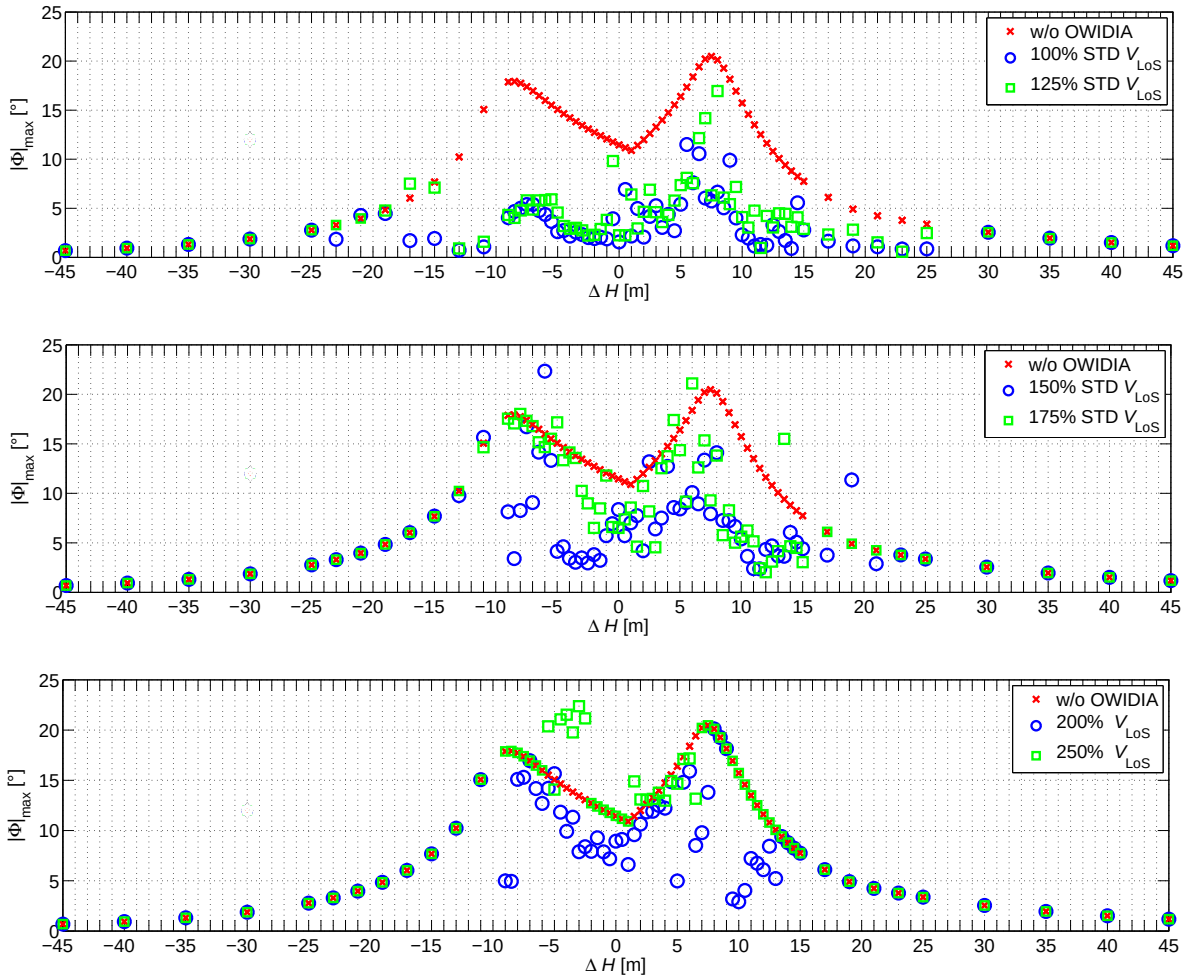

Figure 7.26: Variation of the wake impact alleviation performance at different encounter altitudes with increased standard deviation of the measured line-of-sight velocity of sensor M4-15-5-60

The variation of the standard deviation of the measured LoS velocity of sensor D5-30-10-60_15, presented in Fig. 7.27, shows a more favorable development of the system performance with increasing measurement noise again. From $175\,\%$ standard deviation of the nominally assumed value on the OWIDIA system is already not active anymore (expect for two encounters with negligible alleviation), but with lower measurement noise levels only one encounter with a strong bank angle increase due to the OWIDIA system occurs. Besides the outlier, the alleviation performance of the OWIDIA system is only reduced at smaller increases of the measurement noise but does not aggravate the aircraft response. Compared to the development of the alleviation performance with sensor J4-15-10-75 with increased measurement noise, the system performance of the OWIDIA system applied with sensor D5-30-10-60_15 is more strongly affected by the increase of measurement noise. Sensor J4-15-10-75 seems to have a more favorable measurement geometry, which already leads to a better alleviation performance at its nominal measurement noise level of 0.75 m/s (which is almost the same as the standard deviation of the

line-of-sight velocity of sensor D5-30-10-60_15) and still allows a successful wake characterization with larger standard deviations of the measured line-of-sight velocity, with which sensor D5-30-10-60_15 cannot be applied anymore.

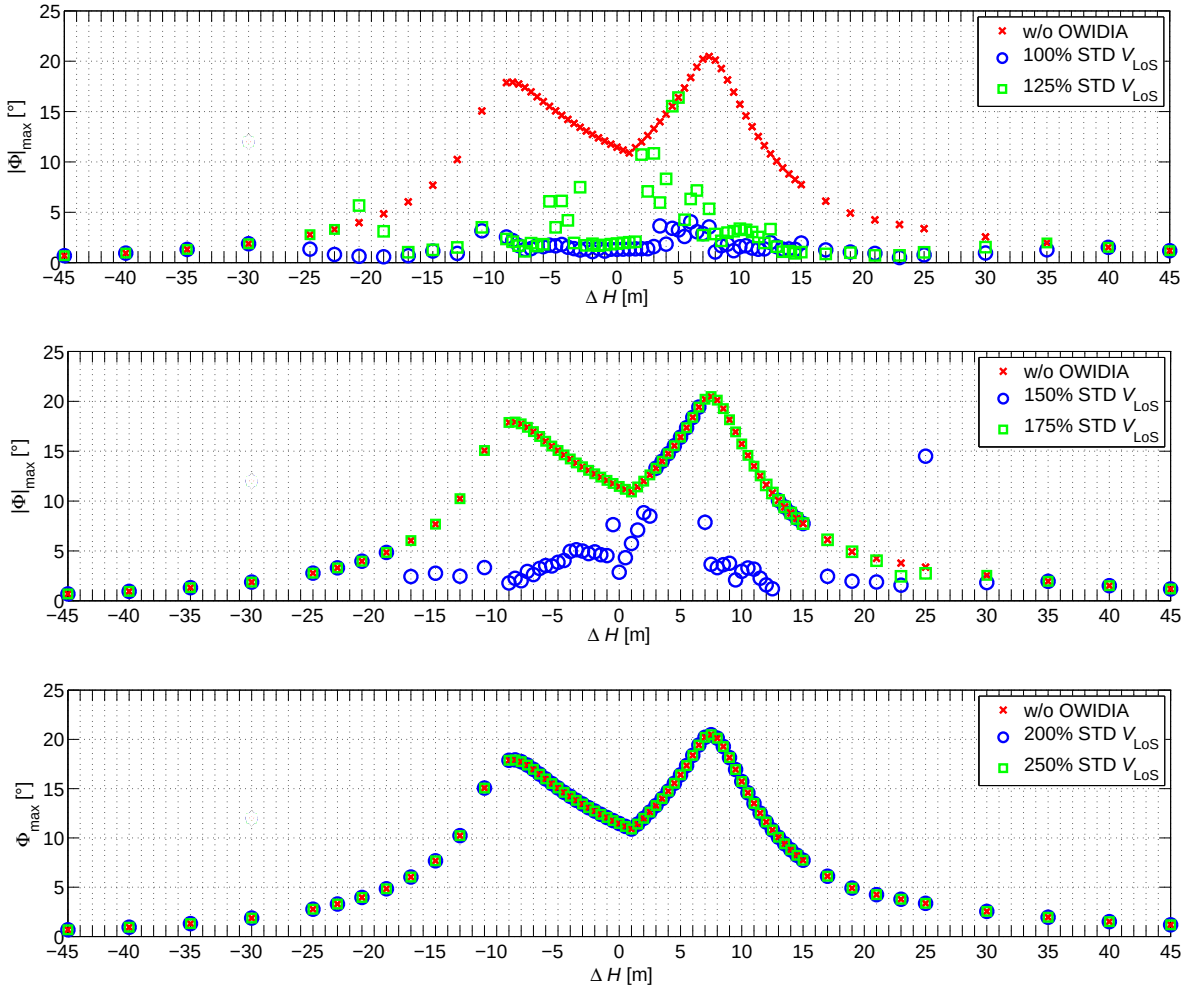

Figure 7.27: Variation of the wake impact alleviation performance at different encounter altitudes with increased standard deviation of the measured line-of-sight velocity of sensor D5-30-10-60_15

The variation of the standard deviation of the LoS velocity of the different lidar sensors shows that the success of the OWIDIA system is not extremely sensitive to the assumed measurement noise. Even though an increase in the measurement noise impairs the wake impact alleviation performance, small deviations from the assumed measurement noise levels do not ruin the benefit of the OWIDIA system yet. Nevertheless, the analysis also shows that in some cases measurements with too high standard deviations can in some cases also lead to increased maximum bank angles. In general, it is, of course, desirable to design the lidar sensor with measurement noise levels as low as possible in order to achieve the best possible alleviation performance.

7.4.6 Variation of Encounter Geometry

In the previous sections the altitude offset between the wake vortex and the aircraft has been varied but the angles between the flight paths of the generator and encountering aircraft have always been $5°$ in lateral and $0°$ in vertical direction. Especially during approach, this is a very likely encounter geometry because the aircraft usually follow the ILS flight path and therefore have very similar trajectories with only very small relative angles. Nevertheless, other encounter geometries can occur, for which the OWIDIA system should work as well. The performance of the OWIDIA system will thus be analyzed for further variations of the vertical and lateral encounter angles in the following. Lateral encounter angles of $5°$, $10°$, $15°$, and $20°$ are considered. Larger lateral encounter angles are not included in the analysis because the wake-induced aircraft response stays comparably small and the wake impact alleviation is not very effective anymore during these steeper encounter angles (cf. section 6.1.1). In vertical direction relative encounter angles of $-5°$, $-3°$, $0°$, $3°$, and $5°$ are analyzed. Larger relative encounter angles are not very likely to occur during approach and are therefore not included in the analysis here. For each combination of encounter angles the range of altitude offsets of the previous studies in section 7.4 is examined again.

Different sensor configurations that showed promising performance in the previous analysis are examined for the increased number of encounter angles. The study showed that the OWIDIA system also works well in other encounter scenarios. A very good bank angle alleviation could be achieved in the vast majority of the scenarios. However, the results also reveal that in the large number of encounter scenarios some encounter geometries are still challenging for the OWIDIA system. None of the examined sensor configurations could prevent increases of the bank angle due to the OWIDIA system in a few cases. In most of the cases, these increases are very small in magnitude and can be considered as negligible though.

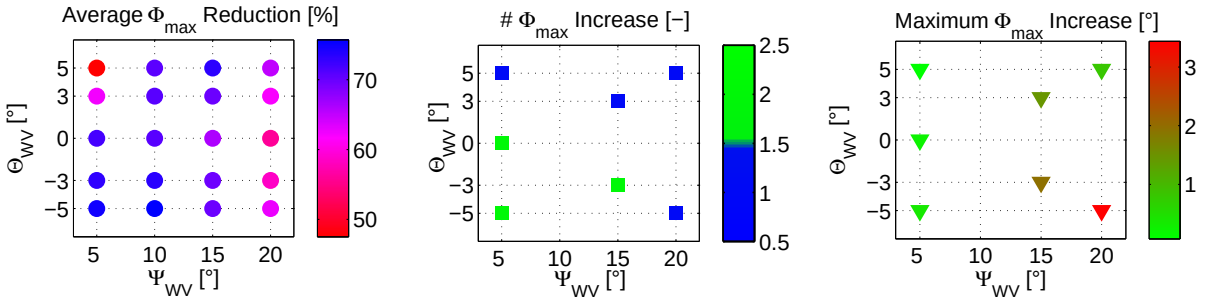

Figure 7.28: Average wake impact alleviation performance of the OWIDIA system with lidar sensor K5-15-5-75 for a range of encounter altitudes and encounter angles

A lidar sensor that allowes a very good wake impact alleviation performance is lidar sensor K5-15-5-75 (cf. table 7.4 for sensor parameters). Figure 7.28 shows the wake impact alleviation performance of this sensor for different encounter angles. For each combination of lateral and vertical encounter angles Ψ_{WV} and Θ_{WV} the displayed parameters represent the summary of all encounter altitudes. Equivalently to the previous figures in section 7.4 the average reduction of the maximum bank angle in the left subplot includes all cases in which the maximum bank during the encounter with an active OWIDIA system is less or equal to the maximum bank

angle during the encounter without OWIDIA. The cases, in which the maximum bank angle is increased due to the OWIDIA system, are shown separately in the remaining two subplots. If no symbol is shown for specific combinations of the lateral and vertical encounter angle in the center and right plot, this means that no increase of the maximum bank angle occurs during the encounters of all altitude offsets.

Figure 7.28 shows that the OWIDIA system in combination with lidar sensor K5-15-5-75 provides excellent alleviation performance in almost all of the encounter scenarios. The average reduction of the maximum bank angle during the encounters is about $70\,\%$ for most of the combinations of lateral and vertical encounter angle. When considering the bank angle alleviation for the different encounter altitudes separately for the different encounter altitudes of specific combinations of lateral and vertical encounter angle, like in Fig. 7.29 to 7.31 for the encounter scenarios $\Psi_{\mathrm{WV}} = 10°$ and $\Theta_{\mathrm{WV}} = 5°$, $\Psi_{\mathrm{WV}} = 5°$ and $\Theta_{\mathrm{WV}} = -3°$, and $\Psi_{\mathrm{WV}} = 10°$ and $\Theta_{\mathrm{WV}} = 0°$, the benefit of the OWIDIA system is demonstrated even more clearly.

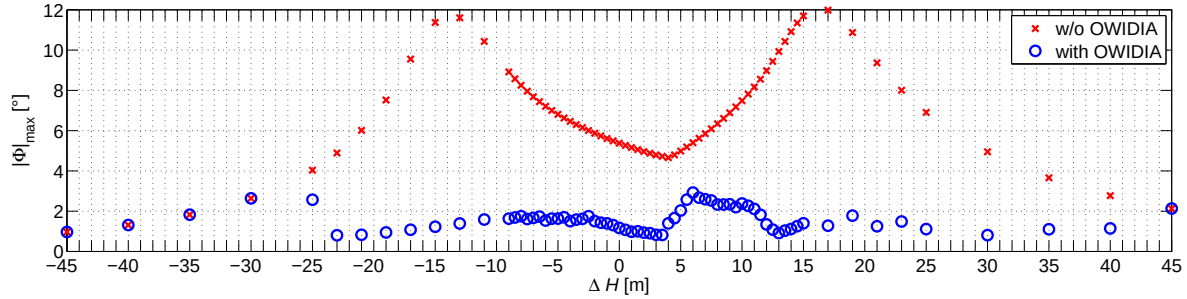

Figure 7.29: Bank angle reduction by the OWIDIA system with lidar sensor K5-15-5-75 for encounters with $\Psi_{\mathrm{WV}} = 10°$ and $\Theta_{\mathrm{WV}} = 5°$ at different encounter altitudes

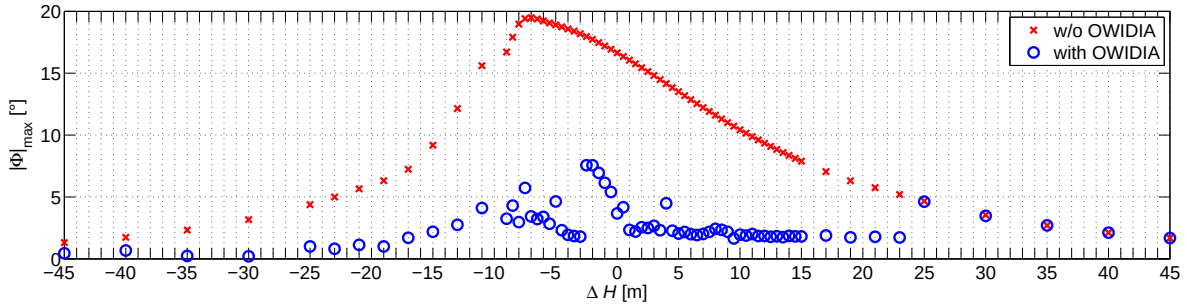

Figure 7.30: Bank angle reduction by the OWIDIA system with lidar sensor K5-15-5-75 for encounters with $\Psi_{\mathrm{WV}} = 5°$ and $\Theta_{\mathrm{WV}} = -3°$ at different encounter altitudes

The increases of the maximum bank angles occur especially during encounters with vertical encounters differing from zero. An increase of the maximum bank angle due to the OWIDIA system is, of course, very undesired. However, it occurs only in a very few cases. Four combinations of the lateral and vertical encounter angle lead to an increase of the bank angle in

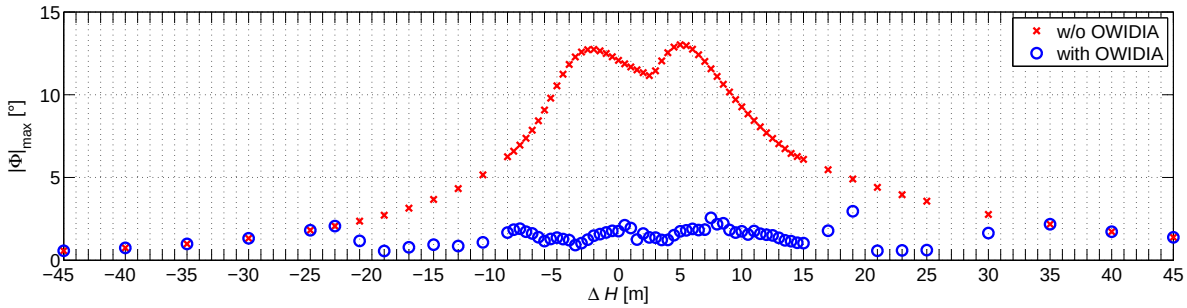

Figure 7.31: Bank angle reduction by the OWIDIA system with lidar sensor K5-15-5-75 for encounters with $\Psi_{WV} = 10°$ and $\Theta_{WV} = 0°$ at different encounter altitudes

one case (i.e. during one of the simulations with different altitude offsets), and in case of four combinations of the lateral and vertical encounter angle the bank angle is increased twice. The magnitude of the bank angle increase is low and stays below $1°$ in almost all cases. Only one simulation with $\Theta_{WV} = 20°$ and $\Psi_{WV} = -5°$ exhibits an increase of the maximum bank angle of $3.5°$. Even though this increase is larger compared to the increases in the other encounter simulations, a difference of $3°$ is still hardly noticeable for the pilot. Furthermore, the lateral and vertical encounter angles of $\Psi_{WV} = 20°$ and $\Theta_{WV} = -5°$ are both comparably large for encounters during approach and thus much less likely to occur than shallower encounters. In total, the increases can thus still be considered as uncritical.

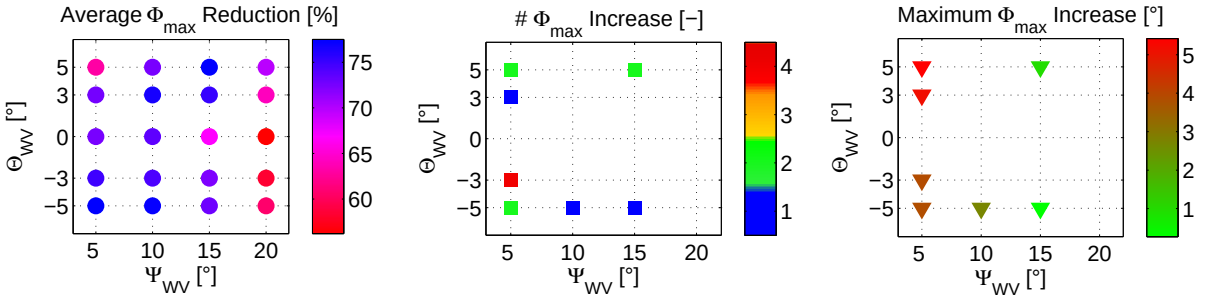

Figure 7.32: Average wake impact alleviation performance of the OWIDIA system with lidar sensor K5-15-5-75_15 for a range of encounter altitudes and encounter angles

If the vertical encounter angle is nonzero, it might be expected that an increased field of view, which did not lead to a significant alleviation performance for encounters with $\Theta_{WV} = 0°$ and $\Psi_{WV} = 5°$ (cf. section 7.4.4), could be beneficial because of the larger vertical distance between the wake vortex and the aircraft flight path. The analysis shows, however, that this is not the case. Figure 7.32 represents the wake impact alleviation performance for the same encounters as in Fig. 7.28 with the lidar sensor K5-15-5-75_15 with an increased vertical field of view of the sensor of +/-$15°$. The average bank angle reduction is slightly higher here compared to the encounters with this sensor with a smaller field-of-view of +/-$10°$. However, the number of cases in which the maximum bank angle is increased rises markedly and the magnitude of the maximum increases rises as well. The field of view of +/-$10°$ thus still seems to be the better choice for encounters with larger vertical encounter angles.

Another interesting observation is the fact that for the considered sensor configurations increases of the maximum bank angle occur particularly often and strongly for encounters with a lateral encounter angle of $\Psi_{WV} = 5°$ and especially in the combination with a vertical encounter angle of $\Theta_{WV} = -3°$. This effect can be found for the majority of the sensor configurations and is clearly visible, for instance, for sensor D-30-10-60 shown in Fig. 7.33.

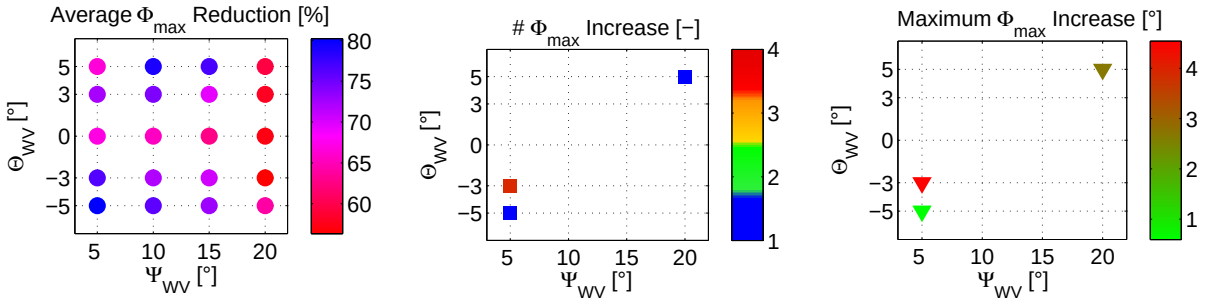

Figure 7.33: Average wake impact alleviation performance of the OWIDIA system with lidar sensor D-30-10-60 for a range of encounter altitudes and encounter angles

A detailed analysis of these cases with an increased bank angle reveales that increases of the maximum bank angle occur if the aircraft flies vertically paralelly to the wake vortex with a few meters vertical offset. This scenario happens in the considered cases because the wake vortex provokes a slight downwards motion of the aircraft, which results in a parallel flight path to the wake as illustrated in Fig. 7.34 for the corresponding case of sensor K5-15-5-75_15.

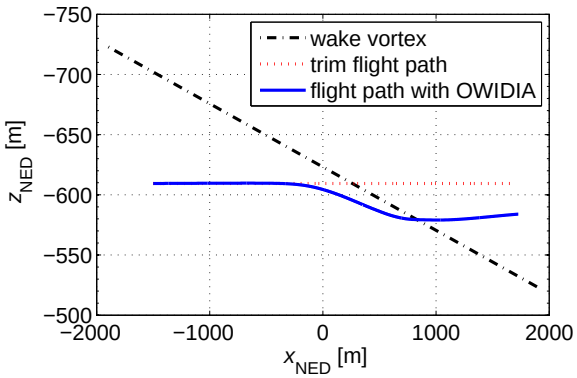

Figure 7.34: Flight path of the aircraft with an active OWIDIA system based on lidar sensor K5-15-5-75_15 during a $\Psi_{WV} = 5°$,$\Theta_{WV} = -3°$ encounter ($\Delta H = 13.5\,\text{m}$) with maximum bank angle increase of $4°$

In this case the wake vortex is sometimes positioned very unfavorably in between the vertical measurement positions of the lidar sensors (cf. Fig. 7.35). Due to the selected scan pattern the measurements are approximately located in an equidistant grid. If the vertical position of the vortex core lies unfavorably between the measurements, this impairs the wake identification and can lead to the increase of the maximum bank angle. Future investigations should put a special

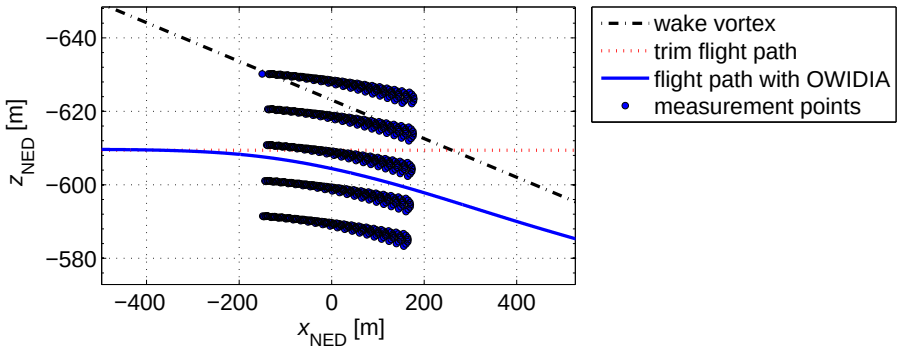

Figure 7.35: Measurement point locations relative to wake vortex during encounter of Fig. 7.34 at $t = 20\,\mathrm{s}$

focus on these encounter scenarios with shallow lateral and vertical encounter angles. An improved performance might be achieved by defining more complex scan patterns with unequal spacing of the measurements in vertical direction.

In summary the variation of the encounter angles demonstrated that the OWIDIA system works well also in different encounter geometries. Even though some cases with increases of the maximum bank angles occurred, the number of these cases was small and the magnitude of the bank angle increases negligible such that the increases can be considered as uncritical. Especially for encounters with large relative vertical encounter angles such as +/-5° it also has to be kept in mind that the occurrence of these encounter scenarios during approach is much less likely than encounters with no vertical encounter angle because the aircraft usually approach other aircraft with the approximately same flight path angle. So altogether a great benefit can be expected from the OWIDIA system.

7.5 Application to LES Vortices

In the previous investigations of the OWIDIA system the wake vortex affecting the aircraft has always been modeled as an analytical Burnham-Hallock wake vortex (cf. section 2.3). This is a simplified wake vortex model, which obviously differs from realistic wake vortices occurring under real flight conditions. For wake vortices of low age the Burnham-Hallock model provides a fair approximation of the vortex flow fields, even though effects such as turbulence are also not included. With increasing vortex age, the vortices deviate more and more from the straight lines assumed in the analytical wake vortex models such as the Burnham-Hallock model. As the wake identification assumes a straight Burnham-Hallock model, it cannot cover very old, deformed vortices. It is thus expected that the current implementation of the OWIDIA does not work for very old vortices. It shall be analyzed, however, up to which vortex age the current implementation still works. For older vortices the vortex model within the OWI needs to be adapted, which goes beyond the scope of this thesis. The purpose of this section is therefore rather to examine the limits of the current realization of the OWIDIA system and to provide an outlook for future extensions of the system.

In the following, the OWIDIA system is applied with wake vortices of different ages ranging from 16 s to 136 s. The corresponding vortices are illustrated in Fig. 7.36. These flow fields are computed using Large Eddy Simulations (LES) under the assumption of atmospheric conditions with moderate turbulence and neutral thermal stratification ($N^* = 0$, $\epsilon^* = 0.23$), as described in section 2.3. They can be considered as much more realistic than analytical wake vortex models because they cover more details of the wake physics such as wake deformation and decay.

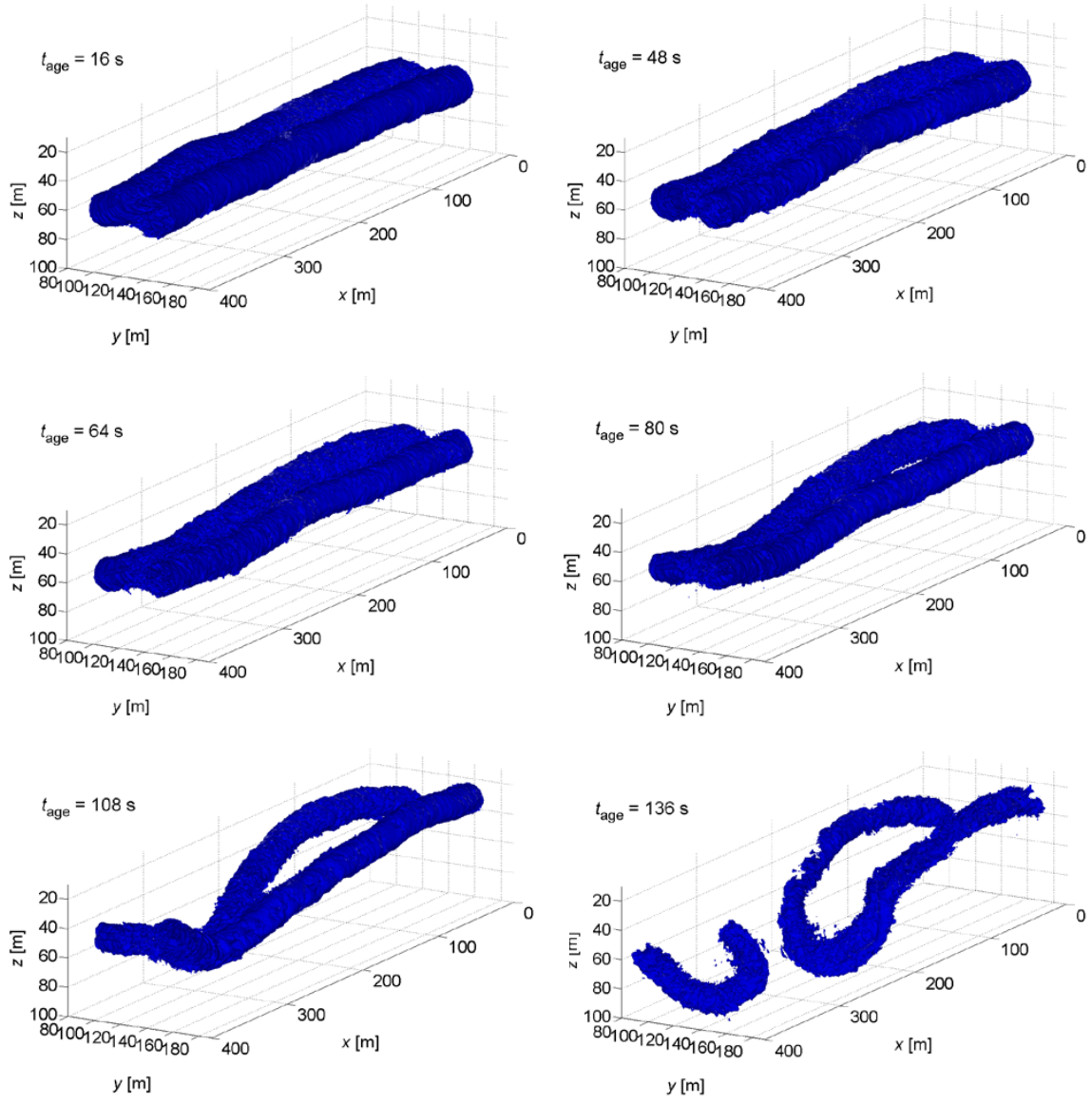

Figure 7.36: LES wake vortices for OWIDIA application to different vortex ages[10]

[10] Vechtel (2016), Paper about the analysis of wake vortex encounters with straight and deformed wake vortices.

Figures 7.37 to 7.42 show the comparison of the maximum bank angles during $5°$ lateral encounters[11] with different altitude offsets for the wake vortices of different ages of Fig. 7.36. The LES vortices are embedded in a three-dimensional field with a different geometrical reference than the reference system used for the analytical vortices presented in the previous sections. This explains the altitude offset of about $55\,\text{m}$ of the z-coordinates of the encounters with LES and Burnham-Hallock wake vortices.[12] For the 16-s-old wake vortex the OWIDIA system works very well. The OWIDIA system leads to a very successful reduction of the wake-induced bank angle during most of the encounters at different altitudes. An increase of the maximum bank angle due to the OWIDIA system compared to the case without OWIDIA occurs in none of the encounter scenarios. The fact that the OWIDIA system works equally well for a 16-s-old LES wake vortex is not self-evident. On the one hand, the lines of the vortex cores are still approximately straight at such a comparably young vortex age and are in this regard similar to a Burnham-Hallock wake vortex model. It could thus be expected that the online wake identification, which uses a straight Burnham-Hallock model as the basis for the identification, can find suitable parameters to match the measured wake vortex. On the other hand, the flow field generated in the LES simulations is more complex than the wind velocities resulting from an analytical Burnham-Hallock wake vortex. It contains turbulence and the vortices are only approximately but not perfectly parallel and straight. The local wind velocities of both flow fields can hence still deviate from each other. Nevertheless, the OWIDIA system can appropriately identify this wake vortex and effectively alleviate its impact on the aircraft. As the LES wake vortex is more realistic than the analytical wake vortex, a successful application of OWIDIA system in combination with these vortices, as it has been demonstrated in Fig. 7.37, is an important step for the realization of the system.

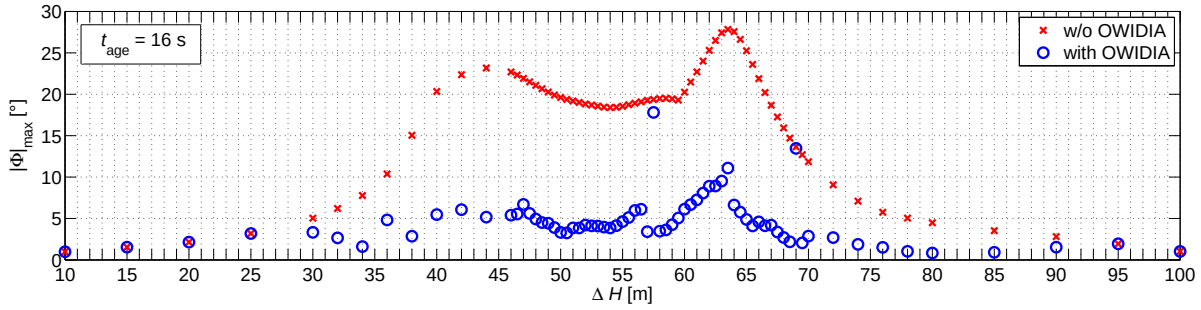

Figure 7.37: Bank angle reduction of the OWIDIA system with lidar sensor K5-15-5-75 during $5°$ lateral encounters at different altitudes with a LES wake vortex of $16\,\text{s}$

For a 48-s-old-LES wake vortex the wake impact alleviation of the OWIDIA system is slightly reduced, as shown in Fig. 7.38. During most of the encounters with medium altitude offsets, which result in large wake-induced bank angles, the OWIDIA system still effects a substantial

[11] Airbus A320 behind Airbus A340, in approach, $0°$ vertical encounter angle, normal active, no pilot inputs, autopilot disengaged.

[12] Positive altitude offsets ΔH still indicate that the wake vortex is located above the center of gravity of the aircraft.

alleviation of the maximum bank angle. However, the relative reduction is lower than in case of the younger 16-s-old wake vortex. Due to the slowly starting deformation of the wake vortex, the differences between the Burnham-Hallock wake vortex model provided by the OWI, on the basis of which the compensating control commands are determined, and the actual wake vortex disturbance become larger in case of the 48-s-old wake vortex. This trend continues for the 64-s-old wake vortex, presented in Fig. 7.39. The wake impact alleviation performance is further impaired but the OWIDIA system is still beneficial during most of the encounters. The increases of the maximum bank angle only occur in very few encounter scenarios of the 48- and 64-s-old vortices and are negligible due to their small magnitude. The current version of the OWIDIA system hence seems to be applicable for deformed wake vortices up to this level of deformation.

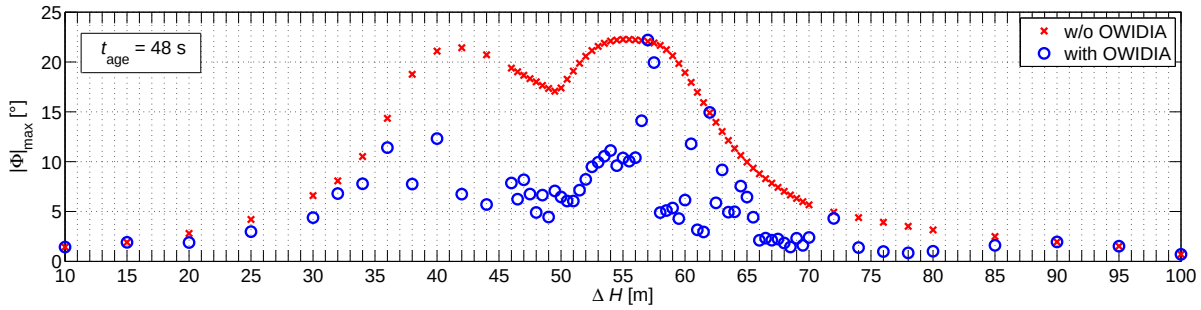

Figure 7.38: Bank angle reduction of the OWIDIA system with lidar sensor K5-15-5-75 during 5° lateral encounters at different altitudes with a LES wake vortex of 48 s

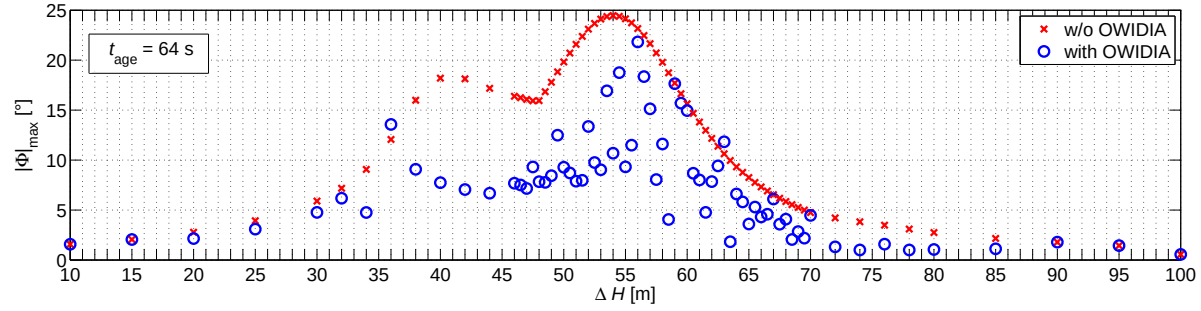

Figure 7.39: Bank angle reduction of the OWIDIA system with lidar sensor K5-15-5-75 during 5° lateral encounters at different altitudes with a LES wake vortex of 64 s

If the vortex age is further increased, like in the case of the 80-s-old wake vortex shown in Fig. 7.40 and the even older and more strongly deformed wake vortices of 108 s and 136 s in Fig. 7.41 and 7.42, the current realization of the OWIDIA system is not applicable anymore. As the underlying Burnham-Hallock wake vortex model differs too strongly from the actual wake-induced flow field in these cases, the OWIDIA system leads to much larger maximum bank angles compared to the encounter without the OWIDIA system during many encounter scenarios and should thus not be applied for these vortices.

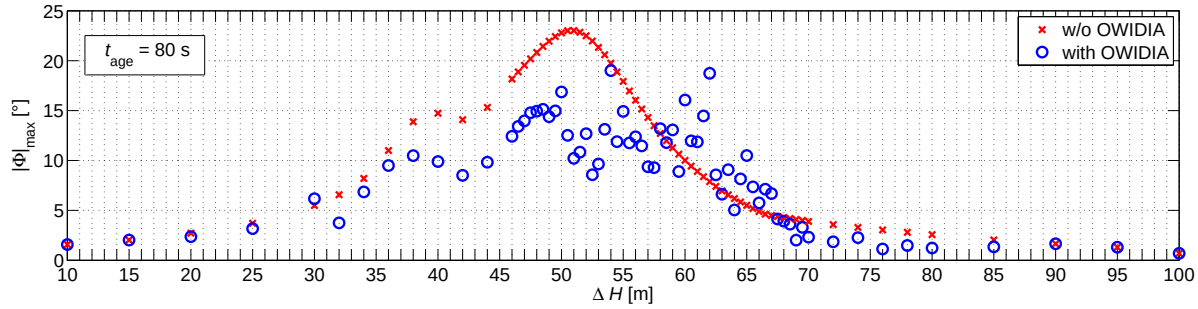

Figure 7.40: Bank angle reduction of the OWIDIA system with lidar sensor K5-15-5-75 during $5°$ lateral encounters at different altitudes with a LES wake vortex of $80\,s$

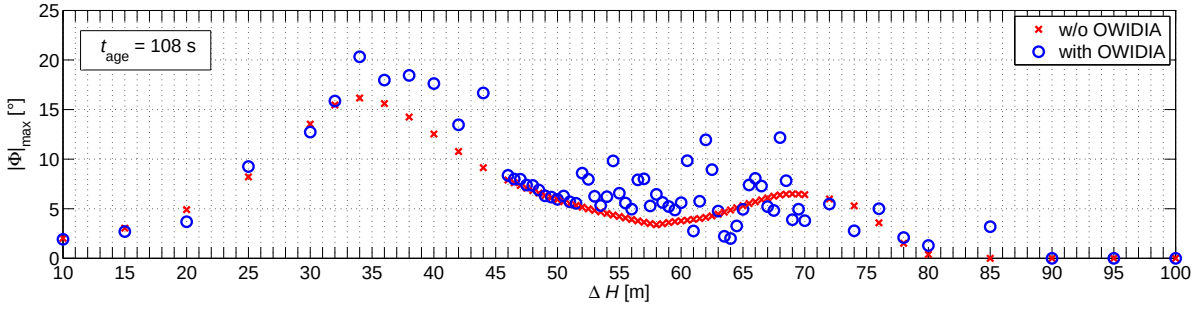

Figure 7.41: Bank angle reduction of OWIDIA system with lidar sensor K5-15-5-75 during $5°$ lateral encounter at different altitudes with LES wake vortex of $108\,s$

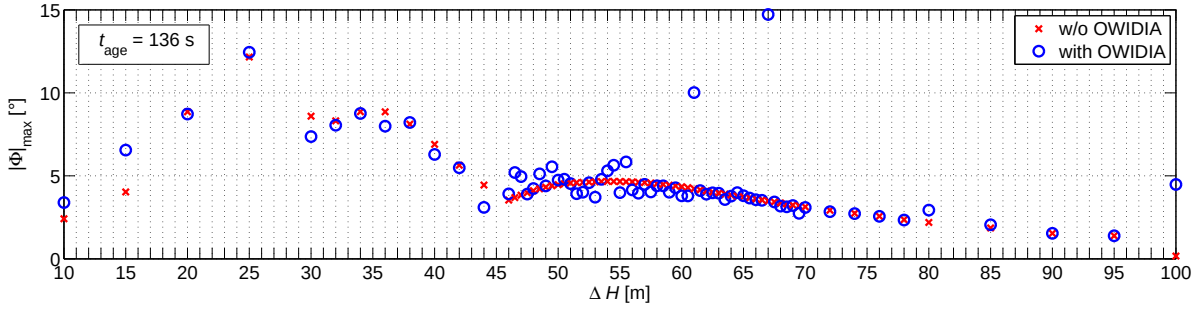

Figure 7.42: Bank angle reduction of the OWIDIA system with lidar sensor K5-15-5-75 during $5°$ lateral encounters at different altitudes with a LES wake vortex of $136\,s$

In order to allow an application of the OWIDIA system with very old, deformed wake vortices, the wake vortex model in the OWI module needs to be revised. The model of the wake identification has to be extended by additional parameters modeling the curved shape of the deformed vortices. Possible approaches for an analytical model of deformed vortices are provided in *Vechtel (2010)*[13] and *Münster (2011)*[14], whereupon the curvature is described by sine-functions. A short outline of a possible application of these models for the OWI is provided in appendix G. In this context, the criteria of the plausibility check of the OWI (cf. section 5.2.5) need to be revised as well. Their current formulation has been developed for straight vortices and might be too limiting for deformed vortices. The implementation and analysis of these extensions of the OWIDIA system goes beyond the scope of this thesis, but should be realized in future works in order to make the system applicable for all possible encounter situations that could occur in real flight. This is particularly important as investigations of the severity of wake encounters revealed that deformed wake vortices can still pose a serious safety hazard for the encountering aircraft (especially for vortex ages close to the transition from curved wake vortices to vortex rings, the so-called linking).[15]

Concerning the current realization of the OWIDIA system the brief analysis with LES vortices showed that

- the current implementation of the OWIDIA system can successfully be applied with realistic LES vortices of a young vortex age. Even though the LES vortices include turbulence and are never perfectly straight, the OWIDIA works equally well for LES vortices of an age of $16\,\mathrm{s}$ (in an atmosphere with moderate turbulence and neutral thermal stratification) as for analytical wake vortex models.
- The OWIDIA system seems to alleviate the wake-induced bank angle acceptably well for wake vortices up to an age of moderate deformation. For moderately deformed wake vortices of an age of $48\,\mathrm{s}$ and $64\,\mathrm{s}$ the current OWIDIA system still reduces the maximum bank about $50\,\%$ during most of the $5°$ lateral encounters and increases of the maximum bank angle occur only at very few encounter altitudes and with negligible magnitude.
- For more strongly deformed wake vortices (such as vortices of an age of $80\,\mathrm{s}$ and older in an atmosphere with moderate turbulence and neutral thermal stratification), the model in the online wake identification has to be extended by parameters allowing curves vortices and vortex rings and the plausibility check of the OWI has to be revised.

For a final evaluation whether the current OWIDIA system can reliably alleviate all wake encounters for vortices up to an age of $64\,\mathrm{s}$ more encounter scenarios need to be considered. The present analysis should only demonstrate the trends of the limits of the applicability of the cur-

[13] Vechtel (2010), DLR institute report about the development of an analytical wake vortex model for deformed vortices.

[14] Münster (2011), DLR institute report about the identification and analysis of an analytical wake vortex model for deformed vortices.

[15] Vechtel (2017), Dissertation about the influence of vortex deformation on the hazard analysis of wake vortex encounters.

rent OWIDIA system. The exact limits are not relevant because the analysis shows that the OWI needs to be extended for the application to old wake vortices anyway. Future works should thus first extend the OWI such that deformations can be included in the wake vortex model and then recheck if the selected lidar sensor configurations are still suitable with the revised OWIDIA system.

The characteristics of suitable sensor configurations for the application of the revised OWIDIA system to deformed vortices are expected to exhibit the same trends as suitable sensor configurations for the application of the current OWIDIA system to straight vortices. It is assumed that the application to deformed vortices also requires a good tradeoff of spacial resolution (especially close to the vortex core, where significant wake-induced wind velocities occur) and measurement noise. Analogously to the application to straight vortices, it likewise has to be assured that the wake vortex is not places unfavorably between the lines of the measurements. It is possible that larger fields of view and buffer sizes might be necessary in order to characterize the curvature of the wake vortex (which has a large wavelength in the order of $400\,\mathrm{m}$). As the wake vortex model in the OWI to describe deformed wake vortices has more parameters, the converge of the parameter estimation algorithm might be more challenging and the definition of these parameters should be selected reasonably in order to avoid numerical problems.

7.6 Estimation of Possible Reduction of Separation Minima

The application of the OWIDIA system under different conditions with varying encounter geometries, vortex ages, and sensor configurations demonstrated that the system has a great potential to alleviate the wake-induced bank angle of the encountering aircraft. In combination with suitable sensor configurations, the OWIDIA system was able to reduce the maximum bank angle by about 70 - $80\,\%$ for the majority of the cases and up to $90\,\%$ for some encounter scenarios. In order to get a feeling of how beneficial this bank angle reduction could be with regards to the overall goal of reducing the separation minima between subsequent aircraft this section provides a very simplified estimation of potential reductions of the separation distances. A final adaptation of the wake-vortex-based separation minima for aircraft with the OWIDIA system is not possible yet at this stage of development. It would require the specification of the exact sensor characteristics, a very detailed analysis of the system performance in combination with this sensor configuration, and the definition of the evaluation metrics describing a safe wake vortex encounter under relaxed separation distances (which has not been agreed on to date). This detailed analysis goes beyond the scope of this thesis. Instead, the present section shall provide a first impression of the order of magnitude of the reduction of separation distances that could possibly be achieved thanks to the OWIDIA system.

For this purpose it is assumed that an aircraft with the OWIDIA system might be allowed to fly closer to the leading aircraft than the current minimum separation standards if its aircraft reaction stays smaller than the aircraft reaction that it would exhibit without the OWIDIA system at the minimum distance of the current ICAO wake-vortex-based separation minima. Figure 7.43 shows the bank angle excursion of the A320 without the OWIDIA system during encounters of

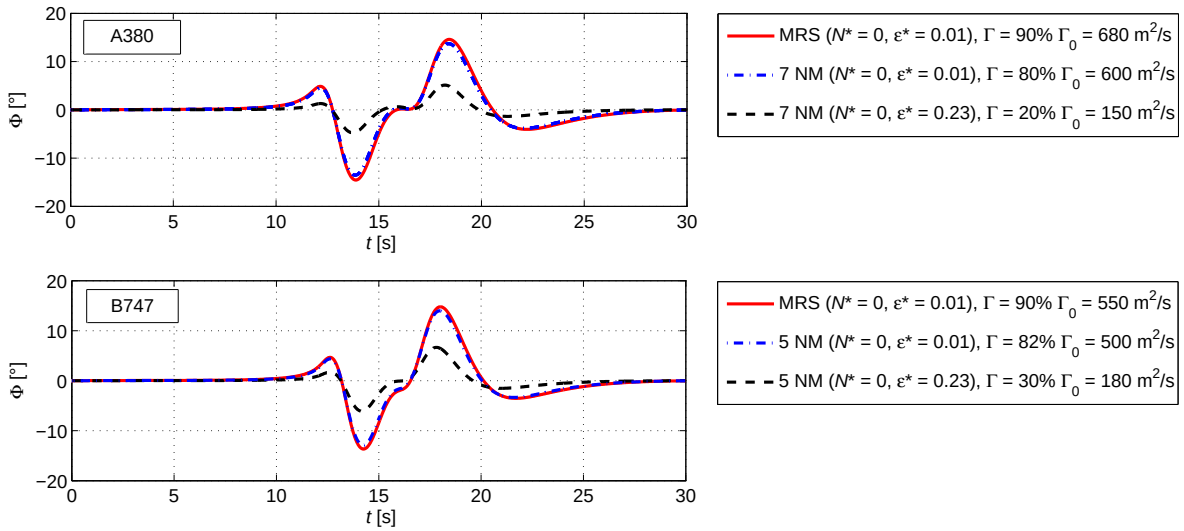

Figure 7.43: Bank angle excursion during encounters with wake vortices of an Airbus A380 and Boeing B747 without the OWIDIA system at different separation distances

the wake vortex of an Airbus A380-800 and Boeing B747-400. The geometry of the encounter scenario represents the standard scenario described in section 4.4 of a $10°$ lateral encounter with no vertical encounter angle and $2\,\text{m}$ altitude offset (wake vortex above the aircraft) during approach.[16] The minimum separation between the A320 behind the Airbus A380 according to the current ICAO standard is $7\,\text{NM}$, the minimum separation behind the Boeing B747, which belongs to the wake-vortex category HEAVY, is $5\,\text{NM}$ (cf. appendix A). The strength of the aircraft reaction occurring during these encounters depends on the vortex strength at these distances, which in turn is strongly dependent on the atmospheric conditions (cf. Fig. 2.4). The blue dash-dot lines in Fig.7.43 depict the bank angle excursion during encounters with a vortex circulation occurring at $7\,\text{NM}$ and $5\,\text{NM}$ respectively under atmospheric conditions with no turbulence and neutral thermal stratification ($N^* = 0$, $\epsilon^* = 0.01$). These conditions correspond to a worst case scenario because they lead to the slowest possible decay of the vortex circulation.[17] The black dashed lines illustrate the aircraft response for encounters with wake vortices with the circulations occurring at $7\,\text{NM}$ and $5\,\text{NM}$ under realistic atmospheric conditions for the lower layer of the atmosphere[20] with moderate temperature and neutral thermal stratification ($N^* = 0$, $\epsilon^* = 0.23$). The aircraft reactions at minimum ICAO separation distances under realistic atmospheric conditions (black dashed line) are used as a conservative reference. The red solid curves in Fig. 7.43 display the bank angle reaction of the A320 under worst case

[16] The aircraft flies in normal law without pilot inputs and autopilot disengaged.

[17] The underlying data of the aircraft weight, wing span, and approach speed in Fig. 7.43 are based on manufacturer data[18,19] and assumed to be the maximum landing weight of $395\,\text{t}$ and $296\,\text{t}$, a wing span of $79.8\,\text{m}$ and $64.9\,\text{m}$, and an approach speed of $71\,\text{m/s}$ and $81\,\text{m/s}$ for the A380 and B747 respectively.

[19] Airbus (2015), Section 3.5.0, Airbus A380 manual about aircraft characteristics.

[19] Boeing (2011), Table of aircraft data of different Boeing aircraft.

[20] Frech et al. (2007), Paper about the production and analysis of a weather database for the terminal area Frankfurt airport.

conditions at Minimum Radar Separation (MRS), which is assumed to be 2.5 NM in this case.[21]

Table 7.6: Maximum bank angles during wake vortex encounters without the OWIDIA system at different separation distances

	$\lvert\Phi\rvert_{\text{max}}$ [°] MRS, $N^* = 0$, $\epsilon^* = 0.01$	$\lvert\Phi\rvert_{\text{max}}$ [°] ICAO, $N^* = 0$, $\epsilon^* = 0.01$	$\lvert\Phi\rvert_{\text{max}}$ [°] ICAO, $N^* = 0$,$\epsilon^* = 0.23$
A380	$14.6°$	$13.7°$	$5.1°$
B747	$14.8°$	$14.0°$	$6.7°$

The assumption, taken here, is that the separation distances can be reduced to MRS if the maximum bank angle during the encounter at MRS with the OWIDIA system is lower than the maximum bank angle without the OWIDIA system at the current ICAO separation under realistic atmospheric conditions. The maximum bank angles occurring without the OWIDIA during the different encounters are shown in table 7.6. In order to get at most the same maximum bank angle as at the ICAO separation minima, the maximum bank angle of the encounter at MRS has to be reduced by $55\,\%$ in case of the B747 and by $65\,\%$ in case of the A380.[22] According to the previous analysis of the OWIDIA system, these reductions of the maximum bank angle seem to be achievable.

It can thus be concluded that the OWIDIA system would most likely be able to allow aircraft spacing at minimum radar separation, which would represent a huge capacity gain compared to the current ICAO wake-vortex-based separation minimum.

[21] Depending on the airport MRS can also be 3 NM.

[22] If the ICAO separation minima with worst case atmospheric conditions were used as a reference the required reduction of the maximum bank angles would only be $5\,\%$ in case of the B747 and by $6\,\%$ in case of the A380. However, as these atmospheric conditions are not very likely it is not clear whether these scenarios can be used as a relevant comparison case for realistic encounters under current ICAO separation standards.

8 Summary and Outlook

8.1 Summary

This thesis covered the development and analysis of a lidar-based wake identification and impact alleviation system. It presented a successful approach to combine a wake identification algorithm, which uses the information of a forward-looking Doppler lidar sensor to identify a wake vortex model, with a disturbance rejection control system to alleviate the impact of wake vortices on encountering aircraft. This control system was integrated into the flight control architecture of a modern transport aircraft and analyzed concerning its potential to reduce the wake-induced aircraft reaction during wake encounters under various conditions. On the basis of this analysis requirements for suitable lidar sensors were derived, which allow a successful wake identification and impact alleviation. This thesis represents the first work that developed a detailed realization of this combination of wake identification and impact alleviation and studied it comprehensively on a system level. The results obtained during the course of this thesis are now analyzed against the underlying scientific questions which form the basis for this thesis.

How can a lidar-based wake identification algorithm and a wake impact alleviation control system be combined and integrated into the flight control architecture of modern aircraft?

The developed system named OWIDIA (Online Wake IDentification and Impact Alleviation) consists of two main components: firstly, the OWI (Online Wake Identification) module which detects and characterizes the wake vortex disturbance and provides a wake vortex model to the second module, and secondly the Wake Impact Alleviation Control (WIAC) system. The WIAC module derives the expected aircraft reaction during the wake encounter on the basis of the provided wake vortex model and generates control commands to prevent the wake-induced rotational motion. In order to allow for a robust onboard application of the wake identification, the OWI considers lidar measurements over a longer time frame from a data buffer and is embedded in a framework with an activation criterion and a plausibility check of the determined wake vortex model. The activation criterion ensures that the identification algorithm is only started if there is a potential chance of a wake vortex encounter. The plausibility check was used to make sure that only wake vortex parameters that were physically plausible and likely were subsequently transferred to the WIAC module.

The application of the wake impact alleviation control system in combination with a basic control system similar to an “Airbus Normal Law” revealed that both control systems interact unfavorably in some respects. An improved integration of the wake impact alleviation controller into the overall flight control architecture could be achieved by two simple modifications of both control systems: On the one hand, the sideslip-angle-induced rolling moment was excluded from the control command computation of the OWIDIA system in order to avoid a double consideration of this component and resulting overcompensation by both control systems. On the other hand, the wake-induced sideslip angle is used as the command value for the yaw control law of the basic control system during the wake encounter such that the yaw controller does not support the intrinsic weathercock stability of the aircraft anymore, which turns the aircraft into

the wind, but pursues the same goal as the wake impact alleviation control system, i.e. to keep the aircraft nose pointed in the direction of flight during the encounter. These modifications led to a significant improvement of the wake impact alleviation performance.

What is the realistic potential of a lidar-based wake impact alleviation system to reduce the aircraft reaction during wake vortex encounters?

To answer the question of the general potential of the OWIDIA system to mitigate the aircraft reaction during wake vortex encounters under realistic boundary conditions, the system performance was studied with regards to its theoretical limits under ideal conditions with a perfectly known wake vortex disturbance, the effect of different artificial errors in the determined wake vortex model and in a realistic setup, including the wake identification, with different sensor configurations and encounter scenarios.

In the theoretical case that the OWI provided a perfect model of the wake vortex disturbance the wake impact alleviation system showed a very good performance. During typical encounters for approach with shallow lateral encounter angles, the most relevant aircraft disturbance, the wake-induced rolling motion, could be almost perfectly compensated and the wake-induced pitching and yawing motion were also alleviated very well. With increasing lateral encounter angles the attainable alleviation of the wake-induced bank angle was reduced because the rate limits of the aileron actuators were saturated. However, the effect that the system was no longer useful due to the saturation of the rate limits only occurred during encounters with comparably large lateral encounter angles which did not lead to significant bank angle excursions anyway. In case of the considered A320 aircraft, the benefit of the wake impact alleviation system was almost gone at 30° lateral encounter angles and above. During a 40° lateral encounter the wake vortex control system did not change the bank angle reaction at all. As the underlying rate limits represent typical values for modern transport aircraft, very similar results can be expected for other aircraft types. An increase in the vortex strength generally yields stronger induced rolling moments such that the deflection limits of the ailerons could be rapidly reached. The investigations in the course of this thesis showed that the wake impact alleviation performance of the considered A320 model was not strongly impaired yet during shallow encounters of 5° in approach for very large vortex circulations up to $850\,\mathrm{m}^2/\mathrm{s}$. Nevertheless, it has to be kept in mind that the available roll control power might be a limiting factor for other aircraft types. Extended concepts such as the preview control approaches proposed by *Kloidt (2007)*[1] could represent a sensible complement for the OWIDIA system for these aircraft if the required roll control ratio during the encounter is much greater than one for a long period of time.

In the longitudinal axis, the current implementation of the OWIDIA system leads to a satisfactory alleviation of the wake-induced pitching moment. However, the investigations showed that the vertical flight path deviation is increased due to the OWIDIA system because it compensates the wake-induced pitch-up moment but does not alleviate the wake-induced vertical force in downwards direction. It has to be noticed that this might be particularly unfavorable

[1] Kloidt (2007), Dissertation about the development of a flight control system for the alleviation of the impact of wake vortices.

for encounters close to ground and that the longitudinal control of the OWIDIA system might have to be modified or not be used at all during these encounters.

Concerning the sensitivity of the bank angle alleviation performance with respect to errors of the different parameters of the wake vortex model, the analysis showed that the lateral distance of the vortex centerline and the wake azimuth are the most sensitive parameters. The vertical position of the wake vortex centerline and the wake elevation are less sensitive and the vortex circulation is the least critical parameter for a successful wake impact allevaition. Nevertheless, all parameters of the wake vortex model should be estimated as precisely as possible in order to allow an optimal wake impact alleviation. How well this parameter estimation works depends on the measurement quality provided by the lidar sensor.

The strong dependency of the wake impact alleviation performance on the characteristics of the lidar sensor has been confirmed in the analysis of the complete OWIDIA system including both modules, the OWI and the WIAC system. Many sensor configurations allowed a very effective alleviation of the maximum bank angle of 70 - $80\,\%$ for the majority of the encounters and up to $90\,\%$ for some encounter scenarios. Other sensor configurations led to an impairment of the maximum bank angle during the wake vortex encounter and are thus not suitable for the application in combination with the current OWIDIA system. The geometric setup of the encounter has shown to have a remarkable influence on the alleviation performance. Especially the vertical altitude offset between the wake vortex and the encountering aircraft strongly influenced the bank angle reduction. In cases with large altitude offsets the wake impact alleviation was less effective because the wake vortex was hardly visible in the field of view of the sensor and thus difficult to detect. However, even for encounters with smaller vertical altitude offsets the alleviation performance with some lidar sensors was still very sensitive to the exact altitude offset. If the sensor had a low spatial resolution of measurement positions in vertical direction an unfavorable vertical position of the vortex cores sometimes led to unsuitable identification results. Furthermore, encounter scenarios with nonzero vertical encounter angles more easily led to increases of the maximum bank angle than encounters with no vertical encounter angle. However, such especially large vertical encounter angles in combination with steep lateral encounter angles are generally much less likely to occur during approach such that small impairments of the wake impact alleviation are less critical in these cases. Altogether it could be shown that the OWIDIA system provides a very efficient bank angle alleviation for analytical Burnham-Hallock wake vortices: It can robustly be applied during encounters with different geometries of the flight paths of the generator and the encountering aircraft and it could most likely allow a relaxation of the current wake-vortex-based separation minima up to minimum radar separation.

The analysis with LES wake vortices demonstrated that the OWIDIA system can also be applied successfully for these much more realistic wake vortices including turbulence, vortex deformation and decay, as long as the vortices are not too strongly deformed. The reduction of the wake-induced bank angle worked very well for young, almost straight LES wake vortices and seems to be beneficial for older vortices up to an age of moderate deformation (such as 64-s-old vortices in atmospheric conditions with moderate turbulence and neutral thermal stratification). The application to older and more deformed wake vortices was not successful anymore and still represents a limit for the current version of the OWIDIA system. In order to make the system

compatible for these strongly deformed wake vortices, the wake vortex model used by the OWI needs to be extended to cope with the curvature of the wake vortices.

What requirements in terms of sensor characteristics can be derived as a prerequisite for a successful application of the lidar-based wake impact alleviation system?

The analysis of the requirements of suitable lidar sensors for the application in combination with the OWIDIA system revealed that a meaningful specification of adequate sensor characteristics is only possible in a comprehensive, coupled simulation environment that comprises all relevant modules of the wake vortex encounter simulation including the aircraft dynamics, the lidar sensor, the identification, and the control systems and respects their complex interdependencies. Due to the complex dependencies between the different modules and the strongly nonlinear influences of the sensor parameters of the overall system performance, it is not possible to specify the requirements of the sensor characteristics as simple functions and threshold values of the different parameters. Instead this thesis presents some suitable sets of sensor parameters and describes the relevant dependencies and trends that should be respected in order to get appropriate sensor configurations for a successful wake identification and impact alleviation.

In general, a good tradeoff between a high spatial resolution of the measurements and low measurement noise is crucial for suitable sensor configurations for the OWIODIA system. The exact limit of the acceptable measurement noise level depends on the other parameters of the sensor configuration as well as the strength of the wake vortex. However, for a ratio of the vortex circulation and reference standard deviations of the measured line-of-sight velocities $\Gamma/(\text{STD } V_{\text{LoS}})$ of less than 200 (i.e. a reference standard deviation of the LoS velocity of more than $1.7\,\text{m/s}$ in the present case with a vortex circulation of $341\,\text{m}^2/\text{s}$) the activation criterion of the OWI was never surpassed for any of the sensor configurations in the analysis. If the spatial resolution is very high, a successful wake identification might still be possible though in case an extended activation criterion is applied.

Concerning the remaining sensor parameters, the following trends could be observed:

- The blur depth and the full scan update rate had only minor influence on the performance of the OWIDIA system. The full scan update rate should be adjusted depending on the number of measurement axes and range gates in order to get a favorable ratio of special resolution and measurement noise.
- Sensor configurations with three, four or five vertical measurement axes allowed an adequate performance of the OWIDIA system, but the usage of four or five vertical measurement axes led by trend to a better performance. Concerning the required number of lateral measurement axes, no universal requirement could be specified, but the number has to be adapted in order to receive a good trade-off of spatial resolution and measurement uncertainty. It has to be assured that the distance between neighboring measurements is small enough such that the wake vortex cannot be located unfavorably in between the measurements.
- If the lidar sensors possessed four or five vertical measurement axes, configuration with ranges to the first measurement point of $60\,\text{m}$, $75\,\text{m}$ and $90\,\text{m}$ were suitable. For sensors

with only three vertical measurement axes, only configurations with a $\text{range}_{\text{MP1}}$ of $60\,\text{m}$ allowed a successful wake impact alleviation.

- Concerning the lateral field of view, all of the three considered lateral scan angle ranges of +/-$16°$, +/-$30°$ and +/-$40°$ provided suitable sensor configurations. For sensor configurations with high noise levels, the information found in the small measurement field of view of +/-$16°$ was often not sufficient and larger lateral fields of view of +/-$30°$ or +/-$40°$ were more favorable. In vertical direction a field of view of +/-$10°$ seemed to be sufficient. The increase of the vertical scan angle range to +/-$15°$ did not provide significant benefits (except for some particular sensor configurations with four or five vertical measurement axes and several range gates).

An example of a sensor configuration that allowed a very good and robust performance of the OWIDIA system in the range of considered encounter geometries and for wake vortices of different ages up to moderate deformation (such as an 64-s-old wake vortex in an atmosphere with moderate turbulence and neutral thermal stratification) is the sensor K5-15-75. It has five vertical and seven lateral measurement axes, one range gate, a field of view of +/-$30°$ x +/-$10°$ in lateral and vertical direction, a full scan update rate of $5\,\text{Hz}$ and a standard deviation of the line-of-sight velocity of $0.67\,\text{m/s}$. However, the results showed that, besides this configuration, many other combinations of sensor parameters are suitable for a successful OWIDIA application as well. According to the analysis of varying measurement noise, these results also seem to be valid if the measurement uncertainty is slightly higher than assumed for the analysis in this thesis. Compared to the state of the art of modern lidar sensors, the determined sensor requirements are optimistic but seem to be feasible for future sensor configurations such that the OWIDIA system could be realizable in the future.

The results concerning the sensor requirements obtained in the course this thesis can be considered as a first starting point for the development for an airborne lidar sensor for wake identification and impact alleviation purposes and can be used as a basis for further iterations with lidar experts and manufactures. Besides the technical results concerning the sensor requirements, the thesis also provided insights with regards to useful methodically approaches for the analysis of the OWIDIA system performance, which could be helpful for further studies of the system and the sensor requirements in the future. These can be summarized as follows:

- An analysis of the wake impact alleviation performance of the OWIDIA system and the resulting requirements for the lidar sensor is only possible in a comprehensive simulation environment that comprises all interdenpencies between the atmospheric influences (in particular the wake vortex), the aircraft dynamics, the basic flight control system, the lidar sensor, the wake identification, and the wake impact alleviation control.[2]

[2] Only in a fully coupled simulation environment effects such as the fact that short measurement ranges of $60\,\text{m}$ are sufficient for a successful wake impact alleviation (because the basic control system compensates slight wake-induced disturbances at the beginning of the encounter and the OWIDIA system is active when strong wake-induced disturbance moments occur) can be observed.

- The analysis of many sensor configurations in a few encounter scenarios in a first step and a detailed investigation of promising sensor configurations in many encounter scenarios in a second step has been shown to be a sensible approach to identify suitable sensor characteristics for the application in combination with the OWIDIA system.
- The analysis revealed that the wake identification and consequently also the wake impact alleviation performance of the OWIDIA system is very sensitive to the altitude offset between the wake vortex and the encountering aircraft. It is thus necessary to investigate a large range of altitudes offsets with tight intervals in order to evaluate the system performance reliably.
- Five key performance parameters were suggested, which allow a systematic comparison of many different sensor configurations in various encounter scenarios. These parameters are the average reduction of the maximum bank angle amplitude, the number of cases in which the OWIDIA system leads to an increase of the maximum bank angle amplitude, the sum of the increase of the maximum bank angle amplitude in all encounters, the maximum increase of the maximum bank angle amplitude in all encounters, and the number of simulations during which the wake impact alleviation control system was never active.
- A worst case scenario for the wake identification and impact alleviation consists of encounter scenarios with a shallow lateral and small (in particular negative) vertical encounter angles (such as $\Psi_{\mathrm{WV}} = 5°$, $\Theta_{\mathrm{WV}} = -3°$). This encounter scenario should necessarily be included in future studies.

Altogether it could be shown in this thesis that the OWIDIA system can be successfully used in combination with different suitable sensor configurations, that it provides a very efficient alleviation of the wake-induced aircraft response and that it can robustly be applied during encounters with different geometries of the flight paths of the generator and encountering aircraft up to vortex ages with medium deformation. It might thus represent a possible answer to the future challenges of improving air traffic capacity and safety and reducing the environmental impact by enabling the reduction of waiting times and delays.

8.2 Outlook

This thesis demonstrated that the OWIDIA system represents a promising approach for the mitigation of the aircraft reaction during wake vortex encounters. In order to further improve the system, however, several aspects could still be enhanced and should be covered in future studies.

The wake identification should be extended in order to allow the application to deformed wake vortices of advanced vortex age. This involves the extension of the identification model by parameters to describe the curvature of the wake vortex as well as a revision of the plausibility check criteria. Furthermore, future analysis should investigate the usefulness of different scan patterns. Especially scan patterns with measurements that are not arranged in an equidistant manner might be helpful for a more robust wake detection and characterization and should be included in future studies. Under the assumption that different sensor technologies might provide other dependencies of the measurement uncertainties, different noise models might be

interesting to investigate. In particular the assumption that additional range gates could be realized without any penalty of the measurement noise might lead to additional suitable sensor configurations. A revision of the current, very simple activation criterion of the OWI is expected to allow the successful application of the OWIDIA system with more sensor configurations (especially those with a high measurement noise but also a high spatial resolution of the measurements) and should thus also be part of future studies. For a practical realization of the OWIDIA system, the system has to be real-time capable. Especially the wake identification needs to be optimized in this regard. Even though the assurance of real-time capabilities of the identification algorithm was not the focus of the present thesis, it would be feasible to optimize the code with respect to real-time application and by using appropriate hardware.

The control module of the OWIDIA system could be improved by combining it with a modified feedback control. During the time of the encounter the feedback gains of the basic control system could be augmented to ensure a more aggressive compensation of the wake vortex disturbance. As the wake detection of the OWIDIA system allows to apply these adapted feedback gains only during the actual encounter, unnecessary high structural loads throughout the entire flight can be avoided. In case of the wake encounter, however, the combined application of the current feedforward disturbance rejection and an additional specific feedback control might further improve the wake impact alleviation. It would also improve the robustness of the system in cases of a suboptimal wake characterization because the imperfectly detected wake vortex model would only impair the performance of the direct disturbance rejection but the feedback control could still successfully alleviate the wake vortex response.
Concerning the control strategy, the exact objective of the wake impact alleviation system still needs to be investigated in detail. This thesis assumed that the alleviation of the wake-induced rotational motion, especially in the roll axis, is the main purpose of the wake impact alleviation controller. Other impacts of the wake vortex on the aircraft such as flight path deviations or vertical accelerations could, however, also be relevant aspects that need to be considered by the control system. The desired behavior during the wake encounter and the priorities of the deviations of different parameters should thus be clarified in a separate analysis and be respected in the design of the control system. The addition of flight path control during the wake encounter might, for instance, be a sensible extension for the mitigation of flight path deviations.

For the final evaluation of the wake impact alleviation system, the system should be investigated by flight tests. Even though the analysis in this thesis demonstrated a promising potential of the system, the studies have so far all been theoretical and based on simulations. A demonstration of the system under real flight conditions would thus be a necessary future step and would allow verifying the applicability and reliability of the system. The remote sensing of the lidar sensor could thereby simultaneously be used for additional applications such as the alleviation of gusts, the detection of clear air turbulence, and the increase of air data redundancy.

References

ATSB (2009): *Wake turbulence event Sydney Airport, NSW 3 November 2008*. Transport Safety Report AO-2008-077. Australian Transport Safety Bureau, 2009.

Airbus (2015): *A380 - Aircraft Characteristics Airport and Maintenace Planning*. 2015. URL: http://www.airbus.com/support/maintenance-engineering/technical-data/aircraft-characteristics/.

Baranov, N. A., Belotserkovski, A. S., Kanaveski, M. I., Pasekunov, I. V., and Spetstekhnika, Zakrytoe Aktsionernoe Obschestvo Rossiyskaya Aktsionernaya Assotsiatsiya (2009): "Method and System for Preventing an Aircraft from Penetrating into a Dangerous Trailing Vortex Aera of a Vortex Generator". Pat. EP1701178A1. 2009.

Bauer, T., Vechtel, D., and Raab, C. (2012): *System and HMI Design of a Wake Encounter Avoidance and Advisory System*. Research report FB 2012-02. DLR, 2012, pp. 171–183.

Bauer, T., Vechtel, D., Abdelmoula, F., and Immisch, T. (2014): "In-Flight Wake Encounter Prediction with the Wake Encounter Avoidance and Advisory System". 6th AIAA Atmospheric and Space Environments Conference. Atlanta, Georgia, USA, 2014. DOI: 10.2514/6.2014-2333.

Boeing (2011): *Airport Reference Code and Approach Speeds for Boeing Airplanes*. 2011. URL: http://www.boeing.com/assets/pdf/commercial/airports/faqs/arcandapproachspeeds.pdf.

Bogue, R. K. and Jentink, H. W (2004): *Optical Air Flow Measurements in Flight*. NASA/TP-2004-210735. NASA, 2004.

Broyden, C. G. (1970): "The Convergence of a Class of Double-rank Minimization Algorithms 1. General Considerations". *IMA Journal of Applied Mathematics* 6 (1 1970), pp. 76–90. DOI: 10.1093/imamat/6.1.76.

Burnham, D.C. and Hallock, J. N. (1982): *Chicago Monoacoustic Vortex Sensing System, Volume IV: Wake Vortex Decay*. Tech. rep. DOT-TSC-FAA-79-18,IV. National Information Service, 1982.

CIAIAC (2011): *Wake turbulence encounter in high-level air space involving an AIRBUS A320 aircraft, registration EC-JDK, operated by Vueling, in route between Barcelona and Santiago de Compostela on 28 May 2006*. report IN-029/2006. Civil Aviation Accident and Incident Investigation Commission, 2011.

Cézard, N., Besson, C., Dolfi-Bouteyre, A., and Lombard, L. (2009): "Airflow Characterization by Rayleigh-Mie Lidars". *Aerospace Lab Journal* (1 2009).

Croom, D. R. (1977): "Evaluation of Flight Spoilers for Vortex Alleviation". *Journal of Aircraft* 14.8 (1977), pp. 823–825. DOI: 823-825,10.2514/3.44620.

Crouch, J. D., Miller, G. D., and P.R., Spalart (2001): "Active-Control System for Breakup of Airplane Trailing Vortices". *AIAA Journal* 39.12 (2001), pp. 2374–2381. DOI: 10.2514/2.1244.

Crow, S. C. (1970): “Stability Terminalheory for a Pair of Trailing Vortices”. *AIAA Journal* 8.12 (1970), pp. 2172–2179. DOI: 10.2514/3.6083.

Crow, S. C. and Bate, E. R. (1976): “Lifespan of trailing vortices in a turbulent atmosphere”. *Journal of Aircraft* 13.7 (1976), pp. 476–482. DOI: 10.2514/3.44537.

De Visscher, I., Winckelmans, G., Lonfils, T., Bricteux, L., Duponcheel, M., and Bourgeois, N. (2010): “The WAKE4D simulation platform for predicting aircraft wake vortex transport and decay: Description and examples of application”. AIAA Atmospheric and Space Environments Conference. Toronto, Canada, 2010. DOI: 10.2514/6.2010-7994.

Dolfi-Bouteyre, A., Augere, B., Valla, M., Goular, D., Fleury, D., Canat, G., Planchat, C., Gaudo, T., Besson, C., Gilliot, A., Cariou, J.-P., Petilon, O., Lawson-Daku, J., Brousmiche, S., Lugan, S., Bricteux, L., and Macq, B. (2009): “Aircraft Wake Vortex Study and Characterization with 1.5 μm Fiber Doppler Lidar,” *Aerospace Lab Journal* (1 2009).

Douxchamps, D., Lugan, S., Verschueren, Y., Mutuel, L., Macq, B., and Chihara, K. (2008): “On-board axial detection of wake vortices using a 2 μm LiDAR”. *IEEE Transactions on Aerospace and Electronic Systems* 44.4 (2008), pp. 1276–1290.

Durston, D. A., Walker, S. M., Driver, D. M., and Smith, S. C. (2005): “Wake-Vortex Alleviation Flowfield Studies”. *Journal of Aircraft* 42.4 (2005), pp. 894–907. DOI: 10.2514/1.7904.

Ehlers, J. and Fezans, N. (2015a): “Airborne Doppler LiDAR Sensor Parameter Analysis for Wake Vortex Impact Alleviation Purposes”. *Advances in Aerospace Guidance, Navigation and Control*. EuroGNC. Toulouse, France, 2015, pp. 433–3543.

Ehlers, J. and Fezans, N. (2015b): “Towards Wake-Resistant Aircraft through LiDAR-Based Wake Impact Alleviation”. WakeNet-Europe Workshop 2015. Amsterdam, Netherlands, 2015.

Ehlers, J., Niedermeier, D., and Fischenberg, D. (2015): “Wake Impact Alleviation Control Based on Wake Identification”. *Journal of Aircraft* 52.6 (2015), pp. 2077–2089. DOI: 10.2514/1.C033157.

Eriksen, P. (2010): “SESAR Joint Undertaking Wake Vortex Research (WP6.8.1)”. Global Wake Conference. San Diego, California, USA, 2010.

Estes, S. L., Koch, M. E., Lunsford, C. R., and Mendolia, A. S. (2011): “Wake Turbulence Avoidance Automation: Evaluation of Feasibility and Impact”. 30th Digital Avionics Systems Conference. Seattle, Washington, USA, 2011. DOI: 10.1109/DASC.2011.6096094.

Eurocontrol (2013): *New study predicts growth in flights and capacity challenges for 2035*. 2013. URL: www.eurocontrol.int/sites/default/files/pressrelease/130708-challenges-of-growth.pdf.

FAA (2014): *Advisory Circular - Aircraft Wake Turbulence*. AC 90-23G. Federal Aviation Administration, 2014.

Fabre, D. and Jacquin, L. (2004): “Short-wave cooperative instabilities in representative aircraft vortices”. *Physics of Fluids* 16.5 (2004), pp. 1366–1378. DOI: 10.1063/1.1686951.

Farineau, J. (1989): “Lateral Electric Flight Control Laws of A Civil Aircraft Based Upon Eigen Structure Assignment Technique”. Guidance, Navigation and Control Conference. Boston, MA, USA, 1989. DOI: 10.2514/6.1989-3594.

Favre, C. (1994): “Fly-by-Wire for Commercial Aircraft: The Airbus Experience”. *International Journal of Control* 59.1 (1994), pp. 139–157. DOI: 10.1080/00207179408923072.

Feuerle, T., Steen, M., and Hecker, P. (2015): “New Concept for Wake-Vortex Hazard Mitigation Using Onboard Measurement Equipment”. *Journal of Aircraft* 52.1 (2015), pp. 42–48.

Fezans, N., Schwithal, J., and Fischenberg, D. (2015): “In-Flight Remote Sensing and Characterization of Gusts, Turbulence, and Wake Vortices”. Deutscher Luft- und Raumfahrtkongress. Rostock, Germany, 2015.

Fischenberg, D. (2002): “Bestimmung der Wirbelschleppencharakteristik aus Flugmessdaten (English: Determination of Wake Vortex Characteristics from Flight Test Data)”. Deutscher Luft- und Raumfahrtkongress. Stuttgart, Germany, 2002.

Fischenberg, D. (2010): “A method to validate wake vortex encounter models from flight test data”. 27th International Congress of the Aeronautical Sciences. Nice, France, 2010.

Fischenberg, D. (2012): *Wake Characterisation Using LIDAR Measurements*. Research report FB 2012-02. DLR, 2012, pp. 144–152.

Fischenberg, D. (2013a): *Online Wake Identification Algorithms Using Forward Looking LIDAR Sensor Measurements*. Institute report IB 111-2013/11. DLR, 2013.

Fischenberg, D. (2013b): “Strömungsermittlungsverfahren/Flow Determination Method/Procédé de détermination d’écoulement”. Pat. EP 2 340 438 B1. 2013.

Fletcher, R. (1970): “A new approach to variable metric algorithms”. *Computer Journal* 13 (3 1970), pp. 317–322. DOI: 10.1093/comjnl/13.3.317.

Fock, H., Hahn, K.-U., and Schwarz, C. W. (2006): *Verwendung von vorausschauenden Strömungssensoren in Pilotenassistenzsystemen für den Wirbelschleppeneinflug (English: Application of forward looking flow sensors for pilot assistance systems for wake vortex encounters)*. Institute report IB 111-2006/12. DLR, 2006.

Focking, J.-A. (2016): *Abschätzung des wirtschaftlichen Nutzens eines Steuerungssystems zur Abmilderung der Flugzeugreaktion bei Wirbelschleppendurchflügen (English: Assessment of the Economic Benefit of Wake Impact Alleviation System)*. Institute report DLR-IB-FT-BS-2016-64. DLR, 2016.

Frech, M., Holzäpfel, F., Tafferner, A., and Gerz, T. (2007): “High-Resolution Weather Database for the Terminal Aera of Frankfurt Airport”. *Journal of Applied Meteorology and Climatology* 46 (2007), pp. 1913–1932. DOI: 10.1175/2007JAMC1513.1.

Gerz, T., Holzäpfel, F., and Darracq, D. (2002): “Commercial aircraft wake vortices”. *Progress in Aerospace Sciences* 38 (3 2002), pp. 181–208. DOI: 10.1016/S0376-0421(02)00004-0.

Gerz, T. and Schwarz, C. W. (2012): *The DLR Project Wetter & Fliegen*. Reserach report FB 2012-02. DLR, 2012.

Ginevsky, A.S. and Zhelannikov, A. I. (2009): *Vortex Wake of Aircrafts*. Springer, 2009.

Goldfarb, D. (1970): "A Family of Variable-Metric Methods Derived by Variational Means". *Mathematics of Computation* 24 (1970), pp. 23–26. DOI: 10.1090/S0025-5718-1970-0258249-6.

Greenblatt, D., Pack-Melton, L. G., Yao, C.-S., and Harris, J. (2005): "Active Control of a Wing Tip Vortex". 23rd AIAA Applied Aerodynamics Conference. 2005. DOI: 10.2514/6.2005-4851.

Hahn, K.-U. (2002): "Coping with Wake Vortex". *23rd International Congress of Aeronautical Sciences Proceedings*. 23rd International Congress of Aeronautical Sciences. Toronto, Canada, 2002, pp. 732.1–732.14.

Hahn, K.-U. and Schwarz, C. W. (2006): "Wake Vortex Avoidance versus Landing Capacity". AIAA Guidance, Navigation, and Control Conference and Exhibit. Keystone, CO, USA, 2006. DOI: 10.2514/6.2006-6322.

Hahn, K.-U. and Schwarz, C. W. (2007): "Safe Limits for Wake Vortex Penetration". AIAA Guidance, Navigation and Control Conference and Exhibit. Hilton Head, SC, USA, 2007. DOI: 10.2514/6.2007-6871.

Hahn, K.-U. and Schwarz, C. W. (2008): "Alleviation of Atmospheric Flow Disturbance Effects on Aircraft Response". *ICAS 2008 Proceedings*. Anchorage, Alaska, USA, 2008.

Hahn, K.-U. and Schwarz, C. W. (2009): *Messflug in die Wirbel (English: Measurement Flight into Wake Vortices)*. DLR Nachrichten 123. 2009.

Hahn, K.-U., Schwarz, C., and Friehmelt, H. (2004): "A Simplified Hazard Area Prediction (SHAPe) Model for Wake Vortex Encounter Avoidance". 24th International Congress of the Aeronautical Sciences. Yokohama, Japan, 2004.

Hahn, K.-U., Fischenberg, D., Niedermeier, D., and Horn, C. (2010): "Wake Encounter Flight Control Assistance Based on Forward-Looking Measurement Processing". AIAA Guidance, Navigation, and Control Conference. Toronto, Ontario, Canada, 2010. DOI: 10.2514/6.2010-7680.

Harris, M., Young, R. I., Köpp, F., Dolfi, A., and Cariou, J.-P. (2002): "Wake vortex detection and monitoring". *Aerospace Science and Technology* 6 (5 2002), pp. 325–331. DOI: 10.1016/S1270-9638(02)01171-9.

Held, K. (2003): "Analyse eines Flugregelungssystems zur Reduzierung des Gefahrenpotentials von Wirbelschleppen während der Landephase (English: Analysis of a Flight Control System for the Mitigation of the Hazard Potential of Wake Vortex Encounters during Landing)". Diploma thesis. Technische Universität Berlin, 2003.

Hemm, R., Shapiro, G., Lee, D., Gribko, J., and Glaser, B. (1999): *Benefit Estimates of Terminal Area Productivity Program Technologies*. Tech. rep. NASA/CR-1999-208989. NASA, 1999.

Hennemann, I. (2010): "Deformation und Zerfall von Flugzeugwirbelschleppen in turbulenter und stabil geschichteter Atmosphäre (English: Deformation and Deacy of Aicraft Wake Vortices in Tubulent and Stratified Atmosphere)". PhD thesis. Techical University of Munich, 2010.

Herbst, J. and Vrancken, P. (2016): "Design of a monolithic Michelson interferometer for fringe imaging in a near-field, UV, direct-detection Doppler wind lidar". *Applied Optics* 55 (25 2016), pp. 6910–6929. DOI: 10.1364/AO.55.006910.

Hill, C. and Harris, M. (2010): *Remote Sensing (UpWind WP6) - Lidar Measurement Report*. QINETIQ/TS/FPPS/TR0900813. QinetiQ, 2010.

Hirschberger, M. C. (2013): "Beiträge zur Erfassung von Wirbelschleppen mit Lidar (English: Contributions to the Detection of Wake Vortices with Lidar)". PhD thesis. Technical University of Munich, 2013.

Holzäpfel, F. (2003): "Probabilistic Two-Phase Wake Vortex Decay and Transport Model". *Journal of Aircraft* 40 (2003), pp. 323–331. DOI: 10.2514/2.3096.

Holzäpfel, F. (2004): "Probabilistic Two-Phase AircraftWake-Vortex Model: Application and Assessment". *Journal of Aircraft* 41.5 (2004), pp. 1117–1126. DOI: 10.2514/1.2280.

Holzäpfel, F. (2005): "Aircraft Wake Vortex Evolution and Prediction". Habilitation. Technical University Munich, 2005.

Holzäpfel, F. (2006): "Probabilistic Two-Phase Aircraft Wake-Vortex Model: Further Development and Assessment". *Journal of Aircraft* 3 (2006), pp. 700–708. DOI: 10.2514/1.16798.

Holzäpfel, F. and Meiko, Steen (2007): "Aircraft Wake-Vortex Evolution in Ground Proximity: Analysis and Parameterization". *AIAA Journal* 45.1 (2007). DOI: 10.2514/1.23917.

Holzäpfel, F., Stephan, A., and Körner, S. (2014): "Wake Vortex Evolution during Approach and Landing With and Without Plate Lines". 52nd Aerospace Sciences Meeting, AIAA SciTech. National Harbor, Maryland, USA, 2014. DOI: 10.2514/6.2014-0925.

Horn, C., Niedermeier, D., and Ehlers, J. (2002): *Wake Impact Alleviation Control Functions and Sensor Requirements*. Research report FB 2012-02. DLR, 2002, pp. 117–129.

IATA (2015): *Air Passenger Market Analysis*. International Air Transport Association, 2015. URL: http://www.iata.org/whatwedo/Documents/economics/passenger-analysis-dec-2015.pdf.

ICAO (2007): *Procedures for Air Navigation Services - Air Traffic Management*. Tech. rep. Doc 4444 ATM/501. ICAO, 2007.

ICAO (2008): *Guidance on A380-800 Wake Vortex Aspects*. Tech. rep. TEC/OPS/SEP - 08-0294.SLG. International Civil Aviation Organization, 2008.

Inokuchi, H., Furuta, M., and Inagaki, T (2014): “High Altitude Turbulence Detection Using an Airborne Doppler Lidar”. 29th Congress of International Council of the Aeronautical Sciences. St. Petersburg, Russia, 2014.

Inokuchi, H., Tanaka, H., and Ando, T. (2008): “Development of an Onboard Doppler LIDAR for Flight Safety”. 26th Congress of International Council of the Aeronautical Sciences. Anchorage, Alaska, USA, 2008.

Inokuchi, H., Tanaka, H., and Ando, T. (2010): “Development of a Long Range Airborne Doppler Lidar”. 27th Congress of International Council of the Aeronautical Sciences. Nice, France, 2010.

Jategaonkar, R., Fischenberg, D., and Gruenhagen, W. v. (2004): “Aerodynamic Modelling and System Identification from Flight Data - Recent Applications at DLR”. *Journal of Aircraft* 41.4 (2004), pp. 681–691. DOI: 10.2514/1.3165.

Johnson, W. A., Teper, G. L., and Rediess, H. A. (1974): “Study of Control System Effectiveness in Alleviating Vortex Wake Upsets”. *Journal of Aircraft* 11.3 (1974), pp. 148–154. DOI: 10.2514/3.60340.

Kameyama, S., Ando, T., Asaka, K., Hirano, Y., and Wadaka, S. (2007): “Compact all-fiber pulsed coherent Doppler lidar system for wind sensing”. *Applied Optics* 46 (11 2007), pp. 1953–1962. DOI: 10.1364/AO.46.001953.

Keane, M., Buckton, D., Redfern, M., Bollig, C., Wedekind, C., Koepp, F., and Berni, F. (2002): “Axial Detection of Aircraft Wake Vortices Using Doppler Lidar”. *Journal of Aircraft* 39.5 (2002), pp. 850–861. DOI: 10.2514/2.3005.

Kloidt, S. (2007): “Beiträge zum Entwurf eines Flugregelungssystems zur Reduktion des Wirbelschleppeneinflusses (English: Contributions to the Design of a Flight Control System for the Alleviation of the Impact of Wake Vortices)”. PhD thesis. Technische Universität Berlin, 2007.

Kocks, S., Bode, S., Feuerle, T., Pätzold, C., Schönhals, S., and Hecker, P. (2010): “An integrated Wake Vortex Visualization Concept for existing Cockpit Display Systems”. ENRI Int. Workshop on ATM/CNS. Tokyo, Japan, 2010.

Köpp, F., Rahm, S., and Smalikho, I. (2004): “Characterization of Aircraft Wake Vortices by 2-μm Pulsed Doppler Lidar”. *Journal of Atmospheric and Oceanic Technology* 21.2 (2004), pp. 194–206.

Köpp, F., Smalikho, I., Rahm, S., Dolfi, A., Cariou, J.-P., Harris, M., Young, R., Weekes, K., and Gordon, N. (2003): “Characterization of Aircraft Wake Vortices by Multiple-Lidar Triangulation”. *AIAA Journal* 41 (2003), pp. 1081–1088. DOI: 10.2514/2.2048.

Köpp, F., Rahm, S., Smakikho, I., Dolfi, A., Cariou, J.-P., Harris, M., and Young, R. (2005): “Comparison of Wake-Vortex Parameters Measured by Pulsed and Continious-Wave Lidars”. *Journal of Aircraft* 42.4 (2005), pp. 916–923. DOI: 10.2514/1.8177.

Kundu, P. K. and Cohen, I.M. (2008): *Fluid Mechanics*. 4th ed. Elsevier, 2008. ISBN: 978-0-12-373735-9.

Lamb, H. (1932): *Hydrodynamics*. 1932, pp. 590–592.

Lang, S. and Lunsford, C. (2013): "RECAT 1: Lessons Learned from MEM". WakeNet-Europe Workshop. Bonneuil-sur-Marne, France, 2013.

Looye, G., Lombaerts, T., and Kier, T. (2012): *Design and Flight Testing of Feedback Control Laws*. Research report FB 2012-02. DLR, 2012, pp. 162–170.

Luckner, R. (2012): "Modeling and Simulation of Wake Vortex Encounters: State-of-the-Art and Challenges". AIAA Modeling and Simlation Technologies Conference. Minneapolis, Minnesota, USA, 2012.

Matalanis, C. G. and Eaton, J. K. (2007a): "Wake Vortex Alleviation Using Rapidly Actuated Segmented Gurney Flaps". *AIAA Journal* 45.8 (2007), pp. 1874–1884. DOI: 10.2514/1.28319.

Matalanis, C. G. and Eaton, J. K. (2007b): "Wake Vortex Control Using Static Segmented Gurney Flaps". *AIAA Journal* 45.2 (2007), pp. 321–328. DOI: 10.2514/1.25956.

Matalanis, C. G., Nelson, G. D., and Eaton, J. K. (2007): "Novel Aerodynamic Device for Wake Vortex Alleviation". *AIAA Journal* 45.9 (2007), pp. 2348–2350. DOI: 10.2514/1.30124.

Matayoshi, N., Asaka, K., and Okuno, Y. (2007): "Flight-Test Evaluation of a Helicopter Airborne Lidar". *Journal of Aircraft* 44.5 (2007), pp. 1712–1720. DOI: 10.2514/1.28338.

Menzies, R. T. and Tratt, D. M. (1997): "Airborne lidar observations of tropospheric aerosols during the Global Backscatter Experiment (GLOBE) Pacific circumnavigation missions of 1989 and 1990". *Journal of Geophysical Research* 102.D3 (1997), pp. 3701–3714. DOI: 10.1029/96JD03405.

Münster, C. (2011): *Modellierung, Identifizierung und Bewertung eines analytischen Modells für gekrümmte Wirbelschleppen (English: Modelling, Identification, and Assessment of an Analytical Model for Curved Wake Vortices)*. Institute report IB 111-2011/09. DLR, 2011.

Münster, C. and Schwarz, C. W. (2010): *Auswertung von Wirbelschleppenmeldungen im US Aviation Safety Reporting System (ASRS) (English: Analysis of Wake Vortec Report of the US Aviation Safety Reporting System (ASRS))*. Institute report IB 111-2010/33. DLR, 2010.

NTSB (1994): *Brief of Accident LAX94FA073*. Tech. rep. National Transportation Safety Board, 1994.

NTSB (2001): *Brief of Accident LAX99LA291*. Tech. rep. National Transportation Safety Board, 2001.

NTSB (2004): *In-Flight Separation of Vertical Stabilizer; American Airlines Flight 587 Airbus Industrie A300-605R, N14053, Belle Harbor, New York, November 12, 2001*. Aircraft Accident Report NTSB/AAR-04/04. Washington, DC, USA: National Transportation Safety Board, 2004.

Nykl, S., Mourning, C., Ghandi, N., and Chelberg, D. (2011): “A Flight Tested Wake Turbulence Aware Altimeter”. *Advances in Visual Computing*. Vol. 6939. 2011, pp. 219–228. DOI: 10.1007/978-3-642-24031-7_22.

Ortega, J. M., Bristol, R. L., and Savas, Ö. (2003): “Experimental Study of the Instability of Unequal-Strength Counter-Rotating Vortex Pairs”. *Journal of Fluid Mechanics* 474 (2003), pp. 35–84. DOI: 10.1017/S0022112002002446.

Petzhold, A. and Kärcher, B. (2012): “Aerosols in the Atmosphere”. *Atmospheric Physics*. Ed. by Schumann, U. Springer, 2012, pp. 37–53. DOI: 10.1007/978-3-642-30183-4_3.

Proctor, F. H., Hamilton, D. W., and Switzer, G. F. (2006): “TASS Driven Algorithms for Wake Prediction”. 44th AIAA Aerospace Sciences Meeting and Exhibit. Reno, Nevada, USA, 2006.

Prokop, G. and Sharp, R.S. (1995): “Performance Enhancement of Limited-Bandwidth Active, Automotive Suspensions by Road Preview”. *IEEE Proceedings - Control Theory and Applications* 142.2 (1995), pp. 140–148. DOI: 10.1049/ip-cta:19951772.

Raab, C. (2010a): *Aerodynamikmodell für das Forschungsflugzeug A320 ATRA (English: Aerodynamic Model of the Research Aircraft A320 ATRA)*. Institute report IB 111-2010/45. DLR, 2010.

Raab, C. (2010b): *Wake Impact Attenuation and Avoidance Systems - Conceptual Design for Operation and Human Machine Interface*. Institute report IB 111-2010/21. DLR, 2010.

Raab, C. (2012): *Flugdynamisches Simulationsmodel A320-ATRA - Validierungsversuche und Bewertung der Modellgüte (English: Flight Dynamics Simulation Model A320-ATRA - Validation Tests and Assessment of the Model Quality)*. Insitute report IB 111-2012/43. DLR, 2012.

Rabadan, G. J., Schmitt, N. P., Pistner, T., and Rehm, W. (2010): “Airborne LIDAR for Automatic Feedforward Control of Turbulent In-Flight Phenomena”. *Journal of Aircraft* 47.2 (2010), pp. 392–403. DOI: 10.2514/1.44950.

Rafi, M. and Steck, J. (2013): “Reponse and Recovery of an MRAC Advanced Flight Control System to Wake Vortex Encounters”. AIAA Infotech@Aerospace (I@A) Conference. Boston, Massachusetts, USA, 2013. DOI: 10.2514/6.2013-5209.

Rahm, S., Smalikho, I., and Köpp, F. (2007): “Characterization of Aircraft Wake Vortices by Airborne Coherent Doppler Lidar”. *Journal of Aircraft* 44.3 (2007), pp. 799–805. DOI: 10.2514/1.24401.

Rees, D. (2014): “UV Imaging Lidar for Wake Vortex Detection - The GreenWake Project”. WakeNet Europe 2014 Workshop. Brétigny, France, 2014.

Reitebuch, O. (2012): “Wind Lidar for Atmospheric Research”. *Atmospheric Physics*. Ed. by Schumann, U. Springer, 2012, pp. 487–507. DOI: 10.1007/978-3-642-30183-4_30.

Robinson, J. (1996): “A Simulation-Based Study of the Impact of Aircraft Wake Turbulence Weight Categories on Airport Capacity”. AGARD-CP-584 "The Characterisation and Modification of Wakes from Lifting Vehicles in Fluid". Trondheim, Norway, 1996, pp. 22.1–22.15.

Rooseleer, F. and Treve, V. (2015): *RECAT-EU - European Wake Turbulence Categorisation and Separation Minima on Approach and Departure*. Eurocontrol, 2015. URL: https://eurocontrol.int/sites/default/files/content/documents/sesar/recat-eu-released-september-2015.pdf.

Rosenhead, L. (1932): “The Formation of Vortices from a Surface of Discontinuity”. *Proceedings of the Royal Society of London*. Vol. 134. 1932, pp. 170–192.

Rossow, V. J., Fong, R. K., Wright, M. S., and Bisbee, L. S. (1996): “Vortex Wakes of Two Transports Measured in 80 by 120 Foot Wind Tunnel”. *Journal of Aircraft* 33.2 (1996), pp. 399–406. DOI: 10.2514/3.46951.

Sarpkaya, T. (2000): “New Model for Vortex Decay in the Atmosphere”. *Journal of Aircraft* 37.1 (2000), pp. 53–61. DOI: 10.2514/2.2561.

Sarpkaya, T., Robins, R. E., and Delisi, D. P. (2001): “Wake-Vortex Eddy-Dissipation Model Predictions Compared with Observations”. *Journal of Aircraft* 38.4 (2001), pp. 687–692. DOI: 10.2514/2.2820.

Schlichting, H. and Truckenbrodt, E. (2001a): *Aerodynamik des Flugzeuges (English: Aerodynamics of the Aircraft), Volume 1*. 3rd ed. Springer, 2001.

Schlichting, H. and Truckenbrodt, E. (2001b): *Aerodynamik des Flugzeuges (English: Aerodynamics of the Aircraft), Volume 2*. 3rd ed. Springer, 2001.

Schlipf, D. (2013): “Lidars and wind turbine control - Part 1”. *Remote sensing for wind energy: DTU Wind Energy-E-Report-0029(EN)*. 2013, pp. 171–191.

Schönhals, S. (2015): “Kopplung der Vorhersage- und Detektionsmethoden für Systeme zum Schutz vor Wirbelschleppen (English: Coupling of Prediction and Detection Methods for Systems for the Protection against Wake Vortices)”. PhD thesis. Technische Universität Braunschweig, 2015.

Schönhals, S., Steen, M., and Hecker, P. (2011): “Wake vortex prediction and detection utilising advanced fusion filter technologies”. *The Aeronautical Journal* 115.1166 (2011), pp. 221–228.

Schwarz, C. W. and Hahn, K.-U. (2006): “Full-Flight simulator study for wake vortex hazard area investigation”. *Aerospace Science and Technology* 10.2 (2006), pp. 136–143. DOI: 10.1016/j.ast.2005.09.005.

Schwarz, C. W. and Hahn, K.-U. (2011): “Automated Pilot Assistance for Wake Vortex Encounters”. *Aerospace Science and Technology* 15 (5 2011), pp. 416–421. DOI: 10.1016/j.ast.2010.09.008.

Schwithal, J. and Niedermeier, D. (2017): “Verfahren zur Reduzierung des Einflusses von Luftströmungsverwirbelungen auf Luftfahrzeuge und Luftfahrzeugregelungseinheit (English: pro-

cedure for the reduction of the influence of airstream turbulence on aircraft and aircraft control unit)". Pat. DE 10 2013 112 059. 2017.

Shanno, D. F. (1970): "Conditioning of Quasi-Newton Methods for Function Minimization". *Mathematics of Computation* 24.111 (1970), pp. 647–656. DOI: 10.1090/S0025-5718-1970-0274029-X.

Shanno, D. F. and Kettler, P. C. (1970): "Optimal Conditioning of Quasi-Newton Methods". *Mathematics of Computation* 24.111 (1970), pp. 657–664. DOI: 10.1090/S0025-5718-1970-0274030-6.

Shen, S., Ding, F., Han, J., Lin, Y.-L., Arya, S., and Proctor, F. (1999): "Numerical Modeling Studies of Wake Vortices: Real Case Simulations". 37th Aerospace Sciences Meeting and Exhibit. Reno, NV, USA, 1999. DOI: 10.2514/6.1999-755.

Sölch, I., Holzäpfel, F., Abdelmoula, F., and Vechtel, D. (2016): "Performance of Onboard Wake - Vortex Prediction Systems Employing Various Meteorological Data Sources". *Journal of Aircraft* (2016). DOI: 10.2514/1.C033732.

Spuler, S. M., Richter, D., Spowart, M. P., and Rieken, K. (2011): "Optical fiber-based laser remote sensor for airborne measurement of wind velocity and turbulence". *Applied Optics* 50 (6 2011), pp. 842–851. DOI: 10.1364/AO.50.000842.

TSB (2010): *Encounter with Wake Turbulence Air Canada Airbus A319-114 C-GBHZ Washinton State, United States 10 January 2008*. Aviation Investigation Report A08W0007. National Transportation Safety Board of Canada, 2010.

Taylor, B. N. and Kuyatt, C. E. (1994): *Guidelines for Evaluating and Expressing the Uncertainty of NIST Measurement Results*. NIST Technical Note 1297. NIST, 1994.

Tinling, B. E. (1977): *Estimates of the Effectiveness of Automatic Control in Alleviating Wake Vortex Induced Roll Excursions*. Technical memorandum TM-73267. NASA, 1977.

Vechtel, D. (2010): *Entwicklung eines analytischen Modells zur Berechnung gekrümmter Wirbelschleppen (English: Development of an Analytical Model for the Evaluation of Deformed Vortices)*. Institute report IB 111-2010/14. DLR, 2010.

Vechtel, D. (2012): *Conflict Resolution for Wake Encounter Prevention*. Institute report IB 111-2012/75. DLR, 2012.

Vechtel, D. (2016): "Simulation study of wake encounters with straight and deformed vortices". *The Aeronautical Journal* 120 (1226 2016), pp. 651–674. DOI: 10.1017/aer.2016.14.

Vechtel, D. (2017): "Wirbeldeformierung und ihr Einfluss auf die Gefährdungsbewertung von Wirbelschleppeneinflügen (English: Vortex Deformation and its Influence on the Hazard Analysis of Wake Vortex Encounters)". Reserach report DLR-FB-2017-24. PhD thesis. Technische Universität Braunschweig, 2017.

Veermann, H., Vrancken, P., and Lombard, L. (2014): “Flight testing DELICAT - A promise for medium-range Clear Air Turbulence protection”. 46th SETP Symposium and 25th SFTE Symposium. Luleå, Schweden, 2014.

Viellette, P.R. (2002): “Data Show That U.S. Wake-turbulence Accidents Are Most Frequent at Low Altitude and During Approach and Landing”. *Flight Safety Digest* 21.3-4 (2002), pp. 1–47.

Voß, G., Carmer, C. v., Konrath, R., Stumpf, E., Krückeberg, C.-P., Meyer, H., and Mattner, H. (2007): “Wake vortex alleviation by differential and oscillating flap setting: a comparative numerical and experimental study”. 1st CEAS European Air and Space Conference. Berlin, Germany, 2007.

Vrancken, P. S. (2016): “Airborne remote detection of turbulence with forward-looking LIDAR”. *Aviation Turbulence - Processes, Detection, Prediction*. Ed. by Sharman, R. and Lane, T. Springer, 2016. ISBN: 9783319236308.

Vrancken, P., Wirth, M., Rempel, D., Ehret, G., Dolfi-Bouteyre, A., Lombard, L., Gaudo, T., Rees, D., Barny, H., and Rondeau, P. (2010): “Clear air turbulence detection and characterisation in the delicat airborne lidar project”. 25th International Laser Radar Conference. St. Petersburg, Russland, 2010.

Weitkamp, C. (2005): *Lidar: Range-Resolved Optical Remote Sensing of the Atmosphere*. Springer, 2005. ISBN: 978-0-387-25101-1.

Winckelmans, G., Thirifay, F., and Ploumhans, P. (2000): “Effect of non-uniform windshear onto vortex wakes: parametric models for operational systems and comparison with CFD studies”. 4th WakeNet Workshop on "Wake Vortex Encounters". Amsterdam, Netherlands, 2000.

Wolkensinger, C. (2010): *Vergleich messtechnischer Konzepte zur bordgestützten Ermittlung atmosphärischer Störphänomene (English: Comparison of Metrological Concepts for Airbone Detection Atmospheric Disturbance Phenomena)*. Institute report IB 111-2010/35. DLR, 2010.

A Wake-Vortex-Based Separation Minima

ICAO Wake Vortex Separation Minima

Table A.1: ICAO wake vortex separation minima[1,2]

Leading aircraft	Following aircraft			
	A380-800	**HEAVY**	**MEDIUM**	**LIGHT**
A380-800	MRS	6 NM	7 NM	8 NM
HEAVY	MRS	4 NM	5 NM	6 NM
MEDIUM	MRS	MRS	MRS	5 NM
LIGHT	MRS	MRS	MRS	MRS

Aircraft (apart from the A380-800) are assigned to the different categories according to their maximum takeoff weight (MTOW). The weight categories are defined as:

HEAVY: MTOW $\geq 136\,\mathrm{t}$
MEDIUM: $7\,\mathrm{t} <$ MTOW $< 136\,\mathrm{t}$
LIGHT: MTOW $\leq 7\,\mathrm{t}$.

MRS denotes minimum radar separation, which is $2.5\,\mathrm{NM}$ or $3\,\mathrm{NM}$ (depending on the airport).

These distance-based separation minima are valid for radar operation, which represents the common case at large airports. For non-radar operations time-based wake vortex separations apply. The minimum Separation Time (SP) of aircraft of the category LIGHT behind MEDIUM or HEAVY aircraft is $3\,\mathrm{min}$ and behind an A380-800 $4\,\mathrm{min}$. MEDIUM aircraft have to maintain minimum separation times of $2\,\mathrm{min}$ behind HEAVY aircraft and $3\,\mathrm{min}$ behind an A380-800 aircraft.

FAA Wake Vortex Separation Minima

Table A.2: FAA wake separation minima[3]

Leading aircraft	Following aircraft				
	SUPER	**HEAVY**	**B757**	**MEDIUM**	**LIGHT**
SUPER	MRS	6 NM	7 NM	7 NM	8 NM
HEAVY	MRS	4 NM	5 NM	5 NM	6 NM
B757	MRS	4 NM	4 NM	4 NM	5 NM
MEDIUM	MRS	MRS	MRS	MRS	4 NM
LIGHT	MRS	MRS	MRS	MRS	MRS

[2] ICAO (2007), ICAO document providing rules for air traffic management.
[2] ICAO (2008), ICAO guidelines for wake turbulence aspects of Airbus A380-800 aircraft.
[3] FAA (2014), Advisory circular of FAA for aircraft wake turbulence.

The weight classes are defined as:

HEAVY:	MTOW $\geq 300\,\text{lb}$
MEDIUM:	$41\,\text{lb} <$ MTOW $< 300\,\text{lb}$
LIGHT:	MTOW $\leq 41\,\text{lb}$.

The category super comprises the aircraft Airbus A380 and Antonov AN225.

Different Aircraft Categorizations based on MTOW

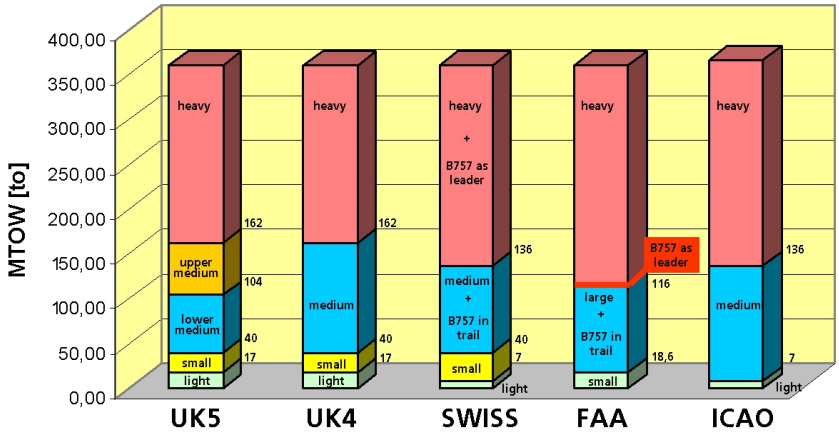

Figure A.1: Different MTOW-based aircraft categorizations for wake vortex separation minima[4]

RECAT-EU

Table A.3: Wake vortex separation minima of RECAT-EU[5]

Leading aircraft	Following aircraft					
	A	**B**	**C**	**D**	**E**	**F**
A	3 NM	4 NM	5 NM	5 NM	6 NM	8 NM
B	MRS	3 NM	4 NM	4 NM	5 NM	7 NM
C	MRS	MRS	3 NM	3 NM	4 NM	6 NM
D	MRS	MRS	MRS	MRS	MRS	5 NM
E	MRS	MRS	MRS	MRS	MRS	4 NM
F	MRS	MRS	MRS	MRS	MRS	3 NM

The aircraft categories are assigned as shown in table A.4.

[4] Hahn and Schwarz (2006), Paper about effects of wake vortex avoidance on landing capacity.
[5] Rooseleer and Treve (2015), Documentation of RECAT-EU.

Table A.4: Aircraft categories of RECAT-EU

Super Heavy	Upper Heavy	Lower Heavy	Upper Medium	Lower Medium	Light
A	**B**	**C**	**D**	**E**	**F**
A388	A332	A306	A318	AT43	FA10
A124	A333	A30B	A319	AT45	FA20
(...)	A342	A310	A320	AT72	D328
	A343	B703	A321	B712	E120
	A345	B752	AN12	B732	BE40
	A346	B753	B736	B733	BE45
	A359	B762	B737	B734	H25B
	B744	B763	B738	B735	JS32
	B748	B764	B739	CL60	JS41
	B772	B783	C130	CJR1	LJ35
	B773	C135	IL18	CJR2	LJ60
	B77L	DC10	MD81	CJR7	SF34
	B77W	DC85	MD82	CJR9	P180
	B788	IL76	MD83	DH8D	C650
	B789	MD11	MD87	E135	C525
	IL96	TU22	MD88	E145	C180
	(...)	TU95	MD90	E170	C152
		(...)	T204	E175	(...)
			TU16	E190	
			(...)	E195	
				F70	
				F100	
				GLF4	
				RJ85	
				RJ1H	
				(...)	

RECAT-US

Table A.5: Wake vortex separation minima of RECAT-US[6]

Leading aircraft	Following aircraft					
	A	**B**	**C**	**D**	**E**	**F**
A	MRS	5 NM	6 NM	7 NM	7 NM	8 NM
B	MRS	3 NM	4 NM	5 NM	5 NM	7 NM
C	MRS	MRS	MRS	3.5 NM	3.5 NM	6 NM
D	MRS	MRS	MRS	MRS	MRS	5 NM
E	MRS	MRS	MRS	MRS	MRS	4 NM
F	MRS	MRS	MRS	MRS	MRS	MRS

The aircraft categories are assigned as shown in table A.6.

Table A.6: Aircraft categories of RECAT-US

A	B	C	D	E	F
A388	B744	MD11	B752	DH8C	E120
	A346	B763	B753	AT72	B190
	B772	A306	B736	RJ1H	C650
	B773		B737	RJ85	H25B
	A333		B738	B462	C525
	A343		B739	B463	
	A332		A321	E170	
			A319	DH8A	
			A320	DH8B	
			A318	CJR9	
			MD82	AT43	
			MD83	AT45	
			F50	GLF4	
			B733	CRJ7	
			B734	SF34	
			B735	CJR2	
			E190	CJR1	
			GLF5	E45X	
			B712	E135	
			DC93	E145	
			DC95		
			DH8D		
			F100		
			F70		

[6] Lang and Lunsford (2013), Presentation about lessons learned from application of RECAT-US at Memphis International Airport.

B Modeling of Measurement Volume of Doppler Lidar Sensor

The measurement volume of the lidar sensor is modeled as a cylindrical volume with a length called blur depth. The diameter of the laser beam is assumed be to very small compared to the length of the volume such that only measurements along a line are considered. The lidar measurement inside the measurement volume is approximated by discrete measurements at different nodes, called blur points, as shown in Fig. B.1. For each measurement volume the different measurements at the blur points are summarized by means of a weighting function and assigned to a single point in space called measurement point.

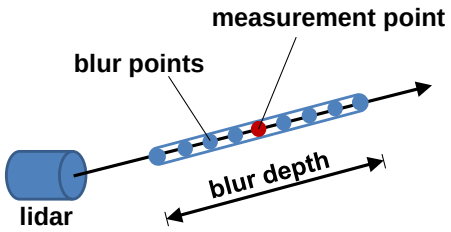

Figure B.1: Model of blur points and the resulting measurement point in a measurement volume of a lidar sensor

C Analytical Wake Vortex Models

Lamb-Oseen model:

$$V_\Theta(r) = \frac{\Gamma}{2\pi r}\left(1 - e^{-\beta\left(\frac{r}{r_c}\right)^2}\right) \tag{3.1}$$

with $\beta = 1.2564$ for a core radius of approximately $0.05b$

Proctor model:

$$V_\Theta(r) = \frac{\Gamma}{2\pi r} 1.4\left(1 - e^{-10\left(\frac{r_c}{b}\right)^{0.75}}\right)\left(1 - e^{-1.2527\left(\frac{r}{r_c}\right)^2}\right) \quad \text{, for } r \leq r_c \tag{3.2a}$$

$$V_\Theta(r) = \frac{\Gamma}{2\pi r}\left(1 - e^{-10\left(\frac{r}{b}\right)^{0.75}}\right) \quad \text{, for } r > r_c \tag{3.2b}$$

Winckelmans model:

$$V_\Theta(r) = \frac{\Gamma}{2\pi r}\left(1 - e^{-\frac{\beta_i\left(\frac{r}{b}\right)^2}{\left(1+\left(\frac{\beta_i}{\beta_o}\left(\frac{r}{b}\right)^{\frac{5}{4}}\right)^p\right)^{\frac{1}{p}}}}\right) \tag{3.3}$$

with $\beta_o = 10$, $\beta_i = 500$, $p = 3$

Jacquin model (two core scales with smooth velocity law, VM2 in *Fabre and Jacquin (2004)*[1]):

$$V_\Theta(r) = \frac{\Gamma}{2\pi a_1^2}\left(\frac{a_1}{a_2}\right)^{1-\alpha} \frac{r}{\left(1 + \left(\frac{r}{a_1}\right)^4\right)^{\frac{1+\alpha}{4}}\left(1 + \left(\frac{r}{a_2}\right)^4\right)^{\frac{1-\alpha}{4}}} \tag{3.4}$$

whereupon α, a_1 and a_2 are shaping parameters with typical values of $\frac{a_2}{a_1} = 10$ and $0.4 < \alpha < 0.6$

Rankine model:

$$V_\Theta(r) = \frac{\Gamma r}{2\pi r_c^2} \quad \text{, for } r \leq r_c \tag{3.5a}$$

$$V_\Theta(r) = \frac{\Gamma}{2\pi r} \quad \text{, for } r > r_c \tag{3.5b}$$

[1] Fabre and Jacquin (2004), Paper about the short-wave cooperative instabilities in vortices of different aircraft.

D Transformation between Wake Vortex Parameters used within Parameter Estimation Process and in WIAC Module

The geometric parameters used for the optimization process within the OWI are illustrated in red in Fig. 5.9 in section 5.2.3. The geometric parameters depicted in blue in Fig. 5.9 are provided by the OWI and used for the wake vortex model within the WIAC module. The vortex circulation and lateral distance between the vortex cores are used in either case. The conversion of the ID-coordinates into the output parameters of the OWI can be performed as follows: The wake azimuth is derived from the current aircraft heading and the x-position of P_1 and y-position P_2, providing the angle between the body-fixed x-axis and the lateral orientation of the wake vortex

$$\Psi_{\mathrm{WV}} = \arctan\left(\frac{-y_2}{x_1}\right) + \Psi_{\mathrm{AC}} \quad \text{, for } x_1 \neq 0, \tag{4.1a}$$

$$\Psi_{\mathrm{WV}} = \Psi_{\mathrm{AC}} \quad \text{, for } x_1 = 0. \tag{4.1b}$$

The delta azimuth angle between the wake vortex and the aircraft heading $\Delta\Psi_{\mathrm{WV}}$ is defined in the range $]-90°, 90°[$. But due to the addition of the current aircraft heading, the wake azimuth angle Ψ_{WV} can reach values outside the interval $[0°, 360°]$. The parameters are thus subsequently limited to this range by a modulo operation.

The wake elevation is derived from the vertical distance and the horizontal distance between the points P_1 and P_2. To get the correct sign of the wake elevation, it needs to be considered that the delta azimuth angle $\Delta\Psi_{\mathrm{WV}}$ only reaches values in the interval $]-90°, 90°[$. The wake elevation is defined, according to the Euler angles, as the vertical angle between the positive x-axis and the horizontal plane. As the angle between the wake vortex and the aircraft-fixed x-axis $\Delta\Psi_{\mathrm{WV}}$ is defined in the interval $]-90°, 90°[$, the wake elevation always needs to be determined for the branch of the wake vortex pointing into the direction of flight of the aircraft. This requires a distinction if the point P_1 lies in front of or behind the origin of the ID coordinate system. In the relevant case for the wake impact alleviation control that the wake vortex lies in front of the point of origin (i.e. $x_1 > 0$) the wake elevation can be determined as:

$$\Theta_{\mathrm{WV}} = \arctan\left(\frac{z_2 - z_1}{\sqrt{x_1^2 + y_2^2}}\right) \quad \text{, for } x_1. \tag{4.2a}$$

If the origin of the coordinate system is located behind the vortex centerline (i.e. $x_1 < 0$), the wake elevation is calculated as:

$$\Theta_{\mathrm{WV}} = \arctan\left(\frac{z_1 - z_2}{\sqrt{x_1^2 + y_2^2}}\right) \quad \text{, for } x_1 < 0. \tag{4.2b}$$

If the denominator $\sqrt{x_1^2 + y_2^2}$ becomes zero, the wake elevation is set to as zero:

$$\Theta_{\mathrm{WV}} = 0 \quad \text{, for } \sqrt{x_1^2 + y_2^2} = 0. \tag{4.2c}$$

The lateral distance between the vortex centerline and the center of gravity of the aircraft Δy_{WV} is derived from the body-fixed x-position of point P_1 and the determined wake azimuth:

$$\Delta y_{\mathrm{WV}} = -\left(x_1 - \Delta x\right) \cdot \sin\left(\Psi_{\mathrm{WV}} - \Psi_{\mathrm{AC}}\right). \tag{4.3}$$

The vertical distance between the vortex centerline and the center of gravity of the aircraft Δz_{WCV} results from the body-fixed x-position of point P_1 and the determined wake elevation:

$$\Delta z_{\mathrm{WV}} = \left(z_2 - \Delta x \cdot \tan\Theta_{\mathrm{WV}}\right) \cdot \cos\Theta_{\mathrm{WV}}. \tag{4.4}$$

E Wake Impact Alleviation without Actuatator Dynamics and Limits

Figure E.1 shows the application of the wake impact alleviation control system for the same encounter[1] as Fig. 5.15 but without actuator dynamics and limits. This implies that there are no limits for the maximum and minimum deflection, rate and acceleration of the control surfaces. The actuator dynamics are replaced by a constant delay of 0.1 s, which corresponds to the delay used within WIAC for the determination of the disturbance forces and moments.

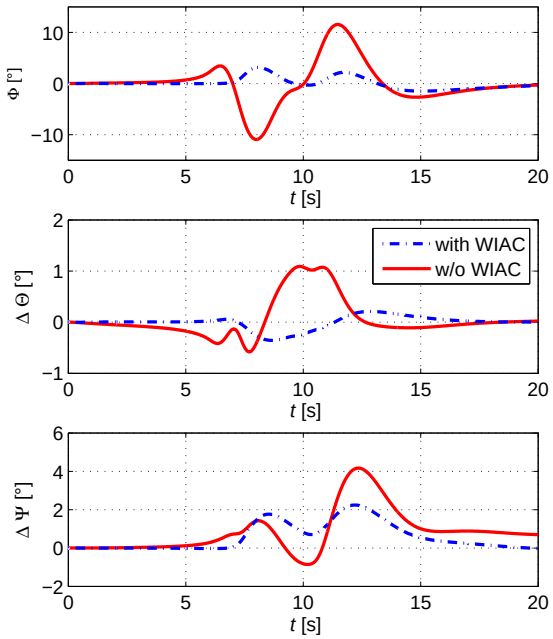

Figure E.1: Wake impact alleviation during $10°$ lateral encounter (with separate implementation of WIAC and basic control system) without actuator dynamics and limits

[1] Airbus A320 flying during approach into the wake of an Airbus A340, $0°$ vertical and $10°$ lateral encounter angle, wake vortex located 2 m above center of gravity of encountering aircraft, no pilot inputs, autopilot disengaged.

F Characteristics of Sensor Configurations of Section 7.1

Table F.1 shows the characteristics of the three sensor sets considered in the exemplary presentation of the wake impact alleviation performance of the OWIDIA system in section 7.1. An illustration of the definition of the sensor parameters is given in Fig. 7.7.

Table F.1: Sensor characteristics of the exemplary presentation of the wake impact alleviation performance

	Number of vertical axes [-]	Number of horizontal axes [-]	Number of MP along axis [-]	Total number of MP [-]	$range_{MP1}$ [m]	Vertical field of view Θ_{scan} [°]	Lateral field of view Ψ_{scan} [°]	Blur depth [m]	Full scan update rate [Hz]	Single axis update rate [Hz]
sensor 1	3	7	1	21	60	+/-10	+/-16	30	5	105
sensor 2	3	7	1	21	90	+/-10	+/-30	30	10	210
sensor 3	3	5	1	15	75	+/-10	+/-16	15	5	75

G Models for Wake Identification of Deformed Wake Vortices

If the OWI shall be applied to deformed wake vortices, the current wake vortex model used for the parameter estimation has to be replaced by a more extended model, which can cover the complexer shape of older wake vortices. For older wake vortices, the cores of the vortex pair are not arranged in two straight lines but show significant oscillations or even form vortex rings. Possible approaches for analytical wake vortex models that could be used in the online wake identification are the formulas of curved vortices and vortex rings suggest by *Münster (2011)*[1]. Münster derived analytical equations of deformed wake vortices from LES wake vortices. He developed two different approaches for the description of the lines of the vortex cores for curved vortices and ring vortices, which are described in detail in section G.1 and G.2. These equations could be used as extended models for the parameter estimation in the OWI. The wake-induced wind velocities at any desired position in space can afterwards be computed by dividing the deformed vortex lines into small finite segments of straight vortices, as suggested by *Vechtel (2010)*[2] and shown in Fig. G.1 and by computing the induced velocities of each segment by means of the law of Biot-Savart[3]. The error resulting from the fact that finite vortex segments are considered instead of the infinite vortex lines assumed by Biot and Savart has been shown by Vechtel to be small.

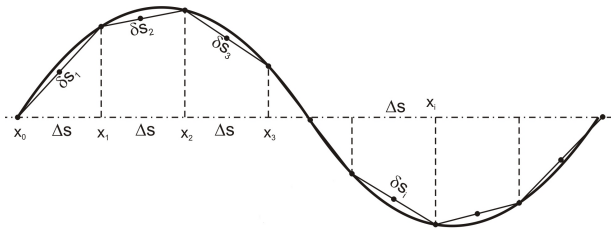

Figure G.1: Discretization of curved wake vortex into small straight segments[2]

G.1 Model of Curved Wake Vortices

The equations for the description of curved wake vortices are based on several sine-functions because the Crow Instability during the decay process of wake vortices leads to a sine-shape. The oscillations occur in a plane that is tilted by approximately $48°$ with respect to the horizontal plane. The model thus needs sine-functions in the x-y- as well as in the x-z-plane, whereupon the x- coordinated is oriented parallelly to the vortex centerline.

[1] Münster (2011), DLR institute report about the identification and analysis of an analytical wake vortex model for deformed vortices.

[2] Vechtel (2010), DLR institute report about the development of an analytical wake vortex model for deformed vortices.

[3] Schlichting and Truckenbrodt (2001a), Reference book of aerodynamics of the aircraft, part 1.

$$y = p_{1y} \cdot \sin\left(p_{2y} \cdot x + p_{3y}\right) + p_{4y} \cdot \sin\left(p_{5y} \cdot x + p_{6y}\right) + p_{7y} \tag{7.1a}$$

$$z = p_{1z} \cdot \sin\left(p_{2z} \cdot x + p_{3z}\right) + p_{4z} \cdot \sin\left(p_{5z} \cdot x + p_{6z}\right) + p_{7z} \tag{7.1b}$$

The analysis of Münster revealed that the superposition of two sine-functions is a good approach for a model of curved wake vortices. The first sine-function models the long-wave Crow Instability and the second sine-function models instabilities of shorter wave-length. As shown in Fig. G.2 adding a third sine-function does not lead to further improvements of the match of the model with the reference wake vortex simulated with LES. However, a single sine-function would not allow an adequate reproduction of the curved wake vortex.

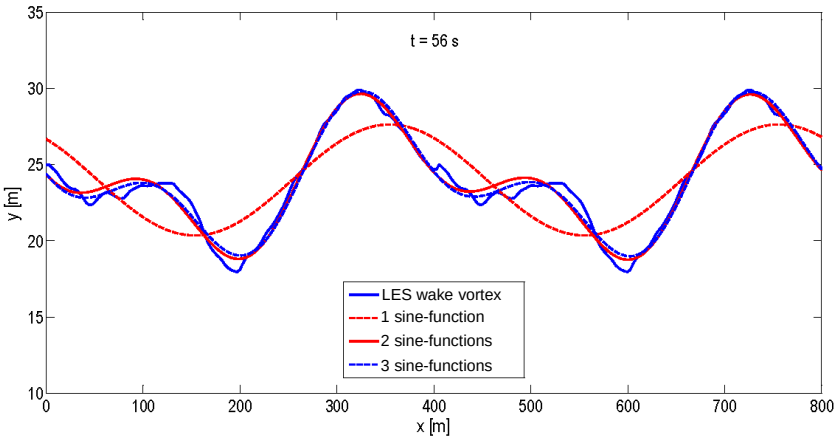

Figure G.2: Comparison of the results of the wake identification based on models with one, two or three superimposed sine-functions with a 56-s-old LES wake vortex (computed for moderate turbulence and neutral thermal stratification, $N^* = 0$, $\epsilon^* = 0.23$)[4]

The parameters p_1 to p_7 for the y- and z-direction are the parameters to be estimated by the OWI. For the initial values of the parameters p_2 and p_5, describing the amplitudes of the sine-functions, Münster recommends the Crow wavelength λ_{Crow} and the half Crow wavelength respectively.

$$p_1 \approx \lambda_{\text{Crow}} = 407.3\,\text{m} \tag{7.2a}$$

$$p_2 \approx \frac{\lambda_{\text{Crow}}}{2} = 203.6\,\text{m} \tag{7.2b}$$

In case of a straight wake vortex all parameters expect for the parameters p_7 in y- and z-direction would result to be zero. The remaining p_7 parameters describe the lateral and vertical position of the straight line of the vortex cores of the port and starboard wake vortex with respect to the vortex centerline. A parallel OWI call with initial values of zero for the parameters p_1 to p_6 in addition to the execution of the OWI for a curved wake vortex model with the initial values of equations 7.2a and 7.2b would enable a faster and more robust converge to the solution of straight wake vortices. The better solution of both OWI calls could be determined by comparing the final values of the cost functions.

[4] Münster (2011), p. 47, DLR institute report about the identification and analysis of an analytical wake vortex model for deformed vortices.

G.2 Model of Vortex Rings

Vortex rings can be modeled by sine-functions along a ring. Münster (2011)[5] suggests the superposition of three sine-functions, whereupon the variable s describes the position along the circumference of the circle. This allows an adequate modeling of irregular ring shapes in 3D. The resulting equations for the coordinates of the vortex centerline are:

$$x = p_{1y} \cdot \sin\left(p_{2x} \cdot s + p_{3x}\right) + p_{4x} \cdot \sin\left(p_{5x} \cdot s + p_{6x}\right) + p_{7x} \cdot \sin\left(p_{8x} \cdot s + p_{9x}\right) + p_{10x}, \tag{7.3a}$$

$$y = p_{1y} \cdot \sin\left(p_{2y} \cdot s + p_{3y}\right) + p_{4y} \cdot \sin\left(p_{5y} \cdot s + p_{6y}\right) + p_{7y} \cdot \sin\left(p_{8y} \cdot s + p_{9y}\right) + p_{10y}, \tag{7.3b}$$

$$z = p_{1z} \cdot \sin\left(p_{2z} \cdot s + p_{3z}\right) + p_{4z} \cdot \sin\left(p_{5z} \cdot s + p_{6z}\right) + p_{7z} \cdot \sin\left(p_{8z} \cdot s + p_{9z}\right) + p_{10z}, \tag{7.3c}$$

with $s \in [0,2\pi]$.

The parameters p_1 to p_{10} of the x-, y- and z-axis have to be estimated by the OWI.

[5] Münster (2011), Identification and analysis of an analytical wake vortex model for deformed vortices.